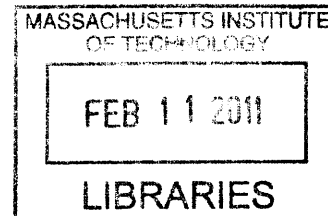


Design and Synthesis of Organic Chromophores for Imaging, Lithography and Organic Electronics

by
Trisha Lionel Andrew

B.Sc. (With Honors) Chemistry
University of Washington, 2005



ARCHIVES

SUBMITTED TO THE DEPARTMENT OF CHEMISTRY IN
PARTIAL FULFILLMENT OF THE REQUIREMENTS FOR THE DEGREE OF

DOCTOR OF PHILOSOPHY IN CHEMISTRY
AT
THE MASSACHUSETTS INSTITUTE OF TECHNOLOGY
FEBRUARY 2011

© Massachusetts Institute of Technology, 2011. All Rights Reserved.

Signature of Author: _____

Department of Chemistry
December 2, 2010

Certified by: _____

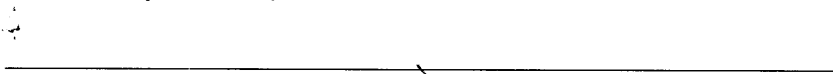
Timothy M. Swager
Professor of Chemistry
Thesis Supervisor

Accepted by: _____

Robert W. Field
Professor of Chemistry
Chairman, Departmental Committee on Graduate Studies

This doctoral thesis has been examined by a
Committee of the Department of Chemistry as follows:


Professor Stephen L. Buchwal
Thesis Committee Chair

A horizontal line with a handwritten signature in black ink above it, extending across the width of the text.

Professor Timothy M. Swager
Thesis Supervisor

A horizontal line with a handwritten signature in black ink above it, extending across the width of the text.

Professor Mohammad Movassaghi
Department of Chemistry

A horizontal line with a handwritten signature in black ink above it, extending across the width of the text.

For my Lion and Lioness

Design and Synthesis of Organic Chromophores for Imaging, Lithography and Organic Electronics

by

Trisha Lionel Andrew

SUBMITTED TO THE DEPARTMENT OF CHEMISTRY ON DECEMBER 2, 2010 IN PARTIAL FULFILLMENT OF THE REQUIREMENTS FOR THE DEGREE OF DOCTOR OF PHILOSOPHY IN CHEMISTRY.

ABSTRACT

The absorption and emission maxima, photostabilities and photoreactivities of small-molecule organic chromophores can be tailored by (a) the choice of an appropriate parent structure and (b) the deliberate introduction of substituents that predictably alter the optical properties and photochemistry of this parent structure. Suitably-designed chromophores can be used in a variety of applications, such as imaging (for example, as fluorescent labeling agents or as indicators for specific analytes), optical lithography and as active components in organic electronic devices.

In Chapter 1, a fluorogenic chemosensor to detect saturated nitramine and nitrate ester explosives was devised based on a photochemical reduction reaction. 10-Methyl-9,10-dihydroacridine (AcrH₂) was found to transfer a hydride ion equivalent to the high explosives RDX and PETN upon irradiation at 313 nm in degassed acetonitrile solutions. Mechanistic photophysical studies indicated that the photoreduction of RDX proceeded via a two-step electron-hydrogen atom transfer reaction, whereas PETN photoreduction proceeded via a three-step electron-proton-electron transfer sequence. A zinc analog was synthesized and found to display an 80- or 25-fold increase in 480 nm emission intensity upon reaction with RDX or PETN, respectively; moreover, the Zn analog was found to be unresponsive to TNT and other common contaminants, in addition to being photostable under ambient conditions.

In Chapter 2, the nitramine-containing explosive RDX and the nitroester-containing explosive PETN were shown to be susceptible to photodegradation upon exposure to sunlight. The products of this photodegradation were identified as reactive, electrophilic NO_x species, such as nitrous and nitric acid, nitric oxide, and nitrogen dioxide. *N,N*-Dimethylaniline was capable of being nitrated by the reactive, electrophilic NO_x photodegradation products of RDX and PETN. A series of 9,9-disubstituted 9,10-dihydroacridines (DHAs) were synthesized from either *N*-phenylanthranilic acid methyl ester or a diphenylamine derivative and were similarly shown to be rapidly nitrated by the photodegradation products of RDX and PETN. An increase in the emission signal at 550 nm was observed upon nitration of DHAs due to the generation of fluorescent donor-acceptor chromophores. Using fluorescence spectroscopy, the presence of ca. 1.2 ng of RDX and 320 pg of PETN could be detected by DHA indicators in the solid state upon exposure to sunlight.

In Chapter 3, optical lithography with organic photochromes is demonstrated. In the past, the formation of microscale patterns in the far field by light has been diffractively limited in resolution to roughly *half* the wavelength of the radiation used. We demonstrated lines with an

average width of 36 nm, about *one-tenth* the illuminating wavelength ($\lambda_1 = 325$ nm), made by applying a film of thermally-stable photochromic molecules above the photoresist. Simultaneous irradiation of a second wavelength ($\lambda_2 = 633$ nm) rendered the film opaque to the writing beam except at nodal sites, which let through a spatially constrained segment of incident λ_1 light, allowing subdiffractional patterning.

In Chapter 4, rylene dyes functionalized with varying numbers of phenyl trifluorovinylether (TFVE) moieties were subjected to a thermal emulsion polymerization to yield shape-persistent, water-soluble chromophore nanoparticles. Perylene and terylene diimide derivatives containing either two or four phenyl TFVE functional groups were synthesized and subjected to thermal emulsion polymerization in tetraglyme. Dynamic light scattering measurements indicated that particles with sizes ranging from 70 – 100 nm were obtained in tetraglyme, depending on monomer concentration. The photophysical properties of individual monomers were preserved in the nanoemulsions and emission colors could be tuned between yellow, orange, red, and deep red. The nanoparticles retained their shape upon dissolution into water and the resulting water suspensions displayed moderate to high fluorescence quantum yield, thus making them attractive candidates for bioimaging applications.

In Chapter 5, a series of substituted 6,6-dicyanofulvenes (DCFs) were synthesized starting from masked, dimeric or monomeric cyclopentadienones. DCFs lacking sufficient steric bulk around the fulvene core tended to reversibly undergo a [4+2] dimerization. In addition to being highly crystalline, DCFs were darkly-colored compounds due to the presence of weak electronic transitions in the visible region of the electromagnetic spectrum. DCFs displayed two distinct, reversible one-electron reductions by cyclic voltammetry. Based on their high crystallinity and suitable electron affinities, and buoyed by their relatively cheap and straightforward synthesis, DCFs are interesting candidates for organic electron-transport materials.

Thesis Supervisor: Timothy M. Swager

Title: John D. MacArthur Professor of Chemistry

CONTENTS

Title Page	1
Signature Page	2
Dedication	3
Abstract	4
CHAPTER 1 – DETECTING HIGH EXPLOSIVES WITH ORGANIC HYDRIDE DONORS	9
1.1 Introduction	10
1.2 <i>N</i> -Methyl-9,10-Dihydroacridine (AcrH ₂)	11
1.3 Other Hydride Donors	16
1.4 Complexes of AcrH ₂	17
1.5 Solid State Sensors and Vapor Phase Detection of RDX and PETN	19
1.6 Conclusions	20
1.7 Experimental Section	20
1.8 References and Notes	25
1.9 Additional Figures	29
CHAPTER 2 – SELECTIVE DETECTION OF EXPLOSIVES VIA PHOTOLYTIC CLEAVAGE OF NITROESTERS AND NITRAMINES	34
2.1 Introduction	35
2.2 Indicator Design	39
2.3 Synthesis	41
2.4 Photophysics	45
2.5 Electrochemistry	47
2.6 Reaction with RDX/PETN Photodegradation Products	50
2.7 Other Nitroesters and Nitramines	53
2.8 Differences in DHA Reaction Mechanisms	53
2.9 Light Sources	54
2.10 Other NO _x Sources	54
2.11 Optical Properties of Nitrated DHAs	55
2.12 Optical Characterization of Indicator Response	56
2.13 Reaction Kinetics	63
2.14 Solid State RDX/PETN Detection	67
2.15 Conclusions	70
2.16 Experimental Section	71
2.17 References and Notes	93
CHAPTER 3 – USING ORGANIC PHOTOCHROMES TO ENABLE OPTICAL NANOPATTERNING	98
3.1 Introduction	99
3.2 Results and Discussion	103
3.3 Conclusions	109
3.4 Experimental Section	109
3.5 References and Notes	118

CHAPTER 4 – THERMALLY-POLYMERIZED RYLENE NANOPARTICLES	121
4.1 Introduction	122
4.2 Monomer Synthesis	124
4.3 Monomer Photophysics	126
4.4 Nanoparticle Synthesis	128
4.5 Nanoparticle Photophysics	133
4.6 Conclusions	135
4.7 Experimental Section	135
4.8 References and Notes	139
CHAPTER 5 – 6,6-DICYANOFULVENES	144
5.1 Introduction	145
5.2 Synthesis of 6,6-Dicyanofulvenes	146
5.3 Electrochemistry	153
5.4 Conclusions	156
5.5 Experimental Section	157
5.6 References and Notes	165
5.7 Additional Figures	169
CURRICULUM VITAE	172
ACKNOWLEDGEMENTS	175
APPENDIX 1: NMR SPECTRA FOR CHAPTER 1	177
APPENDIX 2: NMR SPECTRA FOR CHAPTER 2	180
APPENDIX 3: NMR SPECTRA FOR CHAPTER 3	214
APPENDIX 4: NMR SPECTRA FOR CHAPTER 4	218
APPENDIX 5: NMR SPECTRA FOR CHAPTER 5	225

CHAPTER 1

Detecting High Explosives with Organic Hydride Donors

Adapted and reprinted in part with permission from:
Andrew, T. L.; Swager, T. M. "A Fluorescence Turn-On Mechanism to Detect the High
Explosives RDX and PETN" *J. Am. Chem. Soc.* **2007**, *129*, 7254-7255.

1.1 Introduction

Developing practical sensors for detecting hidden explosive devices in war zones and transportation hubs is a pressing scientific and social concern. Current efforts have focused on sensing three commonly-used powerful explosives: 2,4,6-trinitrotoluene (TNT), 1,3,5-trinitro-1,3,5-triazinane (RDX) and pentaerythritol tetranitrate (PETN) (Figure 1.1). The need for ultra-trace detection of these low-volatility compounds has resulted in an intense interest in fluorescence methods, and the direct detection of TNT vapor by amplifying fluorescent polymers (AFPs) is now an established technology.¹ However analogous examples of direct RDX or PETN detection are sparse and current methods rely heavily on ion mobility spectrometry,^{2a} mass spectrometry,^{2b} and, to a lesser extent, detecting either chemically-modified RDX^{3a} or its degradation products.^{3b}

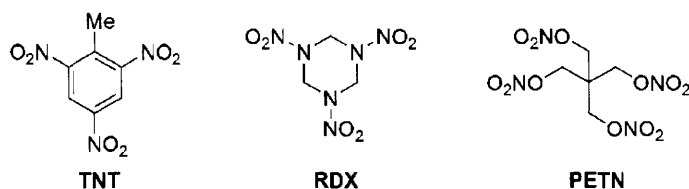


Figure 1.1. Structures of common high explosives.

In the AFP-based detection scheme (developed previously in the Swager lab), the presence of TNT vapor quenches the fluorescence of a conjugated polymer thin film (for example, a thin film of **P1**) due to an energetically-favorable photoinduced electron transfer (PET) pathway made available by the LUMO of TNT (Figure 1.2). In contrast, the analogous PET reaction between **P1** and either RDX or PETN lacks a significant driving force,⁴ thus precluding the observation of significant fluorescence quenching. Another hindrance is the fact

that the vapor pressures of RDX and PETN are three orders of magnitude lower than that of TNT. These challenges to detecting RDX and PETN stimulated our group to explore alternative fluorescence-based detection mechanisms. In particular, we pursued “turn-on” schemes wherein a strong fluorescence signal is generated from a dark background in response to an analyte, as, theoretically, this mechanism has inherently higher sensitivity than a “turn-off” mechanism.

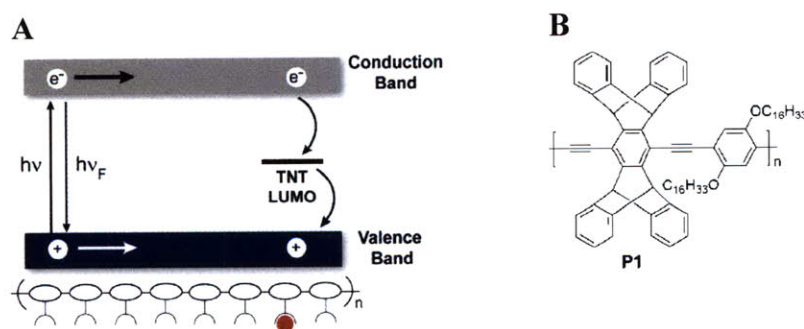


Figure 1.2. (A) Conjugated polymer-based TNT detection scheme. (B) Structure of **P1**, which is able to detect picogram quantities of TNT via amplified fluorescence quenching.^{1b}

1.2 *N*-Methyl-9,10-Dihydroacridine (**AcrH₂**)

Inspired by enzymatic, NADH-mediated reduction of RDX in contaminated wastewater,⁵ we sought to mimic this biological process in a fluorescence-based sensor. Initial studies targeted the NADH analogue *N*-methyl-9,10-dihydroacridine (**AcrH₂**, Figure 1.3) because of its ability to form the *N*-methylacridinium fluorophore (**AcrH⁺**) upon “H⁻” abstraction. As seen in Figure 1.4B, both RDX and PETN generated the green-emitting **AcrH⁺** from the blue-emitting **AcrH₂** upon photolysis at 313 nm in deoxygenated acetonitrile solutions, whereas TNT was ineffective.⁶ Moreover, RDX and PETN were also photoreduced by **AcrH₂** upon exposure of a deoxygenated acetonitrile solution to sunlight (5 minutes in Cambridge winter conditions or 45 seconds in spring weather) (Figure 1.5).

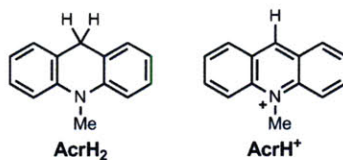


Figure 1.3. Structures of AcrH₂ and its oxidation product AcrH⁺.

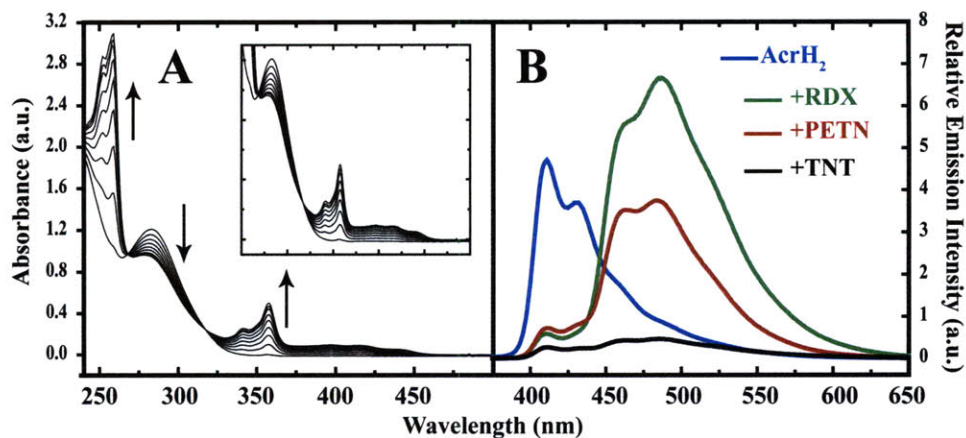


Figure 1.4. (A) Absorbance profile of the photoreaction of AcrH₂ with RDX. (B) Emission profiles of: AcrH₂ in deoxygenated acetonitrile and its mixtures with RDX, PETN or TNT in degassed acetonitrile after a 60.0 second irradiation with 313 nm light.

$$[\text{AcrH}_2] = 2.4 \times 10^{-3} \text{M}, [\text{Explosive}] = 0.012 \text{M}, \lambda_{\text{ex}} = 356 \text{ nm}.$$

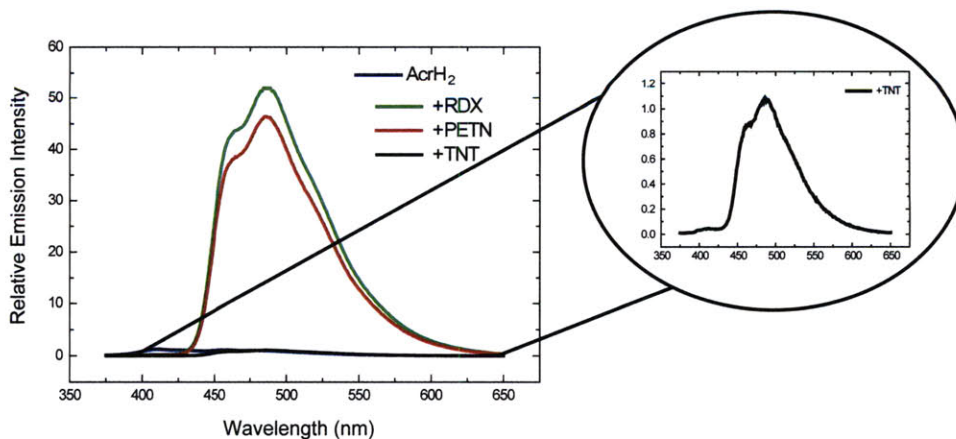
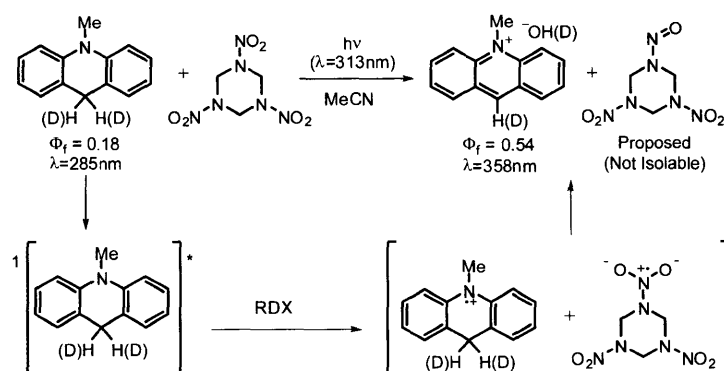


Figure 1.5. Emission profiles of AcrH₂ in deoxygenated acetonitrile and its mixtures with RDX, PETN or TNT after a 45.0 s exposure to sunlight. [AcrH₂] = 4 × 10⁻⁴ M, [Explosive] = 0.012 M.

Whereas the fate of **AcrH₂** could be followed during the course of photoreaction, the structures of reduced RDX or PETN, however, could not be easily discerned. The relatively reactive *N*-nitroso reaction product suggested in Scheme 1.1 stems from a proposed intermediate in enzymatic RDX reduction.⁷ However, we have not been able to unambiguously prove its formation as this compound easily fragments under most ionization conditions, thus rendering mass spectrometric analyses inconclusive.⁸



Scheme 1.1. Proposed photoreaction of **AcrH₂** (**AcrD₂**) with RDX.

In order to better understand the mechanism(s) involved, we measured the quantum yields of RDX, PETN and TNT photoreduction and performed kinetic isotope effect studies. As is common with NADH analogues, we anticipated either of three operative photoreduction mechanisms: a one-step hydride transfer, a two-step electron-hydrogen atom transfer or an electron-proton-electron transfer sequence.⁹ Photoreaction quantum yields (Φ_{rxn}), defined as the ratio of moles **AcrH⁺** produced to moles photons absorbed,¹⁰ were obtained from a series of absorbance profiles for the reactions of RDX, PETN and TNT with **AcrH₂** and its dideuterated analogue, **AcrD₂**. Figure 1.4A shows a typical absorbance profile for the photoreduction reaction

wherein the absorption band corresponding to **AcrH₂** at 285 nm decreased with photolysis, concomitant with an increase in **AcrH⁺** absorbance at 358 nm.

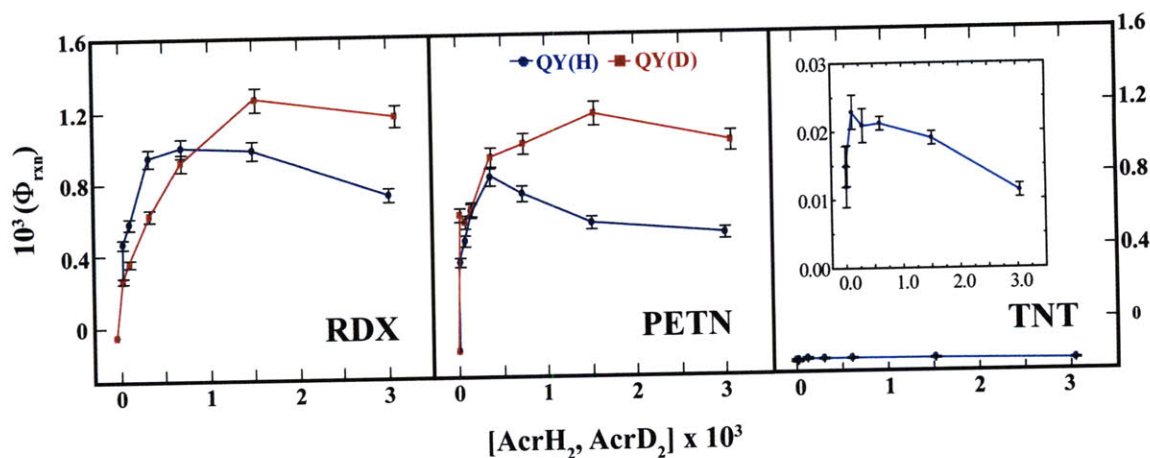


Figure 1.6. Dependence of Φ_{rxn} on $[\text{AcrH}_2, \text{AcrD}_2]$ for the photoreduction of RDX, PETN and TNT. $[\text{Explosive}] = 6.9 \times 10^{-4} \text{ M}$.

Φ_{rxn} values as a function of **AcrH(D)₂** concentration are shown in Figure 1.6. The low Φ_{rxn} values (<0.1%) obtained for our system reflect the inherent inefficiency of a bimolecular photoreaction in dilute solutions and exclude any chain pathways in the photoreduction of either RDX or PETN. At constant [RDX] and [PETN], Φ_{rxn} increased linearly with $[\text{AcrH}_2]$ to a maximum value of 8.5×10^{-4} and 6.1×10^{-4} , respectively, after which it gradually decreased.

A linear increase in quantum yield with increasing reactant concentration is often observed.¹¹ We hypothesize that the singlet excited state of **AcrH₂** reduces RDX or PETN (Scheme 1.1) and can explain, within this context, a linear increase in Φ_{rxn} with $[\text{AcrH}_2]$ based on the fact that a higher **AcrH₂** concentration increases $[\text{AcrH}_2^*]$, the concentration of excited chromophores, which in turn leads to a greater chance of a bimolecular collision with RDX or

PETN within the excited-state lifetime of **AcrH₂**. The concentration of **AcrH₂*** should also be affected by the intensity of incident light and, accordingly, we observe that Φ_{rxn} is linearly dependent on light intensity.

We are not, however, aware of other systems that show quantum yield saturation and subsequent decrease. We found that at sufficiently high concentrations the rate of self-quenching (the collisional deactivation of **AcrH₂*** with **AcrH₂** (GS)) competed with analyte reduction, which lowered the overall efficiency of the photoreaction and lead to the observed decrease in Φ_{rxn} .

In the case of TNT photoreduction, Φ_{rxn} values followed a similar pattern to those of RDX and PETN photoreduction but were significantly lower. This observation is consistent with the emission profiles provided earlier wherein notable **AcrH⁺** formation was not observed in mixtures of **AcrH₂** and TNT. Since TNT functions as an exceptional fluorescence quencher, the initial electron transfer between **AcrH₂*** and TNT is most probably followed by back-electron transfer and regeneration of **AcrH₂** (GS), thus hindering photooxidation of **AcrH₂**.

To distinguish between the three possible mechanisms of RDX photoreduction, we obtained a $\Phi_{\text{H}}/\Phi_{\text{D}}$ value of approximately 1.3 at low [**AcrH₂**], which is consistent with a two-step electron-hydrogen atom transfer oxidation of **AcrH₂**.^{12a,12} The inverse primary kinetic isotope effect (KIE) ($\Phi_{\text{H}}/\Phi_{\text{D}}=0.77$) observed at high [**AcrH₂**] does not have literature parallels but can be explained, once again, by the self-quenching of **AcrH₂** chromophores, in light of reports of an inverse KIE in select quenching processes.¹³ An inverse KIE was also observed at high [**AcrH₂**] for the reduction of PETN; however, a significant KIE is not observed at low [**AcrH₂**], thus implicating an electron-proton-electron transfer sequence as the mechanism of PETN photoreduction.¹⁴

1.3 Other Hydride Donors

The scope of the photochemical hydride transfer reaction was briefly explored by investigating the photoreactions between dihydroanthracenes, xanthene and fluoreneol with RDX, PETN and TNT. As seen in Figure 1.7, 9,10-dihydroanthracene and xanthene behaved similar to **AcrH₂**, although longer irradiation times (approximately 5 times greater) were required to obtain emission intensity changes comparable to that of **AcrH₂**. 2,3,6,7-Tetramethoxy-9,10-dihydroanthracene is interesting for its relative photostability; however, this desirable characteristic came at the loss of reactivity, thus demanding irradiation times greater than 30 minutes to observe an eight-fold increase in 427 nm emission intensity. Trimethylsilane-protected 9-fluoreneol was unstable toward irradiation even in deoxygenated acetonitrile solutions; moreover, surprisingly, we observed efficient hydride transfers to RDX and TNT while PETN did not generate any observable trace of 9-fluorenone, the product of 9-fluoreneol oxidation.

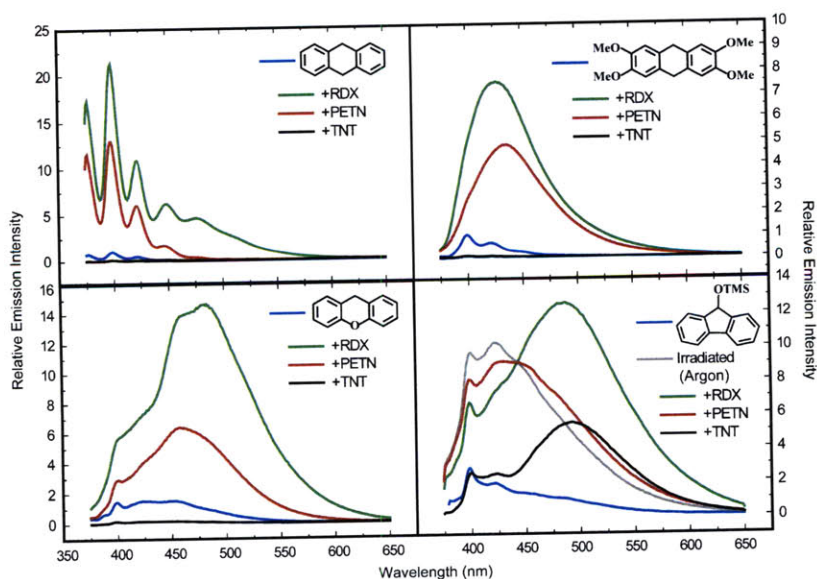


Figure 1.7. Emission profiles of various hydride donors and their mixtures with RDX, PETN and TNT in deoxygenated acetonitrile after irradiation with 313 nm light.

[Hydride Donor] $\approx 4 \times 10^{-4}$ M, [Explosive] = 0.012 M.

1.4 Complexes of AcrH₂

Although most of the hydride donors mentioned thus far were not oxidized in the absence of RDX or PETN in deoxygenated solutions, all compounds were nonetheless oxidized upon irradiation in air. Such oxygen sensitivity limits the utility of a practical chemosensor; therefore, in an effort to fabricate a photostable chemosensor, a zinc analogue of AcrH₂, **1**, was synthesized (Figure 1.8). From an initially weakly emissive, aerated solution of **1**, irradiation at 313 nm in the presence of either RDX or PETN produced an intense peak at 480 nm (Figure 1.9A) due to the formation of an acridine-zinc complex, **2** (Scheme 1.2); this assignment was corroborated by comparing the resulting emission spectrum with that of an independently synthesized zinc-acridine complex.

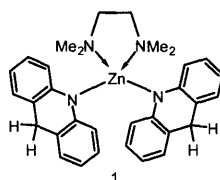


Figure 1.8. Structure of zinc complex **1**.

Irradiating **1** in the absence of an explosive analyte produced an emission band at 400 nm; however, the former 480 nm peak was not formed, even after prolonged (>2 hours) irradiation in air (Figure 1.9A). We believe that **1** slowly photooxidizes to the corresponding ketone, forming an *N*-substituted acridone derivative, **3**, in aerated solutions.¹⁵ Nevertheless, a statistically significant 480 nm emission signal was observed with RDX and PETN concentrations as low as 7×10^{-5} and 1.3×10^{-4} M, respectively.

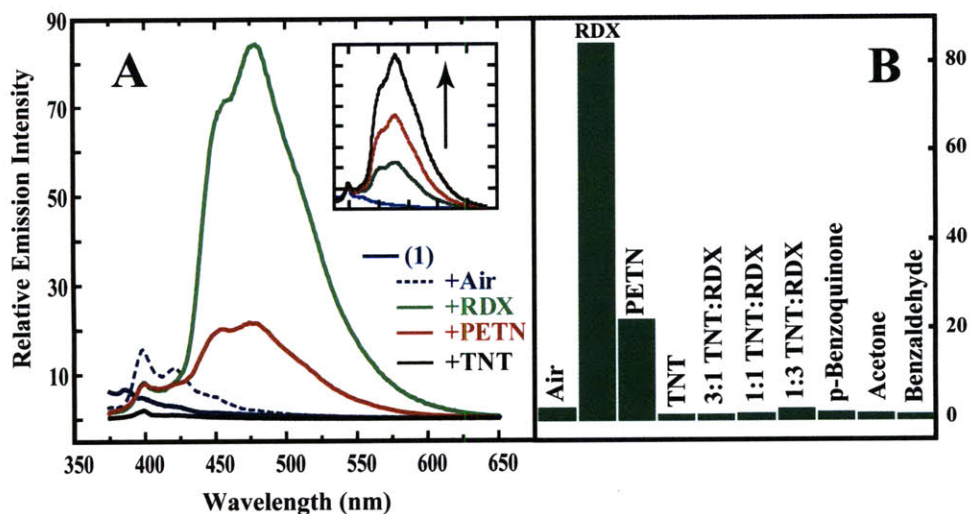
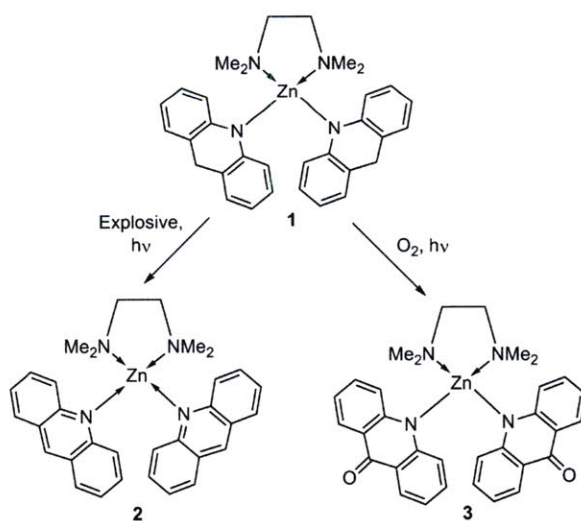


Figure 1.9. (A) Emission profiles of **1** in acetonitrile; **1** after a 120 second irradiation (313 nm) in acetonitrile; and mixtures of **1** and either RDX, PETN or TNT in acetonitrile after a 30.0 second irradiation with 313 nm light. The inset shows growth of the 480 nm peak with increasing irradiation time (10 s intervals). (B) Emission intensity at 480nm resulting from photoreaction of **1** (30.0 second irradiation times) with various explosive analytes, analyte mixtures or select contaminants in aerated acetonitrile. $[1] = 3.1 \times 10^{-4} \text{ M}$, $[\text{Explosive/Analyte}] = 0.012 \text{ M}$, $\lambda_{\text{ex}} = 356 \text{ nm}$.



Scheme 1.2. Reaction of complex **1** with explosive analytes and oxygen.

The selectivity of **1** was examined by monitoring its response to known hydride acceptors, such as *p*-benzoquinone, and mixtures of TNT and RDX. Complex **1** was relatively unresponsive to TNT and, with TNT/RDX mixtures, the emission intensity at 480nm increased approximately proportional to the ratio of RDX (see Figure 1.9B). Most strikingly, unlike the parent **AcrH₂**, **1** did not thermally reduce *p*-benzoquinone and photochemical hydride transfer was found to proceed slowly. Other aliphatic and aromatic ketones and aldehydes (which are common contaminants contained within or found in the proximity of an explosive device) were also comparatively unreactive.

1.5 Solid State Sensors and Vapor Phase Detection of RDX and PETN

In order to obtain a practical, utilizable chemosensor for RDX and PETN, we wished to translate the promising solution state results procured above into a solid state sensor that can be implemented in existing fluorescence-based explosives detection technology.¹⁶ More specifically, our ultimate goal is to fabricate a sensor that possesses sufficient sensitivity to display a direct fluorescence response to equilibrium vapor pressures of RDX and PETN.¹⁷ To realize this goal, we pursued the use of micro- and mesoporous materials with the anticipation that high porosity will enhance analyte diffusion into the sensor and therefore increase the sensitivity of the system.¹⁸

Initial attempts involved the use of zeolites to organize complex **1** in the solid state.¹⁹ A zeolite-included sample of **1** (included in zeolite sodium Y) was coated on a glass slide and a small sample (ca. 0.05 mg) of RDX was allowed to adsorb onto the surface of the slide. As seen in Figure 1.10, a ca. 8-fold increase in emission intensity at 480 nm was observed after a 50.0 second irradiation in the presence of RDX whereas no such change was observed in its absence.

However, a small background emission signal at 480 nm was nonetheless observed, even in the absence of an explosive analyte, because acidic sites within the zeolite cavity oxidized minor quantities of **1** to **2**.

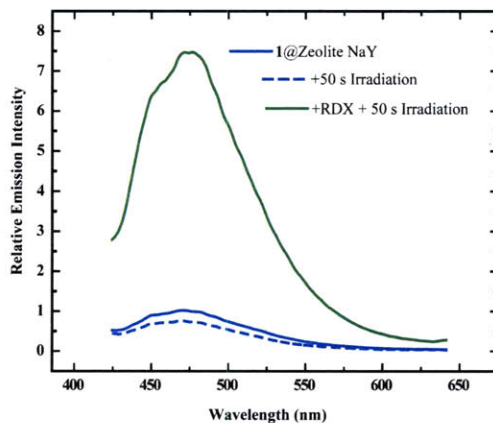


Figure 1.10. Response of zeolite-included **1** coated on a glass slide to RDX.

1.6 Conclusions

We found that *N*-methyl-9,10-dihydroacridine, **AcrH₂**, is capable of selectively transferring a hydride ion equivalent to saturated nitramine and nitroester explosives as part of a photochemical reaction. Its photostable zinc analog, **1**, displayed an 80- and 25-fold increase in 480 nm emission intensity upon reaction with RDX and PETN, respectively. This example of a direct fluorescence response to RDX or PETN is orthogonal to existing conjugated polymer-based detection technology and will enable existing fluorescence methods to detect non-aromatic high explosives.

1.7 Experimental Section

Materials: All solvents used for photophysical experiments were of spectral grade. All reagent grade materials were purchased from Aldrich or Alfa Aesar, and used without further

purification. THF was obtained from J. T. Baker and purified by passing through a Glasscontour dry solvent system. *N*-Methyl-9,10-dihydroacridine (**AcrH₂**) was prepared by sodium borohydride reduction of *N*-methylacridinium iodide according to a literature procedure and recrystallized from ethanol.²⁰ [9,9-²H₂]-*N*-methyl-9,10-dihydroacridine (**AcrD₂**) was prepared by LiAlD₄ reduction of *N*-methylacridone according to a literature procedure and recrystallized from ethanol.²¹

NMR Spectroscopy: ¹H and ¹³C NMR spectra for all compounds were acquired in CD₃CN on a Bruker Avance Spectrometer operating at 400 and 100 MHz, respectively. The chemical shift data are reported in units of δ (ppm) relative to tetramethylsilane (TMS) and referenced with residual CD₃CN.

Mass Spectrometry: High-resolution mass spectra (HRMS) were obtained at the MIT Department of Chemistry Instrumentation Facility using a peak-matching protocol to determine the mass and error range of the molecular ion, employing either electron impact or electrospray as the ionization technique.

Elemental Analyses: Elemental analyses were performed by Desert Analytics Laboratory, Tucson, Az.

Infrared (IR) spectroscopy: IR spectra were recorded on a Perkin-Elmer Model 2000 FT-IR spectrophotometer at the MIT Department of Chemistry Instrumentation Facility and are reported as strong (s), medium (m) or weak (w).

Absorption and Emission Spectroscopy: Fluorescence spectra were measured on a SPEX Fluorolog-τ3 fluorimeter (model FL-321, 450 W Xenon lamp) using right-angle detection. Ultraviolet-visible absorption spectra were measured with an Agilent 8453 diode array spectrophotometer and corrected for background signal with a solvent-filled cuvette.

Fluorescence quantum yields were determined by the optically dilute method²² using quinine sulfate in 0.1M H₂SO₄ as a standard ($\Phi=0.54$) and were corrected for solvent refractive index and absorption differences at the excitation wavelength.

*Photoreaction Quantum Yield Experiments:*²³ Stock solutions of **AcrH₂**, **AcrD₂**, RDX, and PETN were freshly prepared in degassed, spectral grade acetonitrile prior to use. For each measurement, aliquots of each stock solution and degassed acetonitrile were combined in a quartz cuvette such that the final volume equaled 3.0 mL and sparged with argon for 1.0 minute in the dark. Solutions were irradiated at 313 nm using either our SPEX Fluorolog- τ 3 fluorimeter (model FL-321, 450 W Xenon lamp) with a 29.4 nm excitation slit width or a 500 W Mercury Arc Lamp fitted with a 313nm interference filter and varying neutral density filters (0.5, 1.0 or 2.0 OD); both light sources were calibrated with a potassium ferric oxalate actinometer.²⁴ For each measurement, the absorbance at 358 nm was recorded versus irradiation time; both the concentration of **AcrH⁺** formed and the light absorbed by **AcrH₂** were then calculated and the slope of a graph of moles of **AcrH⁺** formed vs. einsteins of light absorbed gave the quantum yield. For each measurement, reaction progress was also monitored in the dark to ensure that there was no thermal contribution to the reduction of RDX or PETN. Each measurement was performed in triplicate.

Complex 2. A flame-dried, two-neck 50 mL round bottom flask equipped with a condenser was charged with 0.289g zinc nitrate hydrate (ca. 1.53 mmol), 0.835g acridine (4.6 mmol, ca. 3eq) and 20mL ethanol under a positive pressure of argon. The resulting solution was refluxed for ten minutes then cooled to room temperature. 0.189g TMEDA (1.62 mmol, ca. 1.05eq) was then added in one portion, the resulting solution refluxed for 12 hours under argon and then cooled to room temperature. A solution of 1.044g sodium tetraphenylborate (3.05 mmol, 2.0eq) in 6 mL

DI water was added dropwise with vigorous stirring and the reaction mixture stirred for 15 minutes under argon before filtering the resulting orange, crystalline solid and washing with cold ethanol, water and ether. The sample was further purified by Soxhlet extraction (diethyl ether) overnight, reprecipitated twice by slow addition of water to an acetonitrile solution and dried *in vacuo* to yield 1.55g of **2** as an orange solid (86% yield). ¹H NMR (400 MHz, CD₃CN) δ 9.27 (s, 2H), 8.24 (dd, *J* = 8.8 Hz, 1.6 Hz, 2H), 8.19 (dd, *J* = 8.8 Hz, 0.8 Hz, 2H), 8.01 (ddd, *J* = 7.6 Hz, 7.2 Hz, 1.6 Hz, 2H), 7.23 (ddd, *J* = 7.6 Hz, 7.2 Hz, 0.8 Hz, 2H), 7.28 (m, 16H), 7.00 (m, 16H), 6.84 (m, 8H), 2.87 (s, 4H), 2.54 (s, 12H). ¹³C NMR (100 MHz, CD₃CN) δ 43.7, 53.6, 122.0, 125.7, 125.9, 126.7, 128.6, 129.3, 130.5, 135.9, 136.3, 149.1, 163.2, 164.2, 164.7. UV-vis (CH₃CN): λ_{max} (log ε) = 356 nm (4.1). Emission (CH₃CN): λ_{max} 478 nm, Φ_F = 0.24. IR (KBr Pellet) 3055 (m), 1640 (m), 1479 (m), 1468 (m), 1427 (m), 1265 (w), 1152 (w), 1032 (w), 782 (s), 741 (s), 707 (s), 604 (m) cm⁻¹. Anal. calcd. for C₃₂H₃₄N₄Zn: %C 81.53, %H 6.33, %N 4.75; found %C 81.61, %H 6.61, %N 4.79.

Complex 1. The 1,4-dihydropyridyl analog of **1** has been synthesized starting from zinc hydride;²⁵ however, the following procedure (adapted from the procedure used to reduce quaternary acridinium compounds²⁰) was followed due to the relative stability of the reactants/reagents involved and the fact that it does not demand manipulations under inert atmosphere. A 50mL two-neck round bottom flask was charged with 0.1g **2** (.085mmol), 15 mL THF and 15 mL DI water under a positive pressure of argon and the resulting solution cooled in an ice bath. 0.185 g sodium borohydride (4.89 mmol) was added to the solution in small portions over half an hour after which the reaction was stirred for one hour at room temperature. The resulting white solid was filtered, washed with copious amounts of cold water and dried *in vacuo* to yield 0.04g **1** as an amorphous white powder (87% yield). Compound **1** has limited solubility

in acetonitrile, pyridine, DMF and DMSO; therefore, satisfactory $^1\text{H-NMR}$ and (especially) $^{13}\text{C-NMR}$ spectra were difficult to obtain, despite several attempts. Absorption/emission spectroscopy and explosive detection experiments were performed in slightly turbid, optically dilute ($\text{OD} < 0.1$) acetonitrile solutions. UV-vis (CH_3CN): λ_{max} ($\log \epsilon$) = 316 nm (4.0). Emission (CH_3CN): λ_{max} 364 nm (λ_{ex} = 316 nm), Φ_{F} = 0.24. IR (KBr Pellet) 3043 (w), 1609 (m), 1582 (m), 1478 (s), 1455 (m), 1419 (w), 1298 (s), 1258 (w), 1164 (w), 1036 (w), 759 (s), 745 (m) cm^{-1} . Anal. calcd. for $\text{C}_{32}\text{H}_{36}\text{N}_4\text{Zn}$: %C 70.90, %H 6.69, %N 10.34; found %C 70.94, %H 6.65, %N 10.56

Complex 3. Attempts at synthesizing complex **3** proved unsuccessful despite the use of various reaction conditions and/or reactant ratios. We were only able to isolate a zinc (II) bis(acridone) complex (**3'**)—i.e., we were only able to synthesize an analog of complex **3** that lacks the N,N,N',N'-tetramethylethylenediamine ligand. A possible explanation for this observation is that, once formed, the insolubility of complex **3'** prevents further reaction.

Complex 3'. 0.194g acridone (0.99 mmol) was added to a solution of 0.093g KOH (1.7 mmol) dissolved in 20 mL ethanol and the mixture refluxed until all the acridone had dissolved (approximately 5 minutes) and a yellow solution (that fluoresces green) was formed. Upon cooling to room temperature a solution of 0.089g zinc nitrate (.47 mmol) dissolved in 5 mL ethanol was added in one portion and the reaction refluxed under argon for 12 hours. The resulting solids were filtered, washed with cold ethanol and water and dried *in vacuo* to afford 0.095g of **3** as a pale yellow-colored powder (45% yield). Compound **3'** was found to be insoluble in ethanol and to have limited solubility in DMF, DMSO and acetonitrile. Attempts at dissolving **3'** in either acetonitrile or DMF at elevated temperatures only resulted in the partial decomposition of the complex into its individual constituents. This observation is not unfounded

as acridone is also relatively insoluble in most organic solvents.²⁶ The limited solubility of **3'** also prevented the procurement of satisfactory ¹H and ¹³C NMR spectra. The limited solubility of **3'** in acetonitrile was, however, sufficient for optical spectroscopy. UV-vis (CH₃CN): λ_{max} (log ε) = 391 nm (4.2). Emission (CH₃CN) λ_{max} 400 nm, Φ_F = 0.43. IR (KBr Pellet)^{26a} 3100 (w), 2994 (w), 2950 (w), 1634 (s), 1599 (s), 1558 (s), 1531 (s), 1472 (s), 1346 (m), 1264 (w), 1159 (w), 937 (w), 752 (m), 673 (m) cm⁻¹. HRMS (ESI): Calcd. for C₂₆H₁₆N₂O₂Zn, [M+H]⁺ 453.0576; found, 453.0578.

1.8 References and Notes

- (1) (a) Toal, S.J.; Trogler, W. C. *J. Mater. Chem.* **2006**, *16*, 2871-2883. (b) Yang, J-S.; Swager, T. M. *J. Am. Chem. Soc.* **1998**, *120*, 5321-5322.
- (2) (a) For a summary of most commercial explosive detection systems see: Bruschini, C. *Subsurface Sensing Tech. and Appl.* **2001**, *2*, 299-336. (b) For a representative example see: Cotte-Rodriguez, I.; Cooks, R. G. *Chem. Commun.* **2006**, *28*, 2968-2970.
- (3) (a) For a representative example see: McHugh, C. J.; Smith, W. E.; Lacey, R.; Graham, D. *Chem. Commun.* **2002**, *21*, 2514-2515. (b) Jungreis, E. *Spot Test Analysis: Clinical, Environmental, Forensic, and Geochemical Applications*, 2nd ed.; J. Wiley: New York, 1997.
- (4) This is because RDX and PETN have reduction potentials that are approximately one volt greater than that of TNT.
- (5) (a) McCormick, N. G.; Cornell, J. H.; Kaplan, A. M. *Appl. Environ. Microbiol.* **1981**, *42*, 817-823. (b) Bhushan, B.; Halasz, A.; Spain, J.; Thiboutot, S.; Ampleman, G.; Hawari, J. *Environ. Sci. Technol.* **2002**, *36*, 3104-3108.

- (6) Formation of AcrH^+ was confirmed by comparing the UV-vis, emission and ^1H NMR spectra of the reaction mixture with those of an independently synthesized sample of *N*-methylacridinium iodide.
- (7) (a) Sheremata, T. W.; Halasz, A.; Paquet, L.; Thiboutot, S.; Ampleman, G.; Hawari, J. *Environ. Sci. Technol.* **2001**, *35*, 1037-1040. (b) Beller, H. R.; Tiemeier, K. *Environ. Sci. Technol.* **2002**, *36*, 2060-2066.
- (8) Additionally, the ^1H and ^{13}C NMR spectra of the proposed *N*-nitroso reduction product do not differ significantly from those of RDX, thus excluding NMR spectroscopy as a meaningful characterization tool. Also, although we observed a few changes in the IR spectrum of the reaction mixture between 1500 and 1750 cm^{-1} during the course of the reaction, we could not satisfactorily deconvolute these changes from the strong IR stretches of the nitro groups of RDX.
- (9) Cheng, J-P. ; Lu, Y. ; Zhu, X.; Mu, L. *J. Org. Chem.* **1998**, *63*, 6108-6114 and references therein.
- (10) The light sources used in all mechanistic photophysical experiments were calibrated using a potassium ferrioxalate actinometer: Hatchard, C. G.; Parker, C. A. *Proc. Royal Soc. London A*, **1956**, *235*, 518-536.
- (11) (a) Fukuzumi, S.; Fijuta, S.; Suenobu, T.; Imahori, H.; Araki, Y.; Ito, O. *J. Phys. Chem. A* **2002**, *106*, 1465-1472. (b) Fukuzumi, S.; Suenobu, T.; Patz, M.; Hirasaka, T.; Itoh, S.; Fujitsuka, M.; Ito, O. *J. Am. Chem. Soc.* **1998**, *120*, 8060-8068. (c) Fukuzumi, S.; Imahori, H.; Okamoto, K.; Yamada, H.; Fujitsuka, M.; Ito, O.; Guldi, D. *J. Phys. Chem. A* **2002**, *106*, 1903-1908.
- (12) Yuasa, J.; Fukuzumi, S. *J. Am. Chem. Soc.* **2006**, *128*, 14281-14292.

- (13) We propose that the rate of vibrational self-deactivation of **AcrD₂^{*}** by **AcrD₂** (GS) is slower than that of **AcrH₂**, thus reducing the detrimental effect of this process on Φ_D and resulting in an inverse KIE. Similarly, the vibrational deactivation of lanthanide luminescence by D₂O is much less efficient than H₂O: (i) Kropp, J. L.; Windsor, M. W. *J. Chem. Phys.* **1965**, *42*, 1599-1608, and references within; (ii) Haas, Y.; Stein, G. *J. Phys. Chem.* **1971**, *75*, 3668-3677.
- (14) Since RDX and PETN have different one-electron reduction potentials, it is plausible that their photoreduction mechanisms differ; see ref 9.
- (15) The formation of complex **3** from **1** upon irradiation in air was confirmed by synthesizing a zinc (II) bis(acridone) complex (**3'**) and characterizing it by ESI MS, IR, UV-vis, and emission spectroscopy.
- (16) For example, we often employ the FIDO sensing platform created by ICx Technologies.
- (17) The equilibrium vapor pressure of RDX is 6×10^{-12} atm (ca. 5-7 ppt) at 25 °C and that of PETN is 2×10^{-11} atm (ca. 30 ppt).
- (18) Tao, S.; Li, G.; Zhu, H. *J. Mater. Chem.* **2006**, *16*, 4521-4528.
- (19) For select examples of using zeolites to organize chromophores and/or as hosts for photoreactions see: (a) McGilvray, K. L.; Chrétien, M. N.; Lukeman, M.; Scaiano, J. C. *Chem. Commun.* **2006**, 4401-4403 and references therein. (b) Minkowski, C.; Pansu, R.; Takano, M.; Calzaferri, G. *Adv. Funct. Mater.* **2006**, *16*, 273-285. (c) Scaiano, J. C.; Garcia, H. *Acc. Chem. Res.* **1999**, *32*, 783-793.
- (20) Roberts, R. M. G.; Ostovic, D.; Kreevoy, M. M. *Faraday Discuss. Chem. Soc.* **1982**, *74*, 257-265.

- (21) Fukuzumi, S.; Tokuda, Y.; Kitano, T.; Okamoto, T.; Otera, J. *J. Am. Chem. Soc.* **1993**, *115*, 8960-8968.
- (22) Demas, J. N.; Crosby, G. A. *J. Phys. Chem.* **1971**, *75*, 991-1024.
- (23) For a representative reference on the procedure followed see: Hill, R.D.; Puddephatt, R. *J. Am. Chem. Soc.* **1985**, *107*, 1218-1225.
- (24) Hatchard, C.G.; Parker, C. A. *Proc. R. Soc. London A* **1956**, *235*, 518-536.
- (25) de Koning, A. J.; Boersma, J.; van der Kerk, G. J. M. *J. Organomet. Chem.* **1980**, *186*, 159-172.
- (26) (a) Albert, A. *The Acridines*, 2nd Ed.; Edward Arnold Publishers Ltd.: London; 1966, pp 372. (b) The IR bands in the 1650-1400 cm⁻¹ region match those reported for the acridone chromophore: Price, J. R.; Willis, J. B. *Austral. J. Chem.* **1959**, *12*, 589-600.

1.9 Additional Figures

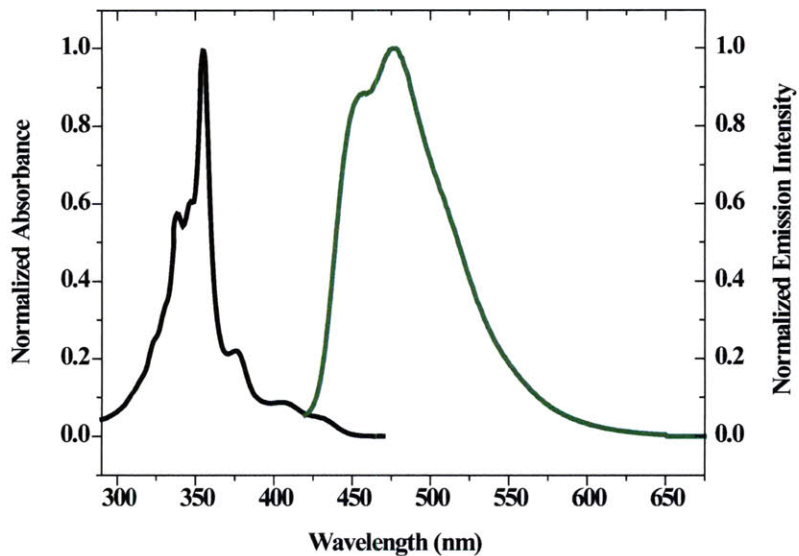


Figure A1. Absorption and emission spectra for complex **2** recorded in acetonitrile.

$$\lambda_{\max} = 356 \text{ nm}; \lambda_{\text{em}} = 478 \text{ nm}; \Phi_{\text{F}} = 0.24.$$

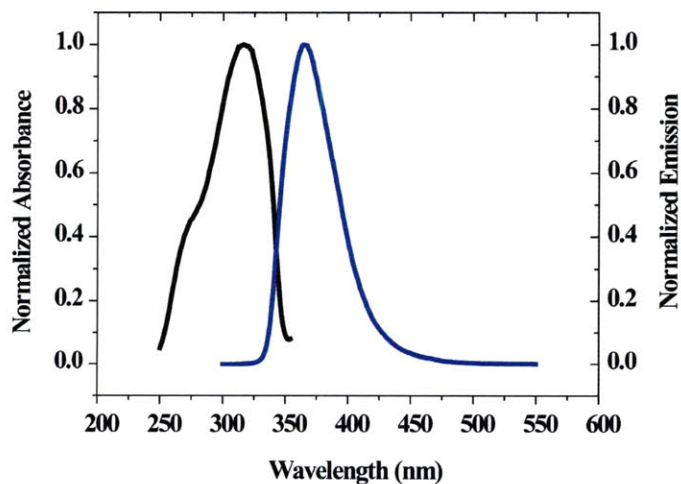


Figure A2. Absorption and emission spectra for complex **1** recorded in acetonitrile.

$$\lambda_{\max} = 316 \text{ nm}; \lambda_{\text{em}} = 364 \text{ nm} (\lambda_{\text{ex}} = 316 \text{ nm}); \Phi_{\text{F}} = 0.24.$$

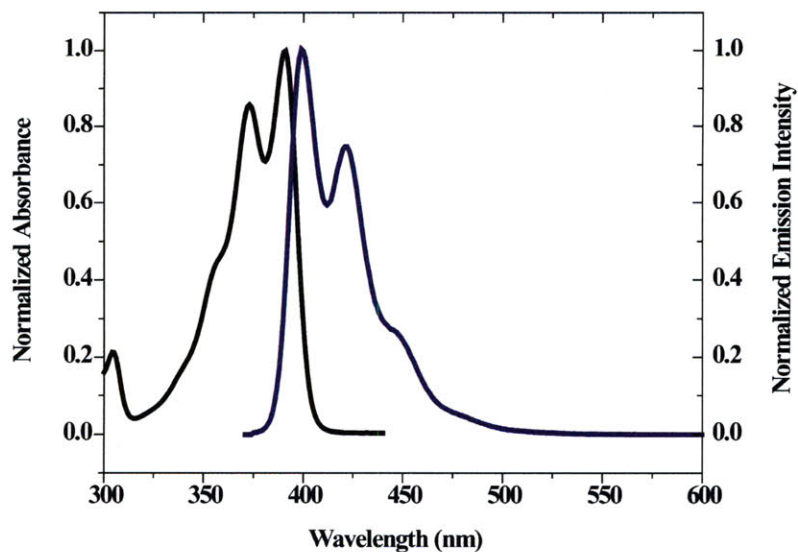


Figure A3. Absorption and emission spectra for compound **3'** recorded in acetonitrile.

$$\lambda_{\max} = 391 \text{ nm}; \lambda_{\text{em}} = 400 \text{ nm}; \Phi_{\text{F}} = 0.43.$$

Mechanistic Photophysical Studies

In addition to [**AcrH₂**, **AcrD₂**] dependence, the effect of [**RDX**, **PETN**] on Φ_{rxn} was also examined:

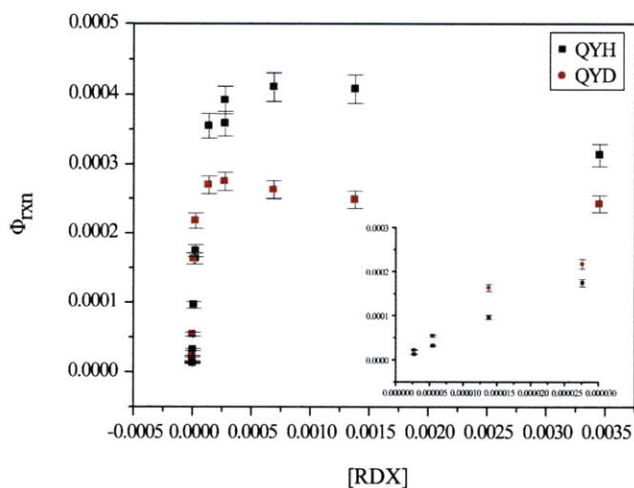


Figure A4. Dependence of Φ_{rxn} on [**RDX**] for **RDX** photoreduction by **AcrH₂**/**AcrD₂**.

$$[\text{AcrH}_2, \text{AcrD}_2] = 7.3 \times 10^{-5} \text{ M.}$$

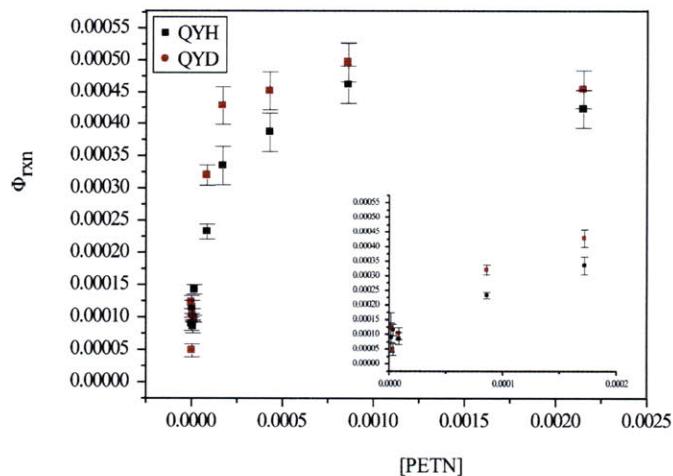


Figure A5. Dependence of Φ_{rxn} on [PETN] for PETN photoreduction by $\text{AcrH}_2/\text{AcrD}_2$.

$$[\text{AcrH}_2, \text{AcrD}_2] = 7.3 \times 10^{-5} \text{ M.}$$

In addition to concentration dependence, Φ_{rxn} was also found to be affected by the intensity of incident light (such behavior has literature precedence; for an example involving AcrH_2 see: Fukuzumi, S.; Fujita, S.; Suenobu, T.; Imahori, H.; Araki, Y.; Ito, O. *J. Phys. Chem. A* **2002**, *106*, 1465-1472.):

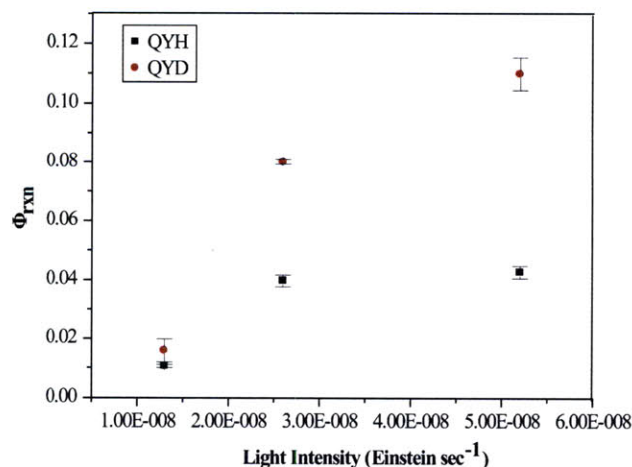


Figure A6. Dependence of Φ_{rxn} on the intensity of incident light for RDX photoreduction by

$$\text{AcrH}_2/\text{AcrD}_2. [\text{AcrH}_2, \text{AcrD}_2] = 1.5 \times 10^{-3} \text{ M, } [\text{RDX}] = 6.9 \times 10^{-4} \text{ M.}$$

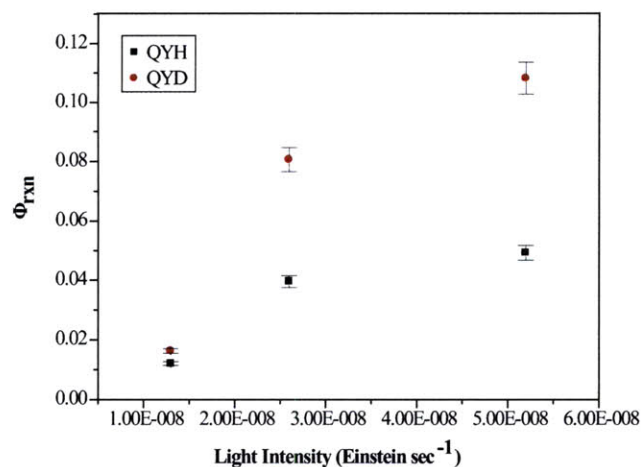


Figure A7. Dependence of Φ_{rxn} on the intensity of incident light for PETN photoreduction by

$\text{AcrH}_2/\text{AcrD}_2$. $[\text{AcrH}_2, \text{AcrD}_2] = 1.5 \times 10^{-3} \text{ M}$, $[\text{PETN}] = 4.3 \times 10^{-4} \text{ M}$.

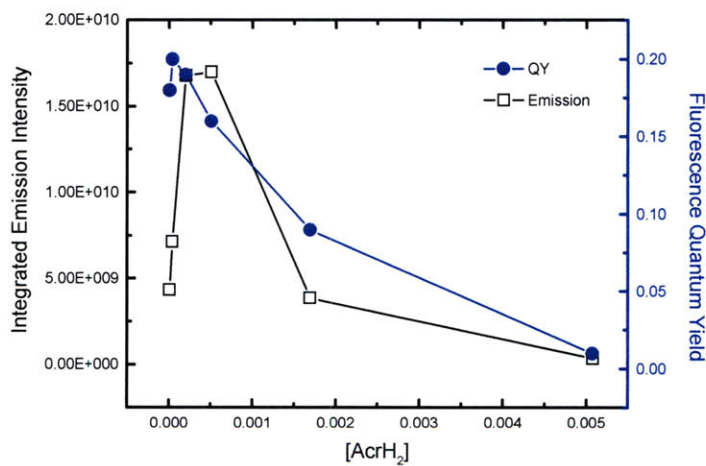


Figure A8. Dependence of AcrH_2 emission intensity and fluorescence quantum yield on $[\text{AcrH}_2]$, in the absence of RDX and PETN, showing self-quenching at high concentrations.

CHAPTER 2

Selective Detection of Explosives via Photolytic Cleavage of Nitroesters and Nitramines

Adapted from:
Andrew, T. L.; Swager, T. M. "Selective Detection of Explosives via Photolytic Cleavage of
Nitroesters and Nitramines" manuscript submitted to *J. Am. Chem. Soc.*

2.1 Introduction

Detecting hidden explosive devices in war zones and transportation hubs is an important pursuit. The three most commonly used highly energetic compounds in explosive formulations are: 2,4,6-trinitrotoluene (TNT), 1,3,5-trinitrotriazinane (RDX), and pentaerythritol tetranitrate (PETN) (Figure 2.1). Numerous technologies are currently capable of detecting the energetic chemical components of explosive devices, including: analytical spot tests;¹ fluorescent sensors using either small-molecule fluorophores² or fluorescent conjugated polymers;³ chemiresistive sensors;⁴ portable mass spectrometers;⁵ and X-ray systems.⁶ Each example listed has unique advantages and limitations. For instance, while X-ray systems are capable of detecting bulk hidden explosive devices and portable mass spectrometers are capable of identifying the exact chemical structures of suspect chemicals, the practical deployment and/or longevity of these technologies in standoff detection requires significant engineering.⁵ Fluorescent sensors are comparatively technology-unintensive and also have desirably low detection limits, but are only capable of identifying *classes* of molecules (such as nitroaromatics) or the presence of particular functional groups.³ Chemical spot tests can be more specific than fluorescent sensors but are not adaptable for standoff detection.

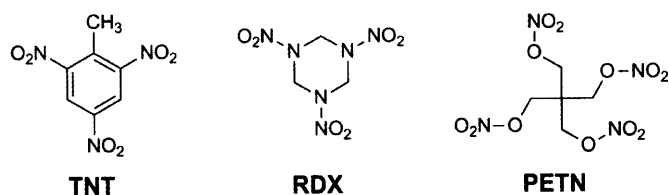


Figure 2.1. Structures of common high explosives.

We previously discussed a chemosensing scheme based on the photoreaction between a hydride donor and either RDX or PETN, wherein the nitramine or nitroester component was photoreduced by 9,10-dihydroacridine (**AcrH₂**, Figure 2.2) or its metalated analogues.⁷ The acridinium products (**AcrH⁺**) of this photoreaction had a high fluorescence quantum yield and resulted in a significant fluorescence turn-on signal in the presence of RDX and PETN.

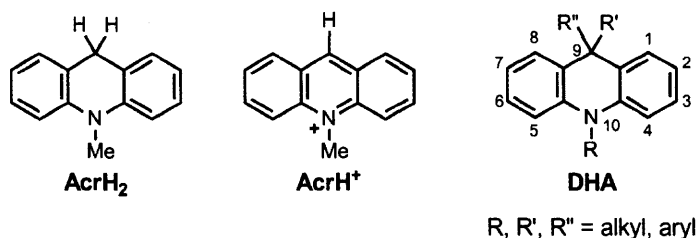


Figure 2.2. Structures of the hydride donor **AcrH₂**, its oxidation product **AcrH⁺**, and the 9,9-disubstituted 9,10-dihydroacridines, **DHAs**, studied herein.

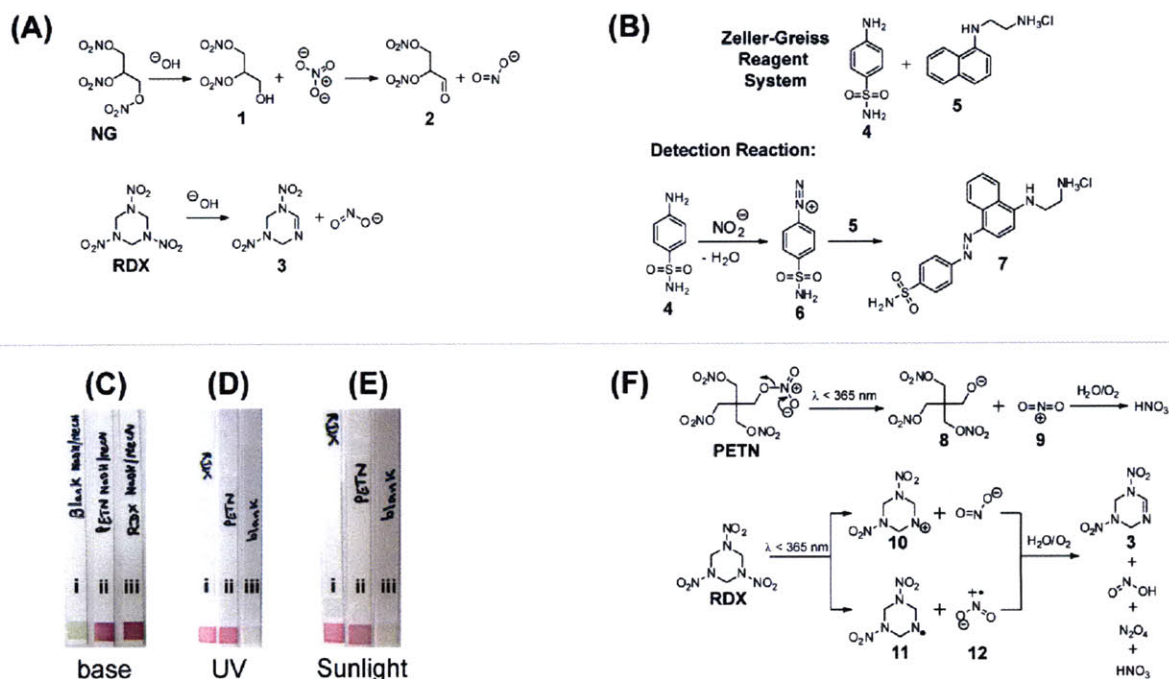
While studying this photoreaction, we became interested in the photochemical stability of nitramine and nitroester compounds under ultraviolet (UV) irradiation. Nitroesters and nitramines have been known to degrade under highly acidic or basic conditions and established spot tests for PETN and RDX detect these degradation products as opposed to directly detecting intact PETN or RDX.¹ The base-promoted digestion of nitroglycerin (NG) has been studied to some extent and is thought to evolve a mixture of nitrate and nitrite anions, among other degradation products (Scheme 2.1A).⁸ Similarly, RDX is also known to decompose in basic media and produce nitrite ions (Scheme 2.1A).⁹ The Greiss test¹⁰ for nitrite ions can, therefore, be employed to confirm the evolution of nitrite upon base-promoted degradation of RDX and PETN. The chemistry behind the Greiss test is shown in Scheme 2.1B; in summary, the reaction of sulfanilamide (**4**) with nitrite forms the diazonium salt **6**, which then reacts with an arylamine

(5) to form a brightly-colored azo dye (7). The original reagent reported by Greiss was composed of sulfanilic acid and α -naphthylamine; however, a more stable version of this formulation (the Zeller-Greiss reagent) containing sulfanilamide and N-(α -naphthyl)-ethylenediamine hydrochloride has since been adopted.¹¹ As seen in Scheme 2.1C, when nitrite test strips impregnated with the modified Greiss reagent were dipped into solutions of either RDX or PETN in 2:1 acetonitrile:1 M NaOH, a bright pink color evolved, indicating the presence of nitrite anions.

Interestingly, when the same nitrite test strips were dipped into base-free acetonitrile solutions of RDX or PETN, dried and irradiated ($\lambda = 254$ nm), formation of the pink azo dye was also observed (Scheme 2.1D), suggesting the evolution of nitrite ions upon the photolysis of RDX and PETN. Photolysis at 313 nm, 334 nm and 365 nm similarly resulted in a positive Greiss test. Moreover, extended exposure (30 minutes) to polychromatic light from solar simulator was also observed to photolyze RDX and PETN and yield a positive Greiss test (Scheme 2.1E).

The photolysis of nitroester and nitramine-based energetic compounds under various conditions has been extensively studied and found to produce a number of small-molecule degradation products, including nitrous and nitric acid, nitric oxide, nitrogen dioxide, formaldehyde and ammonia.¹² The proposed photolytic degradation mechanisms for PETN and RDX are shown in Scheme 2.1F. In the case of PETN, it is hypothesized that heterolytic cleavage of the O-NO₂ bond initially produces an alkoxide (8) and a highly reactive nitronium ion (9) that rapidly forms nitric acid under ambient conditions.¹³ For RDX, evidence of both the homolytic and heterolytic scission of the N-NO₂ bond of RDX (to produce nitrogen dioxide (12) or nitrite, respectively) exists and the exact nature of the initial photoreaction is ambiguous.^{14,12d}

Nevertheless, it can be agreed that the proposed initial products of RDX and PETN photolysis are highly reactive, electrophilic NO_x species, which can conceivably convert sulfanilamide **4** to the diazonium cation **6** necessary to produce a positive result in the Zeller-Greiss test.



Scheme 2.1. (A) Degradation mechanisms of nitroesters and nitramines in basic media.

(B) Active components and detection mechanism of the Zeller-Greiss test for nitrite ions.

(C) Nitrite ion test on base-degraded RDX and PETN. Test strips were dipped into blank 2:1 MeCN: 1M NaOH (i), or 17 mg PETN (ii) or 10 mg RDX (iii) in 3 mL 2:1 MeCN: 1M NaOH. (D) Nitrite ion test on photolyzed RDX and PETN. Test strips were dipped into (i) 10 mg RDX or (ii) 15 mg PETN in 3 mL MeCN, or (iii) neat MeCN and irradiated at 254 nm for one minute. (E) Nitrite ion test on RDX and PETN exposed to sunlight. Test strips were dipped into (i) 10 mg RDX or (ii) 15 mg PETN in 3 mL MeCN, or (iii) neat MeCN and irradiated with polychromatic light from a solar simulator for 30 minutes. (F) Proposed photolytic cleavage pathway of nitroesters and nitramines and select photodegradation products.

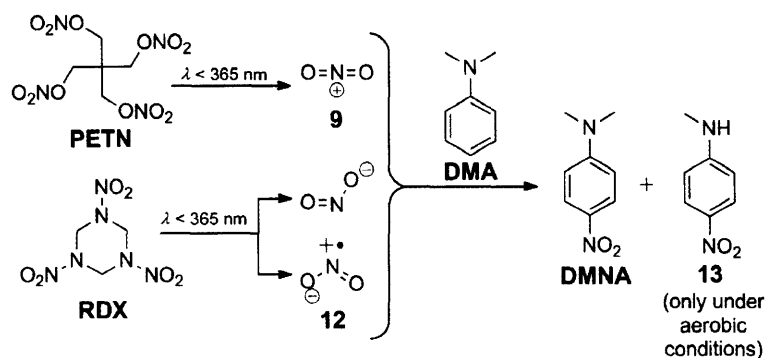
Unfortunately, the Greiss test or variations thereof cannot be adapted to detect RDX and PETN for a few reasons. First, simple standoff detection (detection at a distance) with colorimetric spot tests is not a viable possibility because of the difficulty in getting a clear optical signal returned from a purely absorptive process. Moreover, even with optimized reagent systems, the detection limit of the Greiss test is in the microgram regime,¹⁵ which is not competitive with existing methods to detect RDX and PETN.

Herein, we propose instead a selective sensing scheme based on the photolytic cleavage of nitroester and nitramine compounds and subsequent detection of their photodegradation products via a turn-on fluorescence signal. We envisioned that a pro-fluorescent, or fluorogenic, indicator capable of reacting with the photodegradation products of RDX and PETN would allow for selective and sensitive detection of these explosives.

2.2 Indicator Design

Given the electrophilic nature of the NO_x species generated by the photodegradation of RDX and PETN and their resemblance to the active electrophiles in aromatic nitration reactions, we targeted reactions between electron-rich tertiary aromatic amines and the photodegradation products of RDX and PETN. It was found that photolysis ($\lambda = 313$ nm) of a mixture of *N,N*-dimethylaniline (DMA) and 2 equivalents of either RDX or PETN for 10 minutes in acetonitrile under anaerobic conditions afforded the formation of *N,N*-dimethyl-4-nitroaniline (DMNA) in 14% yield (GC yield). Higher yields of DMNA were obtained with longer photolysis times and DMNA was formed in ca. 80% yield after 1 hour. The photoreaction between DMA and either RDX or PETN under anaerobic conditions was observed to produce only a *single*, yellow-colored product (DMNA) and other side products were not evident by TLC or GC-MS analyses.

The $^1\text{H-NMR}$, IR and high-resolution mass spectra of the isolated yellow product exactly matched those obtained for an authentic commercial sample of DMNA. Conducting the photolysis under aerobic conditions resulted in partial demethylation of DMA¹⁶ and yielded a mixture of DMNA and its demethylated analog, *N*-methyl-4-nitroaniline (**13**) (see Scheme 2.2). Photolysis of DMA with ammonium nitrate was also found to produce DMNA, although longer photolysis times (>30 minutes) were required and greater amounts of demethylated side products were observed (most likely due to the presence of water or other nucleophiles in the solutions).



Scheme 2.2. Nitration of *N,N*-dimethylaniline with the photodegradation products of RDX and PETN.

A distinct absorbance band centered at 400 nm was found to accompany the formation of the nitrated products under both aerobic and anaerobic conditions, which also matched the low-energy charge-transfer band displayed by commercial DMNA. However, DMNA has a very low fluorescence quantum yield¹⁷ and, therefore, a significant turn-on fluorescence signal is not generated upon reaction of DMA with the photodegradation products of RDX and PETN.

To probe the scope of the photonitration reaction, we investigated whether 9,9-dioctylfluorene, anisole and 1,2-dimethoxybenzene could be nitrated by RDX and PETN.

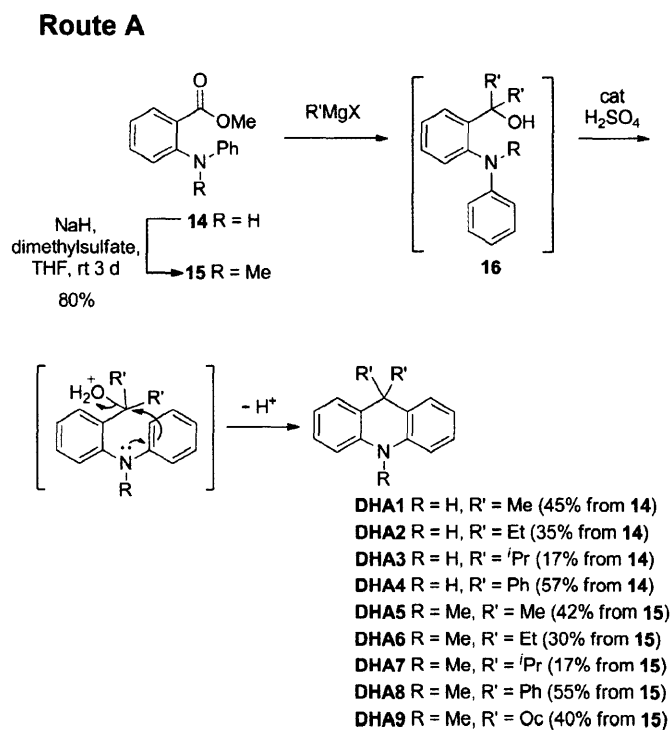
Extended photolysis (5 h) of a mixture of 9,9-dioctylfluorene and either RDX or PETN in 1:1 acetonitrile:THF at either 254, 313, 334, or 356 nm failed to generate any observable products and 9,9-dioctylfluorene was recovered in ca. 90% yield. Photolysis of anisole with RDX or PETN yielded only trace amounts of 4-nitroanisole (<1% GC yield) after 4 hours. Photolysis of 1,2-dimethoxybenzene with either RDX or PETN yielded 1,2-dimethoxy-4-nitrobenzene in only ca. 8% yield after 2 hours; moreover this reaction did not proceed cleanly and numerous polar photoproducts were observed. Therefore, we concluded that anilines were the best candidates for a potential indicator.

To create fluorogenic indicators based on the facile nitration reaction between aromatic amines and the photodegradation products of RDX and PETN, 9,9-disubstituted 9,10-dihydroacridines (DHAs, Figure 2.2) were targeted as chemosensors. We hypothesized that, upon nitration, the comparatively rigid DHAs would generate donor-acceptor chromophores possessing high fluorescence quantum yields.¹⁸

2.3 Synthesis

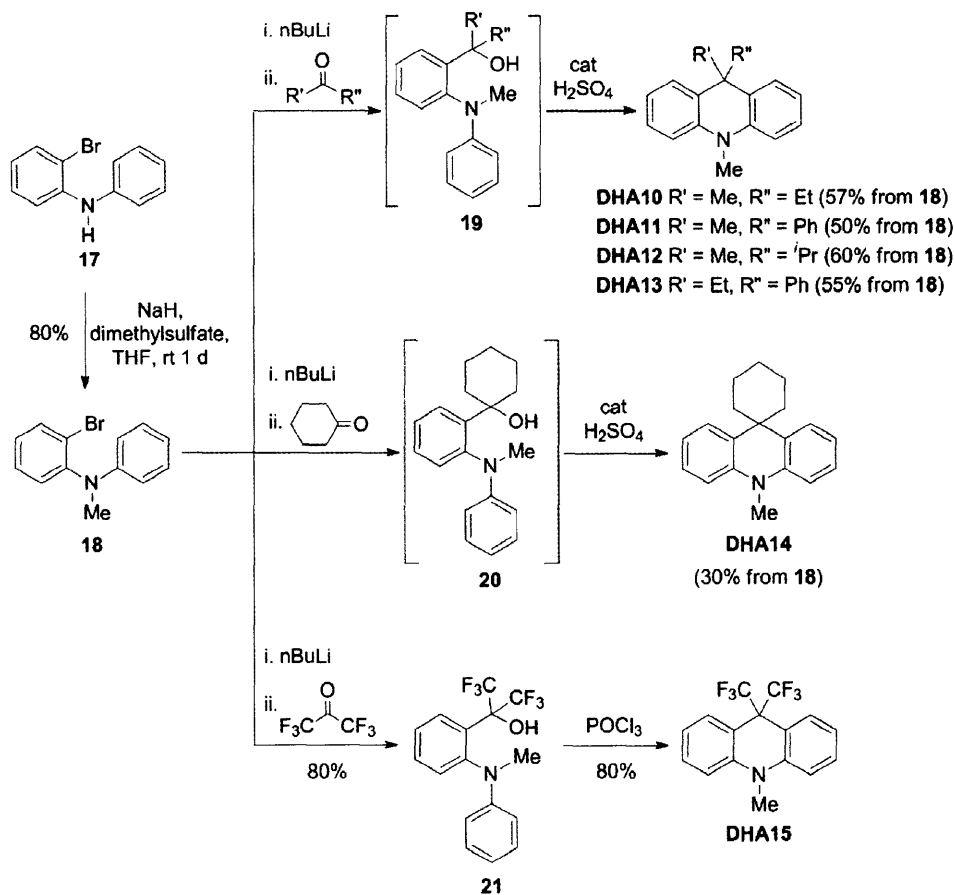
As shown in Schemes 2.3-2.5, a series of 9,9-disubstituted DHAs were synthesized, starting from either *N*-phenylanthranilic acid methyl ester (Routes A and C) or a diphenylamine derivative¹⁹ (Route B). DHAs were accessed by an acid-catalyzed cyclization of a tertiary alcohol intermediate (for example, structure **16**). In Route A (Scheme 2.3), intermediate **16** is accessed by a double 1,2-addition of an alkyl or aryl Grignard reagent to either *N*-phenylanthranilic acid methyl ester (**14**) or its *N*-methyl derivative (**15**); this strategy to synthesize DHAs has previously been reported.²⁰ In Route B (Scheme 2.4), tertiary alcohol intermediates **19-21** are accessed from 1,2-addition of the aryl lithium species derived from **18** to

an appropriate ketone. This strategy was adopted to synthesize unsymmetric DHAs (**DHA10-13**) that have two different substituents at the 9-position, a spiro-DHA (**DHA14**), and a CF₃-containing DHA (**DHA15**).



Scheme 2.3. Route A for the synthesis of 9,9-disubstituted 9,10-dihydroacridines.

Route B



Scheme 2.4. Route B for the synthesis of 9,9-disubstituted DHAs.

In all cases except one, adding a catalytic amount of concentrated sulfuric acid resulted in Friedel-Crafts reaction/cyclization of the respective tertiary alcohol intermediates to yield 9,9-disubstituted DHAs. This transformation is summarized in one step in Scheme 2.3; however, the cyclization is most likely not a concerted process. The X-ray crystal structure of **DHA8** thus obtained is shown in Figure 2.3. The cyclization of compound **21** was uniquely challenging, as neither the use of strong acids, Lewis acids, nor thionyl chloride yielded **DHA15**.²¹ However, it was found that refluxing a solution of **21** in POCl₃ produced **DHA15** in high yield.

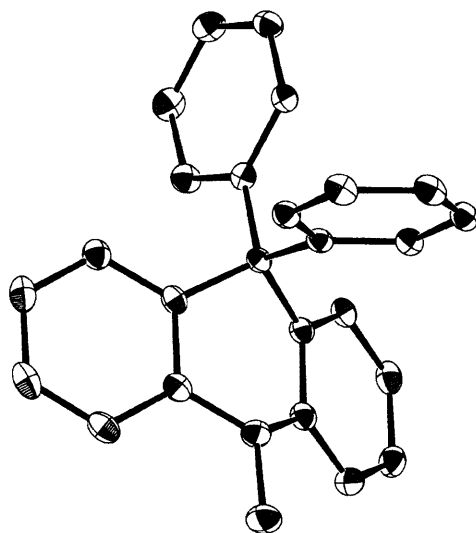
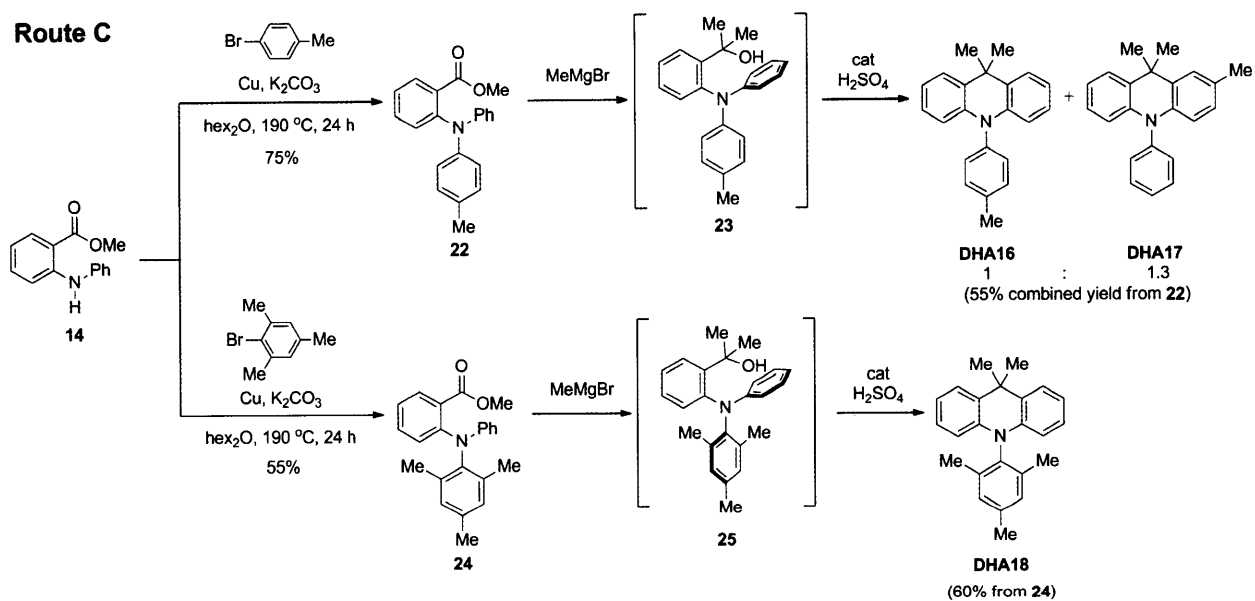


Figure 2.3. X-ray crystal structure of DHA8.



Scheme 2.5. Route C for the synthesis of *N*-aryl DHAs.

Lastly, Route C was followed to synthesize *N*-aryl DHAs (Scheme 2.5). Copper-catalyzed *N*-arylation of **14** with 4-bromotoluene initially furnished **22**, which was then reacted with 2.5 equivalents of methylmagnesium bromide and catalytic concentrated sulfuric acid.

Unfortunately, the Friedel-Crafts cyclization of intermediate **23** yielded a nearly-statistical mixture of **DHA16** and **DHA17** (1:1.3 **DHA16:DHA17**), which could not be acceptably separated by either column chromatography or recrystallization. Therefore, compound **24** was synthesized by copper-catalyzed *N*-arylation of **14** with 2-bromomesitylene and subsequently reacted with methylmagnesium bromide and sulfuric acid to access **DHA18**.

2.4 Photophysics

The optical properties of **DHA1-18** are summarized in Table 2.1. The DHAs reported herein displayed similar UV-vis absorption spectra, with absorption maxima around 290 nm. Additionally, **DHA1-18** generally displayed a single emission band centered at ca. 350 nm and were found to have similar fluorescence quantum yields and excited-state lifetimes.

Table 2.1. Optical Properties of DHAs in acetonitrile.

compd	λ_{\max}/nm ($\log \epsilon$)	$\lambda_{\text{cm}}/\text{nm}$	Φ^{a}	τ/ns
DHA1	284 (4.1)	352	0.18	2.7
DHA2	288 (4.1)	390	0.04	2.2
DHA3	288 (4.1)	376	0.09	2.7
DHA4	285 (4.0), 320 (3.8)	355	0.13	1.6
DHA5	285 (4.1)	355	0.14	2.8
DHA6	246 (4.1), 290 (4.0)	382	0.12	2.3
DHA7	257 (4.1), 298 (3.9)	345	0.10	2.7
DHA8	294 (3.9)	359	0.14	1.7
DHA9^b	247 (4.1), 290 (3.9)	345	0.15	2.8
DHA10	246 (4.3), 290 (4.1)	352	0.12	2.5
DHA11	289 (4.3)	355	0.14	1.7
DHA12	247 (4.0), 292 (3.9)	382	0.06	1.7
DHA13	245 (4.8), 296 (4.4)	355	0.09	2.2
DHA14	247 (4.0), 297 (3.8)	345	0.15	2.4
DHA15	280 (4.3), 311 (4.0)	354	0.18	2.5
DHA16 + DHA17	290 (4.2)	371	0.05	2.7
DHA18	290 (4.2)	371	0.03	2.5

^a Measured against quinine sulfate in 0.1N H₂SO₄ (Φ 0.54) ^b in THF

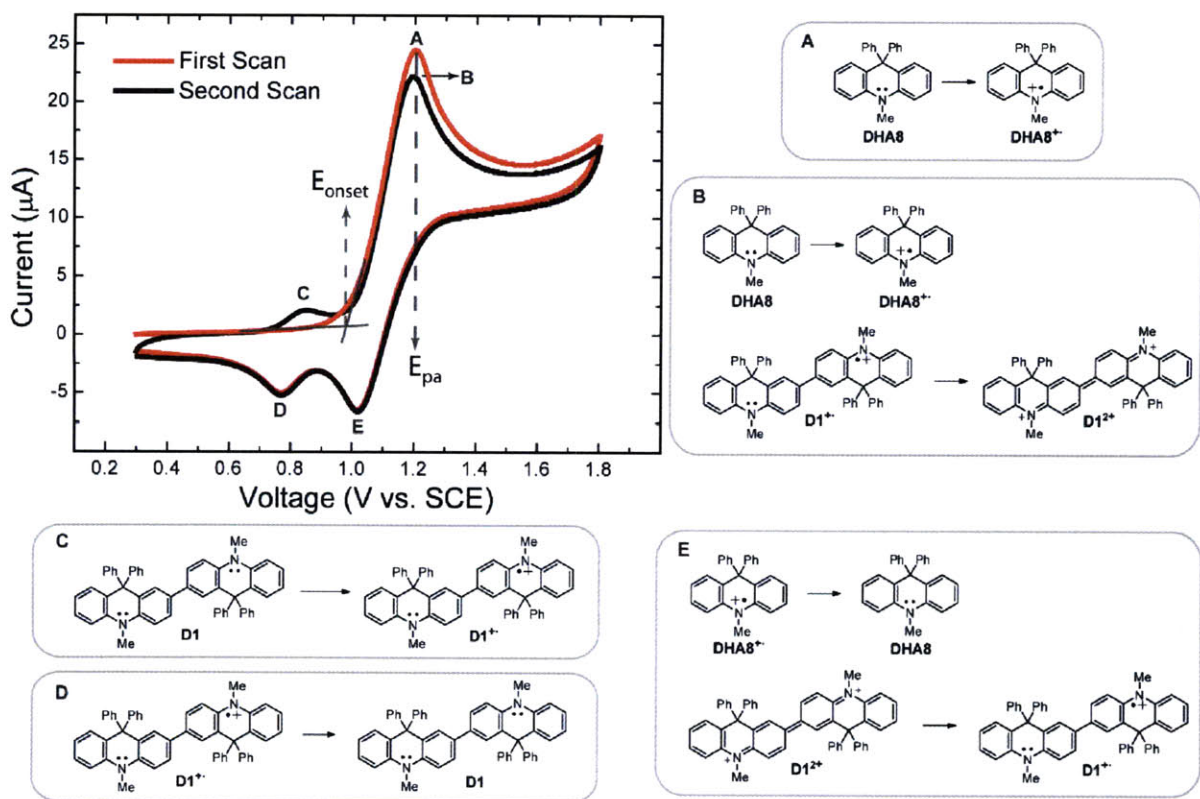


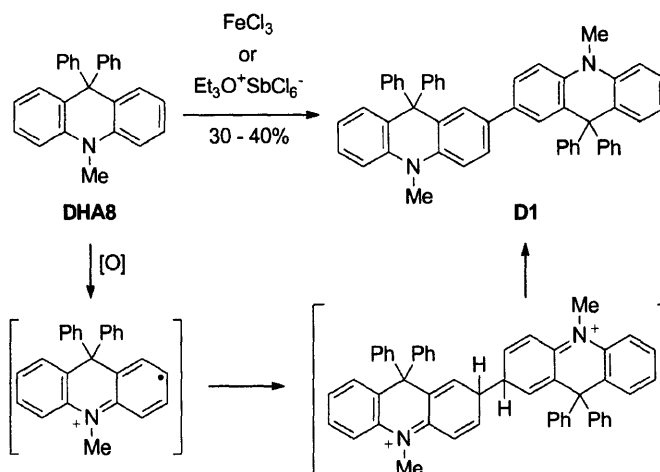
Figure 2.4. Cyclic voltammogram of **DHA8** (Pt button electrode, 0.1 M TBAPF₆ in CH₂Cl₂, 100 mV/s). The redox reactions giving rise to each anodic (A, B and C) and cathodic (D and E) peak are shown, and the first anodic peak potential (E_{pa}) and onset potential (E_{onset}) for the first scan are labeled.

2.5 Electrochemistry

Cyclic voltammograms (CVs) of select DHAs were recorded in CH₂Cl₂ with tetrabutylammonium hexafluorophosphate (TBAPF₆) as a supporting electrolyte and were found to reveal unusual behavior. The CV of **DHA8** is shown in Figure 2.4 as a representative example. The first anodic sweep resulted in a single oxidation peak at ca. 1.20 V vs SCE, which can be ascribed to the formation of the radical cation of **DHA8**. However, the corresponding cathodic sweep revealed two cathodic peaks, arising from the reduction of two different species

in solution. Furthermore, a subsequent anodic sweep displayed two oxidation peaks. Such behavior has been previously observed for triphenylamine (TPA),²² and is attributed to the rapid dimerization of TPA radical cations following oxidation; the electroactive TPA dimer thus formed leads to the growth of an additional anodic and cathodic peak after an initial anodic sweep. Learning from the assignments made for the CV of TPA,²² the redox reactions responsible for the individual anodic and cathodic peaks observed in the CV of **DHA8** were identified and are shown in Figure 3.

The dimerization of radical cations of **DHA8** in the electrochemical cell to form **D1** was confirmed by independently synthesizing **D1**. Oxidation of **DHA8** with FeCl₃ or [Et₃O⁺SbCl₆]⁻²³ afforded **D1** in 30-40% yield (Scheme 2.6). This oxidation reaction was found to proceed cleanly and produced only one product (by TLC and crude ¹H NMR analyses); moreover, we were able to recover the remaining, unreacted **DHA8** upon reaction workup. The use of hydrogen peroxide and *tert*-butyl-hydrogen peroxide was also investigated; however, surprisingly, **D1** was only formed in less than 5% yield with these reagents and **DHA8** was recovered in ca. 90% yield after reaction workup. Interestingly, the oxidative polymerization of **DHA8** does not proceed and only **D1** was isolated. This observation can be explained by the fact that **D1**, once formed, can be oxidized to a stable, closed-shell dication (**D1**²⁺, see Figure 2.4) that cannot participate in subsequent radical coupling reactions to form polymers. Dimer **D1** is a faint-yellow compound that displays an absorption band centered at 457 nm and an emission band centered at 478 nm (Φ 0.20). The CV of **D1** was found to match the second scan of the CV of **DHA8**, thus confirming the aforementioned assignments for the anodic and cathodic peaks observed in the CV of **DHA8**.



Scheme 2.6. Oxidative dimerization of **DHA8** to form **D1**.

The electrochemical behavior of **DHA8** was similar to that of the rest of the reported DHAs and also similar to the electrochemical behavior of DMA—i.e., the respective radical cations dimerized in the electrochemical cell after the first anodic sweep. The values for the first anodic peak potential (E_{pa}) and onset potential (E_{onset}) for the first scan of the CVs of select DHAs, DMA and TPA are summarized in Table 2.2. In general, similar values of E_{pa} and E_{onset} were observed for most DHAs; however, the electron-deficient, CF₃-containing **DHA15** was an outlier and displayed significantly higher E_{pa} and E_{onset} values.

Table 2.2. Electrochemical Properties of Select DHAs.

cmpd	E_{pa}/V vs SCE	E_{onset}/V vs SCE
DHA1	1.19	0.77
DHA2	1.05	0.77
DHA4	1.07	0.87
DHA5	1.27	0.86
DHA6	1.30	0.86
DHA7	1.51	0.92
DHA8	1.20	0.95
DHA9	1.35	0.85
DHA11	1.08	0.87
DHA15	1.65	1.18
DHA16 +	1.04	0.83
DHA17		
DHA18	1.08	0.83
DMA ^a	1.36	0.77
TPA ^b	1.48	0.95

^a *N,N*-Dimethylaniline. ^b Triphenylamine.

2.6 Reaction with RDX/PETN Photodegradation Products

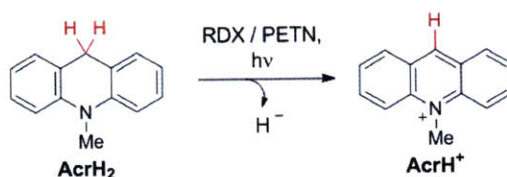
The photoreactions between **DHA1-18** and either RDX or PETN were initially investigated in acetonitrile solutions. In general, irradiating solutions containing **DHA1-18** and either RDX or PETN (which were initially colorless) at 313 nm under aerobic conditions lead to the evolution of a bright yellow/orange color after approximately 30 seconds to 5 minutes. Irradiating solutions of **DHA1-18** in the absence of either RDX or PETN did not result in the same bright yellow/orange color, although faint yellowing of the DHA solutions was noticed after extended exposure (>60 minutes) to UV light under aerobic conditions.

The photolyses (λ 313 nm) of select DHAs with a stoichiometric amount of either RDX or PETN were conducted on a *preparatory* scale in order to isolate and characterize the reaction products formed; long irradiation times (generally 60 minutes) were employed in these cases to ensure complete reactant conversion. TLC and GC-MS analyses of crude reaction mixtures indicated that only a single, highly-colored product was formed in all cases. The yellow-orange products from the reactions of **DHA1**, **DHA4**, and **DHA18** with either RDX or PETN were isolated by flash column chromatography and identified to be the mono-nitrated structures (**26**, **28**, and **30**, respectively) shown in Scheme 7 by their ^1H NMR, FT-IR and high resolution mass spectra. Compounds **26**, **28** and **30** were isolated in 70-80% yield after column chromatography, along with ca. 10-15% of unreacted **DHA1**, **DHA4**, or **DHA18**. Similarly, **DHA5** and **DHA8** were confirmed to produce **27** and **29**, respectively, in approximately 70% yield (GC yield) upon photolysis with RDX or PETN (30 minutes). Additionally, **DHA1** and **DHA4** were independently nitrated under mild conditions using $\text{SiO}_2:\text{HNO}_3$ ²⁴ and the products thus obtained were found to match those isolated from the photoreactions of **DHA1** and **DHA4** with RDX/PETN.

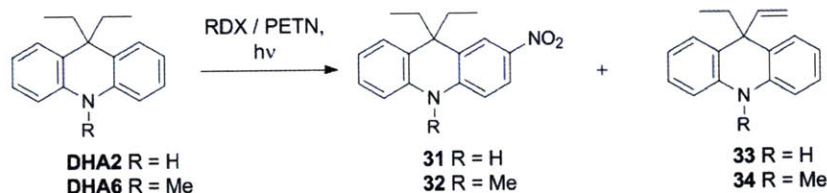
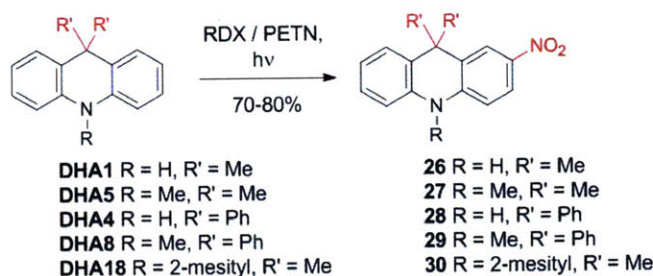
The photoreaction of **DHA2** with either RDX or PETN yielded the nitrated product **31**; however, compound **33** was also isolated from the reaction mixture (Scheme 2.7). The yield of **33** was found to be somewhat dependent on the concentration of **DHA2**, with a higher amount of **33** over **31** observed in dilute solutions. The yield of **33** was also higher relative to that of **31** when the photolysis of **DHA2** and RDX/PETN was conducted in slightly wet acetonitrile. Compounds **31** and **33** were generally isolated in 80% combined yield after flash column chromatography of the photoreactions between **DHA2** and either RDX or PETN. Furthermore,

DHA6 was confirmed to produce **32** and **34** (by GC-MS analysis) upon photolysis in the presence of RDX/PETN.

Photoreduction of RDX/PETN by Hydride Donors:



Nitration of Aromatic Amines by the Photodegradation Products of RDX/PETN:



Scheme 2.7. Photoreactions of various 9,10-dihydroacridines with RDX and PETN. The photoreduction of RDX/PETN by **AcrH₂** has been previously reported.⁷

GC-MS analyses of the photoreactions between the remaining DHAs (**DHA3**, **DHA7**, **DHA9**, **DHA10-17**) and either RDX or PETN similarly revealed the formation of mono-nitrated derivatives of the respective DHAs.

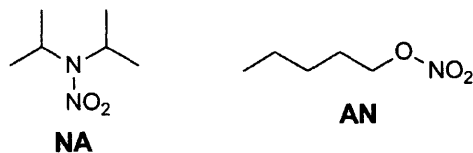


Figure 2.5. Structures of a model nitramine, *N,N*-diisopropylnitramine (**NA**), and a model nitroester, amyl nitrate (**AN**).

2.7 Other Nitroesters and Nitramines

The photoreactions between **DHA1-18** and either a model nitramine or nitroester compound—*N,N*-diisopropylnitramine (**NA**) and amyl nitrate (**AN**), respectively (Figure 2.5)—were also investigated. The reaction products observed upon photolysis (λ 313 nm) of mixtures of **DHA1-18** and either **NA** or **AN** were exactly similar (as established by TLC and GC-MS analyses) to the aforementioned nitrated products observed with RDX and PETN. However, the observed yields (GC yields) of nitrated DHAs were significantly lower with **NA/AN**, as compared to RDX/PETN. For example, whereas **26** was formed in 75% yield upon photolysis with either RDX or PETN for 30 minutes, the photolysis of **DHA1** with **NA** or **AN** afforded **26** in only 30% yield under identical reaction conditions. Therefore, it can be tentatively inferred that RDX and PETN are more susceptible to photolytic cleavage than their respective model compounds.

2.8 Differences in DHA Reaction Mechanisms

As shown in Scheme 2.7, it is interesting to note the difference in photochemical reaction mechanisms between various 9,10-dihydroacridines. As previously reported,⁷ *N*-methyl-9,10-dihydroacridine (**AcrH₂**) participates in a hydride transfer reaction with either RDX, PETN, **NA**

or AN. Dialkylation or diarylation of the 9-position of **AcrH₂** effectively nullifies its ability to donate a hydride ion and promotes the photonitration reaction detailed herein.

2.9 Light Sources

Importantly, precise timing and sophisticated, high-intensity light sources were not found to be necessary to effect the reaction between **DHA1-18** and the degradation products of either RDX or PETN. Simply exposing a mixture of **DHA1-18** and RDX/PETN to polychromatic light from a solar simulator effected the photolytic cleavage of RDX/PETN and subsequent formation of mono-nitrated DHAs. For example, compounds **26** and **28** could both be isolated in 75% yield (after flash column chromatography) after a mixture of RDX or PETN and **DHA1** or **DHA4**, respectively, in acetonitrile were exposed to simulated sunlight for 45 minutes. The yields of compounds **26** and **28** thus obtained are similar to those reported earlier for photolysis at 313 nm.

2.10 Other NO_x Sources

The (photo)reactions of **DHA1-18** with sodium nitrite, potassium nitrate, and NO were also investigated to judge the limitations of using **DHA1-18** as stand-off indicators for RDX/PETN. Exposing a mixture of either **DHA1**, **DHA5**, **DHA4** or **DHA8** and excess sodium nitrite in 2:1 acetonitrile:water to simulated sunlight for 2 hours did not result in significant nitration of these DHAs (<1% GC yields of **26-29** were generally observed). However, upon addition of 100 μ L acetic acid to the same reaction mixtures, compounds **26-29** were formed in approximately 8% yield in the *absence* of light. Protonating nitrite salts generates nitrous acid, which is known to decompose and form HNO₃ (among other species), which most likely nitrated the DHAs in this case.

The addition of a large excess of monomeric NO gas to dry, oxygen-free solutions of the aforementioned DHAs failed to generate the characteristic yellow-orange color of **26-29**; however, upon introduction of oxygen to these solutions, the nitrated DHAs were observed to be formed by eye (in the absence of light). Subsequent GC-MS analyses confirmed that **26-29** were formed in ca. 20% yield. Once again, NO is known to form nitrogen dioxide upon exposure to oxygen, which most likely resulted in nitration of the DHAs.

Mixtures of **DHA1**, **DHA5**, **DHA4** or **DHA8** and a large excess of potassium nitrate in 2:1 acetonitrile:water did not immediately result in nitration. If left standing for 24 h, **26-29**, along with multiply-nitrated derivatives of the aforementioned DHAs, were formed in less than 5% combined yield (GC yield). Adding acetic acid to DHA/KNO₃ mixtures resulted in the formation of multiply nitrated DHAs, with 2,7-dinitro DHAs being the major products. Exposing mixtures of either **DHA1**, **DHA5**, **DHA4** or **DHA8** and a large excess of potassium nitrate in 2:1 acetonitrile:water to simulated sunlight for 60 minutes similarly yielded multiply-nitrated derivatives of these DHAs in approximately 20% combined yield. Stoichiometric or sub-stoichiometric amounts of potassium nitrate, or shorter irradiation times failed to generate observable quantities of nitrated DHAs.

2.11 Optical Properties of Nitrated DHAs

The photophysical properties of select nitrated DHAs, which were either isolated from the photolysis reactions between DHAs and RDX/PETN or synthesized by nitrating an appropriate DHA, are listed in Table 2.3. In general, the nitrated DHAs displayed similar absorbance bands as DMNA, with the lowest energy bands centered at ca. 400 nm. Additionally, emission bands centered at ca. 540 nm were observed for all isolated mono-nitrated DHAs. The

fluorescence quantum yields of the compounds listed in Table 3 were found to be solvent dependent, with the lowest quantum yields observed in acetonitrile.²⁵ Moreover, compounds **26**, **28**, **30** and **31** were found to display significant emission in the solid state (in cellulose acetate films containing 10 wt% of the appropriate compound).

Table 2.3. Optical properties of select mono-nitrated DHAs.

cmpd	λ_{\max}^a (log ϵ)	λ_{em}^a	Φ
DMNA	395 (3.9)	530	<0.01 (MeCN) ^b 0.09 (CHCl ₃) ^b 0.17 (film) ^{c,d}
26	408 (4.1)	535	0.09 (MeCN) ^b 0.27 (CHCl ₃) ^b 0.35 (film) ^{c,d}
28	410 (4.1)	540	0.10 (MeCN) ^b 0.30 (CHCl ₃) ^b 0.42 (film) ^{c,d}
30	413 (4.2)	548	0.14 (MeCN) ^b 0.37 (CHCl ₃) ^b 0.45 (film) ^{c,d}
31	409 (4.1)	539	0.05 (MeCN) ^b 0.22 (CHCl ₃) ^b 0.33 (film) ^{c,d}

^a in MeCN ^b Measured against perylene in EtOH (Φ 0.94) ^c 10 wt% in cellulose acetate ^d Measured against 10 wt% perylene in PMMA (Φ 0.78)

2.12 Optical Characterization of Indicator Response

The absorption and emission profiles for the reaction between **DHA5** and RDX under aerobic conditions are shown in Figure 2.6. An absorption band centered at ca. 408 nm was observed to evolve when **DHA5** is photolyzed (λ 313 nm) with RDX, which corresponds to the

formation of **27**. An emission band at approximately 540 nm concomitantly evolved, which can be assigned to emission from **27** based on the emission profile recorded for its *N*-H analog **26**. A ca. 27-fold increase in the emission intensity at 540 nm was generated after 2 minutes of UV irradiation. Exactly similar absorption and emission profiles were obtained for the photoreaction between **DHA5** and PETN. Moreover, the presence or absence of oxygen did not noticeably change the observed optical response.

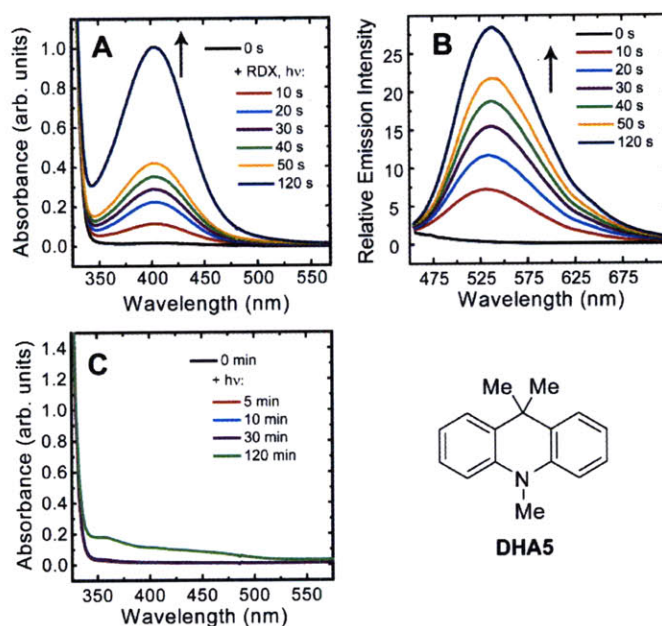


Figure 2.6. Absorption (A) and emission (B, $\lambda_{\text{ex}} = 415 \text{ nm}$) profiles of the photoreaction of **DHA5** with RDX in acetonitrile upon irradiation at 313 nm. $[\text{DHA5}] = 1.3 \times 10^{-4} \text{ M}$. $[\text{RDX}] = 5.4 \times 10^{-5} \text{ M}$. Identical profiles are observed for the photoreactions of **DHA5** with PETN. The presence or absence of oxygen similarly does not affect the observed absorption and emission profiles. The absorption profile for the extended irradiation of a blank, aerated solution of **DHA5** is also shown (C).

Photolysis of **DHA5** under aerobic conditions in the absence of RDX/PETN failed to generate a distinct absorbance band at 408 nm. Surprisingly, electron-rich **DHA5** was found to be relatively photostable: 30 minutes of continuous UV irradiation did not result in a noticeable change in the absorption spectrum of **DHA5** (Figure 2.6C), and its emission peak at 355 nm (see Table 2.1) was found to be bleached by only 10%. Further UV irradiation eventually lead to slight yellowing of **DHA5** solutions, and poorly-defined absorbance peaks at 356 nm and ca 440 nm appeared in the absorption spectrum after 2 hours of continuous UV irradiation under air (Figure 2.6C). These new absorption peaks most likely correspond to the formation of radical cations, *N*-demethylated species, and/or *N*-oxide derivatives of **DHA5**. Notably, though, a significant portion of this photolyzed **DHA5** solution remained unoxidized after 2 hours, and, therefore, the subsequent addition of RDX or PETN nonetheless lead to evolution of a 408 absorbance peak and 540 nm emission peak (5-fold emission turn-on) after a 20 second exposure to 313 nm light.

As seen in Figure 2.7, exposing a mixture of **DHA5** and RDX to broad-band light from a solar simulator lead to the evolution of the same 408 nm peak observed with irradiation at 313 nm. The rate of formation of the 408 nm peak upon exposure to simulated sunlight also matched that observed upon exposure to monochromatic 313 nm light from a xenon arc lamp (Figure 2.7B). Therefore, simulated sunlight was preferentially used as the light source in subsequent studies to prove that the DHAs can function as technology-unintensive, fluorogenic indicators for RDX/PETN under ambient sunlight.

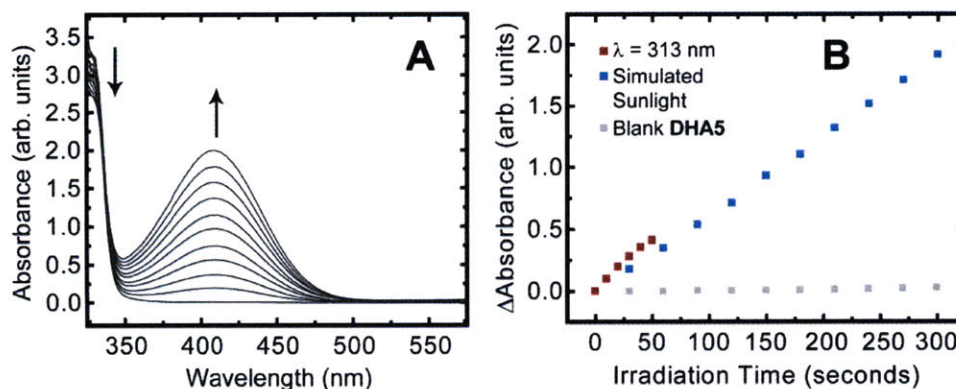


Figure 2.7. (A) Absorption profile of the photoreaction of **DHA5** and RDX in acetonitrile upon exposure to broad-band light from a solar simulator. $[\text{DHA5}] = 1.3 \times 10^{-4} \text{ M}$. $[\text{RDX}] = 5.4 \times 10^{-5} \text{ M}$. (B) The rate of formation of the 408 nm absorbance peak in the presence of RDX upon exposure to either simulated sunlight or monochromatic 313 nm light.

The absorption and emission profiles for the reaction between **DHA6** and PETN upon exposure to simulated sunlight are shown in Figure 2.8. **DHA6** behaved similar to **DHA5** in terms of its optical response: an absorbance peak at 409 nm evolved in the presence of either RDX or PETN, accompanied with evolution of an emission band at 540 nm. The presence or absence of oxygen did not affect the observed optical response to RDX/PETN. **DHA6** was also found to be relatively photostable, with no change in its absorption spectrum and a 5% bleaching of its emission band at 382 nm (see Table 2.1) observed after 30 minutes of continuous exposure to sunlight. The only significant difference between **DHA5** and **DHA6** was the rate of formation of the 409 nm /540 nm absorption/emission peaks: **DHA5** was found to yield a turn-on signal approximately three times faster than **DHA6**. We hypothesize that this comparatively slow response is because **DHA6** forms a mixture of **32** and **34** upon reacting with RDX/PETN (see Scheme 2.7). Compound **32** is responsible for the 409 nm/540 nm absorption/emission bands,

whereas **34** is not green-fluorescent and is responsible for the 356 nm absorption peak seen in Figure 2.8A.

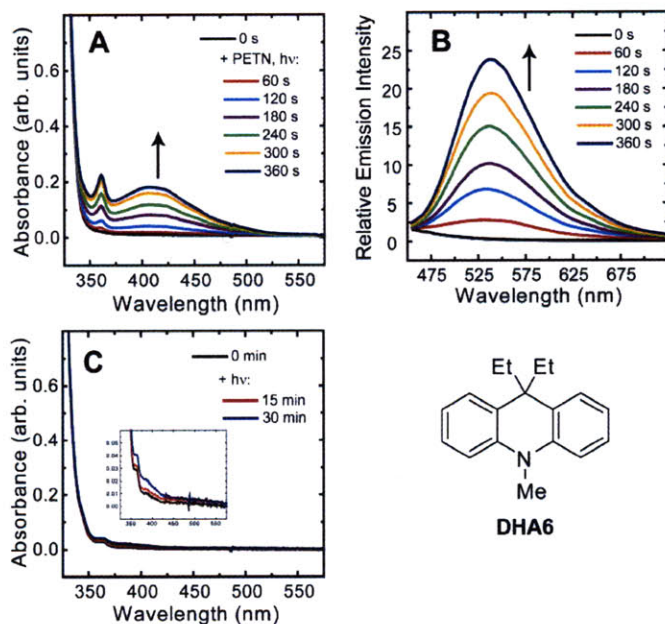


Figure 2.8. Absorption (A) and emission (B, $\lambda_{\text{ex}} = 415 \text{ nm}$) profiles of the photoreaction of **DHA6** with PETN in acetonitrile upon exposure to simulated sunlight. $[\text{DHA6}] = 1.3 \times 10^{-4} \text{ M}$. $[\text{PETN}] = 5.4 \times 10^{-5} \text{ M}$. The absorption profile for the extended irradiation of a blank, aerated solution of **DHA6** is also shown (C).

The optical response of **DHA18** to either RDX or PETN (Figure 2.9) was similar to that of **DHA5**. An absorbance band at 413 nm and an emission peak at 550 nm evolved upon exposure to simulated sunlight in the presence of either RDX or PETN. **DHA18** was also relatively photostable, with no change in its absorption spectrum and a 5% bleach of its emission

band at 371 nm (see Table 1) observed after continuous exposure to simulated sunlight for 30 minutes. The rate of photoreaction of **DHA18** with RDX/PETN was slower than that of **DHA5** but faster than that of **DHA6**.

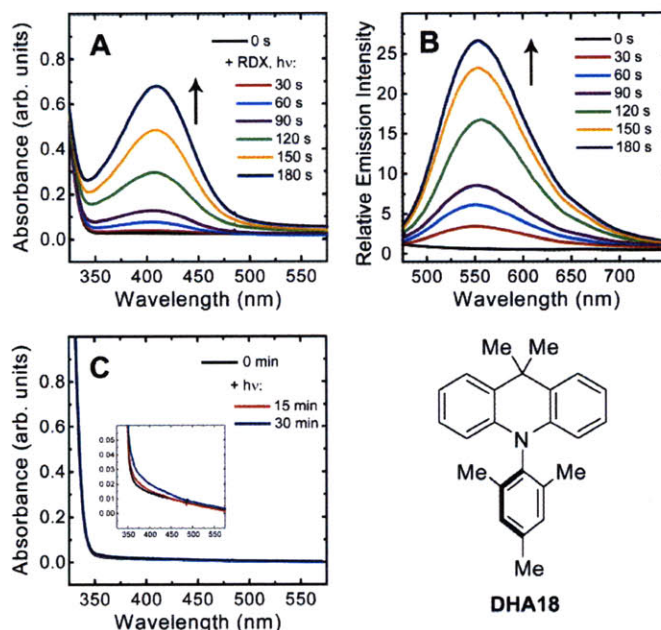


Figure 2.9. Absorption (A) and emission (B, $\lambda_{\text{ex}} = 415 \text{ nm}$) profiles of the photoreaction of **DHA18** with RDX in acetonitrile upon exposure to simulated sunlight. $[\text{DHA18}] = 1.3 \times 10^{-4} \text{ M}$. $[\text{RDX}] = 5.4 \times 10^{-5} \text{ M}$. The absorption profile for the extended irradiation of a blank, aerated solution of **DHA18** is also shown (C).

9,9-Diphenyl-substituted **DHA8** differed slightly from the other DHAs explored in this work, as an absorbance band centered at 470 nm, as opposed to ca. 410 nm, evolved during its photoreaction with either RDX or PETN (Figure 2.10). Based on accompanying GC-MS

analyses, this absorbance band could be assigned to the formation of **29**. An emission band at 550 nm was also observed to evolve concomitantly. An approximately 25-fold increase in the emission intensity at 550 nm was generated in the presence of either RDX or PETN upon exposure to simulated sunlight for 40 seconds. The rates of reaction of **DHA5** and **DHA8** with RDX/PETN were approximately similar.

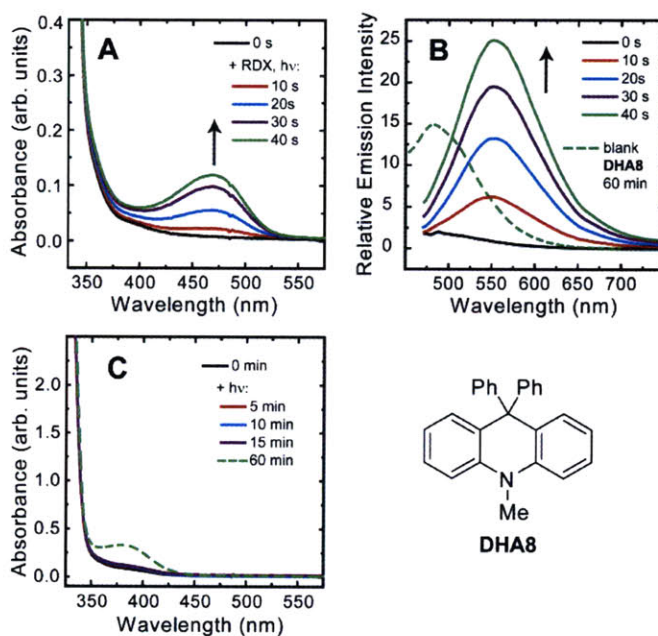


Figure 2.10. Absorption (A) and emission (B, $\lambda_{\text{ex}} = 470 \text{ nm}$) profiles of the photoreaction of **DHA8** with RDX in acetonitrile upon exposure to simulated sunlight. $[\text{DHA8}] = 1.3 \times 10^{-4} \text{ M}$. $[\text{RDX}] = 5.4 \times 10^{-5} \text{ M}$. The dashed green line depicts the emission spectrum obtained for a blank solution of **DHA8** after irradiation under either aerobic or anaerobic conditions for 60 minutes. The absorption profile for the irradiation of a blank, aerated solution of **DHA8** is also shown (C); the same profile is also obtained for oxygen-free solutions of **DHA8**.

Unlike **DHA5**, **DHA6** and **DHA18**, exposing solutions of **DHA8** to sunlight (or monochromatic UV light) in either the presence or absence of oxygen lead to the formation of a distinct absorbance band at 380 nm, with an accompanying emission band centered at 478 nm. Exactly similar photoreactivity was also observed for other DHAs that contained at least one phenyl substituent in the 9-position (**DHA4**, **DHA11** and **DHA13**). Since these absorption/emission bands were observed to evolve even in the absence of oxygen, they are most likely not generated by simple photooxidation products of **DHA8**. Moreover, the evolution of the absorbance band at 380 nm cannot be ascribed to a photodimerization event, as the product of such a reaction, **D1** (Scheme 2.6), has an absorption maximum of 457 nm. We are currently unsure as to the origin of the photoproduct responsible for the 380 nm/478 nm absorption/emission peak but suspect that a photocyclization reaction occurs in DHAs with at least one phenyl substituent in the 9-position. Nevertheless, for the purposes of this work, it can be seen in Figure 2.10 that the competing photoreaction in blank solutions of **DHA8** is slower than the photonitration of **DHA8** in the presence of RDX/PETN and an emission peak at 550 nm is cleanly generated by these explosives in under 10 seconds.

2.13 Reaction Kinetics

The most significant difference between the DHAs reported in this work involved the rate of formation of the nitrated photoproducts upon reaction with RDX or PETN. By following the evolution of the characteristic low-energy charge transfer band (centered at ca. 400 nm) of the nitrated DHAs with irradiation time, we were able to identify differences in the reactivities of **DHA1-18** (Figures 2.11 and 2.12). As can be seen in Figure 2.11, the substituents at the 9-position of DHAs significantly affected their reactivities. DHAs with at least one methyl or

phenyl substituent at the 9-position were rapidly nitrated in the presence of RDX or PETN. DHAs with alkyl (other than methyl) substituents at the 9-position displayed relatively slower rates of nitration, with isopropyl substituents leading to the slowest reaction rates. Replacing the 9-methyl substituents with trifluoromethyl moieties also retarded the reaction rate. Nominally faster reaction rates were generally observed with PETN over RDX for all DHAs. 9,9-Dioctylfluorene was used as a negative control for these studies and, in all cases, the DHAs reported in this work yielded a significant absorption signal at 400 nm over background.

The nature of the *N*-substituent was also found to affect the rate of photonitration in the presence of RDX/PETN. As seen in Figure 2.12, for DHAs with ethyl or isopropyl substituents at the 9-position, the *N*-H analogues reacted faster than the *N*-Me analogues. For DHAs with phenyl or methyl substituents in the 9-position, this trend was reversed and *N*-Me analogues displayed the fastest reaction rates. Moreover, *N*-arylation was found to significantly retard the rate of photonitration.

Lastly, the rate of formation of nitrated DHAs was compared to the formation of DMNA from DMA. As seen in Figure 2.13, the reactivity of **DHA5**, which displayed the fastest rate of nitration among **DHA1-18**, is comparable to that of DMA.

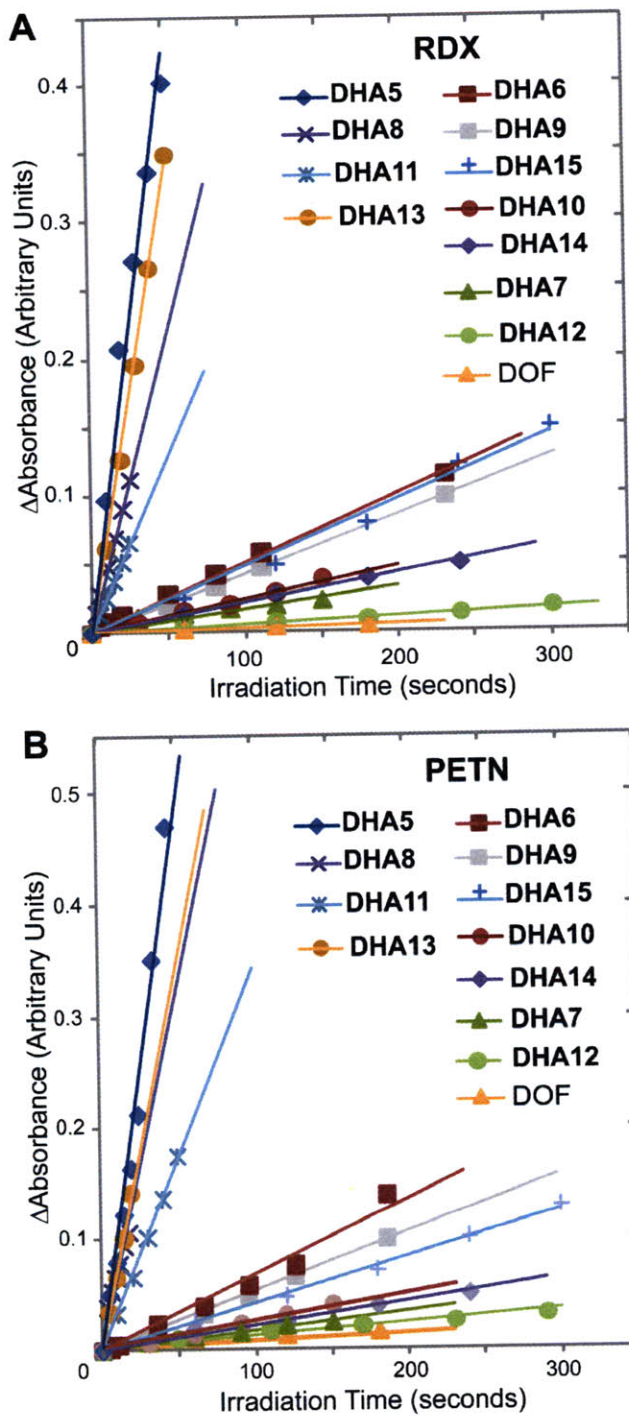


Figure 2.11. The effect of the substituents at the 9-position of DHAs on their photoreactions with RDX and PETN. Shown are the rates of evolution of the absorbance peak at 410 nm (470 nm for **DHA8**) for the photoreactions between **DHA5-15** and (A) RDX or (B) PETN. DOF is 9,9-dioctylfluorene, which was used as a negative control.

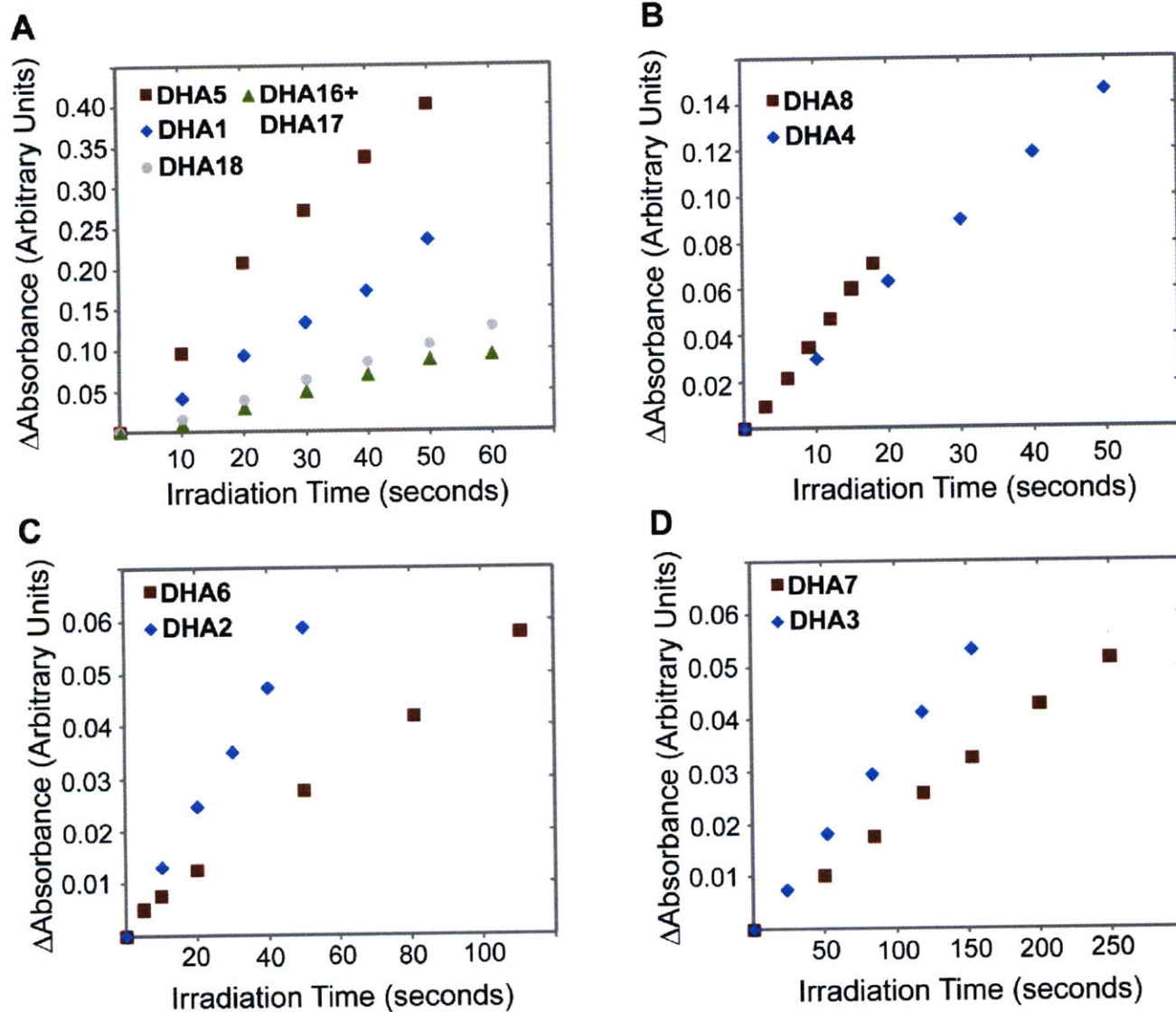


Figure 2.12. The effect of the *N*-substituent of DHAs on their photoreactions with RDX. Shown are the rates of evolution of the absorbance peak at 410 nm (470 nm for **DHA8**) for the photoreactions between various DHAs and RDX.

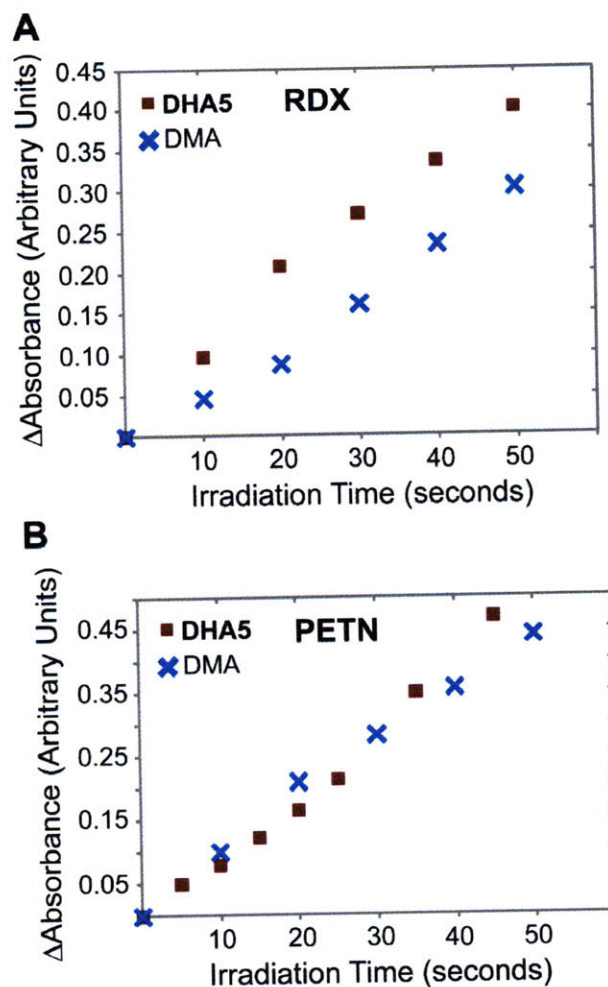


Figure 2.13. Comparison of the rates of nitration of **DHA5** vs DMA in the presence of (A) RDX or (B) PETN.

2.14 Solid State RDX/PETN Detection

Based on the previously-detailed rates of nitration of **DHA1-18** by the photodegradation products of RDX and PETN, we initially chose to focus on **DHA5**, **DHA8**, **DHA11** and **DHA13** as potential indicators for RDX and PETN, as they displayed the fastest rates of reaction. Between these four DHAs, **DHA5** and **DHA8** were favored because their nitrated products displayed high fluorescence quantum yields. We chose to use **DHA5** to demonstrate detection of

RDX/PETN in the solid state; however, similar results and detection limits were also obtained with **DHA8**.

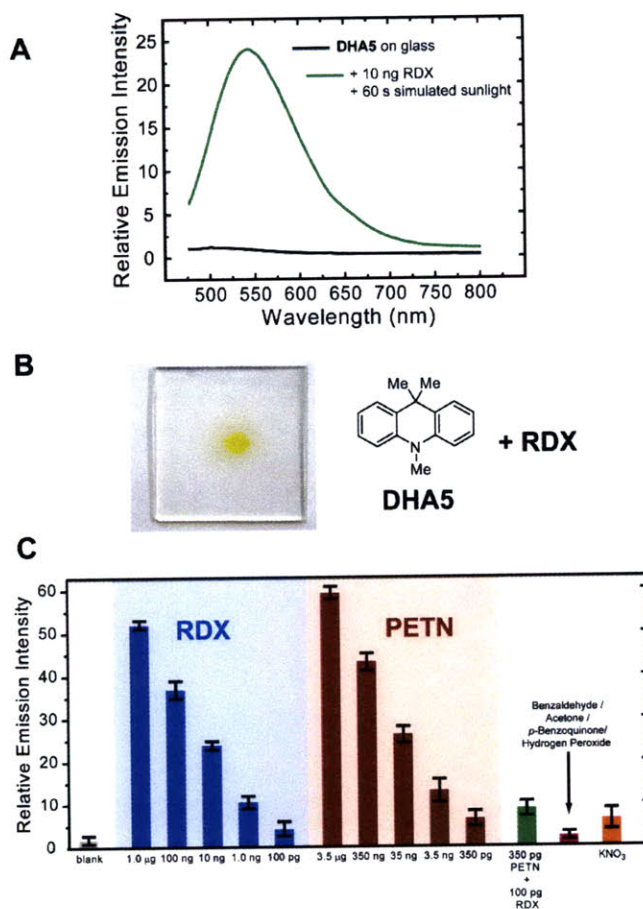


Figure 2.14. (A) Emission profile (λ_{ex} 420 nm) of a glass slide coated with **DHA5** (black line) and the same slide after spotting with ca. 10 ng of RDX and irradiating with a solar simulator for 60 seconds (green line). (B) Picture of a glass slide coated with **DHA5**, spotted with ca. 10 ng RDX and exposed to simulated sunlight for 120 s. (C) Limits of solid-state detection of RDX and PETN as measured by monitoring the change in emission intensity at 540 nm

upon exposure to simulated sunlight.

In order to evaluate the utility of **DHA5** as a fluorescent indicator for RDX and PETN, the solid-state response of **DHA5** to RDX and PETN was investigated. For this study, glass slides coated with **DHA5** were prepared by dipcoating into 8×10^{-3} M solutions of the indicator in acetonitrile and air drying. RDX and PETN solutions of varying concentration were spotted onto the surface and the slides then irradiated with a solar simulator for no longer than 120 seconds.

As shown in Figure 2.14A, an acceptable turn-on emission signal at 540 nm was generated by 10 ng of RDX after 60 seconds of irradiation with a solar simulator. In addition to a fluorescence signal, the distinct yellow color of **27** could also be observed by eye, as shown in Figure 2.14B. The limits of detection of the **DHA5** chemosensor were estimated by spotting RDX or PETN solutions of varying concentrations onto the **DHA5**-coated slides and are shown in Figure 2.14C. In general, a greater emission signal at 540 nm was generated by PETN over RDX, possibly because PETN is more susceptible to photodegradation than RDX.

Select interferents, such as ketones and aldehydes, did not produce a significant emission signal at 540 nm. Moreover, consistent with observations made during the synthesis of **D1**, hydrogen peroxide did not react readily with **DHA5** and most likely only formed a small quantity of the radical cation of **DHA5**, which is non-emissive and therefore did not produce any emission at 540 nm.

Aqueous potassium nitrate solutions of varying concentrations were also spotted onto the **DHA5**-coated glass slides in order to gauge the response of the **DHA5** indicator to nitrate contaminants. Consistent with previous observations, sub-micromolar solutions of potassium nitrate did not generate a significant emission signal at 540 nm after one hour in either the absence or presence of simulated solar irradiation. Using a 30 mM solution of potassium nitrate, an approximately 8-fold increase in the emission intensity at 540 nm was observed after a 10

minute exposure to simulated sunlight. However, given the high nitrate concentration and relatively long irradiation time necessary to effect this emission signal, interference from nitrates during RDX/PETN detection can, in theory, be surmounted.

Within experimental error, approximately 100 pg of RDX and PETN can be detected by the **DHA5** indicator under aerobic conditions by monitoring the emission intensity at 540 nm. In the presence of nitrate interferents, this detection limit is conservatively estimated as ca. 1 ng.

2.15 Conclusions

We have found that the nitramine-containing explosive RDX and the nitroester-containing explosive PETN are susceptible to photodegradation upon exposure to sunlight to produce reactive NO_x species, such as nitrogen dioxide and nitric acid. *N,N*-Dimethylaniline and 9,9-disubstituted 9,10-dihydroacridines (DHAs) are capable of being selectively nitrated by the reactive, electrophilic NO_x photodegradation products of RDX and PETN. This nitration reaction proceeds rapidly and yields only one major, singly-nitrated product. A roughly 25-fold increase in the emission signal at 550 nm is observed upon nitration of DHAs due to the generation of fluorescent donor-acceptor chromophores. By monitoring the emission intensity at ca. 550 nm, the presence of approximately 100 pg of RDX or PETN can be detected within one minute by these indicators in the solid state upon exposure to sunlight. The photonitration reaction presented herein is a unique and selective detection mechanism for nitroester and nitramine explosives that is distinct from a previously-reported photoreduction reaction to detect explosives. The rapid nitration of 9,9-diphenyl or -dimethyl substituted DHA chemosensors in the presence of RDX or PETN and the resulting strong, turn-on emission signal qualifies these

DHAs as cheap, impermanent indicators for the selective, stand-off identification of nitroester and nitramine explosives.

2.16 Experimental Section

Materials. Synthetic manipulations that required an inert atmosphere (where noted) were carried out under argon using standard Schlenk techniques. All solvents were of ACS reagent grade or better unless otherwise noted. All solvents used for photophysical experiments were of spectroscopic grade. Anhydrous tetrahydrofuran, diethyl ether, toluene and dichloromethane were obtained from J. T. Baker and purified by passing through a Glasscontour dry solvent system. Spectroscopic-grade acetonitrile was degassed and stored over 4Å sieves. Silica gel (40-63 μm) was obtained from SiliCycle Inc. All reagent grade materials were purchased from Aldrich or Alfa Aesar, and used without further purification. *N*-Phenylanthranilic acid was purchased from Alfa Aesar and esterified following a literature procedure.²⁶ RDX and PETN were obtained from K-9 training units, which consisted of RDX/PETN adsorbed onto sand. RDX and PETN were extracted from the sand with spectral grade acetonitrile and precipitated by the addition of DI water. The solids thus isolated were recrystallized three times from chloroform / acetonitrile and stored in the dark at -4 °C.

NMR Spectroscopy. ¹H and ¹³C NMR spectra for all compounds were acquired in CHCl₃ on a Bruker Avance Spectrometer operating at 400 and 100 MHz, respectively. The chemical shift data are reported in units of δ (ppm) relative to tetramethylsilane (TMS) and referenced with residual CHCl₃. ¹⁹F NMR spectra were recorded on a Varian Mercury Spectrometer at 380 MHz. Trichlorofluoromethane was used as an external standard (0 ppm) and upfield shifts are reported as negative values. In some cases, signals associated with the CF₃ groups and proximal

quaternary centers were not reported in the ^{13}C -NMR spectra due to C-F coupling and low signal-to-noise ratios.

Mass Spectrometry. High-resolution mass spectra (HRMS) were obtained at the MIT Department of Chemistry Instrumentation Facility using a peak-matching protocol to determine the mass and error range of the molecular ion, employing either electron impact or electrospray as the ionization technique.

Gas Chromatography/Mass Spectrometry. GC-MS data were recorded on an Agilent 5973N Gas Chromatograph/Mass Spectrometer equipped with a unit mass electron impact mass spectrometer. The GC was operated in the temperature range of 100-350°C under a vacuum of at least 10^{-5} torr. GC retention times are reported in minutes.

Infrared (IR) spectroscopy. IR spectra were recorded on a Perkin-Elmer Model 2000 FT-IR spectrophotometer at the MIT Department of Chemistry Instrumentation Facility and are reported as strong (s), medium (m) or weak (w).

X-Ray Diffraction. X-ray crystal structures were determined with a Siemens Platform three-circle diffractometer coupled to a Bruker-AXS Smart Apex CCD detector with graphite-monochromated Mo K α radiation ($\lambda = 0.71073 \text{ \AA}$), performing ϕ - and ω -scans. All structures were solved by direct methods using SHELXS²⁷ and refined against F on all data by full-matrix least squares with SHELXL-97. All non-hydrogen atoms were refined anisotropically.

Cyclic Voltammetry. All electrochemical measurements were made with an Autolab PGSTAT 20 potentiostat (EcoChemie) using a quasi-internal Ag wire reference electrode (BioAnalytical Systems) submersed in 0.01 M AgNO₃/0.1 M *n*-Bu₄NPF₆ in anhydrous MeCN. Typical CVs were recorded using a platinum button electrode as the working electrode and a platinum coil

counter electrode. The ferrocene/ferrocenium (Fc/Fc⁺) redox couple was used as an external reference.

Absorption and Emission Spectroscopy. Ultraviolet-visible absorption spectra were measured with an Agilent 8453 diode array spectrophotometer and corrected for background signal with either a solvent-filled cuvette (solutions) or a blank microscope slide (films). Fluorescence spectra were measured on a SPEX Fluorolog- τ 3 fluorimeter (model FL-321, 450 W Xenon lamp) using either right-angle (solutions) or front-face (22.5°) detection (thin films). Fluorescence quantum yields were determined by the optically dilute method²⁸ using quinine sulfate in 0.1M H₂SO₄ as a standard ($\Phi=0.53$) and were corrected for solvent refractive index and absorption differences at the excitation wavelength. Fluorescence lifetimes were measured via frequency modulation using a Horiba-Jobin-Yvon MF2 lifetime spectrometer equipped with a 365 nm laser diode and using the modulation of POPOP as a calibration reference.

*Photolysis Experiments.*²⁹ Solutions were irradiated under air at 313 nm using either: (1) a SPEX Fluorolog- τ 3 fluorimeter (model FL-321, 450 W Xenon lamp) with a 29.4 nm excitation slit width; (2) a 500 W Mercury Arc Lamp fitted with a 313 nm interference filter (or a 334 nm or 365 nm interference filter) and varying neutral density filters (0.5, 1.0 or 2.0 OD); or (3) a Newport Oriel Class A Solar Simulator Model 91190A equipped with a 450 W Xenon arc lamp, with a spectral output of 1.3 suns under AM 1.5 conditions. The first two light sources were calibrated with a potassium ferric oxalate actinometer.³⁰ For each measurement, reaction progress was also monitored in the dark to ensure that there was no thermal contribution to the nitration of aromatic amines by RDX and PETN. Each experiment was performed in triplicate.

***N,N*-Dimethyl-4-nitroaniline (DMNA).** A mixture of 0.4mL DMA and 0.1g of either RDX or PETN were dissolved in 3.0 mL dry, degassed acetonitrile and the solution photolyzed with a

xenon arc lamp at 313 nm for 60 minutes. The reaction mixture was sampled every 10 minutes to determine the GC yield of the DMNA product. Approximately 80% of DMNA (GC yield) was formed after 60 minutes of photolysis. The yellow DMNA was isolated by flash column chromatography using 50/50 hexanes/dichloromethane as an eluent. ^1H NMR (400 MHz, CHCl_3) δ 3.11 (s, 6H), 6.59 (d, $J = 8.2$ Hz, 2H), 8.09 (d, $J = 8.2$ Hz, 2H). ^{13}C NMR (100 MHz, CHCl_3) δ 40.2, 110.2, 126.0, 136.9, 154.3. HRMS (ESI) calc for $\text{C}_8\text{H}_{11}\text{N}_2\text{O}_2$ $[\text{M}+\text{H}]^+$ 167.0815, found 167.0819. IR (KBr plate) 695 (s), 750 (s), 820 (s), 1067 (m), 1118 (m), 1232 (m), 1347 (m), 1383 (w), 1456 (s), 1483 (s), 1582 (s), 1615 (w), 2924 (m) cm^{-1} .

General procedure for the synthesis of 9,9-disubstituted-9,10-dihydroacridines (DHA1-4). A flame-dried Schlenk flask was charged with 1.0 g methyl *N*-phenylanthranilate (**14**, 4.4 mmol) and 45 mL dry, degassed Et_2O under argon and cooled to 0 °C in an ice bath. 3.5 Equivalents of the appropriate Grignard reagent in Et_2O was added dropwise and the reaction allowed to stir at room temperature under argon for 3 d. After quenching with saturated ammonium chloride, the organic layer was separated, washed with brine and water and dried over MgSO_4 , and the solvent evaporated under reduced pressure. The crude tertiary alcohol thus formed was carried on to the next step without purification. To the neat oil isolated from the previous step was added 1-2 mL of concentrated H_2SO_4 under argon and the reaction stirred at room temperature for 1 h under argon. After dilution with 30 mL DI H_2O the reaction was poured into a 10% (v/v) aqueous ammoniacal solution and extracted with ether (5 x 50mL). The combined organic layers were washed with saturated sodium bicarbonate, brine and water and dried over MgSO_4 , and the solvent evaporated under reduced pressure. The residue was purified by flash column chromatography to yield the desired compound.

9,9-Dimethyl-9,10-dihydroacridine (DHA1). Synthesized using 3.0 M methyl magnesium bromide in Et₂O and purified by flash column chromatography using gradient elution, starting with 10% dichloromethane in hexanes and progressing to 50% dichloromethane in hexanes. 0.41 g (45%) of a white solid was isolated. m.p. 120 °C. ¹H NMR (400 MHz, CHCl₃) δ 1.54 (s, 6H), 6.11 (s, 1H), 6.67 (dd, *J* = 0.8 Hz, 7.6 Hz, 2H), 6.90 (m, 2H), 7.09 (m, 2H), 7.37 (d, *J* = 7.6 Hz, 2H). ¹³C NMR (100 MHz, CHCl₃) δ 30.7, 36.4, 113.6, 120.8, 125.7, 126.9, 129.3, 138.6. HRMS (ESI) calc for C₁₅H₁₅N [M+H]⁺ 210.1277, found 210.1284. IR(KBr plate) 745 (s), 886 (m), 1037 (m), 1318 (m), 1452 (m), 1479 (s), 1507 (m), 1580 (m), 1606 (m), 2966 (m), 3359 (m) cm⁻¹.

9,9-Diethyl-9,10-dihydroacridine (DHA2). Synthesized using 3.0 M ethyl magnesium bromide in Et₂O and purified by flash column chromatography using hexanes as the eluent. 0.36 g (35%) of a clear oil was isolated. ¹H NMR (400 MHz, CHCl₃) δ 0.91 (t, *J* = 7.6 Hz, 3H), 0.97 (t, *J* = 7.6 Hz, 3H), 2.24 (q, *J* = 7.6 Hz, 2H), 2.35 (q, *J* = 7.6 Hz, 2H), 5.74 (s, 1H), 6.90 (m, 3H), 7.06 (m, 5H). ¹³C NMR (100 MHz, CHCl₃) δ 13.0, 13.1, 13.9, 14.8, 24.3, 31.7, 115.9, 116.8, 118.2, 118.5, 120.3, 120.5, 121.0, 121.2, 123.0, 124.9, 127.4, 127.5, 129.5, 129.7, 130.1, 130.2, 134.3, 140.1, 140.3, 141.2, 143.5, 143.7. HRMS (ESI) calc for C₁₇H₁₉N [M+H]⁺ 238.1590, found 238.1591. IR (KBr plate) 692 (m), 745 (s), 1309 (m), 1451 (m), 1507 (s), 1575 (m), 1593 (s), 2871 (m), 2930 (m), 2965 (m), 3041 (m), 3403 (m) cm⁻¹.

9,9-Diisopropyl-9,10-dihydroacridine (DHA3). Synthesized using 2.0 M isopropyl magnesium chloride in Et₂O and purified by flash column chromatography using hexanes as the eluent. 0.19 g (17%) of a clear oil was isolated. ¹H NMR (400 MHz, CHCl₃) δ 0.77 (d, *J* = 6.8 Hz, 3H), 1.02 (d, *J* = 6.8 Hz, 3H), 1.46 (s, 3H), 1.87 (s, 3H), 3.06 (septet, *J* = 6.8 Hz, 1H), 5.75 (s, 1H), 6.88 (m, 5H), 7.20 (m, 4H). ¹³C NMR (100 MHz, CHCl₃) δ 19.7, 20.9, 22.4, 22.2, 30.6, 115.5, 118.6, 119.8, 121.2, 127.1, 129.5, 129.8, 130.0, 130.7, 136.8, 141.0, 143.5. HRMS (ESI) calc for

$C_{19}H_{24}N$ $[M+H]^+$ 266.1903, found 266.1904. IR (KBr plate) 693 (s), 745 (s), 1079 (m), 1309 (s), 1450 (s), 1508 (s), 1576 (s), 1594 (s), 2961 (m), 3399 (s) cm^{-1} .

9,9-Diphenyl-9,10-dihydroacridine (DHA4). Synthesized using 3.0 M phenyl magnesium bromide in Et_2O and purified by flash column chromatography using gradient elution, starting with 10% dichloromethane in hexanes and progressing to 50% dichloromethane in hexanes. 0.83 g (57%) of a white solid was isolated. m.p. 230 °C. 1H NMR (400 MHz, $CHCl_3$) δ 6.25 (s, 1H), 6.86 (m, 9H), 7.16 (m, 8H). ^{13}C NMR (100 MHz, $CHCl_3$) δ 30.1, 56.7, 113.5, 120.2, 125.6, 126.1, 126.2, 127.1, 127.4, 127.6, 127.6, 127.9, 128.5, 130.0, 130.2, 130.2, 139.7, 146.0, 149.3. HRMS (ESI) calc for $C_{25}H_{19}N$ $[M+H]^+$ 334.1590, found 334.1584. IR (KBr plate) 699 (m), 734 (m), 753 (m), 907 (m), 1315 (m), 1474 (s), 1604 (m), 3057 (w), 3393 (m) cm^{-1} .

Methyl *N*-methyl-*N*-phenylanthranilate (15). A flame-dried two-neck round bottom flask was charged with 8 g *N*-phenylanthranilic acid (37.5 mmol), 0.3 mL 15-crown-5, 300 mL dry THF and 100 mL dimethoxyethane under argon. The solution was cooled to 0 °C in an ice bath, 5 g of a 60 wt% dispersion of NaH in mineral oil (3 g NaH, 125mmol) was added to the reaction mixture in small portions under argon and 15 mL dimethyl sulfate (19.99 g, 15 8mmol) was added via syringe. After stirring at room temperature for 5 d under argon the reaction was poured carefully onto 800g ice and extracted with Et_2O (5 x 50mL). The organic layers were combined, washed thoroughly with saturated sodium bicarbonate (3x 25 mL), brine and water, dried over $MgSO_4$ and the solvent evaporated under reduced pressure. The resulting oil was purified by flash column chromatography using gradient elution, starting with 100% hexanes and progressing to 30% dichloromethane in hexanes to yield 7.2 g (80%) of a yellow oil. 1H NMR (400 MHz, $CHCl_3$) δ 3.28 (s, 3H), 3.58 (s, 3H), 6.63 (dd, $J = 8.8$ Hz, $J = 1.2$ Hz, 2H), 6.73 (td, , $J = 6$ Hz, $J = 1.2$ Hz, 1H), 7.16 (td, $J = 7.2$ Hz, $J = 1.6$ Hz, 2H), 7.27 (m, 2H), 7.53 (td, $J = 8$ Hz, $J = 1.2$ Hz, 1H).

= 1.6 Hz, 1H), 7.79 (dd, J = 7.6 Hz, J = 1.6 Hz, 1H). ¹³C NMR (100 MHz, CHCl₃) δ 40.5, 52.3, 114.4, 118.1, 125.4, 129.1, 129.2, 129.4, 131.6, 133.4, 148.3, 129.4, 167.7. HRMS (ESI) calc for C₁₅H₁₅NO₂ [M+H]⁺ 242.1176, found 242.1170. IR (KBr plate) 2924 (s), 2853 (s), 1728 (m), 1594 (m), 1500 (m), 1454 (m), 1391 (w), 1253 (s), 1214 (s), 1062 (m), 1005 (m), 758 (m), 575 (m) cm⁻¹.

General procedure for the synthesis of 9,9-disubstituted-10-methyl-9,10-dihydroacridines (DHA5-9). A flame-dried Schlenk flask was charged with 1.0 g methyl *N*-methyl-*N*-phenylanthranilate (**15**, 4.1 mmol) and 45 mL dry, degassed Et₂O under argon and cooled to 0 °C in an ice bath. 2.5 Equivalents of the appropriate Grignard reagent in Et₂O was added dropwise and the reaction allowed to stir at room temperature under argon for 3 d. After quenching with saturated ammonium chloride, the organic layer was separated, washed with brine and water and dried over MgSO₄, and the solvent evaporated under reduced pressure. The crude tertiary alcohol thus formed was carried on to the next step without purification. To the neat oil isolated from the previous step was added 1-2 mL of concentrated H₂SO₄ under argon and the reaction stirred at room temperature for 1 h under argon. After dilution with 30 mL DI H₂O the reaction was poured into a 10% (v/v) aqueous ammoniacal solution and extracted with ether (5 x 50 mL). The combined organic layers were washed with saturated sodium bicarbonate, brine and water and dried over MgSO₄, and the solvent evaporated under reduced pressure. The residue was purified by flash column chromatography to yield the desired compound.

9,9-Dimethyl-10-methyl-9,10-dihydroacridine (DHA5). Synthesized using 3.0 M methyl magnesium bromide in Et₂O and purified by flash column chromatography using gradient elution, starting with 10% dichloromethane in hexanes and progressing to 50% dichloromethane in hexanes. 0.39 g (42%) of a light yellow solid was isolated. m.p. 93 °C. ¹H NMR (400 MHz, in hexanes.

CHCl₃) δ 1.52 (s, 6H), 3.43 (s, 3H), 6.96 (m, 4H), 7.21 (m, 2H), 7.38 (d, *J* = 1.6 Hz, 2H). ¹³C NMR (100 MHz, CHCl₃) δ 27.4, 33.5, 36.7, 112.3, 120.8, 123.8, 126.8, 132.8, 142.4. HRMS (ESI) calc for C₁₆H₁₇N [M+H]⁺ 224.1434, found 224.1429. IR (KBr plate) 751 (s), 1046 (m), 1268 (s), 1340 (s), 1450 (s), 1470 (s), 1590 (s), 2900 (m), 2950 (s), 2980 (s), 3050 (m) cm⁻¹.

9,9-Diethyl-10-methyl-9,10-dihydroacridine (DHA6). Synthesized using 3.0 M ethyl magnesium bromide in Et₂O and purified by flash column chromatography using hexanes as the eluent. 0.31 g (30%) of a clear oil was isolated. ¹H NMR (400 MHz, CHCl₃) δ 0.81 (t, *J* = 7.6 Hz, 3H), 0.84 (t, *J* = 7.6 Hz, 3H), 2.14 (q, *J* = 7.6 Hz, 2H), 2.27 (q, *J* = 7.6 Hz, 2H), 3.06 (s, 3H), 6.65 (m, 3H), 7.17 (m, 5H). ¹³C NMR (100 MHz, CHCl₃) δ 14.2 (2), 14.3, 22.5, 22.8, 23.2, 23.4, 29.6, 30.4, 31.0, 31.2, 31.7, 37.1, 39.4, 39.6, 114.0, 114.1, 117.2, 117.3, 125.5, 125.9, 127.8, 128.1, 128.2, 128.4, 128.7, 128.9, 130.5, 132.0, 132.5, 140.0, 140.1, 141.5, 143.4, 146.1, 147.0, 149.3, 149.5. HRMS (ESI) calc for C₁₈H₂₁N [M+H]⁺ 252.1747, found 252.1742. IR (KBr plate) 692 (s), (748 (s), 1342 (m), 1444 (m), 1487 (s), 1500 (s), 1568 (m), 1592 (s), 1602 (s), 2810 (m), 2870 (m), 2963 (m), 3024 (m) cm⁻¹.

9,9-Diisopropyl-10-methyl-9,10-dihydroacridine (DHA7). Synthesized using 2.0 M isopropyl magnesium chloride in Et₂O and purified by flash column chromatography using hexanes as the eluent. 0.19 g (17%) of a clear oil was isolated. ¹H NMR (400 MHz, CHCl₃) δ 0.85 (d, *J* = 7.2 Hz, 3H), 0.89 (d, *J* = 7.6 Hz, 3H), 1.46 (s, 3H), 1.80 (s, 3H), 2.84 (septet, *J* = 7.2 Hz, 1H), 3.03 (s, 3H), 6.74 (m, 3H), 6.98 (m, 1H), 7.13 (m, 5H). ¹³C NMR (100 MHz, CHCl₃) δ 21.6, 22.3, 23.8, 31.8, 39.0, 114.6, 117.4, 120.6, 121.4, 125.2, 127.4, 127.8, 128.0, 128.7, 129.4, 133.6, 140.0, 141.2, 147.2, 149.6. HRMS (ESI) calc for C₂₀H₂₅N [M+H]⁺ 280.2060, found 280.2058. IR (KBr plate) 748 (m), 1499 (m), 1601 (m), 2820 (m), 2910 (m) 3040 (m) cm⁻¹.

9,9-Diphenyl-10-methyl-9,10-dihydroacridine (DHA8). Synthesized using 3.0 M phenyl magnesium bromide in Et₂O and purified by flash column chromatography using gradient elution, starting with 10% dichloromethane in hexanes and progressing to 50% dichloromethane in hexanes. 0.79 g (55%) of a light yellow solid was isolated. m.p. 165 – 166 °C. ¹H NMR (400 MHz, CHCl₃) δ 3.29 (s, 3H), 6.84 (m, 2H), 6.91 (m, 8H), 7.18 (m, 6H), 7.26 (m, 2H). ¹³C NMR (100 MHz, CHCl₃) δ 33.6, 57.3, 112.1, 120.0, 126.4, 127.4, 127.7, 130.1, 130.6, 131.4, 142.7, 146.2. HRMS (ESI) calc for C₂₆H₂₁N [M+H]⁺ 348.1747, found 348.1732. IR (KBr plate) 638 (m), 699 (m), 733 (m), 755 (m), 1270 (m), 1348 (m), 1468 (s), 1590 (m), 1589 (m), 2815 (w), 2873 (w), 3056 (m) cm⁻¹.

9,9-Di-*n*-octyl-10-methyl-9,10-dihydroacridine (DHA9). Synthesized using 2.0 M octyl magnesium bromide in Et₂O and purified by flash column chromatography using hexanes as the eluent. 0.7 g (40%) of a clear oil was isolated. ¹H NMR (400 MHz, CHCl₃) δ 0.85 (t, *J* = 7.6 Hz, 3H), 0.88 (t, *J* = 7.2 Hz, 3H), 1.22 (bm, 22H), 2.08 (q, *J* = 7.2 Hz, 2H), 2.25 (t, *J* = 7.6 Hz, 2H), two overlapping singlets: δ 3.08, 3.10, total 3H, 5.35 (t, *J* = 7.6 Hz, 1H), 6.67 (m, 3H), 7.17 (m, 6H). ¹³C NMR (100 MHz, CHCl₃) δ 14.4, 22.9 (3), 28.3, 28.7, 29.0, 29.3, 29.5 (2), 29.6, 29.7 (2), 29.8, 30.0, 30.3, 31.1, 32.1 (2), 37.4, 39.4, 39.6, 114.0, 114.1, 117.2, 117.3, 125.5, 125.9, 128.0 (2), 128.2, 128.4, 128.6, 128.9, 130.7, 132.0, 132.5, 140.0, 140.7, 141.3, 143.4, 146.1, 146.9, 149.3, 149.5. HRMS (ESI) calc for C₃₀H₄₅N [M+H]⁺ 420.3625, found 420.3613. IR (KBr plate) 692 (m), 747 (m), 1095 (w), 1342 (m), 1499 (s), 1592 (s), 1602 (s), 2854 (s), 2924 (s), 2955 (s), 3024 (w) cm⁻¹.

2-Bromo-N-methyl-N-phenylaniline (18). A flame-dried two-neck round bottom flask was charged with 2-bromo-N-phenylaniline (3 g, 12.2 mmol), 0.1 mL 15-crown-5, 200 mL dry THF and 50 mL dimethoxyethane under argon. The solution was cooled to 0 °C in an ice bath, 0.6 g of

a 60 wt% dispersion of NaH in mineral oil (0.36 g NaH, 15 mmol) was added to the reaction mixture in small portions under argon and 1.4 mL dimethyl sulfate (1.89 g, 15 mmol) was added via syringe. After refluxing for 20 h under argon the reaction was poured carefully onto 500 g ice and extracted with Et₂O (5 x 50mL). The organic layers were combined, washed thoroughly with saturated sodium bicarbonate (3 x 25mL), brine and water, dried over MgSO₄ and the solvent evaporated under reduced pressure. The resulting oil was purified by flash column chromatography using gradient elution, starting with 100% hexanes and progressing to 30% dichloromethane in hexanes to yield 2.5 g (80%) of a clear oil. ¹H NMR (400 MHz, CHCl₃) δ 3.22 (s, 3H), 6.56 (d, *J* = 7.6 Hz, 2H), 6.75 (t, *J* = 7.6 Hz, 1H), 7.15 (m, 3H), 7.25 (dd, *J* = 8.0 Hz, *J* = 2.0 Hz, 1H), 7.32 (td, *J* = 7.6 Hz, *J* = 1.2 Hz, 1H), 7.66 (dd, *J* = 8.0 Hz, *J* = 1.6 Hz, 1H). ¹³C NMR (100 MHz, CHCl₃) δ 39.1, 113.5, 117.8, 124.4, 127.9, 128.4, 129.1, 129.2, 130.6, 134.3, 147.0, 148.7. HRMS (ESI) calc for C₁₃H₁₂BrN [M+H]⁺ 262.0226, found 262.0234. IR (KBr plate) 654 (s), 691 (s), 748 (s), 872 (s), 1139 (s), 1137 (s), 1273 (s), 1346 (s), 1438 (m), 1467 (s), 1499 (s), 1580 (s), 1601 (s), 2813 (m), 2824 (s), 3058 (m), 3089 (m) cm⁻¹.

9-ethyl-9,10-dimethyl-9,10-dihydroacridine (DHA10). A flame-dried two-necked flask was charged with 2-bromo-N-methyl-N-phenylaniline (1.0g, 3.8mmol) and 100mL dry THF under argon and cooled to -78°C in a dry ice-acetone bath. 2.6mL of a 1.6M solution of *n*-BuLi in hexanes (4.16 mmol) was added dropwise over 5 minutes and the reaction stirred at -78°C under argon for 1 h. Methyl ethyl ketone (0.302g, 4.2mmol) was added in one portion to the reaction mixture at -78°C, the reaction allowed to warm to room temperature and stirred overnight under argon. After quenching with saturated ammonium chloride, the reaction was extracted with Et₂O, the organic layers combined, washed with brine and water and dried over anhydrous MgSO₄ and the solvent evaporated under reduced pressure. To the neat residue thus obtained was added 2mL

of concentrated H₂SO₄ under argon and the mixture stirred at room temperature for 1 h under argon. After dilution with 30mL DI H₂O, the reaction was extracted with Et₂O (5x 50mL), the organic layers were combined, washed with brine and water and dried over anhydrous MgSO₄, and the solvent was evaporated under reduced pressure. The residue was purified by flash column chromatography using hexanes as the eluent to yield 0.57g (57%) of the desired compound as a clear oil. ¹H NMR (400 MHz, CHCl₃) δ 1.66 (dd, *J* = 6.8 Hz, *J* = 0.8 Hz, 3H), 1.78 (t, *J* = 1.2 Hz, 3H), 3.10 (s, 3H), 5.49 (m, 1H), 6.66 (m, 3H), 7.18 (m, 6H). ¹³C NMR (100 MHz, CHCl₃) δ 14.2, 15.2, 16.5, 24.2, 39.2, 39.6, 113.8, 114.1, 117.1, 117.4, 122.4, 124.4, 125.7, 125.9, 128.0, 128.2, 128.5, 128.8, 128.9, 130.6, 131.5, 136.4, 140.4, 144.3, 145.8, 146.9, 149.2, 149.4. HRMS (ESI) calc for C₁₇H₁₉N [M+H]⁺ 238.1590, found 238.1587. IR (KBr plate) 692 (m), 747 (m), 1345 (m), 1444 (m), 1499 (s), 1592 (s), 1602 (s), 2918 (m), 3024 (m) cm⁻¹.

9-Methyl-9-phenyl-10-methyl-9,10-dihydroacridine (DHA11). A flame-dried two-necked flask was charged with 2-bromo-N-methyl-N-phenylaniline (1.0 g, 3.8mmol) and 100mL dry THF under argon and cooled to -78°C in a dry ice-acetone bath. 2.6mL of a 1.6M solution of *n*-BuLi in hexanes (4.16 mmol) was added dropwise over 5 minutes and the reaction stirred at -78 °C under argon for 1 h. Acetophenone (0.49 mL, 0.51 g, 4.2mmol) was added in one portion under argon at -78°C, the reaction allowed to warm to room temperature and stirred overnight under argon. After quenching with saturated ammonium chloride, the reaction was extracted with Et₂O, the organic layers combined, washed with brine and water and dried over anhydrous MgSO₄ and the solvent evaporated under reduced pressure. To the neat residue thus obtained was added 2mL of concentrated H₂SO₄ under argon and the mixture stirred at room temperature for 1 h under argon. After dilution with 30mL DI H₂O, the reaction was extracted with Et₂O (5x 50mL), the organic layers were combined, washed with brine and water and dried over

anhydrous MgSO₄, and the solvent was evaporated under reduced pressure. The desired product was purified by flash column chromatography using gradient elution, starting with 20% dichloromethane in hexanes and progressing to 50% dichloromethane in hexanes to yield 0.55 g (50%) of a light yellow solid. m.p. 184 °C. ¹H NMR (400 MHz, CHCl₃) δ 1.83 (s, 3H), 3.37 (s, 3H), 6.93 (m, 6H), 7.24 (m, 8H). ¹³C NMR (100 MHz, CHCl₃) δ 27.4, 28.2, 31.2, 33.6, 112.1 (2), 112.3, 113.7, 113.9, 116.9, 120.0, 120.4, 120.8, 123.8, 126.2, 126.4, 126.76, 126.7, 127.1, 127.38, 127.5, 127.7, 127.8, 127.9, 128.0, 128.5, 128.7, 128.8, 128.9, 130.1, 130.5, 131.4, 132.5, 142.0, 142.7, 146.2, 148.9. HRMS (ESI) calc for C₂₁H₁₉N [M+H]⁺ 286.1590, found 286.1590. IR (KBr plate) 650 (m), 699 (m), 743 (m), 798 (m), 1290 (m), 1353 (m), 1468 (s), 1595 (m), 1631 (m), 2803 (w), 2898 (w), 3042 (m) cm⁻¹.

9-Isopropyl-9,10-dimethyl-9,10-dihydroacridine (DHA12). A flame-dried two-necked flask was charged with 2-bromo-N-methyl-N-phenylaniline (1.0g, 3.8mmol) and 100mL dry THF under argon and cooled to -78°C in a dry ice-acetone bath. 2.6mL of a 1.6M solution of *n*-BuLi in hexanes (4.16 mmol) was added dropwise over 5 minutes and the reaction stirred at -78°C under argon for 1 h. Isopropyl methyl ketone (0.361g, 4.2mmol) was added in one portion to the reaction mixture at -78°C, the reaction allowed to warm to room temperature and stirred overnight under argon. After quenching with saturated ammonium chloride, the reaction was extracted with Et₂O, the organic layers combined, washed with brine and water and dried over anhydrous MgSO₄ and the solvent evaporated under reduced pressure. To the neat residue thus obtained was added 2mL of concentrated H₂SO₄ under argon and the mixture stirred at room temperature for 1 h under argon. After dilution with 30mL DI H₂O, the reaction was extracted with Et₂O (5x 50mL), the organic layers were combined, washed with brine and water and dried over anhydrous MgSO₄, and the solvent was evaporated under reduced pressure. The residue was

purified by flash column chromatography using hexanes as the eluent to yield 0.62g (60%) of the desired compound as a clear oil. ¹H NMR (400 MHz, CHCl₃) δ 1.51 (s, 3H), 1.64 (s, 3H), 1.70 (s, 3H), 3.04 (s, 3H), 6.64 (m, 3H), 7.12 (m, 6H). ¹³C NMR (100 MHz, CHCl₃) δ 21.5, 22.2, 23.8, 31.8, 39.0, 114.6, 117.4, 120.6, 121.4, 125.1, 127.4, 127.8, 128.0, 128.7, 129.3, 133.6, 140.0, 141.1, 147.2, 149.5. HRMS (ESI) calc for C₁₈H₂₁N [M+H]⁺ 252.1747, found 252.1742. IR (KBr plate) 692 (m), 747 (s), 1137 (m), 1342 (m), 1443 (m), 1486 (s), 1499 (s), 1591 (s), 1601 (s), 2911 (m), 2984 (m) cm⁻¹.

9-Ethyl-9-phenyl-10-methyl-9,10-dihydroacridine (DHA13). A flame-dried two-necked flask was charged with 2-bromo-N-methyl-N-phenylaniline (1.0g, 3.8mmol) and 100mL dry THF under argon and cooled to -78 °C in a dry ice-acetone bath. 2.6mL of a 1.6M solution of *n*-BuLi in hexanes (4.16 mmol) was added dropwise over 5 minutes and the reaction stirred at -78°C under argon for 1 h. Propiophenone (0.56 mL, 0.56 g, 4.2mmol) was added in one portion to the reaction mixture under argon at -78°C, the reaction allowed to warm to room temperature and stirred overnight under argon. After quenching with saturated ammonium chloride, the reaction was extracted with Et₂O, the organic layers combined, washed with brine and water and dried over anhydrous MgSO₄ and the solvent evaporated under reduced pressure. To the neat residue thus obtained was added 2mL of concentrated H₂SO₄ under argon and the mixture stirred at room temperature for 1 h under argon. After dilution with 30mL DI H₂O, the reaction was extracted with Et₂O (5x 50mL), the organic layers were combined, washed with brine and water and dried over anhydrous MgSO₄, and the solvent was evaporated under reduced pressure. The desired product was purified by flash column chromatography using 10% dichloromethane in hexanes as the eluent to yield 0.62 g (55%) of a light yellow oil. ¹H NMR (400 MHz, CHCl₃) δ 0.74 (t, *J* = 7.2 Hz, 3H), 2.22 (q, *J* = 7.2 Hz, 2H), 3.38 (s, 3H), 6.75 (m, 4H), 6.89 (m, 2H), 7.17

(m, 3H), 7.27 (m, 4H). ^{13}C NMR (100 MHz, CHCl_3) δ 9.7, 33.8, 34.6, 50.5, 111.9, 113.1, 113.8, 114.0, 116.9, 119.9, 125.4, 125.6, 125.9, 126.4, 126.5, 126.6, 126.7, 127.0, 127.3, 127.5, 127.8, 127.9, 128.2, 128.3, 128.8, 128.9, 129.2, 129.4, 129.6, 130.2, 132.9, 138.7, 141.3, 142.0, 143.5, 147.3, 148.5, 149.5. HRMS (EI) calc for $\text{C}_{22}\text{H}_{21}\text{N}$ $[\text{M}]^+$ 299.1669, found 299.1673. IR (KBr plate) 633 (m), 693 (s), 747 (s), 1032 (w), 1260 (w), 1349 (m), 1448 (m), 1499 (s), 1575 (m), 1590 (s), 1601 (s), 2927 (m), 3024 (m) cm^{-1} .

10-methyl-10H-spiro[acridine-9,1'-cyclohexane] (DHA14). A flame-dried two-necked flask was charged with 2-bromo-N-methyl-N-phenylaniline (1.0g, 3.8mmol) and 100mL dry THF under argon and cooled to -78°C in a dry ice-acetone bath. 2.6mL of a 1.6M solution of *n*-BuLi in hexanes (4.16 mmol) was added dropwise over 5 minutes and the reaction stirred at -78°C under argon for 1 h. Cyclohexanone (0.43mL, 0.412g, 4.2mmol) was added in one portion to the reaction mixture at -78°C , the reaction allowed to warm to room temperature and stirred overnight under argon. After quenching with saturated ammonium chloride, the reaction was extracted with Et_2O , the organic layers combined, washed with brine and water and dried over anhydrous MgSO_4 and the solvent evaporated under reduced pressure. To the neat residue thus obtained was added 2mL of concentrated H_2SO_4 under argon and the mixture stirred at room temperature for 1 h under argon. After dilution with 30mL DI H_2O , the reaction was extracted with Et_2O (5x 50mL), the organic layers were combined, washed with brine and water and dried over anhydrous MgSO_4 , and the solvent was evaporated under reduced pressure. The residue was purified by flash column chromatography using hexanes as the eluent to yield 0.3g (30%) of the desired compound as a clear oil. ^1H NMR (400 MHz, CHCl_3) δ 1.53 (m, 4H), 2.10 (m, 4H), 3.12 (s, 3H), 5.65 (m, 1H), 6.66 (m, 3H), 7.18 (m, 6H). ^{13}C NMR (100 MHz, CHCl_3) δ 22.0, 23.0, 25.6, 28.2, 39.2, 113.7, 116.9, 125.6, 126.3, 127.7, 128.2, 128.5, 130.3, 137.9, 142.8, 145.6,

149.0. HRMS (ESI) calc for $C_{19}H_{21}N$ $[M+H]^+$ 264.1747, found 264.1758. IR (KBr plate) 693 (m), 747(m), 1069 (s), 1155 (m), 1263 (m), 1345 (m), 1499 (s), 1602(s), 2853 (m), 2921 (s) cm^{-1} .

1,1,1,3,3,3-hexafluoro-2-(2-(methyl(phenyl)amino)phenyl)propan-2-ol (21). A flame-dried two-necked flask equipped with a dry ice/acetone condenser was charged with 2-bromo-N-methyl-N-phenylaniline (1.0g, 3.8mmol) and 100mL dry THF under argon and cooled to $-78^{\circ}C$ in a dry ice-acetone bath. 2.6mL of a 1.6M solution of *n*-BuLi in hexanes (4.16 mmol) was added dropwise over 5 minutes and the reaction stirred at $-78^{\circ}C$ under argon for 1 h. Making sure that the dry ice/acetone condenser remained filled, anhydrous hexafluoroacetone (HFA) gas was bubbled into the reaction flask at $-78^{\circ}C$ under a positive pressure of argon for a total duration of 3 minutes; the pressure reading on the HFA tank was noted to be 22psi. The reaction was allowed to warm to room temperature and the HFA allowed to reflux for an additional 3h (making sure the dry ice/acetone condenser remained full for the duration) after which the excess HFA was removed by bubbling through a saturated KOH solution for 1h. The reaction was quenched with saturated ammonium chloride and extracted with Et_2O (3x 50mL). The organic layers were combined, washed with brine and water and dried over $MgSO_4$, and the solvent was evaporated under reduced pressure. The residue was purified by flash column chromatography using 50% dichloromethane in hexanes as the eluent to yield g 1.1g (80%) of the desired compound as a white crystalline solid after drying in vacuo for 3d. 1H NMR (400 MHz, $CHCl_3$) δ 3.08 (s, 3H), 6.87 (dd, $J = 8.0$ Hz, $J = 1.6$ Hz, 2H), 6.98 (m, 2H), 7.21 (m, 2H), 7.36 (m, 2H), 7.75 (d, $J = 8.0$ Hz, 1H), 11.51 (s, 1H). ^{13}C NMR (100 MHz, $CHCl_3$) δ 40.3, 80.3 (quintet), 115.0, 115.5, 118.8, 119.2 (2), 119.4, 120.6 121.5, 121.6, 122.0, 122.1, 122.9, 124.9 (3), 127.2, 127.7, 127.8, 127.9, 128.3, 128.9 (2), 129.0, 129.2, 129.3, 129.4, 129.6, 132.3, 149.2, 151.6.

^{19}F NMR (380 MHz, CHCl_3) δ -76.4, -75.1. HRMS (ESI) calc for $\text{C}_{16}\text{H}_{13}\text{F}_6\text{NO}$ $[\text{M}+\text{H}]^+$ 350.0974, found 350.0961. IR (KBr plate) 479 (m), 693 (s), 709 (s), 754 (s), 848 (m), 936 (m), 954 (s), 968 (s), 1121 (s), 1147 (m), 1192 (s), 1260 (s), 1496 (s), 1577 (m), 1603 (m), 2719 (m), 2973 (m), 3066 (m), 3854 (broad) cm^{-1} .

10-methyl-9,9-bis(trifluoromethyl)-9,10-dihydroacridine (DHA15). 1,1,1,3,3,3-hexafluoro-2-(2-(methyl(phenyl)amino)phenyl)propan-2-ol (0.2g, 0.57mmol) was dissolved in 15mL POCl_3 and the solution refluxed under argon for 3d. Excess POCl_3 was distilled off using a short path distillation head, the residue was dissolved in CHCl_3 , poured into a 10% (v/v) aqueous ammoniacal solution and the biphasic system stirred at room temperature for one hour. The organic layer was separated and the aqueous layer extracted with Et_2O (3x50mL). The organic layers were combined, washed with brine and water and dried over MgSO_4 , and the solvent evaporated under reduced pressure. The residue was purified by flash column chromatography using 10% dichloromethane in hexanes as the eluent to yield 0.15 g (80%) of the desired compound as a light-blue oil. ^1H NMR (400 MHz, CHCl_3) δ 3.46 (s, 3H), 7.00 (m, 4H), 7.42 (m, 2H), 7.89 (m, 2H). ^{13}C NMR (100 MHz, CHCl_3) δ 29.8, 35.1, 111.8, 114.7, 120.3, 130.3 (quintet), 130.7, 141.8. ^{19}F NMR (380 MHz, CHCl_3) δ -65.9. HRMS (EI) calc for $\text{C}_{16}\text{H}_{11}\text{F}_6\text{N}$ $[\text{M}]^+$ 332.0868, found 332.0874. IR (KBr plate) 479 (m), 693 (s), 709 (s), 758 (s), 848 (m), 954 (s), 1116 (s), 1163 (m), 1192 (s), 1260 (s), 1489 (s), 1573 (m), 1594 (m), 2840 (m), 2972 (m), 3054 (m) cm^{-1} .

Methyl *N*-(*p*-tolyl)-*N*-phenylanthranilate (22). A flame-dried Schlenk flask was charged with **14** (5 g, 22 mmol), 4-bromotoluene (3 mL, 4.17 g, 24 mmol), copper powder (1.56 g, 24 mmol), copper (I) iodide (100 mg), potassium carbonate (3.3 g, 24 mmol), and 5 mL hexyl ether under argon. The resulting mixture was heated to 190 °C in a sand bath for 24 h. Upon cooling to room

temperature, the reaction mixture was diluted with dichloromethane, passed through a celite plug and the solvents evaporated under reduced pressure. The residual oil thus obtained was purified by flash column chromatography (30% dichloromethane in hexanes) to yield 5.2 g (75%) of an off-white solid. m.p. 110-111 °C. ¹H NMR (400 MHz, CHCl₃) δ 2.28 (s, 3H), 3.42 (s, 3H), 6.91 (m, 7H), 7.15 (m, 4H), 7.39 (t, *J* = 7.6 Hz, 1H), 7.66 (d, *J* = 7.6 Hz, 1H). ¹³C NMR (100 MHz, CHCl₃) δ 20.7, 51.7, 121.6, 122.0, 123.5, 123.8, 128.5, 128.7, 128.8, 129.6, 131.1, 132.1, 132.5, 145.1, 146.7, 148.0, 167.9. HRMS (EI) calc for C₂₁H₁₉NO₂ [M+H]⁺ 318.1489, found 318.1481. IR (KBr plate) 693 (m), 713 (m), 753 (m), 813 (m), 1085 (m), 1125 (m), 1244 (s), 1271 (s), 1289 (s), 1320 (s), 1448 (s), 1492 (s), 1508 (s), 1594 (s), 1722 (s), 2947 (m), 3026 (m) cm⁻¹.

9,9-Dimethyl-10-(*p*-tolyl)-9,10-dihydroacridine (DHA16) + 2,9,9-Trimethyl-10-phenyl-9,10-dihydroacridine (DHA17). A flame-dried Schlenk flask was charged with 1.0 g methyl *N*-(*p*-tolyl)-*N*-phenylanthranilate (**22**, 3.1 mmol) and 45 mL dry, degassed Et₂O under argon and cooled to 0 °C in an ice bath. 2.5 Equivalents of 3.0 M methyl magnesium bromide in Et₂O (2.7 mL) was added dropwise and the reaction allowed to stir at room temperature under argon for 3 d. After quenching with saturated ammonium chloride, the organic layer was separated, washed with brine and water and dried over MgSO₄, and the solvent evaporated under reduced pressure. The crude tertiary alcohol thus formed was carried on to the next step without purification. To the neat oil isolated from the previous step was added 1-2 mL of concentrated H₂SO₄ under argon and the reaction stirred at room temperature for 1 h under argon. After dilution with 30 mL DI H₂O the reaction was poured into a 10% (v/v) aqueous ammoniacal solution and extracted with ether (5 x 50 mL). The combined organic layers were washed with saturated sodium bicarbonate, brine and water and dried over MgSO₄, and the solvent evaporated under reduced pressure. The residue was purified by flash column using gradient elution, starting with 10%

dichloromethane in hexanes and progressing to 50% dichloromethane in hexanes. 0.52 g (55%) of a mixture of **DHA16** and **DHA17** as white solid was isolated. **DHA16** and **DHA17** could not be separated from each other. m.p. 100-102 °C. ¹H NMR (400 MHz, CHCl₃) δ 1.66 (s, 9H), 2.27 (s, 3H), 2.46 (s, 3H), 6.13 (d, *J* = 8.4 Hz, 1H), 6.22 (dd, *J* = 1.2, 8.0 Hz, 1H), 6.26 (dd, *J* = 1.2 Hz, 8.0 Hz, 1H), 6.74 (dd, *J* = 1.2, 8.0 Hz, 1H), 6.92 (m, 5H), 7.18 (d, *J* = 8.4 Hz, 2 H), 7.30 (d, *J* = 8.4 Hz, 2H), 7.43 (m, 5H), 7.59 (m, 2H). ¹³C NMR (100 MHz, CHCl₃) δ 21.0, 21.6, 31.5, 31.6, 35.0, 36.2, 114.1, 114.3, 114.3, 120.4, 120.6, 125.4, 125.5, 126.1, 126.5, 126.6, 127.2, 128.4, 129.8, 130.1, 130.1, 130.2, 131.1, 131.2, 131.6, 131.8, 138.2, 138.7, 139.0, 141.3, 141.7. HRMS (ESI) calc for C₂₂H₂₁N [M+H]⁺ 300.1747, found 300.1756. IR (KBr plate) 745 (s), 886 (m), 1037 (m), 1318 (m), 1452 (m), 1479 (s), 1507 (m), 1580 (m), 1606 (m), 2966 (m) cm⁻¹.

Methyl *N*-(2-mesityl)-*N*-phenylanthranilate (24). A flame-dried Schlenk flask was charged with **14** (5 g, 22 mmol), 2-bromomesitylene (3.67 mL, 4.77 g, 24 mmol), copper powder (1.56 g, 24 mmol), copper (I) iodide (100 mg), potassium carbonate (3.3 g, 24 mmol), and 5 mL hexyl ether under argon. The resulting mixture was heated to 190 °C in a sand bath for 24 h. Upon cooling to room temperature, the reaction mixture was diluted with dichloromethane, passed through a celite plug and the solvents evaporated under reduced pressure. The residual oil thus obtained was purified by flash column chromatography (30% dichloromethane in hexanes) to yield 4.18 g (55%) of an off-white solid. m.p. 90 °C. ¹H NMR (400 MHz, CHCl₃) δ 2.03 (s, 6H), 2.30 (s, 3H), 3.26 (s, 3H), 6.65 (dd, *J* = 0.8 Hz, 8.4 Hz, 1H), 6.81 (m, 3H), 6.93 (m, 3H), 7.11 (m, 2H), 7.21 (m, 1H), 7.60 (dd, *J* = 1.6, 7.6 Hz, 1H). ¹³C NMR (100 MHz, CHCl₃) δ 19.0, 21.2, 51.5, 114.2, 117.3, 119.4, 121.1, 121.3, 122.5, 122.7, 123.2, 129.0, 129.3, 129.3, 129.6, 130.3, 130.5, 131.4, 131.9, 132.7, 134.3, 136.4, 136.9, 137.8, 138.1, 140.9, 145.0, 148.4, 168.9.

HRMS (EI) calc for $C_{23}H_{23}NO_2$ $[M+H]^+$ 346.1802, found 346.1804. IR (KBr plate) 741 (m), 756 (m), 1238 (m), 1319 (m), 1448 (s), 1483 (s), 1593 (s), 1719 (s), 2857 (m), 2918 (m), 2948 (m), 3026 (m) cm^{-1} .

9,9-Dimethyl-10-(2-mesityl)-9,10-dihydroacridine (DHA18). A flame-dried Schlenk flask was charged with 1.0 g methyl *N*-(2-mesityl)-*N*-phenylanthranilate (**24**, 2.9 mmol) and 45 mL dry, degassed Et_2O under argon and cooled to 0 °C in an ice bath. 2.5 Equivalents of 3.0 M methyl magnesium bromide in Et_2O (2.4 mL) was added dropwise and the reaction allowed to stir at room temperature under argon for 3 d. After quenching with saturated ammonium chloride, the organic layer was separated, washed with brine and water and dried over $MgSO_4$, and the solvent evaporated under reduced pressure. The crude tertiary alcohol thus formed was carried on to the next step without purification. To the neat oil isolated from the previous step was added 1-2 mL of concentrated H_2SO_4 under argon and the reaction stirred at room temperature for 1 h under argon. After dilution with 30 mL DI H_2O the reaction was poured into a 10% (v/v) aqueous ammoniacal solution and extracted with ether (5 x 50 mL). The combined organic layers were washed with saturated sodium bicarbonate, brine and water and dried over $MgSO_4$, and the solvent evaporated under reduced pressure. The residue was purified by flash column using gradient elution, starting with 10% dichloromethane in hexanes and progressing to 50% dichloromethane in hexanes. 0.57 g (60%) of a white solid was thus isolated. m.p. 85 °C. 1H NMR (400 MHz, $CHCl_3$) δ 1.69 (s, 6H), 1.96 (s, 6H), 2.37 (s, 3H), 6.07 (dd, $J = 1.6, 8.4$ Hz, 2H), 6.90 (m, 4H), 7.06 (s, 2H), 7.44 (dd, $J = 1.6, 7.6$ Hz, 2H). ^{13}C NMR (100 MHz, $CHCl_3$) δ 18.0, 20.2, 21.4, 33.5, 36.1, 112.7, 119.8, 120.4, 120.7, 126.3, 127.2, 128.6, 128.6, 129.3, 129.7, 130.4, 135.2, 138.1, 138.5, 138.7. HRMS (ESI) calc for $C_{22}H_{21}N$ $[M+H]^+$ 300.1747, found

300.1756. IR (KBr plate) 745 (s), 886 (m), 1315 (m), 1484 (s), 1507 (m), 1580 (m), 1606 (m), 2966 (m) cm^{-1} .

Compound D1. A flame-dried Schlenk flask was charged with **DHA8** (1.0 g, 2.8 mmol) and 10 mL dry dichloromethane under argon. Triethyloxonium hexachloroantimonate (1.26 g, 2.8 mmol) was added to this solution in one portion under argon. The reaction was stirred at room temperature for 12 h. A 10% aqueous solution of sodium thiosulfate was then added, the organic layer separated, washed with brine and water and dried over MgSO_4 , and the solvent evaporated under reduced pressure. The residue was purified by flash column using 50% dichloromethane in hexanes as eluent. 0.40 g (40%) of a faint-yellow solid was thus isolated. m.p. 340 °C (decomp.). ^1H NMR (400 MHz, CHCl_3) δ 3.27 (s, 6H), 6.88 (m, 18H), 7.17 (m, 16H). ^{13}C NMR (100 MHz, CHCl_3) δ 33.6, 57.4, 112.0, 112.4, 120.0, 125.3, 125.9, 126.3, 126.5, 127.4, 127.5, 127.7, 127.9, 128.3, 128.7, 130.2, 130.3, 130.5, 131.3, 131.8, 132.7, 141.5, 142.7, 146.0. HRMS (ESI) calc for $\text{C}_{52}\text{H}_{41}\text{N}$ $[\text{M}+\text{H}]^+$ 693.3264, found 693.3267. IR (KBr plate) 638 (m), 697 (m), 733 (m), 755 (m), 1270 (m), 1357 (m), 1463 (s), 1590 (m), 1589 (m), 2815 (w), 2873 (w), 3056 (m) cm^{-1} .

9,9-Dimethyl-2-nitro-9,10-dihydroacridine (26). A mixture of 0.5 g **DHA1** (2.3 mmol) and 0.8 g of either RDX or PETN were dissolved in 3.0 mL dry, degassed acetonitrile and the solution photolyzed with a solar simulator (1.3 suns AM 1.5) for 60 minutes. The reaction mixture was sampled every 10 minutes to determine the GC yield of the nitrated product. Approximately 80% of **26** (GC yield) was formed after 60 minutes of photolysis. Compound **26** was isolated by flash column chromatography using 50/50 hexanes/dichloromethane as an eluent. ^1H NMR (400 MHz, CHCl_3) δ 1.62 (s, 6H), 6.64 (s, 1H), 6.69 (d, $J = 8.8$ Hz, 1H), 6.75 (d, $J = 8.8$ Hz, 1H), 7.03 (m, 1H), 7.15 (m, 1H), 7.40 (d, $J = 7.6$ Hz, 1H), 8.02 (dd, $J = 2.4, 8.8$ Hz, 1H), 8.30 (s, 1H). ^{13}C NMR (100 MHz, CHCl_3) δ 30.7, 36.4, 113.6, 121.8, 126.7, 127.9, 130.2, 148.6. HRMS (ESI)

calc for $C_{15}H_{14}N_2O_2$ $[M+H]^+$ 255.1128, found 255.1123. IR (KBr plate) 753 (s), 1053 (m), 1232 (m), 1347 (m), 1383 (w), 1456 (s), 1483 (s), 1582 (s), 1615 (w), 2924 (m) cm^{-1} .

2-Nitro-9,9-diphenyl-9,10-dihydroacridine (28). Method A. A mixture of 0.5 g **DHA4** (1.5 mmol) and 0.8 g of either RDX or PETN were dissolved in 3.0 mL dry, degassed acetonitrile and the solution photolyzed with a solar simulator (1.3 suns AM 1.5) for 60 minutes. The reaction mixture was sampled every 10 minutes to determine the GC yield of the nitrated product. Approximately 80% of **28** (GC yield) was formed after 60 minutes of photolysis. Compound **28** was isolated by flash column chromatography using 50/50 hexanes/dichloromethane as an eluent. 1H NMR (400 MHz, $CHCl_3$) δ 7.12 (broad m, 16H), 8.02 (dd, $J = 8.8, 2.2$ Hz, 1H), 8.30 (d, $J = 2.2$ Hz, 1H). ^{13}C NMR (100 MHz, $CHCl_3$) δ 56.7, 113.5, 120.2, 125.6, 126.1, 126.2, 127.1, 127.4, 127.5, 127.6, 127.9, 128.5, 131.0, 133.2, 137.3, 142.7, 146.0, 149.3. HRMS (ESI) calc for $C_{25}H_{19}N_2O_2$ $[M+H]^+$ 379.1441, found 393.1447. IR (KBr plate) 699 (m), 762 (m), 907 (m), 1300 (m), 1330 (m), 1483 (s), 1529 (m), 1585 (s), 2922 (m), 3410 (m) cm^{-1} . **Method B.** Compound **28** was also synthesized by nitrating **DHA4**: A 25 mL round bottom flask was charged with 0.5 g **DHA4** (1.5 mmol) and 20 mL dry dichloromethane under argon and the solution was cooled to $-78^\circ C$ in an acetone/dry ice bath. Approximately 0.2 g of 25% HNO_3 on silica gel was then added to the solution and the reaction stirred at $-78^\circ C$ for 1 h. Upon warming to room temperature, the reaction was filtered and the solvent evaporated under reduced pressure. The residue was purified by flash column chromatography using 50/50 hexanes/dichloromethane as eluent. 40% of the mononitrated product (**28**) and 30% of the dinitrated product was thus isolated.

9,9-Dimethyl-2-nitro-10-(2-mesityl)-9,10-dihydroacridine (30). A mixture of 0.5 g **DHA18** (1.5 mmol) and 0.8 g of either RDX or PETN were dissolved in 3.0 mL dry, degassed

acetonitrile and the solution photolyzed with a solar simulator (1.3 suns AM 1.5) for 60 minutes. The reaction mixture was sampled every 10 minutes to determine the GC yield of the nitrated product. Approximately 82% of **30** (GC yield) was formed after 60 minutes of photolysis. Compound **30** was isolated by flash column chromatography using 50/50 hexanes/dichloromethane as an eluent. ¹H NMR (400 MHz, CHCl₃) δ 1.74 (s, 6H), 1.96 (s, 6H), 2.41 (s, 3H), 6.11 (d, *J* = 9.2 Hz, 1H), 6.17 (dd, *J* = 2.8, 8.0 Hz, 1H), 7.01 (m, 2H), 7.11 (s, 2H), 7.48 (m, 1H), 7.84 (dd, *J* = 2.4, 9.2 Hz, 1H), 8.36 (d, *J* = 2.8 Hz, 1H). ¹³C NMR (100 MHz, CHCl₃) δ 17.8, 21.4, 33.6, 36.3, 68.8, 112.4, 113.8, 122.8, 123.2, 123.9, 126.4, 127.7, 129.7, 130.0, 130.7, 134.1, 137.0, 137.5, 139.1, 141.0, 144.1. HRMS (ESI) calc for C₂₄H₂₅N₂O₂ [M+H]⁺ 373.1911, found 373.1913. IR (KBr plate) 750 (m) 848 (m), 1289 (s), 1306 (s), 1320 (s), 1475 (s), 1496 (s), 1592 (m), 1651 (s), 2918 (m), 2969 (m) cm⁻¹.

9,9-Diethyl-2-nitro-9,10-dihydroacridine (31) and Compound 33. A mixture of 0.5 g **DHA2** (2.1 mmol) and 0.8 g of either RDX or PETN were dissolved in 3.0 mL dry, degassed acetonitrile and the solution photolyzed with a solar simulator (1.3 suns AM 1.5) for 60 minutes. Compounds **31** and **33** were isolated by flash column chromatography using 50/50 hexanes/dichloromethane as an eluent. Compound **33** co-eluted with unreacted **DHA2** and, therefore, could not be completely separated from **DHA2**. **Compound 31:** ¹H NMR (400 MHz, CHCl₃) δ 0.59 (t, *J* = 7.2 Hz, 6H), 1.96 (quartet, *J* = 7.2 Hz, 4H), 6.47 (s, 1H), 6.60 (d, *J* = 8.8 Hz, 1H), 6.67 (d, *J* = 1.2 Hz, 1H), 7.00 (m, 1H), 7.12 (m, 1H), 7.24 (m, 1H), 7.97 (d, *J* = 2.8 Hz, 1H), 8.00 (s, 1H). ¹³C NMR (100 MHz, CHCl₃) δ 9.7, 38.8, 46.3, 112.9, 114.1, 122.8, 123.9, 124.1, 124.5, 125.2, 127.0, 127.4, 137.6, 145.2. HRMS (ESI) calc for C₁₇H₁₉N₂O₂ [M+H]⁺ 283.1441, found 283.1443. IR (KBr plate) 746 (m), 823 (m), 1242 (s), 1282 (s), 1294 (s), 1329 (m), 1462 (m), 1487 (s), 1530 (s), 1578 (9s), 1609 (m), 2932 (m), 2968 (m), 3352 (s) cm⁻¹.

Compound 33: ^1H NMR (400 MHz, CHCl_3) δ 0.91 (t, $J = 7.6$ Hz, 3H), 0.97 (t, $J = 7.6$ Hz, 3H), 1.48 (d, $J = 6.8$ Hz, 2H), 1.79 (d, $J = 6.8$ Hz, 3H), 2.24 (q, $J = 7.6$ Hz, 2H), 2.35 (q, $J = 7.6$ Hz, 2H), 5.48 (m, 1H), 5.72 (m, 1H), 5.74 (s, 1H), 6.90 (m, 4H), 7.06 (m, 5H). ^{13}C NMR (100 MHz, CHCl_3) δ 13.0, 13.1, 13.9, 14.8, 24.3, 31.7, 115.9, 116.8, 118.2, 118.5, 120.3, 120.5, 121.0, 121.2, 123.0, 124.9, 127.4, 127.5, 129.5, 129.7, 130.1, 130.2, 134.3, 140.1, 140.3, 141.2, 143.5, 143.7. HRMS (ESI) calc for $\text{C}_{17}\text{H}_{17}\text{N}$ $[\text{M}+\text{H}]^+$ 236.1434, found 236.1438. IR (KBr plate) 692 (m), 745(m), 1309(m), 1451 (m), 1506(s), 1575 (m), 1594 (s), 2925(m), 2963(m), 3405 (m) cm^{-1} .

2.17 References and Notes

- (1) Jungreis, E. in *Spot Test Analysis: Clinical, Environmental, Forensic, and Geochemical Applications*, 2nd ed., J Wiley, New York, 1997.
- (2) For representative examples see: (a) Che, Y.; Yang, X.; Liu, G.; Yu, C.; Ji, H.; Zuo, J.; Zhao, J.; Zang, L. *J. Am. Chem. Soc.* **2010**, *132*, 5743-5750. (b) Lan, A.; Li, K.; Wu, H.; Olson, D. H.; Emge, T. J.; Ki, W.; Hong, M.; Li, J. *Angew. Chem. Int. Ed.* **2009**, *48*, 2334-2338. (c) Tao, S.; Yin, J.; Li, G. *J. Mater. Chem.* **2008**, *18*, 4872-4878.
- (3) (a) Toal, S. J.; Trogler, W. C. *J. Mater. Chem.* **2006**, *16*, 2871-2883. (b) Yang, J.-S.; Swager, T. M. *J. Am. Chem. Soc.* **1998**, *120*, 5321-5322.
- (4) Engel, Y.; Elnathan, R.; Pevzner, A.; Davidi, G.; Flaxer, E.; Patolsky, F. *Angew. Chem. Int. Ed.* **2010**, *49*, 6830-6835.
- (5) (a) Bruschini, C. *Subsurf. Sens. Technol. Appl.* **2001**, *2*, 299-336. (b) Takats, Z.; Cotte-Rodriguez, I.; Talaty, N.; Chen, H.; Cooks, R. G. *Chem. Commun.* **2005**, 1950-1952.
- (6) Eilbert, R. F. in *Aspects of Explosives Detection*, Eds: M. Marshall, J. C. Oxley, Elsevier, London, **2009**, pp. 89-130.

- (7) Andrew, T. L.; Swager, T. M. *J. Am. Chem. Soc.* **2007**, *129*, 7254-7255.
- (8) Cope, W. C.; Barab, J. *J. Am. Chem. Soc.* **1917**, *39*, 504-514.
- (9) Balakrishnan, V. K.; Halasz, A.; Hawari, J. *Environ. Sci. Technol.* **2003**, *37*, 1838-1843.
- (10) Greiss, P. *Ber. Dtsch. Chem. Ges.* **1879**, *12*, 427-434.
- (11) Zeller, H. D. *Analyst*, **1955**, *80*, 632-640.
- (12) (a) Hawari, J.; Halasz, A.; Groom, C.; Deschamps, S.; Paquet, L.; Beaulieu, C.; Corriveau, A. *Environ. Sci. Technol.* **2002**, *36*, 5117-5123. (b) Just, C. L.; Schnoor, J. L. *Environ. Sci. Technol.* **2004**, *38*, 290-295. (c) Burton, D. T.; Turley, S. D. *Bull. Environ. Contam. Toxicol.* **1995**, *55*, 89-95. (d) Glover, D. J.; Hoffsommer, J. C. Technical Report for Naval Surface Weapons Center: Silver Spring, MD, February **1979**.
- (13) (a) Sanchez, J. C.; Trogler, W. C. *J. Mater. Chem.* **2008**, *18*, 3143-3156. (b) Roos, B. D.; Brill, T. B. *Combust. Flame.* **2002**, *128*, 181-190.
- (14) (a) Peyton, G. R.; LaFaivre, M. H.; Maloney, S. W. CERL Technical Report for US Army Corps of Engineers: Champaign, IL, November 1999. (b) Gowenlock, B. G.; Pfab, J.; Young, V. M. *J. Chem. Soc., Perkin Trans. 2*, **1997**, 915-919. (c) Pace, M. D. *J. Phys. Chem.* **1994**, *98*, 6251-6257.
- (15) Bark, L. S.; Catterall, R. *Mikrochim. Acta.* **1960**, *4*, 553-558.
- (16) Demethylation of DMA has been observed in other cases: (a) Macdonald, T. L.; Gutheim, W. G.; Martin, R. B.; Guengerich, F. P. *Biochemistry*, **1989**, *28*, 2071-2077. (b) Doyle, M. P.; Can Lente, M. A.; Mowat, R.; Fobare, W. F. *J. Org. Chem.* **1980**, *45*, 2570-2575.
- (17) DMNA generally displays a low fluorescence quantum yield because it is susceptible to photolytic cleavage upon excitation: (a) Costela, A.; Garcia-Moreno, I.; Garcia, O.;

- Sastre, R. *Chem. Phys. Lett.* **2001**, *347*, 115-120 (laser irradiation at 337 nm); (b) Görner, H.; Döpp, D. *Photochem. Photobiol. Sci.* **2002**, *1*, 270-277.
- (18) Donor-acceptor anilines containing a nitro group as the “acceptor” component have been previously shown to be acceptable fluorophores. For example, see: Gruen, H.; Görner, H. *J. Phys. Chem.* **1989**, *93*, 7144-7152.
- (19) Compound **17** was synthesized following a previously published procedure: Campeau, L.-C.; Parisien, M.; Jean, A.; Fagnou, K. *J. Am. Chem. Soc.*, **2006**, *128*, 581-590, but is also commercially available.
- (20) Oka, H.; Kouno, H.; Tanaka, H. *J. Mater. Chem.* **2007**, *17*, 1209-1215.
- (21) The poor reactivity of the hexafluoroisopropanol group toward Friedel-Crafts reactions has been observed before: Amara, J. P.; Swager, T. M. *Macromolecules*, **2006**, *39*, 5753-5759 and references therein.
- (22) Seo, E. T.; Nelson, R. F.; Fritsch, J. M.; Marcoux, L. S.; Leedy, D. W.; Adams, R. N. *J. Am. Chem. Soc.* **1966**, *88*, 3498-3503.
- (23) Rathore, R.; Kumar, A. S.; Lindeman, S. V.; Kochi, J. K. *J. Org. Chem.* **1998**, *63*, 5847-5856.
- (24) Nitric acid on silica gel (SiO₂:HNO₃) was previously used to controllably mono-nitrate electron rich calixarenes: Xu, B.; Swager, T. M. *J. Am. Chem. Soc.* **1993**, *115*, 1160-1162.
- (25) Strongly solvent-dependent fluorescence quantum yields have been previously observed for donor-acceptor chromophores. For example, see ref. 18.
- (26) Craig, D. *J. Am. Chem. Soc.* **1935**, *57*, 195.

- (27) (a) Sheldrick, G. M. *Acta Cryst. A* **1990**, *46*, 467. (b) Sheldrick, G. M. SHELXL 91, Universität Göttingen, Göttingen, Germany, 1997
- (28) Demas, J. N.; Crosby, G. A. *J. Phys. Chem.* **1971**, *75*, 991.
- (29) For a representative reference on the procedure followed see: Hill, R.D.; Puddephatt, R. *J. J. Am. Chem. Soc.* **1985**, *107*, 1218.
- (30) Hatchard, C.G.; Parker, C. A. *Proc. R. Soc. London A* **1956**, 235, 518.

2.18 Additional Figures

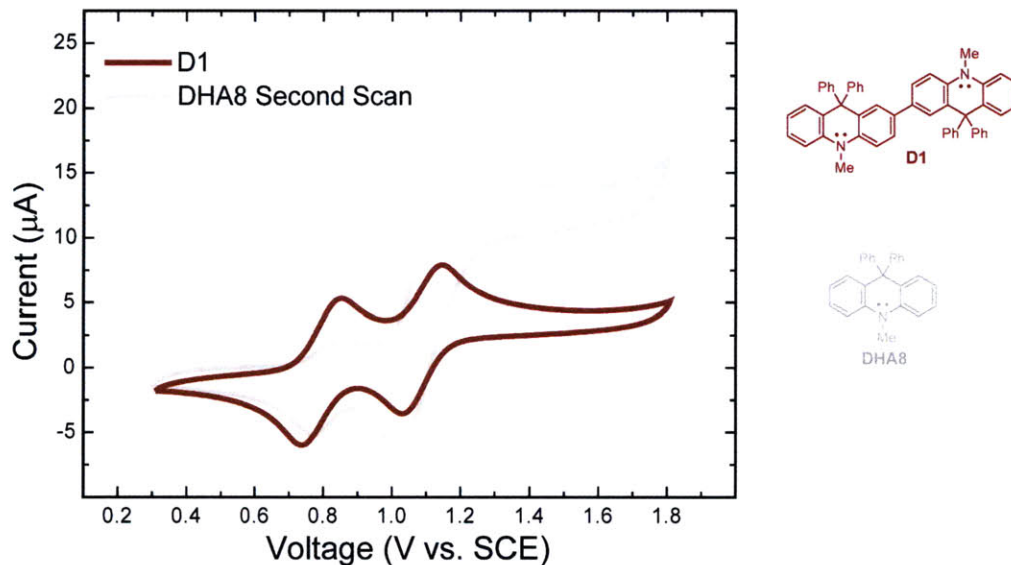


Figure A1. Cyclic voltammogram (CV) of **D1** (red line) and the second scan of the CV of **DHA8** (grey line). The CV of **D1** displays the same peaks observed to appear after an initial oxidative sweep of **DHA8**, thus confirming that **DHA8** dimerizes in the electrochemical cell.

CHAPTER 3

Using Organic Photochromic Molecules to Enable Optical Nanopatterning

Completed in collaboration with Professor Rajesh Menon¹ and Hsin-Yu Tsai²

Adapted and reprinted in part with permission from:
Andrew, T. L.; Tsai, H.-Y.; Menon, R. “Confining Light to Deep Subwavelength Dimensions to
Enable Optical Nanopatterning” *Science*, **2009**, 324, 917-921.

3.1 Introduction

Optical patterning is the primary enabler of microscale devices. However, the Achilles heel of optics is resolution. The far-field diffraction barrier limits the resolution of optical systems to approximately half the wavelength,³ and therefore restricts nanoscale patterning at visible wavelengths. Scanning-electron-beam patterning has thus become the preferred method for fabricating nanostructures. However, electrons are affected by extraneous electromagnetic fields, limiting the accuracy to which patterns can be placed relative to one another.⁴ Furthermore, electron-flux is limited by mutual repulsion effects, constraining the patterning speed.⁵ The vacuum environment and electron lenses increase system complexity and cost. Alternatively, the diffraction barrier can be overcome in the optical near-field.⁶ The high spatial frequencies present in the optical near-field are evanescent, and hence, the recording medium needs to be placed at a precisely controlled nanometric distance from the source of the optical near-field.⁷ By placing a pre-patterned photomask in intimate contact with the photoresist, the optical near-field may be recorded.⁸ In this case, high resolution is achieved at the expense of an inflexible and costly photomask, and the high probability of contamination of the contacted surfaces. An alternative approach scans one or many nanoscale tips in close proximity to the sample.⁹ Precisely maintaining the gap between the tip (or tips) and the sample is problematic, especially when patterning over large areas or with multiple near-field probes.¹⁰ Plasmonic lenses can alleviate some of these problems,¹¹ but they still require sub-100 nm gaps and nanometric gap control.¹²

To overcome these limitations, we have used a thin photochromic film on top of the recording photoresist layer. The molecules chosen to comprise the film adopt two isomeric forms that interconvert on respective absorption of light at ultraviolet (λ_1) and visible (λ_2)

wavelengths.¹³ We simultaneously apply both colors in an interference pattern that overlaps peaks at λ_1 with nodes at λ_2 . Absorption at λ_1 generates the isomer transparent at that wavelength, but regions exposed to λ_2 revert to the initial isomer and continue to absorb at λ_1 , protecting the photoresist. Only at the λ_2 nodes does a stable, transparent aperture form (see Figure 3.1A).¹⁴ Photons at λ_1 tunnel through this aperture, forming a nanoscale writing beam that can pattern the underlying photoresist. The size of the aperture decreases as the ratio of the intensity at λ_2 with respect to that at λ_1 increases.^{14,15} This technique, which we refer to as absorbance modulation, can therefore, confine light to spatial dimensions far smaller than the wavelength.

Furthermore, because the photochromic molecules recover their initial opaque state, spatial periods smaller than the incident wavelengths can be achieved by repeated patterning.¹⁶ In Figure 3.1B, we plot the simulated full-width at half-maximum (FWHM) of the transmitted light at λ_1 as a function of the ratio of intensities at the two wavelengths, illustrating that the transmitted light is spatially confined to dimensions far below the wavelength. In other words, optical near-fields are generated without bringing a physical probe into close proximity with the sample. In the past, we used an interferometric setup to illuminate an azobenzene-polymer based photochromic film with a standing wave at λ_2 and uniform illumination at λ_1 .¹⁵ Although linewidths as small as $\lambda_1/4$ were demonstrated, the thermal instability of the azobenzene polymer as well as the non-negligible sensitivity of the underlying photoresist to λ_2 prevented further scaling below 100 nm.

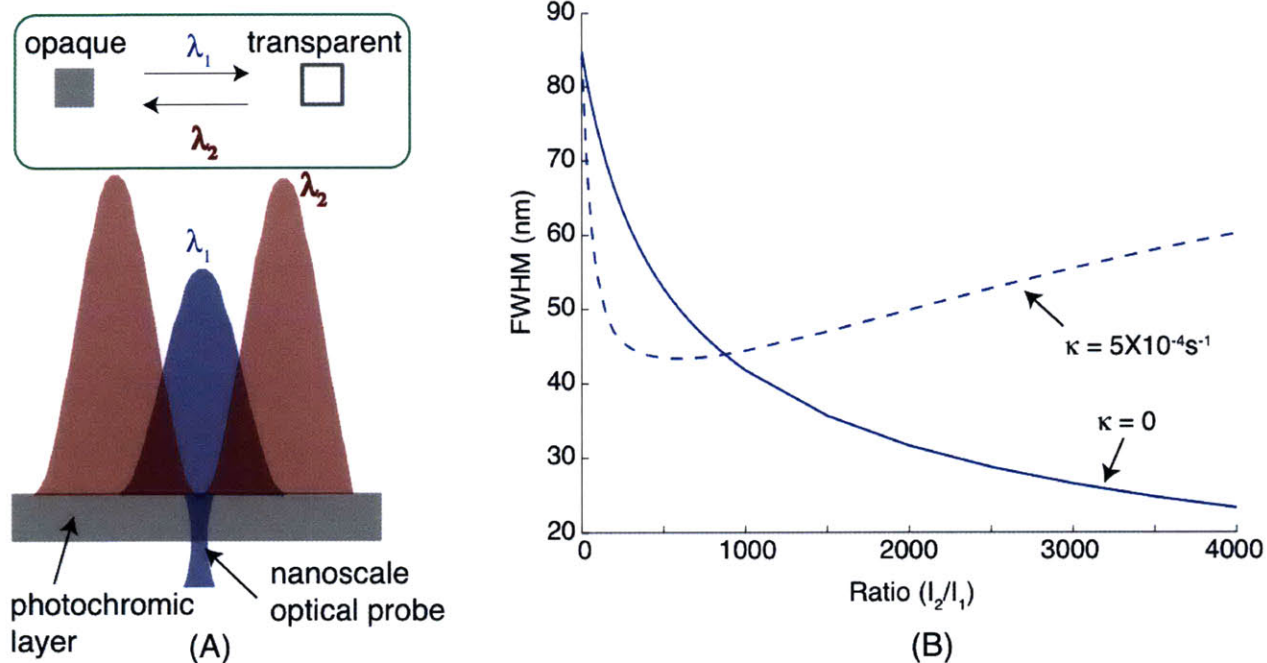


Figure 3.1. The scheme of absorbance modulation. (A) The photochromic layer turns transparent upon exposure to λ_1 and opaque upon exposure to λ_2 . When illuminated with a node at λ_2 coincident with a peak at λ_1 , a sub-wavelength transparent region (or aperture) is formed through which photons at λ_1 penetrate, forming a nanoscale optical writing beam. (B) Full-width at half-maximum (FWHM) of the intensity distribution at λ_1 directly beneath the photochromic layer as a function of the ratio of the peak intensities at the two wavelengths. When the photochromic molecules are thermally stable (the thermal rate constant, $\kappa = 0$), the size of the writing beam decreases monotonically, far below the wavelength. However, when a thermal instability is present ($\kappa = 5 \times 10^{-4} \text{ s}^{-1}$), the smallest beam size is limited, as shown by the dashed line.

For optimum performance, it is essential that the photochromic molecules are thermally stable; otherwise the size of the writing beam becomes dependent on the absolute intensities rather than their ratio alone. If the photochromic molecule in the transparent state is thermally unstable, then at low λ_1 intensities, the thermal back-reaction overwhelms the forward (opaque-to-transparent) reaction, essentially closing the aperture. The FWHM of the resulting beam shows a minimum. This is illustrated in Figure 3.1B, where the photochromic parameters of compound **1** (see Figure 3.2b) were assumed.¹⁷ A thermal rate constant of $5 \times 10^{-4} \text{ s}^{-1}$ was assumed for the dashed curve. The incident illumination is modelled as standing waves of period 350 nm ($\lambda_2 = 633 \text{ nm}$) and 170 nm ($\lambda_1 = 325 \text{ nm}$). Both curves were calculated by decreasing the peak intensity of the λ_1 standing wave while maintaining the peak intensity of the λ_2 standing wave equal to 1 KW/m^2 , and repeating the numerical simulation for each intensity ratio. Although this deleterious effect can be overcome by using higher intensities at both wavelengths while maintaining the required intensity ratio, it is highly desirable to achieve nanoscale resolution at low intensities.

For this reason, we turned our attention to thermally-stable classes of photochromes, such as fulgides¹⁸ and diarylethenes.¹⁹ In both these classes of photochromes, photoinduced (conrotatory) electrocyclic rearrangements transform a colorless (*i.e.*, UV-absorbing) triene system into a highly-colored cyclohexadiene photoproduct, and vice-versa. Due to steric hinderance, the barrier to electrocyclization/retrocyclization in these systems is high and cannot be practically overcome thermally.¹⁹ Therefore, conversion between the open-ring and closed-ring isomers is primarily photoinitiated, and the thermal contribution to this isomerisation is negligible.

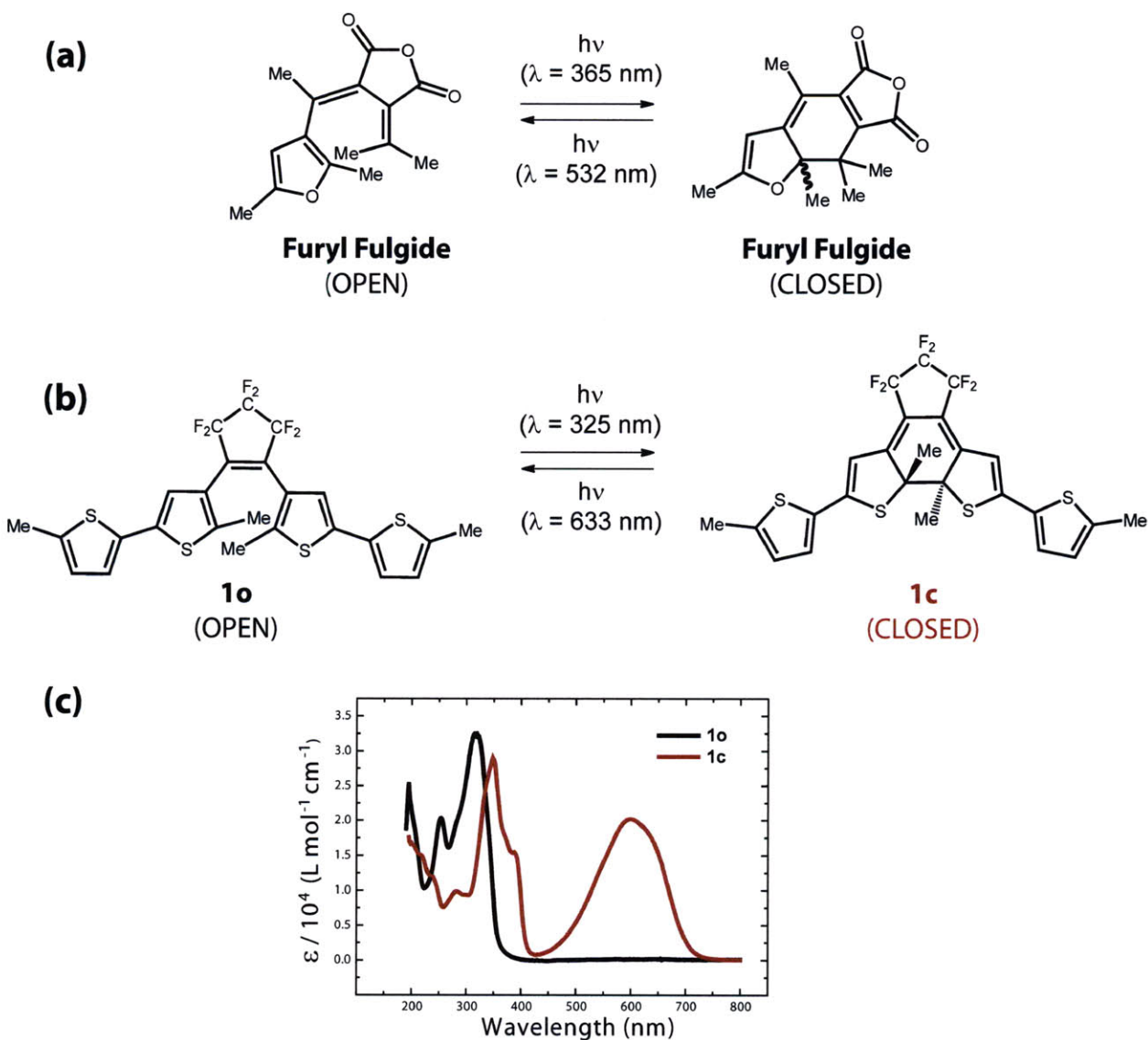


Figure 3.2. (a) Structures of the open- and closed-ring isomers of (a) furyl fulgide and (b) 1,2-bis(5,5'-dimethyl-2,2'-bithiophen-yl) perfluorocyclopent-1-ene or compound **1**. (c) Absorbance spectra of **1** in the open and closed forms in hexane. ϵ is the decadic molar absorptivity.

3.2 Results and Discussion

Initial investigations of furyl fulgide²⁰ (Figure 3.2a) as the active component in the absorbance-modulation layer (AML) revealed a susceptibility to photodegradation that significantly reduced the concentration of this photochrome in the AML with prolonged

irradiation. cursory analysis of some fulgides reported in the chemical literature confirmed that many fulgides display a lack of fatigue resistance due to photooxidation of either their triene or heterocyclic moieties.¹⁸ Therefore, we explored a comparatively photostable class of thiophene-substituted fluorinated cyclopentenones as potential photochromes for absorbance modulation. The perfluorinated bridge in these systems prevents photooxidation of the active triene moiety and suppresses competing, non-productive isomerization pathways. Specifically, 1,2-bis(5,5'-dimethyl-2,2'-bithiophen-yl) perfluorocyclopent-1-ene (**1**, shown in Figure 3.2(b)) was chosen for use in the AML because it displayed an absorption band centered at 313 nm in the open state and one centered at 582 nm in the closed state. These spectral features allowed use of the 325 nm line of the helium-cadmium laser and the 633 nm line of the helium-neon laser for the writing and the confining beams, respectively. High intensities could be applied at the nodal wavelength, λ_2 because 633 nm light has no effect on most photoresists.

Pertinent photophysical constants, such as absorption coefficients and photoreaction quantum yields, were measured for compound **1** at room temperature in hexane solution (Table 3.1, Experimental Section).

In order to spin-cast the photochromic layer, we used a 30 mg/ml solution of poly(methyl methacrylate) (PMMA) in anisole doped with 92 wt% compound **1** (with respect to PMMA). The photochromic layer was to be placed atop a photoresist layer to record the transmitted light at λ_1 . The solvent for the PMMA matrix, anisole, distorts the development rate of the photoresist. Therefore, a barrier layer of poly(vinyl alcohol) (PVA) was placed in between the two layers. The barrier layer also prevents any inter-diffusion between the two layers. Because the high-spatial-frequency content of the nanoscale writing beam is evanescent, it is important to keep the thickness of the PVA layer as small as possible.

In order to illustrate the effect of the thickness of the PVA layer on the linewidth of the pattern, we simulated the transmission of light through a sub-wavelength aperture in a metal film using custom-software that implements the finite-difference-time domain (FDTD) method.²¹ When a sub-wavelength aperture is illuminated, the transmitted light is primarily composed of evanescent high-spatial frequency components. These components decay exponentially away from the aperture increasing the FWHM of the transmitted light. Illumination of a one-dimensional aperture of width 75 nm was simulated with a plane wave of wavelength 325 nm as shown in the schematic in Figure 3.3A. The electric field of the incident wave was polarized normal to the plane of the figure. The time-averaged intensity of the scattered light was calculated at steady state. Cross-sections of the normalized intensity distribution in planes parallel to the aperture at varying distances from the aperture were computed and plotted in Figure 3.3B. Clearly, the transmitted light is significantly broadened with distance from the aperture. Furthermore, the peak intensity at the center of the line also falls exponentially with distance from the aperture.

These theoretical predictions were qualitatively confirmed by our experimental results. Figures 3.4A and 3.4B show scanning-electron micrographs of the cross-sections of exposed and developed photoresist with PVA barrier layer thicknesses of 25 nm and 8 nm, respectively. For the 25 nm layer, the exposed line exhibits significant broadening with depth into the photoresist. The sidewall profile bears a qualitative resemblance to the intensity contours in Figure 3.3A. For the thinner PVA, this linewidth broadening is significantly curtailed and the photoresist exhibits vertical sidewalls. This result also suggests that an ultra-thin photoresist layer may be necessary to faithfully record the high spatial frequencies in the near-field, which is in agreement with earlier work.²²

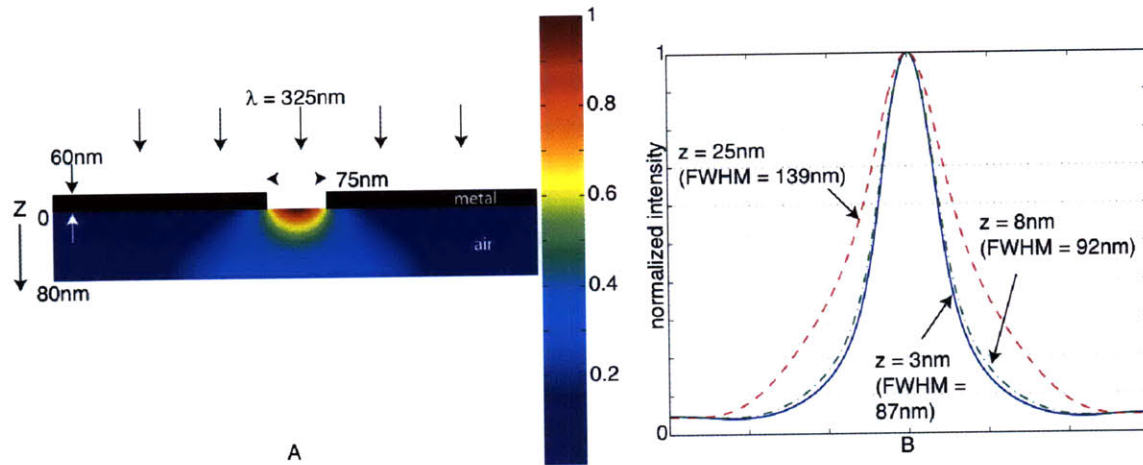


Figure 3.3. Effect of barrier-layer thickness on the patterned linewidth. (A) FDTD simulation of light transmission through a one-dimensional sub-wavelength aperture. The incident light was assumed to be a uniform plane wave with electric field polarized into the plane of the figure. The metal was assumed to have $\epsilon = 0.85 + i2.01$. The metal film was placed in air. (B) Cross-sections of the normalized intensity distributions at different distances from the aperture. The evanescent high spatial frequencies die away from the aperture, and the linewidth increases.

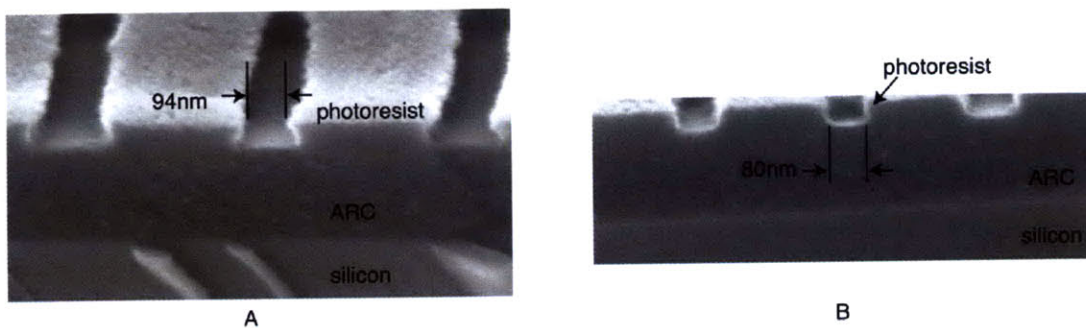


Figure 3.4. Scanning-electron micrographs of cross-sections of exposed and developed lines in photoresist where the PVA barrier layer thickness was (A) 25 nm and (B) 8 nm, respectively. Clearly, the thinner the PVA layer, the straighter the resist sidewall, and smaller the exposed line. In both cases, the period of the lines is 350 nm, corresponding to the period of the λ_2 standing wave.

To minimize this effect of line broadening, we used a PVA film thickness of 8 nm, which was found to be sufficient to protect the photoresist from the solvent for the photochromic layer. Samples consisted of a silicon substrate spin-coated with 200 nm of anti-reflection coating (ARC), 200 nm of photoresist, 8 nm of PVA and 410 nm of the photochromic layer. After exposure, the samples were rinsed in de-ionized water in a sonicator for about five minutes, which removed the PVA layer as well as the photochromic overlayer. The photoresist was baked on a hot-plate at 120 °C for 90 seconds, and developed in 0.26 N tetramethyl ammonium hydroxide (TMAH) for 60 seconds. The resulting patterns were inspected in a scanning-electron microscope after sputter-coating with about 2nm of a palladium/gold alloy.

The exposure system was a modified Lloyd's-mirror interferometer (see Figure 3.8, Experimental Section), comprising a mirror at right-angles to a vacuum chuck that held the sample. This configuration was illuminated at $\lambda_1 = 325$ nm and $\lambda_2 = 633$ nm. The angles of incidence of the two wavelengths were adjusted such that the resulting standing waves on the sample had periods of 350 nm at $\lambda_2 = 633$ nm and 170 nm at $\lambda_1 = 325$ nm. As illustrated in Figure 3.5A, the nodes of the λ_2 standing wave approximately coincide with every other peak of the λ_1 standing wave. Photokinetic simulation using the extracted photochromic parameters reveal that the transmitted light at λ_1 is significantly narrower than the diffraction limit. The scanning-electron micrograph in Figure 3.5B shows that the average width of the lines recorded in the photoresist was 36 nm, which is close to one-tenth of λ_1 . Furthermore, the narrow lines were spaced by 350 nm, which corresponds to the period of the λ_2 standing wave. We separately confirmed that the photoresist is not sensitive to the λ_2 photons. Those λ_1 peaks that coincide with the λ_2 peaks were suppressed beyond the photochromic layer. We confirmed this experimentally by recording lines at lower intensity ratios and examining their cross-sections in

the scanning-electron microscope (Figure 3.9, Experimental Section). In our current setup, in order to maintain high intensity in the λ_2 peaks, it was necessary to forgo spatial-filtering of the λ_2 illumination. High-frequency noise therefore persisted in the λ_2 standing wave, causing line-edge roughness as well as the line-width variation in the photoresist patterns. Nevertheless, these results clearly demonstrate the feasibility of deep sub-wavelength localization of light using absorbance modulation.

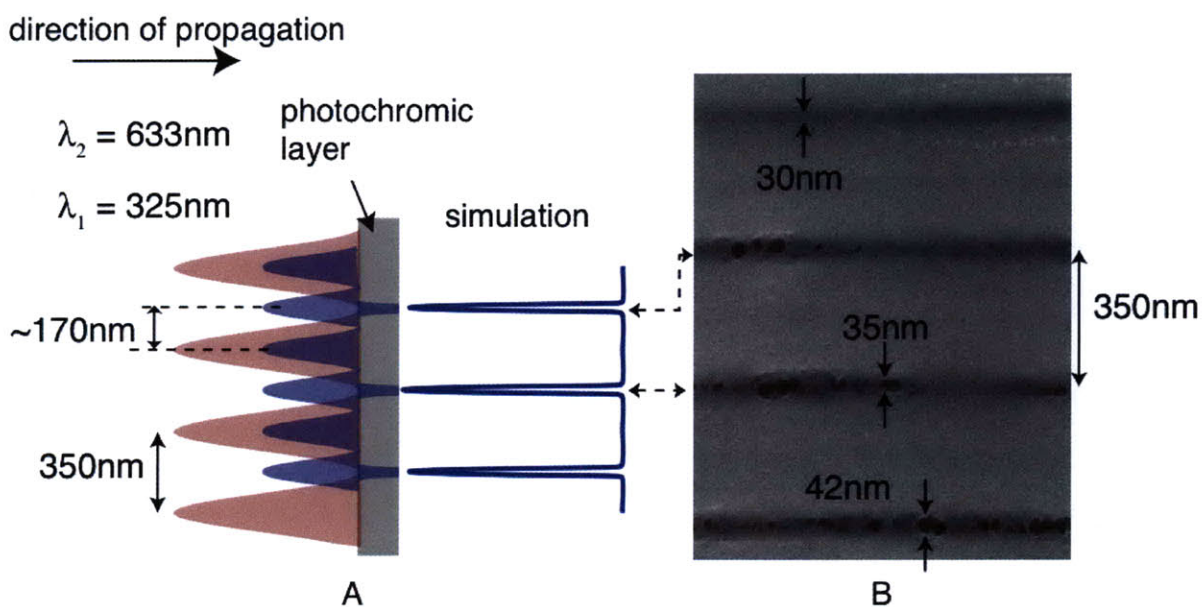


Figure 3.5. Deep sub-wavelength patterning using absorbance modulation. (A) The photochromic layer is illuminated by two overlapping standing waves of period 350 nm ($\lambda_2 = 633\text{ nm}$) and 170 nm ($\lambda_1 = 325\text{ nm}$), respectively. Simulating the transmitted light at λ_1 supported narrow lines where the peaks of the λ_1 standing wave coincided with the nodes of the λ_2 standing wave. (B) Scanning-electron micrograph of lines exposed in photoresist. Lines as narrow as 30 nm were resolved. The average linewidth was about 36 nm . The narrow lines were spaced by 350 nm corresponding to the period of the λ_2 standing wave. The transmitted light at λ_1 is suppressed where the peaks at the two wavelengths overlap.

Furthermore, these results also demonstrate the feasibility of patterning periodic lines far smaller than their spatial period. Since the absorbance of the AML is reversible, interspersed multiple exposures could pattern lines spaced apart by a distance far smaller than the far-field diffraction limit of the optical system. Although the current demonstration utilized one-dimensional standing waves, we anticipate straightforward extension to two-dimensional peaks and nodes, which can be generated by diffractive micro-optics.²³ Furthermore, such nanoscale optical beams may also be useful for optical nanoscopy.²⁴

3.3 Conclusions

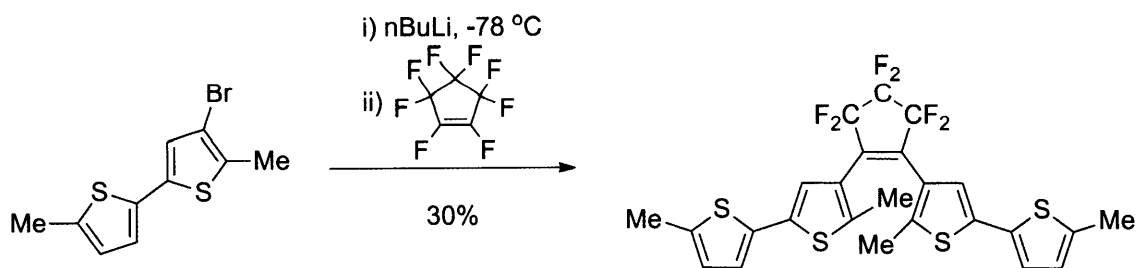
In the past, the formation of microscale patterns in the far field by light has been diffractively limited in resolution to roughly *half* the wavelength of the radiation used. Here, we demonstrated lines with an average width of 36 nm, about *one-tenth* the illuminating wavelength ($\lambda_1 = 325$ nm), made by applying a film of thermally-stable photochromic molecules above the photoresist. Simultaneous irradiation of a second wavelength ($\lambda_2 = 633$ nm) rendered the film opaque to the writing beam except at nodal sites, which let through a spatially constrained segment of incident λ_1 light, allowing subdiffractive patterning. The same experiment also demonstrated a patterning of periodic lines whose widths were about one-tenth their period, which is far smaller than what has been thought to be lithographically possible.

3.4 Experimental Section

Sample preparation. A silicon wafer was spin-coated with a solution of BarLi anti-reflection coating at 6000 rpm for 60 seconds and baked on a hot-plate at 175 °C for 90 seconds to form a 200 nm layer. Then, the sample was spin-coated with the photoresist at 4000 rpm for

60 s and baked on a hot-plate at 90 °C for 90 s to form a 200 nm layer. The photoresist was comprised of a blend of a chemically amplified positive-tone photoresist, TDUR-P308 (Tokyo Ohka Kogyo Co. Ltd.) and a photoacid generator, CGI-725 (CIBA Specialty Chemicals, Inc.) in the ratio of approximately 5:1 by weight. Then, the sample was spin-coated with a solution of PVA in water (5.7 μg/ml) at 6000 rpm and air-dried for 5 minutes to form a film of thickness 8 nm. Finally, the sample was spin-coated with the PMMA solution doped with the photochromic molecules at 500 rpm and air-dried for 5 minutes to form a layer of thickness 410 nm. The results shown in Figure 3.3 were conducted in the same manner, except that the photoresist comprised of a blend of TDUR-P308 (Tokyo Ohka Kogyo Co. Ltd.) and a photoacid generator, Irgacure PAG-103 (CIBA Specialty Chemicals, Inc.) in the ratio 20:1 by weight. The thickness of this photoresist layer was 73 nm.

Photochrome Synthesis and Characterization. Furyl fulgide was synthesized according to a literature procedure.²⁰ Compound **1o** was synthesized as shown in Scheme 3.1 following a literature procedure²⁵ and isolated in 30% yield.



Scheme 3.1. Synthesis of **1o**

Compound **1o** was recrystallized from pentanes and stored in the dark to exclude formation of **1c**. Compound **1c** was synthesized by irradiating a degassed solution of **1o** in hexanes for 30

minutes at 313 nm and by purifying the resulting reaction mixture via high performance liquid chromatography (HPLC).

The decadic molar absorption coefficients of the open and closed forms of compound **1** at 325 (λ_1) and 633 nm (λ_2) (ϵ_{1open} , $\epsilon_{1closed}$, ϵ_{2open} , $\epsilon_{2closed}$) were calculated using the integrated form of the Beer-Lambert Law ($\alpha = \epsilon lc$, where α is absorbance, l is the optical path length and c is the concentration) as follows. A known quantity of pure compound **1** (open) and compound **1** (closed) was dissolved in hexanes in the dark. Approximately 3 mL of these two solutions were placed in quartz cuvettes with an optical path length of 1 cm and the absorbance spectrum recorded. The absorbance values thus obtained at 313, 325 and 633 nm were used in the integrated Beer-Lambert equation to calculate the experimental absorption coefficients.

The quantum yield of cyclization was defined as the moles compound **1** (closed) formed per mole photon absorbed by the sample. Cyclization quantum yields were obtained by irradiating hexane solutions (of known concentrations) of compound **1** (open) at 313 or 325 nm and monitoring the change in absorbance at 633 nm at 5 s intervals. Figure 3.6(a) shows the absorbance profile of the photocyclization reaction recorded every 5 seconds. A 500 W Xenon arc lamp was used as the light source and the irradiation wavelength isolated by passing the light through two monochromators. The irradiation density was measured using a power meter and this value converted to moles photons sec^{-1} using Einstein's equation ($E_{\text{mol}} = N_A h\nu$, where N_A is Avogadro's number). The moles of photons absorbed by the compound **1** sample was calculated from the irradiation duration and corrected with the α_{313} or α_{325} of the solution immediately prior to irradiation. The moles of compound **1** (closed) formed were calculated from α_{633} using the integrated Beer-Lambert equation and the $\epsilon_{2closed}$ obtained above.

The quantum yield of ring-closing was defined as the moles compound **1** (open) formed per mole of photon absorbed. Ring-opening quantum yields were obtained in a similar fashion to cyclization quantum yields, by irradiating solutions of compound **1** (closed) with 633 nm light and monitoring the change in absorbance at 313 nm. The moles of compound **1** (open) formed were calculated using the integrated Beer-Lambert equation and the absorption coefficient of compound **1** (open) at 313 nm obtained above. Figure 3.6(b) shows the absorption profile of the ring-opening photoreaction recorded every 50 minutes.

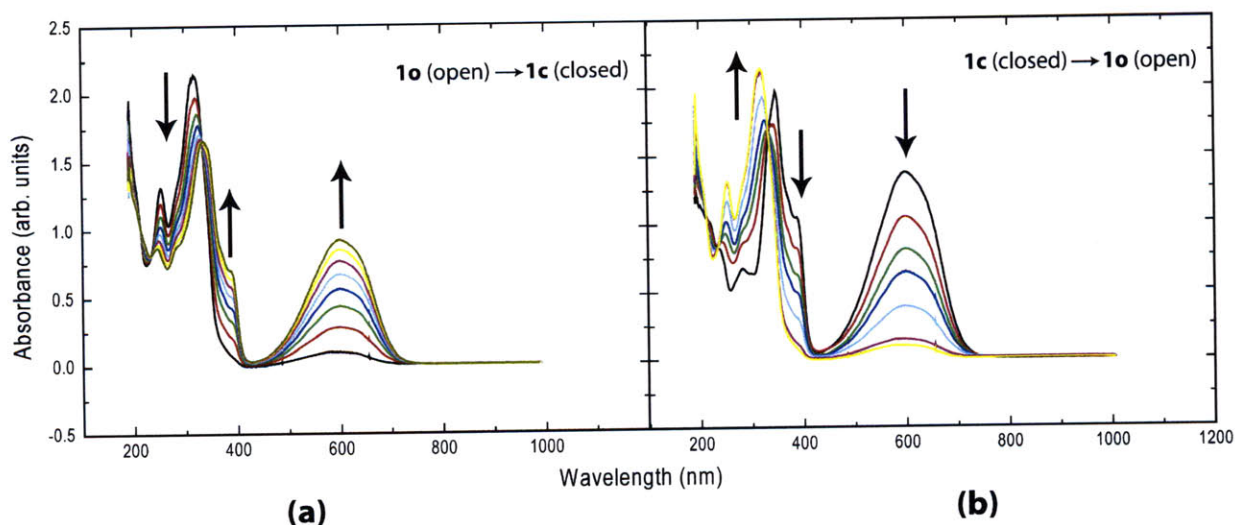


Figure 3.6. (a) Absorbance profile of the photocyclization reaction of compound **1** (open) recorded every 5 seconds. (b) Absorbance profile of the ring-opening photoreaction of compound **1** (closed) recorded every 50 minutes.

The photochromic film was spun-cast under yellow light in a class 10 clean-room. Since the closed form is accessible only via photo-reaction, this ensures that the thin film contained predominantly the open form. The spectrophotometer used in the above measurements was not suitable for measuring absorbance values above 3. Hence, the dispersion curve of the film was

measured using a spectroscopic ellipsometer (Figure 3.7). The thickness of the film was estimated from the dispersion curve as 410 nm. The absorbance of this film was calculated using the equation, $\alpha = 4\pi k/\lambda$, where k is the imaginary part of the refractive index. The integrated form of the Beer-Lambert law was then used to calculate the initial concentration of the open form in the film.

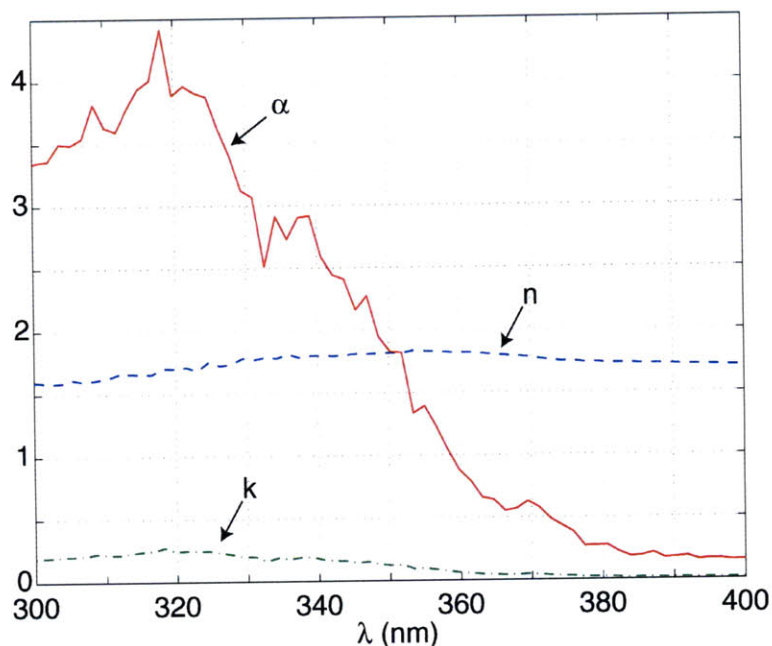


Figure 3.7. Dispersion curve of the photochromic film (primarily open form of compound **1** in a PMMA matrix). The real part (n) and the imaginary part (k) of the refractive index are plotted in blue and green colors, respectively. The absorbance is plotted in red.

In order to investigate the thermal stability of compound **1**, solutions of **1o** and **1c** in toluene were heated to 100 °C in the dark for 60 min and their absorbance spectra were recorded every 10 minutes. Additionally, thin films of ca. 92 wt% **1o** or **1c** in PMMA were heated to 120 °C for 60 minutes and their absorption spectra recorded every 10 minutes. No changes in

absorbance spectra were observed within the measurement error of our spectrophotometer (~0.01 O. D.). Considering the 60 minutes of observation time, we concluded that the thermal reaction rate constant, κ , is less than $\sim 3 \times 10^{-6} \text{ s}^{-1}$.

The calculated photochromic parameters are summarized in Table 3.1.

Table 3.1. Photochromic parameters of compound **1**. ϵ 's are the decadic molar absorptivities, Φ 's are the quantum efficiencies, κ is the thermal rate constant, and $[\text{open}_0]$ is the initial concentration of the open form of compound **1** in the photochromic film.

$\epsilon_{1\text{open}} = 31136 \text{ L mol}^{-1} \text{ cm}^{-1}$	$\epsilon_{1\text{closed}} = 10521 \text{ L mol}^{-1} \text{ cm}^{-1}$
$\epsilon_{2\text{open}} = 158 \text{ L mol}^{-1} \text{ cm}^{-1}$	$\epsilon_{2\text{closed}} = 20035 \text{ L mol}^{-1} \text{ cm}^{-1}$
$\Phi_{\text{open} \rightarrow \text{closed}} = 0.24$	$\Phi_{\text{closed} \rightarrow \text{open}} = 8.8 \times 10^{-4}$
$\kappa < 3 \times 10^{-6} \text{ s}^{-1}$	$[\text{open}_0] = 2.99 \text{ M}$

Compounds **1o** and **1c** are thermally stable and were not observed to interconvert at elevated temperatures ($T < 120 \text{ }^\circ\text{C}$). The absorption onset value for compound **1o** is approximately 370 nm, which corresponds to an excitation energy of 3.35 eV. In other words, photons with energy of at least 3.35 eV are necessary to excite **1o** and effect cyclization to form **1c**. Since 633 nm photons correspond to an energy of 1.96 eV, we can effectively conclude that cyclization does not occur when **1o** is irradiated at 633 nm.

As for the retrocyclization of **1c** to **1o**, we assumed that the quantum yield of ring-opening is constant across all absorbed wavelengths because of Kasha's rule.²⁶ Kasha's rule states that for photochemical reactions we need consider only the lowest excited singlet (S_1) or the lowest triplet (T_1) state as likely candidates for the initiation of a reaction because rapid radiationless conversion from higher excited states ($S_{n>1}$ or $T_{n>1}$) to S_1 or T_1 competes favorably with higher-order processes; specifically, for most organic molecules the rate of internal

conversion from $S_{n>1} \rightarrow S_1$ falls in the range of 10^{11} - 10^{13} sec^{-1} . The absorption onset for **1c** occurs at 700 nm (1.77 eV) and therefore, photons with energy of at least 1.77 eV are necessary to excite **1c**. Assuming that the lowest energy absorption band centered at 582 nm corresponds to the $S_0 \rightarrow S_1$ transition of **1c**, we can claim that the quantum yield of ring-opening from the S_1 state is 8.8×10^{-4} . Upon absorption of higher-energy 325 nm photons, **1c** can access the S_2 (or higher) state, but subsequent relaxation to the S_1 state via internal conversion should be faster than ring-opening; thus, although different excited states can be accessed at different wavelengths, ring-opening is most likely to occur from the comparatively long-lived S_1 state. Therefore, we assumed that the quantum yield of ring-opening is independent of wavelength.

Lloyd's mirror setup. A schematic of the dual-wavelength Lloyd's-mirror interferometer is shown in Figure 3.8. Light from a helium-cadmium laser ($\lambda_1 = 325\text{nm}$) is spatial-filtered and allowed to expand over a distance of about 1m. This generates an approximately uniform plane wave at the Lloyd's mirror. Light from a helium-neon laser ($\lambda_2 = 633\text{nm}$) is introduced at an angle as shown. Approximately, half of each beam is incident on the mirror, which reflects that portion of the beam onto the sample surface, where it interferes with the remaining portion of the incident beam (that is directly incident on the sample). This interference produces a standing wave. The angles of incidence of λ_1 and λ_2 beams were adjusted such that the periods of their standing waves were 170 nm and 350 nm, respectively. In this situation, many of the peaks of the λ_1 standing wave overlap with nodes of the λ_2 standing wave, creating the ideal illumination for absorbance modulation in one dimension.

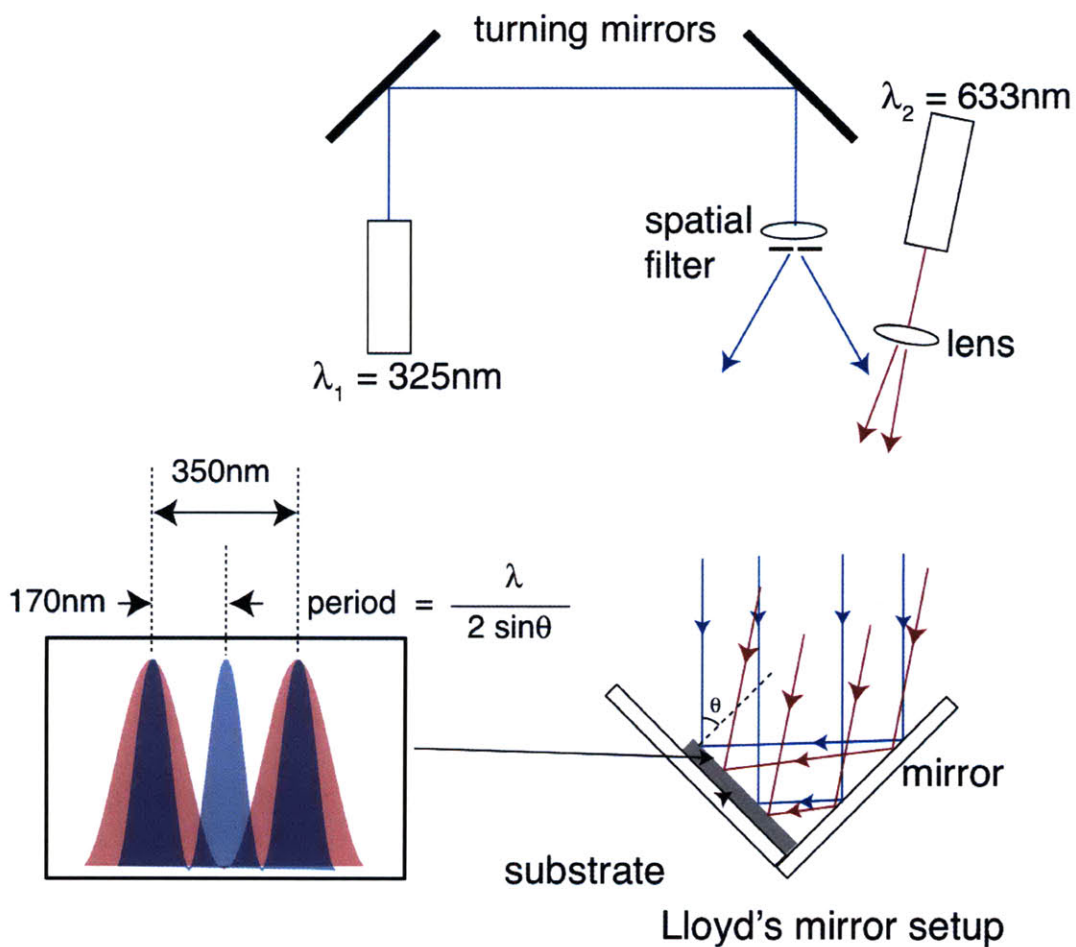


Figure 3.8. Schematic of the dual-wavelength Lloyd's-mirror interferometer. The inset shows the interlaced pair of standing waves incident on the substrate. The angles of incidence of the two wavelengths are adjusted so as to form standing waves of period 350 nm at λ_2 and 170 nm at λ_1 .

Polarization of both the beams was ensured to be pointing into the plane of the figure to maximize the contrast of the standing waves. The intensity at λ_1 as measured at the Lloyd's mirror was 0.365 W/m^2 . The λ_2 beam was expanded perpendicular to the axis of the Lloyd's mirror via a cylindrical lens placed at a distance of $\sim 61\text{cm}$ from the Lloyd's mirror. The beam profile of the λ_2 illumination at the Lloyd's mirror was captured with a camera, and the resulting peak intensity at the Lloyd's mirror was estimated to be about $1 \times 10^3 \text{ W/m}^2$.

Exposure Results. In the Lloyd's-mirror interferometer, the standing waves at λ_2 and λ_1 overlap such that each node at λ_2 approximately coincides with each alternate peak at λ_1 . Those peaks at λ_1 that coincide with the peaks at λ_2 are suppressed beyond the photochromic layer. We investigated this phenomenon by performing exposures at various intensity ratios. Figure 3.9(a) shows the scanning-electron micrograph of a portion of the pattern on the same sample as in Figure 3.3b, but at a different location. Due to the lower intensity of λ_2 at this location, the "suppressed λ_1 peaks" are weakly recorded in the underlying photoresist. This effect is more pronounced in Figure 3.9(b), where the scanning-electron micrograph of a cross-section through the lines recorded in photoresist reveal that the "suppressed peaks" are indeed shallower than the others. The period of the main peaks in both micrographs is equal to 350 nm, the period of the λ_2 standing wave.

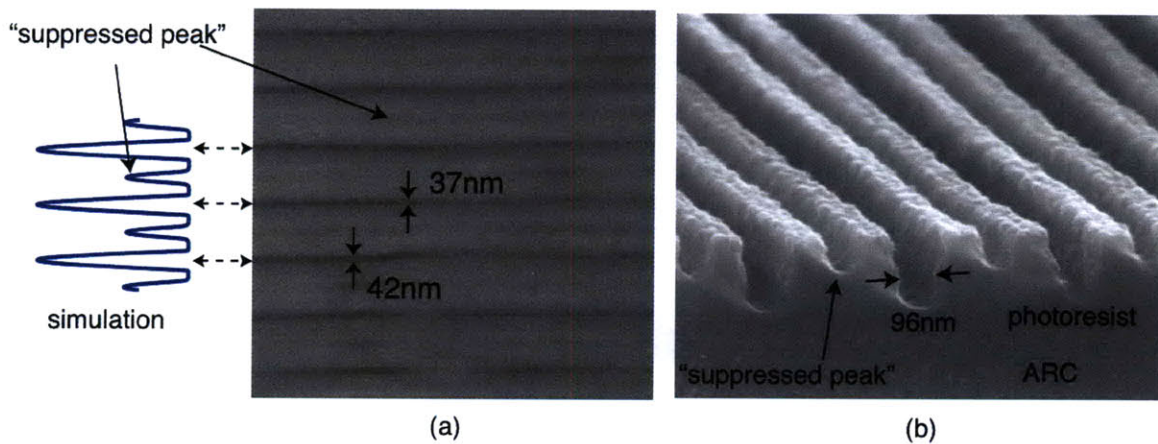


Figure 3.9. (a) Top-down scanning-electron micrograph of a different region of the same sample as in Figure 3.3(b). Due to the slightly lower intensity at λ_2 , the "suppressed peaks" at λ_1 are weakly recorded in the photoresist. (b) Scanning-electron micrograph of a cross-section through exposed lines in photoresist from a sample where the intensity ratio is smaller. The "suppressed peaks" are correspondingly shallower than the other peaks. The period of the main peaks in both micrographs is equal to 350 nm, the period of the λ_2 standing wave.

3.5 References and Notes

- (1) Current affiliation: University of Utah, Department of Electrical and Computer Engineering
- (2) Massachusetts Institute of Technology, Research Laboratory of Electronics, Department of Electrical Engineering, Henry I. Smith group.
- (3) Abbé, E. *Arch. Mikrosk. Anat. Entwicklungsmech.* **1873**, *9*, 413.
- (4) Murooka, K.; Hattori, K.; Iizuka, O. *J. Vac. Sci. Technol. B.* **2003**, *21*, 2668.
- (5) Pease, R. F. W. *Microelectron. Eng.* **2005**, *78*, 381.
- (6) Ash, E. A.; Nichols, G. *Nature* **1972**, *237*, 510.
- (7) (a) Betzig, E.; Trautman, J. K.; Harris, T. D.; Weiner, J. S.; Kostelak, R. L. *Science* **1991**, *251*, 1468. (b) Novotny, L.; Hecht, B.; Pohl, D. *Ultramicroscopy* **1998**, *71*, 341. (c) Frey, H. G.; Keilmann, F.; Kriele, A.; Guckenberger, R. *Appl. Phys. Lett.* **2002**, *81*, 5030.
- (8) Ito, T.; Yamada, T.; Inao, Y.; Yamaguchi, T.; Mizutani, N.; Kuroda, R. *Appl. Phys. Lett.* **2006**, *89*, 033113.
- (9) Yin, X.; Fang, N.; Zhanga, X.; Martini, I. B.; Schwartz, B. J. *Appl. Phys. Lett.* **2002**, *81*, 3663.
- (10) Chovin, A.; Garrigue, P.; Manek-Hönniger, I.; Sojic, N. *Nano. Lett.* **2004**, *4*, 1965.
- (11) Ozbay, E. *Science* **2006**, *311*, 189.
- (12) (a) Fang, N.; Lee, H.; Sun, C.; Zhang, X. *Science* **2005**, *308*, 534. (b) Jacob, Z.; Alekseyev, L. V.; Narimanov, E. *Opt. Exp.* **2006**, *14*, 8247.
- (13) Crano, J. C.; Guglielmetti, R. J., Eds. *Organic Photochromic and Thermochromic Compounds*, v. 2; Plenum Press: New York, **1999**.
- (14) Menon, R.; Smith, H. I. *J. Opt. Soc. Am. A* **2006**, *23*, 2290.

- (15) Menon, R.; Tsai, H.-Y.; Thomas, S. W. *Phys. Rev. Lett.* **2007**, *98*, 043905/1.
- (16) Tsai, H.-Y.; Wallraff, G. W.; Menon, R. *Appl. Phys. Lett.* **2007**, *91*, 094103.
- (17) See experimental section for the measurement of these parameters.
- (18) Yokoyama, Y. *Chem. Rev.* **2000**, *100*, 1685.
- (19) Irie, M. *Chem. Rev.* **2000**, *100*, 1685.
- (20) Darcy, P. J.; Heller, H. G.; Strydom, P. J.; Whittall, J. J. *Chem. Soc. Perkin Trans.* **1981**, *1*, 202.
- (21) Taflove, A.; Hagness, S. C. *Computational Electrodynamics: The Finite-Difference Time-Domain Method*; 2nd ed.; Artech House: Norwood, MA **2000**.
- (22) Ito, T.; Yamada, T.; Inao, Y.; Yamaguchi, T.; Mizutani, N.; Kuroda, R. *Appl. Phys. Lett.* **2006**, *89*, 033113.
- (23) (a) Menon, R.; Tsai, H.-Y.; Rogge, P. *J. Opt. Soc. Am. A.* **2009**, *26*, 297. (b) Tsai, H.-Y.; Smith, H. I.; Menon, R. *Opt. Lett.* **2008**, *33*, 2916.
- (24) Hell, S. W. *Nat. Biotech.* **2003**, *27*, 1347.
- (25) (a) Saika, T.; Irie, M.; Shimidzu, T. *Chem. Commun.* **1994**, 2123. (b) Peters, A.; Branda, N. R. *Chem Commun.* **2003**, 954.
- (26) Kasha, M. *Disc. Faraday Soc.*, **1950**, *9*, 14.

CHAPTER 4
Thermally-Polymerized
Rylene Nanoparticles

Adapted from:
Andrew, T. L.; Swager, T. M. “Thermally-Polymerized Rylene Nanoparticles” manuscript
submitted to *Adv. Funct. Mater.*

4.1 Introduction

Chromophore and conjugated polymer (CP) nanoparticles and nanocomposites¹ have recently found prominence in various applications, including optoelectronics,² and biological imaging and sensing.³ In certain cases, CP nanoparticles displayed desirable properties that were either absent (water solubility) or not as prominent (two-photon absorption cross section) in CP thin films or solutions.^{3,4} Additionally, there is considerable interest in using CP nanoparticles to improve or control the nanoscale composition of CP blends to improve the efficiency of polymer LEDs and photovoltaics.^{2,5} Fluorescence energy transfer in small molecule chromophore-containing nanoparticles has also been investigated for live cell imaging.^{3e,6}

CP nanoparticles are predominantly fabricated by microprecipitation methods, where a small aliquot of a dilute solution of the CP in a good solvent (such as tetrahydrofuran) is added to a poor solvent (such as water) with sonication.⁴ In the case of small molecule chromophores, emulsions of monomers containing polymerizable functional groups are first formed (sometimes in the presence of surfactants) and then the monomers are polymerized within the microcapsules (using either radical initiators or metal catalysts) to yield shape-persistent chromophore or CP nanoparticles.⁷ Rylene dyes, particularly 3,4,9,10-perylene tetracarboxydiimides (PDIs), are frequently used as the chromophore component owing to their brilliant colors, large extinction coefficients, near-unity fluorescence quantum yields and remarkable photostability.⁸ Recent examples of rylene-containing nanoparticles almost always utilize methacrylate-functionalized chromophores, which are then polymerized in microemulsions by established controlled radical polymerization processes.^{3c-f}

Aryl trifluorovinyl ethers (TFVEs) are a unique class of molecules that have been shown to undergo a thermal dimerization reaction to generate perfluorocyclobutane (PFCB) derivatives

(Figure 4.1A).⁹ Smith and coworkers have synthesized numerous, high molecular-weight polymers by thermally polymerizing monomers containing multiple TFVE moieties.¹⁰ Moreover, due to the availability of a key synthetic intermediate (**1**, Figure 4.1B), the straight-forward incorporation of phenyl TFVE moieties into a variety of chromophore skeletons is possible.¹¹ In the past decade, TFVE-containing chromophore thermosets have been explored as thermally-stable nonlinear optical polymers,¹² optical waveguides¹³ and electroluminescent polymers.¹⁴

Thus far, the thermal, radical initiator-free fabrication of shape-persistent nanoparticles has not been demonstrated. We anticipated that the thermal reactivity of TFVEs would allow access to such nanoparticles. Herein we describe the synthesis of rylene dyes functionalized with two or more phenyl TFVE moieties and the fabrication of rylene nanoparticles via a thermal emulsion polymerization.

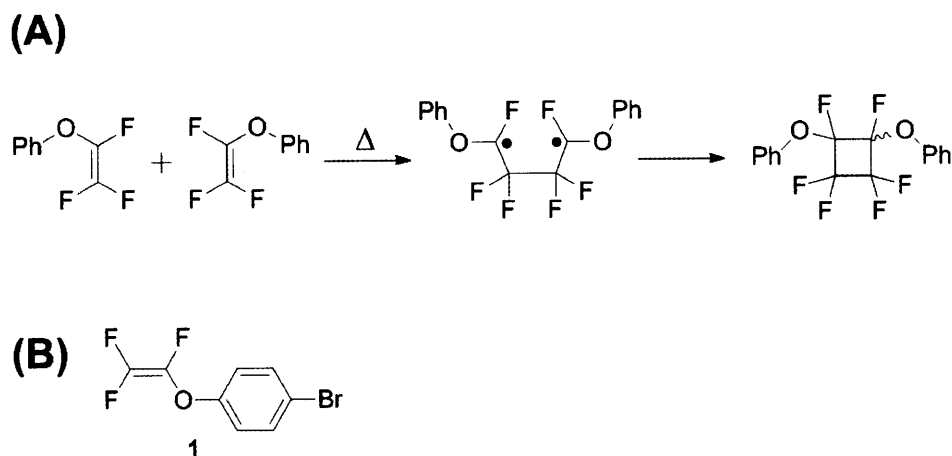
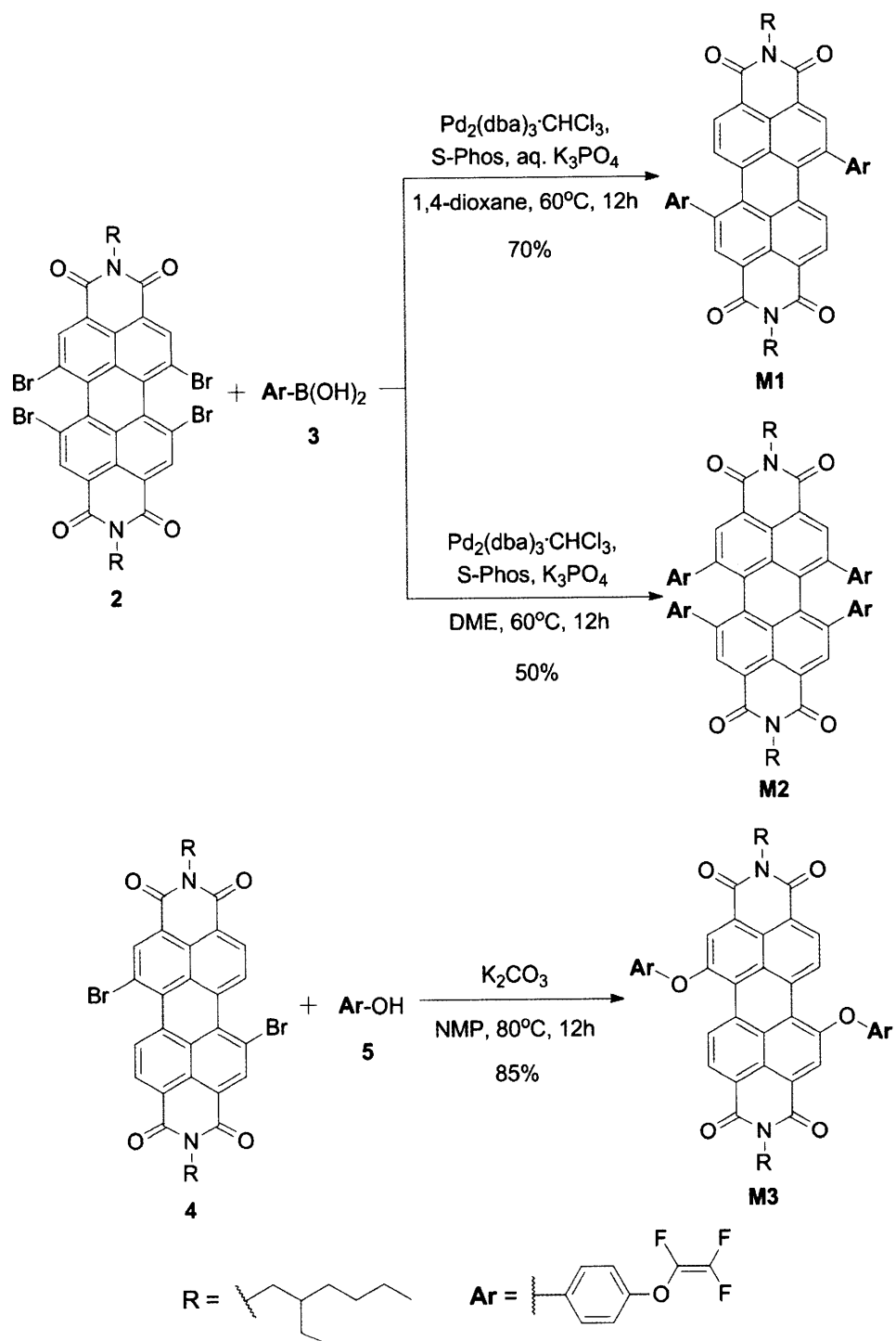


Figure 4.1. (A) Thermal dimerization reaction of aryl trifluorovinyl ethers (TFVEs), shown for phenyl TFVE. (B) Structure of 4-bromophenyl TFVE (**1**).

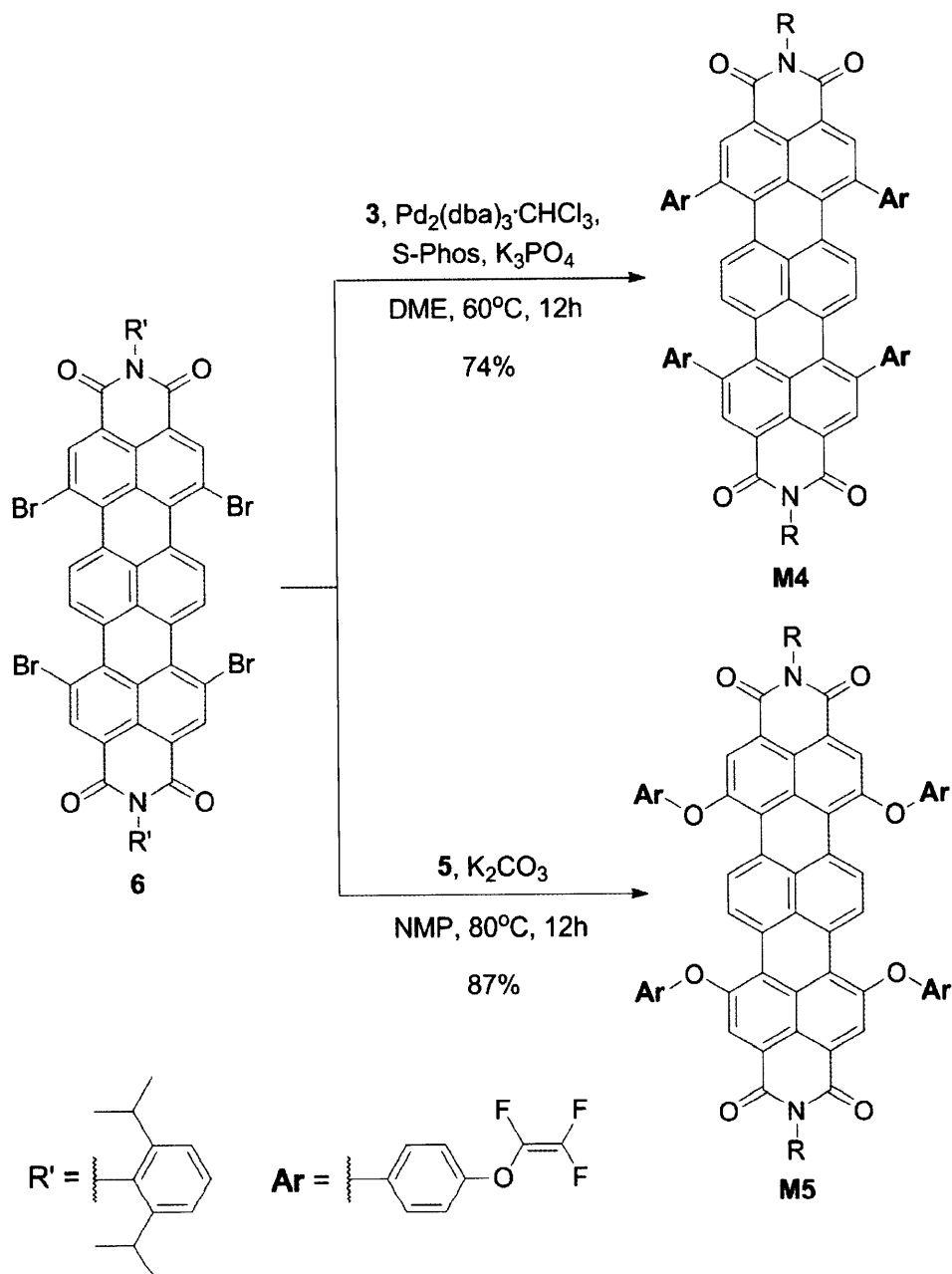
4.2 Monomer Synthesis

PDI_s were bay-functionalized with phenyl TFVE moieties starting from either tetrabromide **2**¹⁵ or dibromide **4**¹⁶ (Scheme 4.1). Following the previously reported synthesis and CsF/Ag₂O mediated tetraarylation of **2**,¹⁵ we initially aimed to perform a four-fold Suzuki-Miyaura coupling between **2** and **3**. However, the TFVE moiety was found to be slightly susceptible to nucleophilic addition of fluoride in the presence of the CsF/Ag₂O base system and the resulting hydro-1,2,2-fluoroethane-containing (-O-CHF-CF₃) side products could not be separated from the reaction mixture. Instead, a four-fold Suzuki-Miyaura cross coupling under the modified Buchwald conditions was pursued. When aqueous potassium phosphate was employed as a base, tetrabromide **2** was partially dehalogenated and monomer **M1**, with two phenyl TFVE moieties, was isolated in 70% yield. Upon switching the base to rigorously anhydrous potassium phosphate, tetraarylated monomer **M2** was isolated in 50% yield. Taking advantage of the electron-deficient nature of the PDI skeleton, monomer **M3** was synthesized via an S_NAr reaction between **4** and **5**.

The synthesis of TFVE-functionalized terylene diimide (TDI) monomers is shown in Scheme 4.2. Similar to **M2**, the tetraarylated TDI monomer **M4** was synthesized starting from tetrabromide **6** via a modified Suzuki-Miyaura cross-coupling reaction with anhydrous potassium phosphate. Tetraaryloxy monomer **M5** was synthesized by an S_NAr reaction between **6** and **5**.



Scheme 4.1. Synthesis of perylene diimide-containing thermoset monomers.



Scheme 4.2. Synthesis of terylene diimide-containing thermoset monomers.

4.3 Monomer Photophysics

The photophysical properties of monomers **M1-5** (in CHCl_3 solutions) are summarized in Table 4.1. In general, the TFVE moieties were not observed to significantly affect the optical

properties of rylene dyes. The absorption and emission maxima and fluorescence quantum yields of monomers **M3** and **M5** were similar to phenyloxy-substituted PDI^{17a} and TDI,^{17b} respectively. Monomer **M2** displayed similar absorption and emission maxima to the previously-reported tetraphenyl PDI. Consistent with similar observations for biphenyl-containing fluorophores,¹⁸ phenyl substitution was found to increase the otherwise-small Stokes' shift of rylene dyes and decrease their fluorescence quantum yields. Moreover, the excited-state lifetimes of the phenyl-substituted rylenes, **M1**, **M2** and **M4**, were found to be significantly longer than their parent rylene diimides (4.5 ns for *N*-(2-ethylhexyl)-PDI and 3.5 ns for *N*-(2,6-diisopropylphenyl)-TDI), most likely due to excited state planarization across the biphenyl linkage.

Table 4.1. Photophysical properties (in CHCl₃) of phenyl TFVE-containing rylene diimides.

Compound	λ_{\max} / nm (log ϵ)	λ_{em} / nm	Φ	τ / ns
M1	553 (4.4)	602	0.88 ^a	8.7
M2	592 (4.3)	640	0.61 ^a	9.8
M3	536 (4.4)	563	0.81 ^a	5.8
M4	720 (3.9)	765	0.08 ^b	5.7
M5	680 (4.2)	700	0.17 ^b	2.4

^a Measured against Rhodamine B in ethanol (Φ 0.71) ^b Measured against zinc phthalocyanine in 1% pyridine in toluene (Φ 0.30)

4.4 Nanoparticle Synthesis

A linear polymer from **M1** was initially synthesized in order to study the desired thermal polymerization of TFVE-substituted rylene diimides by the formation of perfluorocyclobutane (PFCB) moieties. A polymer with M_n 9900 g/mol (DP 11, PDI 1.4) was obtained by heating **M1** in mesitylene at 190 °C for 72 h. The ^{19}F NMR spectra of **M1** and its resulting linear polymer are shown in Figure 4.2.

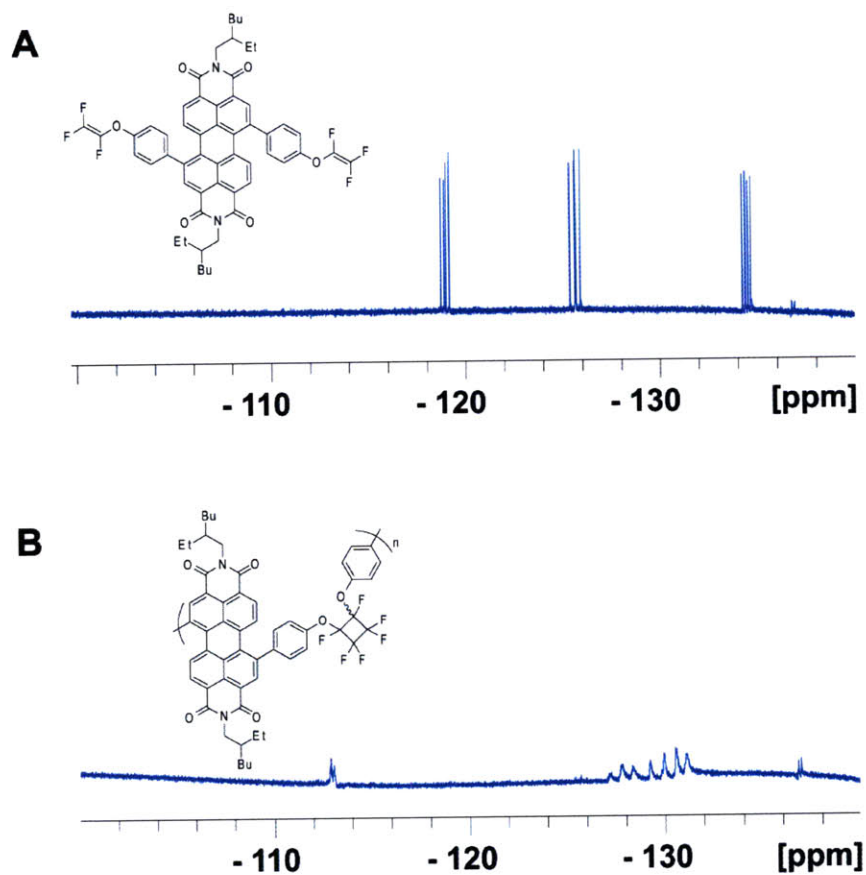
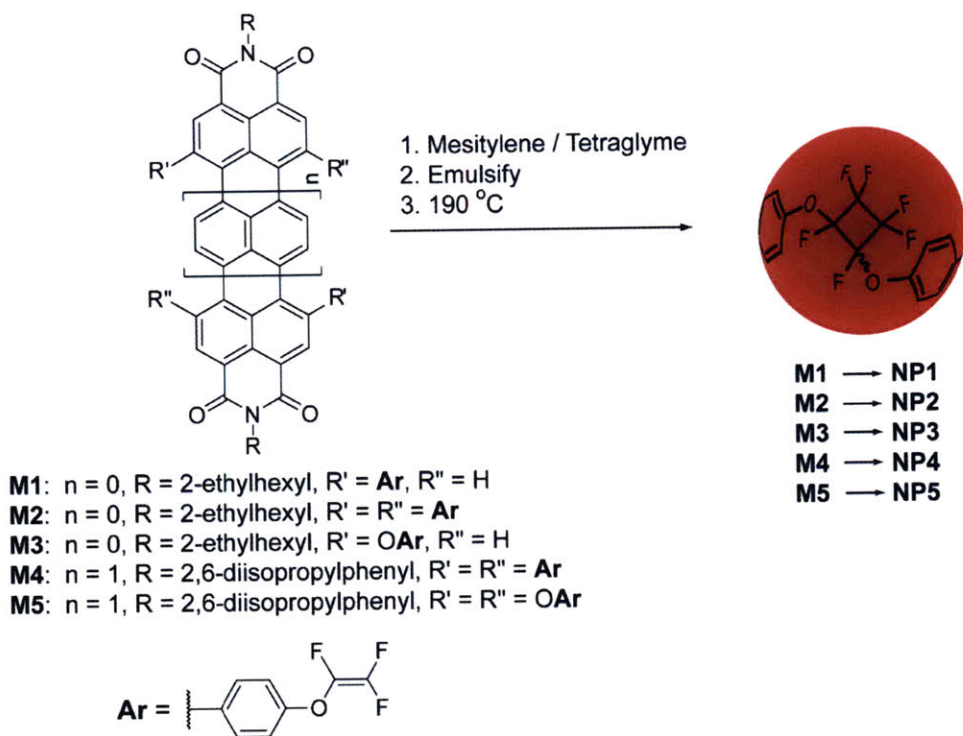


Figure 4.2. ^{19}F NMR spectra of **M1** (A) and its linear polymer formed by thermal polymerization in mesitylene (B).



Scheme 4.3. Thermal formation of shape-persistent rylene nanoparticles.

Rylene nanoparticles were synthesized by adding mesitylene solutions of monomers **M1-5** to tetraglyme and either homogenizing or sonicating the resulting biphasic system. This homogeneous mixture was then thermally crosslinked by heating to 190 °C for twelve hours (Scheme 4.3). Scanning electron micrograph (SEM) images of the drop-cast reaction mixture thus obtained from **M2** revealed the presence of polydisperse, submicron particles (Figure 4.3). Dynamic light scattering (DLS) measurements on the thermally-polymerized mixtures fabricated from **M1-5** indicated that particles with hydrodynamic radii between ca. 70 and 100 nm in tetraglyme were obtained (see Figure 4.4A). A significant difference was not observed in the size of the nanoparticles obtained from perylene (**NP1-3**) versus terrylene (**NP4-5**) diimide

monomers. The size of the dye particles in tetraglyme could be controlled within the 70 – 100 nm range by varying the concentration of monomer in the starting mesitylene solution (see Figure 4.4B). DLS measurements indicated that **NP1-5** did not coagulate in tetraglyme for at least six months (the stability of the nanoparticles as colloids in tetraglyme was only monitored for six months).

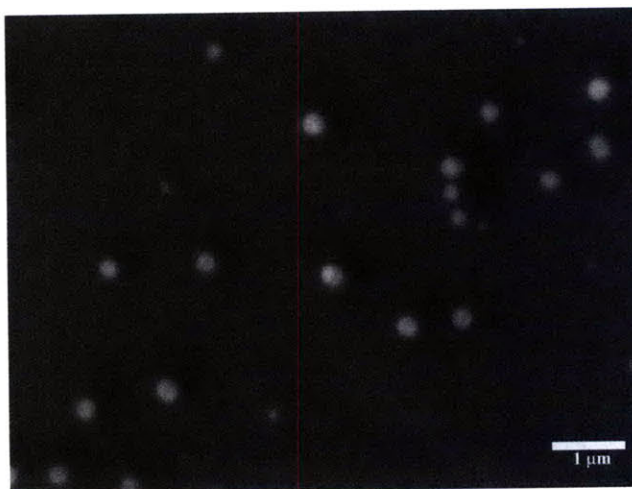


Figure 4. 3. SEM micrograph of the thermally-polymerized reaction mixture obtained from **M2**.

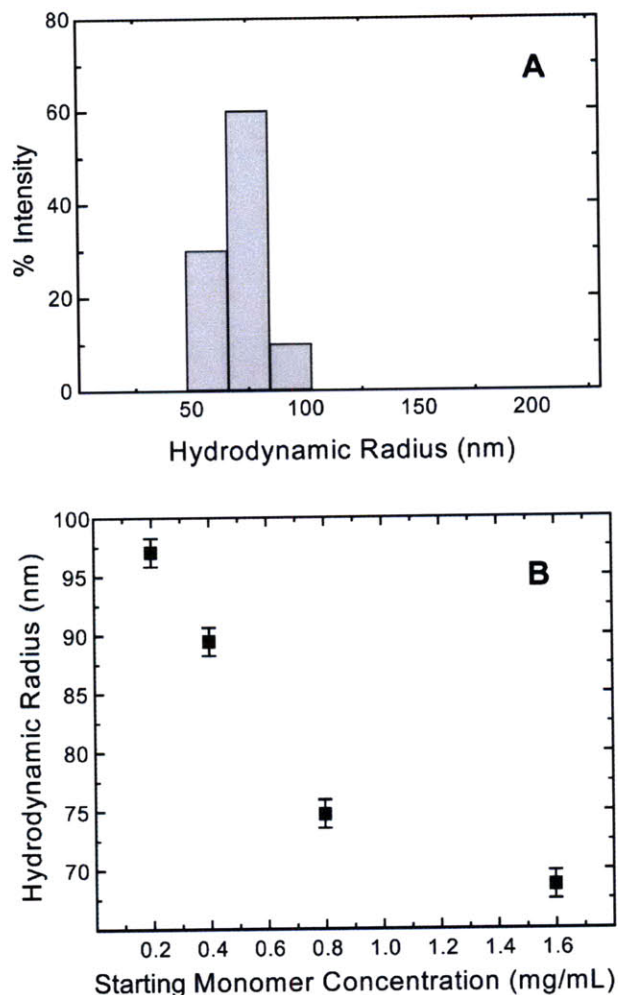


Figure 4.4. (A) Typical distribution of hydrodynamic radii in tetraglyme for the thermally-polymerized mixtures fabricated with **M1-5**, as measured by dynamic light scattering (DLS); the particle size distribution for **NP2** is shown (1.6 mg/mL starting monomer concentration in mesitylene). (B) The average hydrodynamic radii of particles obtained by varying the concentration of rylene monomer in the starting mesitylene solution.

Once thermally polymerized, the chromophore nanoparticles could be extracted into organic solvents from the tetraglyme suspension. ^{19}F -NMR spectra of the *toluene-d₈* extract of the thermally-polymerized reaction mixture obtained from **M2** indicated that the desired

formation of PFCBs had proceeded, as the three characteristic doublet of doublets arising from the TFVE moiety^{9c} were not observed (see Figure 4.5). Additionally, undesired side products from the addition of water or other nucleophiles to the TFVE moiety were not evident in the ¹⁹F spectrum of **NP2**. Nanoparticles **NP2**, **NP4** and **NP5** were observed to retain their shape upon extraction into organic solvents (toluene and CHCl₃); however, the hydrodynamic radii of these particles were observed to increase by approximately 30% in organic solvents (see Figure 4.6).

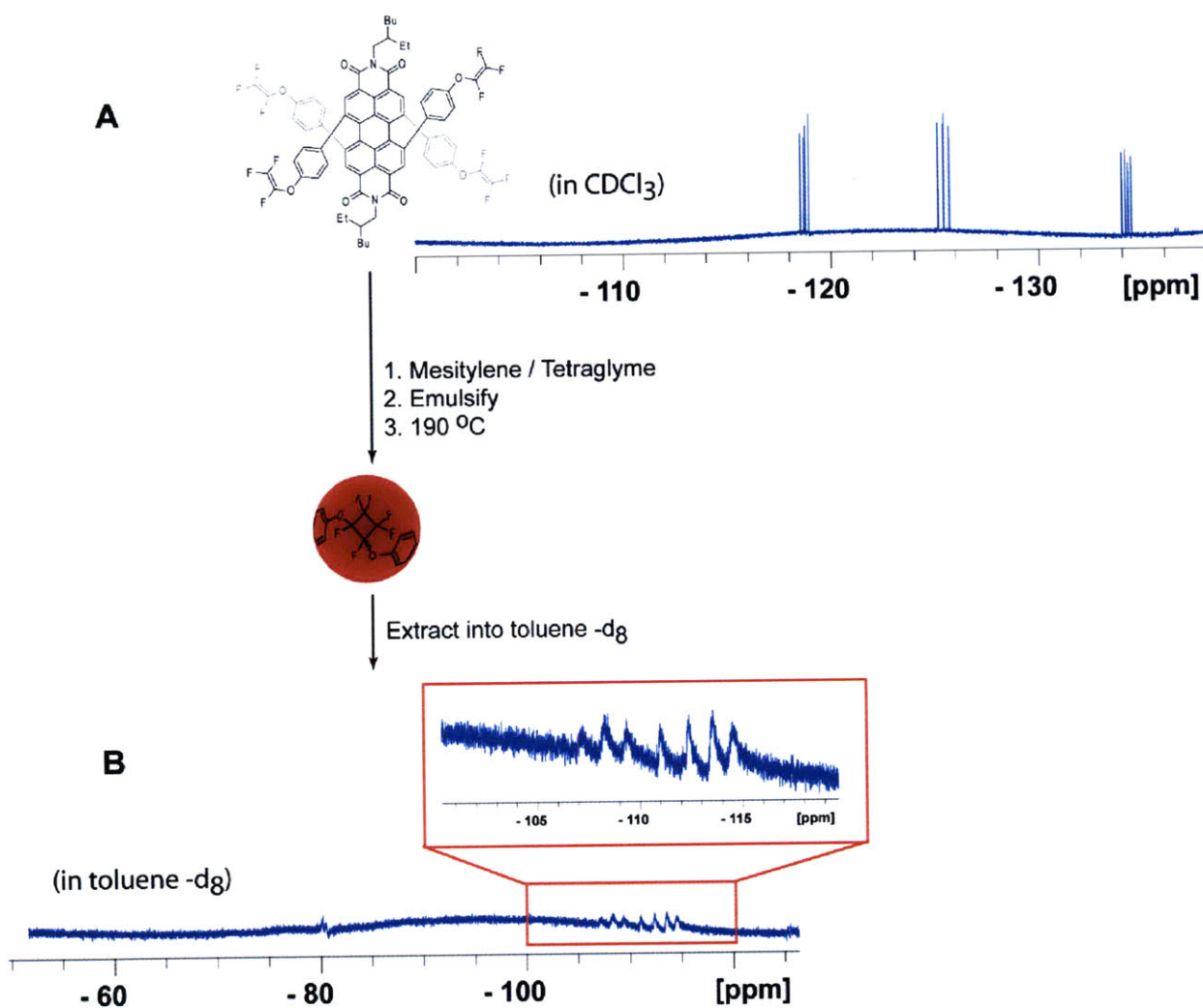


Figure 4.5. ¹⁹F NMR spectrum of **M2** (A) and the ¹⁹F NMR spectrum of the toluene-d₈ extract of the thermally-polymerized reaction mixture obtained from **M2**.

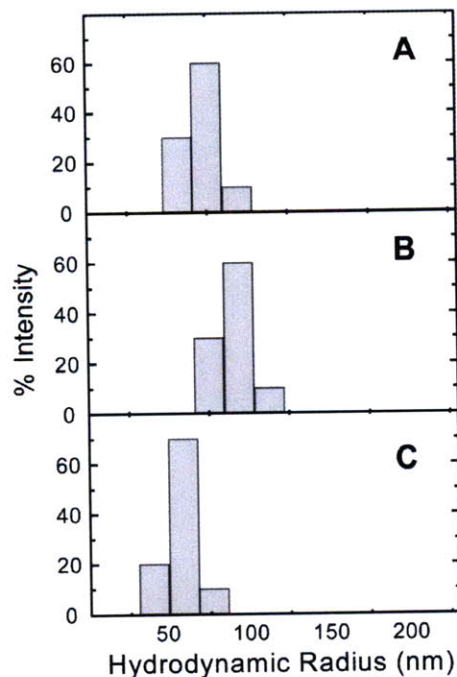


Figure 4.6. Typical changes in the measured hydrodynamic radii for **NP2**, **NP4** and **NP5** with changing solvents. The particle size distribution for **NP2** (fabricated with 1.6 mg/mL starting monomer concentration in mesitylene) is shown in (A) tetraglyme, (B) toluene and (C) water.

4.5 Nanoparticle Photophysics

The absorption and emission spectra of colloidal **NP1-5** in tetraglyme (Figure 4.7A) were, overall, similar to those of their respective monomers in chloroform or toluene solutions, with two notable differences: the absorption and emission bands of the rylene nanoparticles were broadened and their emission maxima were hypsochromically shifted by approximately 15 nm relative to their corresponding monomers. The fluorescence quantum yields of the nanoparticles in tetraglyme were also slightly lower than those of the starting monomers—a ca. 5% loss in fluorescence quantum yield was generally observed after thermal emulsion polymerization in tetraglyme.

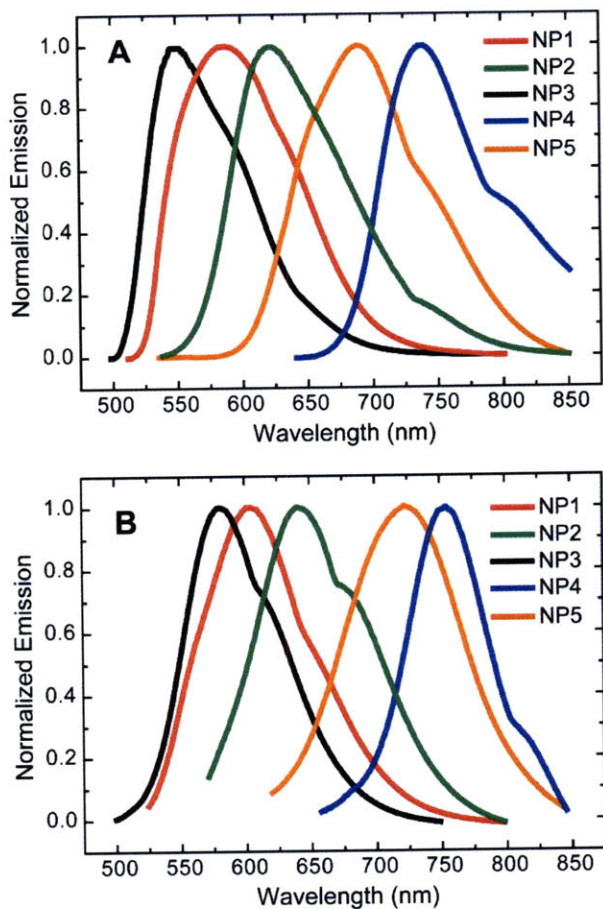


Figure 4.7. Emission spectra of **NP1-5** as colloidal suspensions in tetraglyme (A) and as dilute suspensions in water (B, 1:50 dilution of the tetraglyme suspension into DI water).

The nanoparticle suspensions in tetraglyme were diluted into water (1:50 dilution) and the resulting aqueous mixtures were filtered through a 0.2 μm PTFE filter to remove large aggregates. The filtered aqueous solutions were homogenous and nanoparticle precipitation was not evident by eye. DLS measurements revealed that the hydrodynamic radii of **NP1-5** in water decreased by ca. 35% relative to those measured in tetraglyme (see Figure 4.6). The emission spectra of **NP1-5** in water are shown in Figure 4.7B. The emission maxima of **NP1-5** in water are very similar to those of their corresponding monomers in chloroform solutions. Aqueous

solutions of the perylene diimide nanoparticles **NP1**, **NP2** and **NP3** displayed good fluorescence quantum yields (63%, 50% and 60%, respectively); however, the fluorescence quantum yields of aqueous solutions of the terrylene diimide nanoparticles **NP4** and **NP5** were relatively low (3% and 11%, respectively).¹⁹

4.6 Conclusions

Rylene dyes functionalized with varying numbers of phenyl trifluorovinylether (TFVE) moieties were synthesized and subjected to a thermal emulsion polymerization to yield shape-persistent, water-soluble chromophore nanoparticles. The reported thermal emulsion polymerization is unique from previously-reported methods to fabricate chromophore or conjugated polymer nanoparticles, as it does not involve the use of radical initiators or metal catalysts. Aqueous solutions of perylene diimide-containing nanoparticles remained homogenous for at least three months and displayed desirable fluorescence quantum yields. Due to these attributes, the rylene nanoparticles reported herein are attractive candidates for bioimaging applications.

4.7 Experimental Section

General Considerations: Synthetic manipulations were carried out under argon using dry solvents and standard Schlenk techniques. All solvents were of ACS reagent grade or better unless otherwise noted. 1,4-Dioxane and 1,2-dimethoxyethane were purified by distillation over activated alumina. Silica gel (40-63 μm) was obtained from SiliCycle Inc. $\text{Pd}_2(\text{dba})_3 \cdot \text{CHCl}_3$ and S-Phos were purchased from Strem Chemicals and used without further purification. Tetraglyme was purchased from VWR and purified by passing through a plug of activated neutral alumina.

Compounds **2**,¹⁵ **3**,^{9c} **4**,¹⁶ **5**,^{9c} and **6**^{17c} were synthesized following published procedures. Ultraviolet-visible absorption spectra were measured with an Agilent 8453 diode array spectrophotometer and corrected for background signal with a solvent-filled cuvette. Fluorescence spectra were measured on a SPEX Fluorolog- τ 3 fluorimeter (model FL-321, 450 W Xenon lamp) using right-angle detection. Fluorescence lifetimes were measured via frequency modulation using a Horiba-Jobin-Yvon MF2 lifetime spectrometer equipped with a 365 nm laser diode and using the modulation of POPOP as a calibration reference. Mesitylene/tetraglyme biphasic mixtures were emulsified with either an IKA Ultra-Turrax T25 Basic high-shear disperser (at a shear rate of 24/min) or a Misonix Microson Ultrasonic Cell Disruptor. DLS measurements were performed at the MIT Biophysics Instrumentation Facility using a Wyatt Technologies DynaPro Titan Dynamic Light Scatterer equipped with a 830 nm diode laser. Data were fitted to a globular protein model, taking into account solvent refractive indices and viscosities (CHCl₃: 0.57 cP at 20 °C, toluene: 0.59 cP at 20 °C, tetraglyme: 4.1 cP at 20 °C, water: 1.00 cP at 20 °C).

General Procedure for the synthesis of M1, M2, and M4: A flame-dried 50 mL Schlenk flask was charged with the appropriate rylene bromide, **3** (1.5 eq. per bromine substituent), Pd₂(dba)₃·CHCl₃ (0.05 eq), S-Phos (0.2 eq), and anhydrous potassium phosphate (20 eq.) under a positive flow of argon. Dry, degassed 1,2-dimethoxyethane (15mL) was introduced via cannula addition and the resulting mixture heated at 60 °C for twelve hours. The reaction was cooled to room temperature and passed through a celite plug and the solvent evaporated under reduced pressure. The resulting residue was purified by flash column chromatography using 50/50 hexanes/dichloromethane as the eluent.

M1. Isolated in 70% as a deep red solid from **2** following the procedure described above, with the sole substitution of 3.0M aqueous potassium phosphate for anhydrous potassium phosphate. ¹H NMR (400 MHz, CDCl₃, δ): 8.56 (s, 2H), 8.18 (d, *J* = 8.4 Hz, 2H), 7.80 (d, *J* = 8.4 Hz, 2H), 7.56 (d, *J* = 8.0 Hz, 4H), 7.23 (d, *J* = 8.0 Hz, 4H), 4.11 (m, 4H), 1.92 (m, 2H), 1.55 (s, 6H), 1.32 (m, 20H), 0.91 (m, 14H); ¹³C NMR (100 MHz, CDCl₃, δ): 163.8, 139.9, 139.4, 136.8, 136.1, 135.0, 131.1, 130.3, 130.1, 129.8, 128.6, 122.5, 121.4, 117.8, 44.5, 38.1, 30.9, 28.9, 24.2, 23.2, 14.3, 10.8; ¹⁹F NMR (376 MHz, CDCl₃, δ) -119.00 (dd, *J* = 98, 60 Hz, 1F), -126.69 (dd, *J* = 109, 98 Hz, 1F), -134.47 (dd, *J* = 109, 60 Hz, 1F); UV-vis (CHCl₃): λ_{max} (log ε) = 400 (3.8), 475(3.2), 519 (4.0), 553 (4.4); HRMS (ESI, *m/z*): [M + H]⁺ calcd for C₅₆H₄₉F₆N₂O₆, 959.3495; found, 959.3493.

M2. Isolated in 50% as a deep red solid from **2** following the procedure described above. ¹H NMR (400 MHz, CDCl₃, δ): 8.29 (s, 4H), 7.56 (d, *J* = 8.0 Hz, 8H), 7.23 (d, *J* = 8.0 Hz, 8H), 4.11 (m, 4H), 1.92 (m, 2H), 1.55 (s, 6H), 1.32 (m, 20H), 0.91 (m, 14H); ¹³C NMR (100 MHz, CDCl₃, δ): 163.7, 139.8, 139.4, 136.8, 135.8, 135.0, 131.1, 130.3, 130.1, 128.6, 122.5, 121.4, 117.8, 44.5, 38.1, 30.9, 28.9, 24.2, 23.2, 14.3, 10.8; ¹⁹F NMR (376 MHz, CDCl₃, δ) -119.00 (dd, *J* = 98, 60 Hz, 1F), -126.69 (dd, *J* = 109, 98 Hz, 1F), -134.47 (dd, *J* = 109, 60 Hz, 1F); UV-vis (CHCl₃): λ_{max} (log ε) = 400 (3.8), 558 (4.0), 592 (4.3); HRMS (ESI, *m/z*): [M + H]⁺ calcd for C₇₂H₅₅F₁₂N₂O₈, 1303.3767; found, 1303.3769.

M4. Isolated in 74% as a greenish-blue solid from **6** following the procedure described above. ¹H NMR (400 MHz, CDCl₃, δ): 8.37 (s, 4H), 7.98 (s, 4H), 7.56 (d, *J* = 8.4 Hz, 8H), 7.27 (t, *J* = 4.8 Hz, 2H), 7.23 (d, *J* = 8.4 Hz, 8H), 7.01 (d, *J* = 4.8 Hz, 4H), 2.68 (m, 4H), 1.08 (s, 24H); ¹³C NMR (100 MHz, CDCl₃, δ): 163.3, 155.0, 153.2, 147.8, 145.8, 134.6, 132.1, 132.0, 129.7, 129.2, 129.2, 129.0, 128.9, 128.4, 127.4, 127.3, 126.1, 125.8, 125.5, 124.1, 123.4, 122.7, 122.0, 119.3,

34.7, 29.2, 21.6; ^{19}F NMR (376 MHz, CDCl_3 , δ) -119.00 (dd, $J = 98, 60$ Hz, 1F), -126.69 (dd, $J = 109, 98$ Hz, 1F), -134.47 (dd, $J = 109, 60$ Hz, 1F); UV-vis (CHCl_3): λ_{max} ($\log \epsilon$) = 410 (3.0), 610 (3.1), 665 (3.7), 720 (3.9); HRMS (ESI, m/z): $[\text{M} + \text{H}]^+$ calcd for $\text{C}_{90}\text{H}_{59}\text{F}_{12}\text{N}_2\text{O}_8$, 1523.4080; found, 1523.1520.

General Procedure for the synthesis of M3 and M5: A flame-dried 50 mL Schlenk flask was charged with the appropriate rylene bromide, **5** (1.1 eq. per bromine substituent), and anhydrous potassium carbonate (1.1 eq. per bromine substituent) under a positive flow of argon. Dry, degassed *N*-methyl-2-pyrrolidone (10mL) was introduced via cannula addition and the resulting mixture heated at 80 °C for twelve hours. The reaction was cooled to room temperature, diluted with 1 M HCl and extracted with CHCl_3 (3x 30 mL). The organic layers were combined, dried over magnesium sulfate and the solvent evaporated under reduced pressure. The resulting residue was purified by flash column chromatography using 60/40 hexanes/dichloromethane as the eluent.

M3. Isolated in 85% as a deep red solid from **4** following the procedure described above. ^1H NMR (400 MHz, CDCl_3 , δ): 9.47 (d, $J = 8.4$ Hz, 2H), 8.57 (d, $J = 8.4$ Hz, 2H), 8.23 (s, 1H), 7.18 (m, 8H), 4.04 (m, 4H), 1.87 (m, 2H), 1.57 (s, 4H), 1.28 (m, 22H), 0.88 (m, 16H); ^{13}C NMR (100 MHz, CDCl_3 , δ): 163.7, 155.3, 139.4, 132.1, 130.5, 129.3, 129.0, 125.3, 124.1, 123.9, 122.4, 121.3, 118.3, 44.5, 38.1, 30.9, 28.9, 24.2, 23.2, 14.3, 10.8 ; ^{19}F NMR (376 MHz, CDCl_3 , δ) -119.00 (dd, $J = 98, 60$ Hz, 1F), -126.69 (dd, $J = 109, 98$ Hz, 1F), -134.47 (dd, $J = 109, 60$ Hz, 1F); UV-vis (CHCl_3): λ_{max} ($\log \epsilon$) = 400 (3.8), 461 (3.8), 502 (4.1), 536 (4.4); HRMS (ESI, m/z): $[\text{M} + \text{H}]^+$ calcd for $\text{C}_{56}\text{H}_{49}\text{F}_6\text{N}_2\text{O}_8$, 991.3393; found, 991.3398.

M5. Isolated in 87% as a deep blue solid from **6** following the procedure described above. ^1H NMR (400 MHz, CDCl_3 , δ): 9.47 (s, 4H), 8.27 (s, 4H), 7.40 (d, $J = 8.4$ Hz, 8H), 7.27 (t, $J =$

4.8 Hz, 2H), 7.09 (d, $J = 8.4$ Hz, 8H), 7.01 (d, $J = 4.8$ Hz, 4H), 2.68 (m, 4H), 1.08 (s, 24H); ^{13}C NMR (100 MHz, CDCl_3 , δ): 163.3, 155.0, 153.2, 147.8, 145.8, 134.6, 132.1, 132.0, 129.7, 129.2, 129.2, 129.0, 128.9, 128.4, 127.4, 127.3, 126.1, 125.8, 125.5, 124.1, 123.4, 122.7, 122.0, 119.3, 34.7, 29.2, 21.6; ^{19}F NMR (376 MHz, CDCl_3 , δ) -119.00 (dd, $J = 98$, 60 Hz, 1F), -126.69 (dd, $J = 109$, 98 Hz, 1F), -134.47 (dd, $J = 109$, 60 Hz, 1F); UV-vis (CHCl_3): λ_{max} ($\log \epsilon$) = 410 (3.2), 569 (3.8), 623 (4.0), 680 (4.2); HRMS (ESI, m/z): $[\text{M} + \text{H}]^+$ calcd for $\text{C}_{90}\text{H}_{59}\text{F}_{12}\text{N}_2\text{O}_{12}$, 1587.3876; found, 1587.3877.

Poly(MI). A 5 mL Teflon-capped Schlenk tube was charged with 57 mg (0.060 mmol) **M1** and 800 μL dry, degassed mesitylene under a positive flow of argon. The tube was then sealed and heated to 190 $^\circ\text{C}$ for 72 h. The solvent was evaporated under reduced pressure to yield 0.057 mg of a dark red powder. GPC M_n 9900 g/mol (DP 11), PDI 1.4.

Nanoparticle Synthesis. 0.5 mL of a solution of the appropriate TFVE-functionalized rylene diimide monomer in mesitylene (0.2 – 1.6 mg/mL) was added to 5.0 mL tetraglyme. The resulting biphasic mixture was either homogenized with a high-shear disperser or sonicated to yield a homogeneous emulsion, which was then heated to 190 $^\circ\text{C}$ under argon for 12 h.

4.8 References and Notes

- (1) (a) Tuncel, D.; Demir, H. V. *Nanoscale*, **2010**, 2, 484. (b) Pecher, J.; Mecking, S. *Chem. Rev.* **2010**, 110, 6260-6279.
- (2) (a) Kietzke, T.; Nehrer, D.; Landfester, K.; Montenegro, R.; Güntner, R.; Scherf, U. *Nat. Mater.* **2003**, 2, 408. (b) Mauthner, G.; Landfester, K.; Köck, A.; Brückl, H.; Kast, M.; Stepper, C.; List, E. J. W. *Org. Electron.* **2008**, 9, 164. (c) Fisslthaler, E.; Blümel, A.; Landfester, K.; Scherf, U.; List, E. J. W. *Soft Matter*, **2008**, 4, 2448.

- (3) (a) Wu, C.; Szymanski, C.; Cain, Z.; McNeill, J. *J. Am. Chem. Soc.* **2007**, *129*, 12904. (b) Zhu, M.-Q.; Zhu, L.; Han, J. J.; Wu, W.; Hurst, J. K.; Li, A. D. Q. *J. Am. Chem. Soc.* **2006**, *128*, 4303. (c) Tian, Z.; Wu, W.; Wan, W. Li, A. D. Q. *J. Am. Chem. Soc.* **2009**, *131*, 4245. (d) Zhu, L.; Wu, W.; Zhu, M.-Q.; Han, J. J.; Hurst, J. K.; Li, A. D. Q. *J. Am. Chem. Soc.* **2007**, *129*, 3524. (e) Moon, J. H.; McDaniel, W.; MacLean, P.; Hancock, L. F. *Angew. Chem. Int. Ed.* **2007**, *46*, 8223.
- (4) (a) Wu, C.; Szymanski, C.; McNeill, J. *Langmuir*, **2006**, *22*, 2956. (b) Szymanski, C.; Wu, C.; Hooper, J.; Salazar, M. A.; Perdomo, A.; Dukes, A.; McNeill, J. *Phys. Chem. B*, **2005**, *109*, 8543. (c) Wu, C.; McNeill, J. *Langmuir*, **2008**, *24*, 5855.
- (5) (a) Zhuang, D.; Hogen-Esch, T. E. *Macromolecules*, **2010**, *43*, 8170. (b) Piok, T.; Gamerith, S.; Gadermaier, C.; Plank, H.; Wenzl, F. P.; Patil, S.; Montenegro, R.; Kietzke, T.; Nehrer, D.; Scherf, U.; Landfester, K.; List, E. J. W. *Adv. Mater.* **2003**, *15*, 800. (b) Kietzke, T.; Nehrer, D.; Kumke, M.; Montenegro, R.; Landfester, K.; Scherf, U. *Macromolecules*, **2004**, *37*, 4882.
- (6) (a) Grigalevicius, S.; Forster, M.; Ellinger, S.; Landfester, K.; Scherf, U. *Macromol. Rapid Commun.* **2006**, *27*, 200. (b) Wu, C.; Peng, H.; Jiang, Y.; McNeill, J. *J. Phys. Chem. B*, **2006**, *110*, 14148.
- (7) (a) Landfester, K.; Montenegro, R.; Scherf, U.; Güntner, R.; Asawapirom, U.; Patil, S.; Neher, D.; Kietzke, T. *Adv. Mater.* **2002**, *14*, 651. (b) Landfester, K. *Annu. Rev. Mater. Res.* **2006**, *36*, 231. (c) Müller, K.; Klapper, M.; Müllen, K. *Macromol. Rapid Commun.* **2006**, *27*, 586. (d) Berkefeld, A.; Mecking, S. *Angew. Chem. Int. Ed.* **2006**, *45*, 6044. (e) Baier, M. C.; Huber, J.; Mecking, S. *J. Am. Chem. Soc.*, **2009**, *131*, 14267. (f) Pecher, J.; Mecking, S. *Macromolecules*, **2007**, *40*, 7733.

- (8) (a) Zollinger, H. *Color Chemistry*, 3rd ed.; VCH: Weinheim, **2003**. (b) Würthner, F. *Chem. Commun.* **2004**, 1564.
- (9) (a) Smart, B. E. In *Organofluorine Chemistry Principles and Commercial Applications*. Banks, R. E.; Smart, B. E.; Tatlow, J. C., Eds. Plenum Press: New York, **1994**; p 73. (b) Bartlett, P. D.; Montgomery, L. K.; Seidel, B. *J. Am. Chem. Soc.* **1964**, *86*, 616. (c) Spraul, B. K.; Suresh, S.; Jin, J.; Smith, D. W., Jr. *J. Am. Chem. Soc.* **2006**, *128*, 7055.
- (10) (a) Smith, D. W., Jr.; Chen, S.; Kumar, S.; Ballato, J.; Shah, H.; Topping, C.; Foulger, S. *Adv. Mater.* **2002**, *14*, 1585. (b) Jin, J.; Smith, D. W., Jr.; Topping, C.; Suresh, S.; Chen, S.; Foulger, S.; Rice, N.; Mojazza, B. *Macromolecules* **2003**, *36*, 9000. (c) Jin, J.; Topping, C.; Suresh, S.; Foulger, S.; Rice, N.; Mojazza, B.; Smith, D. W., Jr. *Polymer* **2005**, *46*, 6923. (d) Smith, D. W., Jr.; Babb, D. A. *Macromolecules* **1996**, *29*, 852.
- (11) (a) Neilson, A. R.; Budy, S. M.; Ballato, J. M.; Smith, D. W., Jr. *Macromolecules*, **2007**, *40*, 9378. (b) Iacono, S. T.; Budy, S. M.; Moody, J. D.; Smith, R. C.; Smith, D. W., Jr. *Macromolecules*, **2008**, *41*, 7490. (c) Spraul, B. K.; Suresh, S.; Glaser, S.; Perahia, D.; Smith, D. W., Jr. *J. Am. Chem. Soc.* **2004**, *126*, 12773.
- (12) (a) Ma, H.; Jen, A. K.-Y.; Dalton, L. R. *Adv. Mater.* **2002**, *14*, 1339. (b) Budy, S. M.; Suresh, S.; Spraul, B. K.; Smith, D. W., Jr. *J. Phys. Chem. C* **2008**, *112*, 8099.
- (13) Kang, S. H.; Luo, J.; Ma, H.; Barto, R. R.; Frank, C. W.; Dalton, L. R.; Jen, A. K.-Y. *Macromolecules*, **2003**, *36*, 4355.
- (14) (a) Carlson, B.; Phelan, G. D.; Kaminsky, W.; Dalton, L. R.; Jiang, X.; Liu, S.; Jen, A. K.-Y. *J. Am. Chem. Soc.* **2002**, *124*, 14162. (b) Niu, Y.-H.; Tung, Y.-L.; Chi, Y.; Shu, C.-G.; Kim, J. H.; Chen, B.; Luo, J.; Carty, A. J.; Jen, A. K.-Y. *Chem. Mater.* **2005**, *17*, 3532.

- (15) Qiu, W.; Chen, S.; Sun, X.; Liu, Y.; Zhu, D. *Org. Lett.* **2006**, *8*, 867.
- (16) (a) Zhan, X.; Tan, Z.; Domercq, B.; An, Z.; Zhang, X.; Barlow, S.; Li, Y.; Zhu, D.; Kippelen, B.; Marder, S. R. *J. Am. Chem. Soc.* **2007**, *129*, 7246. (b) Ahrens, M. J.; Fuller, M. J.; Wasielewski, M. R. *Chem. Mater.* **2003**, *15*, 2684.
- (17) (a) Li, X.-Q.; Zhang, X.; Ghosh, S.; Würthner, F. *Chem. Eur. J.* **2008**, *14*, 8074. (b) Nolde, F.; Qu, J.; Kohl, C.; Pschirer, N. G.; Reuther, E.; Müllen, K. *Chem. Eur. J.* **2005**, *11*, 3959. (c) Weil, T.; Reuther, E.; Beer, C.; Müllen, K. *Chem. Eur. J.* **2004**, *10*, 1398.
- (18) Rose, A.; Tovar, J. D.; Yamaguchi, S.; Nesterov, E. E.; Zhu, Z.; Swager, T. M. *Phil. Trans. R. Soc. A* **2007**, *365*, 1589.
- (19) Fluorescence quantum yields for **NP1-3** were measured against Rhodamine B in ethanol, which has a quantum yield of 0.71: Demas, J. N.; Crosby, G. A. *J. Phys. Chem.* **1971**, *75*, 991-1024. Fluorescence quantum yields for **NP4-5** were measured against zinc phthalocyanine in 1% pyridine in toluene, which has a quantum yield of 0.30: Vincett, P. S.; Voigt, E. M.; Rieckhoff, K. E. *J. Chem. Phys.* **1971**, *55*, 4131-4140.

CHAPTER 5

6,6-Dicyanofulvenes

Adapted and reprinted in part with permission from:
Andrew, T. L.; Cox, J. R.; Swager, T. M. "Synthesis, Reactivity, and Electronic Properties of
6,6-Dicyanofulvenes" *Org Lett.* **2010**, *12*, 5302-5305.

5.1 Introduction

During the past decade, intense research efforts have yielded numerous optimized, air-stable, *p*-type (hole-transporting) organic semiconductors with conductivities and hole mobilities that are competitive with inorganic analogs.¹ Recently, several examples of *n*-type (electron-conducting) organic materials have been utilized in thin-film organic field-effect transistors (OFETs) and photovoltaic cells,² but the electronic and solid-state packing properties, air-stability, and processability of *n*-type semiconductors are far from being as optimized as their *p*-type counterparts.³

The discovery of new molecular building blocks for *n*-type materials remains germane, as the diversity in the chemical structures of proven electron-conductors does not match the large population of known organic hole-conductors. To date, polymeric / oligomeric / small molecule oxadiazoles,⁴ benzothiadiazoles,⁵ arylene imides,⁶ perfluorinated⁷ or perfluoroalkyl-containing arenes,⁸ fullerenes,⁹ pyridiniums,¹⁰ and dicyanovinylene¹¹ or tricyanovinylene-substituted arenes¹² have been demonstrated as suitable *n*-type materials. Notably, nitrile incorporation is an interesting design strategy, as it both results in desirable electronic properties (low LUMO energies)¹³ and is capable of transforming a *p*-type organic system into an electron-accepting material.¹⁴

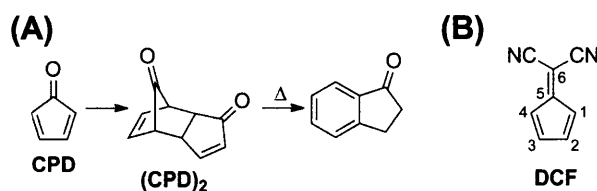


Figure 5.1. (A) Structures of the unisolable cyclopentadienone, CPD, and its isolable dimer, (CPD)₂. (B) Structure of 6,6-dicyanofulvene (DCF), depicting the numbering convention for a fulvene skeleton.

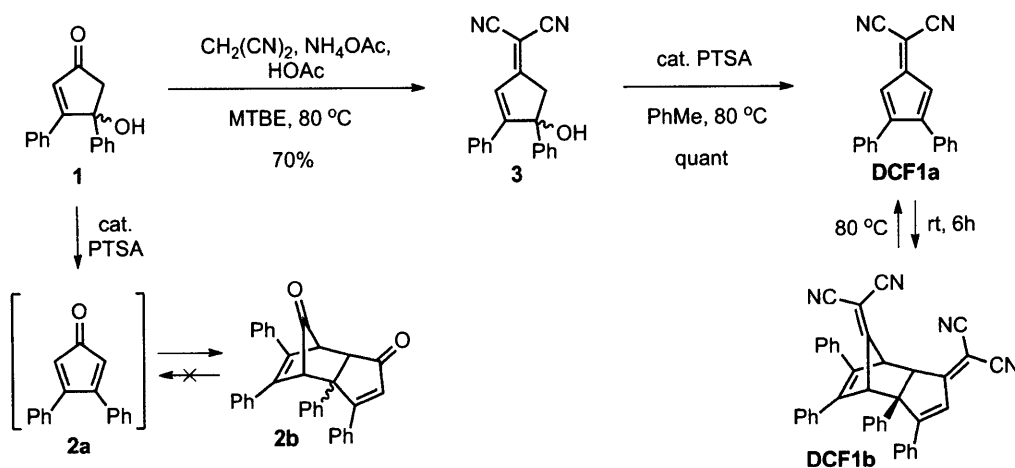
Cyclopentadienones (CPDs) and fulvenes have received little attention as *n*-type building blocks and have only been considered indirectly, as structural subunits in indenofluorenone and indenofluorene bis(dicyanovinylene) chromophores.^{11a,b} Wudl et al. reported a donor-acceptor polymer containing a dithienylcyclopentadienone moiety in its repeat unit, where the CPD served as the “acceptor” component;¹⁵ however, this polymer displayed complex electrochemistry and did not demonstrate *n*-type behavior in an OFET. The paucity of CPD- or fulvene-based building blocks could also be attributed to the reactivity and instability of these classes of molecules: many CPDs are unisolable in their monomeric form¹⁶ (see Figure 5.1A) and the electrochemical stability of fulvenes is suspect.¹⁷

We propose, instead, the use of 6,6-dicyanofulvenes (DCFs, Figure 5.1B) as building blocks for electron-transport materials. In this chapter, we explore the synthesis of DCFs, their chemical stabilities, and their optical and electrochemical properties.

5.2 Synthesis of 6,6-Dicyanofulvenes

Informed by the instability of monomeric cyclopentadienone, we first synthesized a diphenyl derivative of 6,6-dicyanofulvene (Scheme 5.1) based on the hypothesis that two phenyl substituents would provide enough steric protection from dimerization. 2,3-Diphenyl-6,6-dicyanofulvene (**DCF1a**) was synthesized in two steps from the 4-hydroxy-2-cyclopenten-1-one derivative **1**, which was prepared by an aldol condensation between acetone and benzil.¹⁸ Acid-catalyzed dehydration of **1** generates the corresponding cyclopentadienone **2a**, which either irreversibly undergoes a [4+2] homodimerization¹⁶ or can be trapped by suitable dienophiles to generate 1,2-diphenylbenzene derivatives after decarbonylation.¹⁸ To avoid such undesirable side reactions, only transformations of the masked cyclopentadienone **1** were pursued. The 1,2-

addition of malononitrile to compound **1** proceeded smoothly to yield **3**. We initially anticipated the occurrence of a number of detrimental rearrangement reactions competing with the 1,2-addition of malononitrile; however, as supported by the crystal structure of **3** (Figure 5.2A), the desired product was the sole isolated compound. Dehydration of **3** by a catalytic amount of PTSA at elevated temperatures quantitatively generated a dark brown solution of **DCF1a**; however this dicyanofulvene was found to dimerize at room temperature to **DCF1b**. As seen in the crystal structure of dimer **DCF1b** (Figure 5.2B), the endo adduct was the major isolated product.



Scheme 5.1. Synthesis of **DCF1**.

Dimerization was reversible and was accompanied by disappearance of the dark brown color of the starting **DCF1a** solution. The monomeric fulvene could be recovered by heating **DCF1b** to 80 °C and we were able to cycle between monomeric and dimeric forms multiple times with little to no decomposition noticeable by ¹H-NMR spectroscopy. This observation is in contrast to the behavior of **2a**, for which dimerization is an irreversible phenomenon (heating

results in decarbonylation).¹⁶ Moreover, the tendency of **DCF1a** to undergo [4+2] dimerization is not shared by other 6,6-disubstituted fulvenes, such as a 6,6-dimethylfulvene.¹⁷

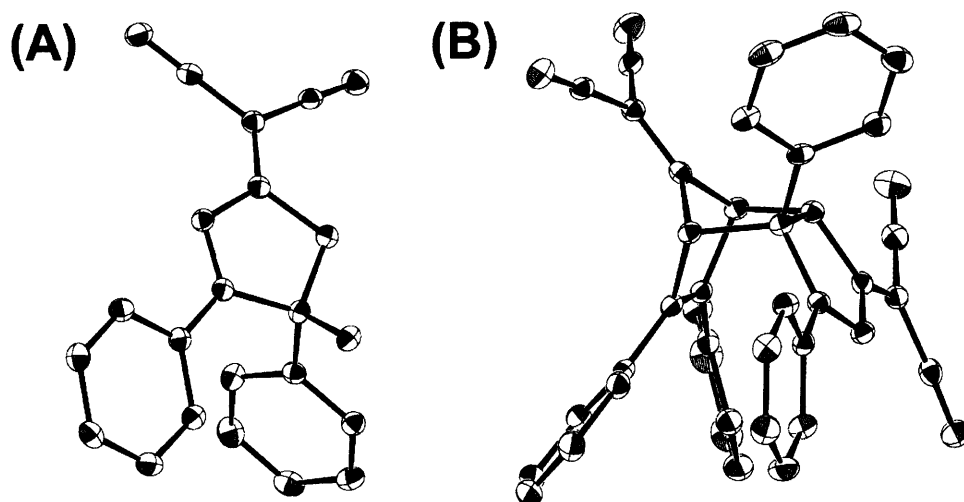
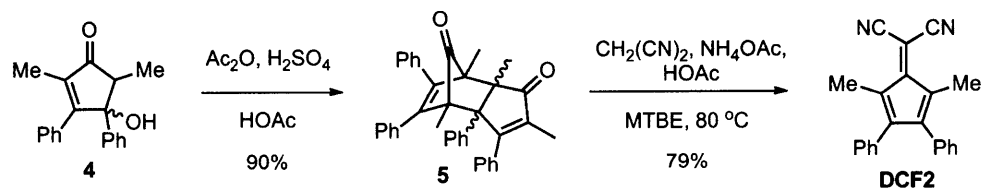


Figure 5.2. Crystal structures of (A) **3** and (B) **DCF1b**.



Scheme 5.2. Synthesis of **DCF2**.

In an attempt to isolate a monomeric 6,6-dicyanofulvene, two methyl substituents were introduced at the 2- and 5-positions of the starting hydroxy-2-cyclopenten-1-one. Compound **4** was obtained from the aldol condensation of 3-pentanone with benzil and was subsequently dehydrated to yield the cyclopentadienone dimer **5**. Compound **5** is a member of a subclass of

cyclopentadienones that can be reversibly cracked to their monomeric forms at elevated temperatures, unlike the parent CPD.¹⁶ Therefore, **DCF2** was directly accessed from **5** by conducting the 1,2-addition of malononitrile at 80 °C. Notably, dark purple, crystalline **DCF2** was isolated in its monomeric form (see Figure 5.3) while the corresponding cyclopentadienone dimerizes at room temperature.

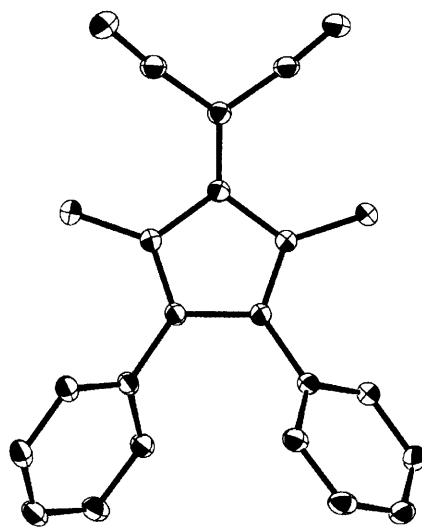
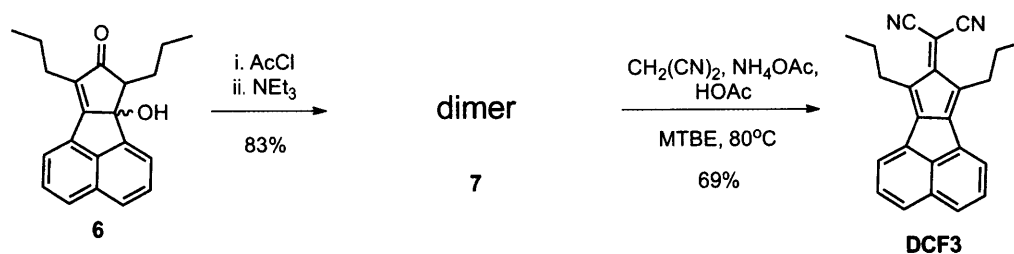


Figure 5.3. X-ray crystal structure of **DCF2**.



Scheme 5.3. Synthesis of **DCF3**.

Wudl and co-workers have previously demonstrated that acenaphthene-containing cyclopentadienones are exceptionally planar compounds that display desirable π - π stacking interactions in the solid state.¹⁵ Therefore, the synthesis of an acenaphthene-containing DCF was investigated. Compound **6** was obtained from the aldol condensation of 5-nonanone with acenaphthenequinone and was isolated as a 1:1 mixture of diastereomers (Scheme 5.3). Attempts to dehydrate **6** with acetic anhydride in the presence of a catalytic amount of sulfuric acid only yielded a complex mixture of acetates. Instead, a two-step dehydration procedure involving acetyl chloride and a tertiary amine base¹⁹ cleanly afforded a dimeric cyclopentadienone, **7**.

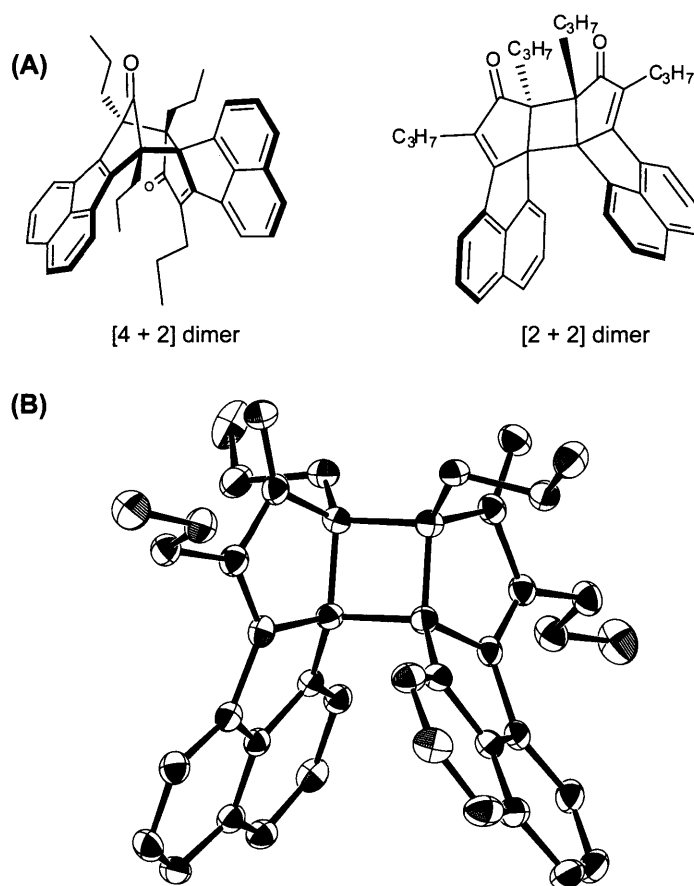


Figure 5.4. (A) Two possible structures for the dimeric cyclopentadienone **7**. (B) X-ray crystal structure of the isolated dimer **7**.

Based on the previously-detailed dimerization behavior of cyclopentadienones, we initially assumed that the isolated CPD dimer **7** was the product of a [4 + 2] cycloaddition reaction (Figure 5.4A). However, as seen in Figure 5.4B, the X-ray crystal structure of **7** revealed that it was, in fact, the product of a [2 + 2] cycloaddition reaction. The presence of the [4 + 2] dimer was, surprisingly, not observed. The [2 + 2] dimerization reaction was reversible and a pale salmon color (stemming from the monomer CPD) quickly evolved when **7** was dissolved in chloroform; heating **7** to 60 °C, in either chloroform solutions or in the solid state resulted in the evolution of a deep pink compound, which can be assigned as the monomeric CPD. The yellow [2 + 2] dimer was cleanly re-isolated upon subsequent cooling to room temperature. To the extent of our knowledge, the formation of **7** is not a photochemical process, as the same [2 + 2] dimer can be isolated when the dehydration of **6** is conducted in the dark. Similar behavior in a 1,4-dimethyl analog of **7** was briefly communicated by Jones and McDonald;²⁰ however, we are currently unsure as to the electronic origins of the thermal [2 + 2] dimerization reaction of acenaphthene-containing CPDs.

Similar to **DCF2**, **DCF3** was directly accessed from dimer **7** by conducting the 1,2-addition of malononitrile at 80 °C. Also similar to **DCF2**, dark green, crystalline **DCF3** was isolated in its monomeric form (see Figure 5.5) while the corresponding cyclopentadienone dimerizes at room temperature.

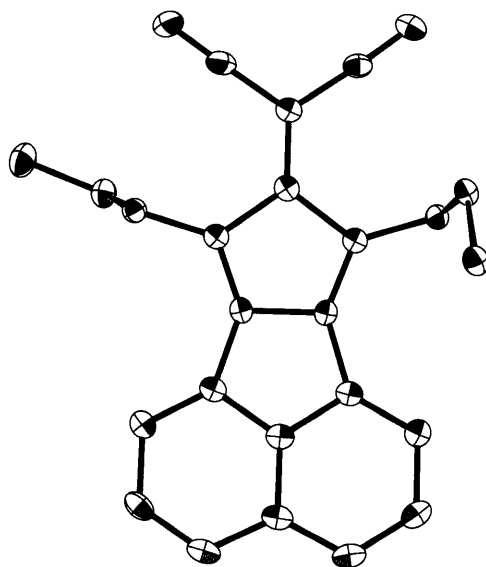
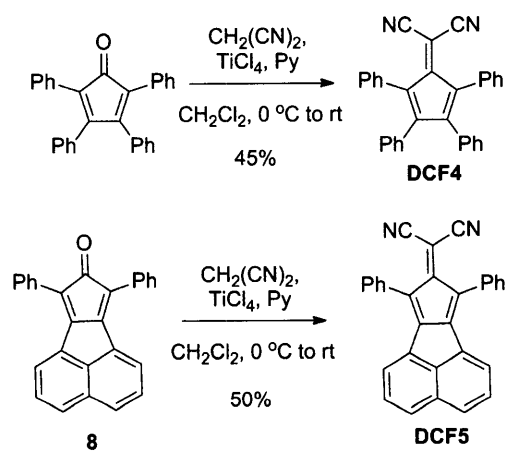


Figure 5.5. X-ray crystal structure of **DCF3**.



Scheme 5.4. Synthesis of 1,4-diphenyl-6,6-dicyanofulvenes.

It was found that introduction of phenyl substituents at the 1,4-positions of the fulvene skeleton hindered the 1,2-addition of malononitrile and therefore, the reaction conditions used in the synthesis of **DCF1-3** failed to generate the dicyanofulvene analogs of tetracyclone and **8**.

Nevertheless, the use of a strong Lewis acid, such as $\text{BF}_3\cdot\text{OEt}_2$ or TiCl_4 , in combination with pyridine afforded the desired cyanofulvenes **DCF4** and **DCF5** (Scheme 5.4). In these instances, the progress of the reaction can be witnessed optically: deep purple tetracyclone forms pea green **DCF4** while navy blue **8** forms emerald green **DCF5**.

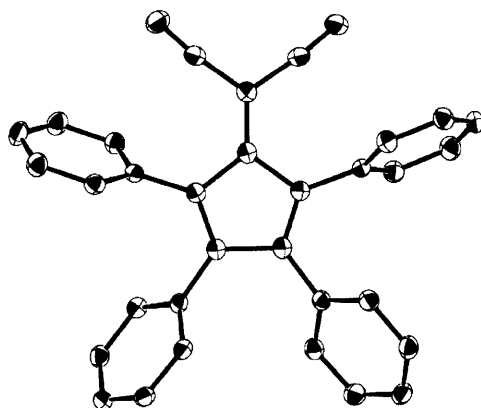


Figure 5.6. X-ray crystal structure of **DCF4**.

The crystal structure of **DCF4** is shown in Figure 5.6. Both **DCF2** and **DCF4** do not display edge-to-face packing in the solid state, preferring instead weak π - π interactions between fulvene cores (see Additional Figures).

5.3 Electrochemistry

Cyclic voltammograms (Figure 5.4) of all monomeric dicyanofulvenes were recorded in order to judge their suitability as electron-transport materials in electronic devices. The electrochemical properties of **DCF2-5** are summarized in Table 5.1. In general, the dicyanofulvenes displayed two distinct, reversible one-electron reduction peaks. The first one-electron reduction for **DCF4** and **DCF5**, which contain two phenyl substituents in the 1,4-

positions, occurred at slightly lower potentials than in DCFs with alkyl substituents in the 1,4-positions.

For cases where the parent CPDs are monomeric, such as with **DCF4-5**, it was possible to evaluate the effects of the dicyanovinylene moiety on the electronic properties of select cyclopentadiene systems. As previously reported, cyclic voltammograms of CPDs generally display a single two-electron reduction peak²¹ (see Additional Figures) and the intermediate radical anion product of one-electron reduction is observed only in select cases.¹⁵ In contrast, the intermediate radical anions of DCFs are stable and therefore, cyclic voltammograms of DCFs display two distinct, one-electron reduction peaks. Additionally, the formal reduction potentials of DCFs are globally lower than those of the corresponding CPDs.

The electron affinities (EA) of **DCF2-5** were calculated from their formal reduction potentials using the formula $EA = E_{\text{red}} + 4.4 \text{ eV}^{10}$ and are listed in Table 5.1. With average electron affinities of 3.9 eV, DCFs are comparable to PCBM (EA 4.0 eV) as electron acceptors.

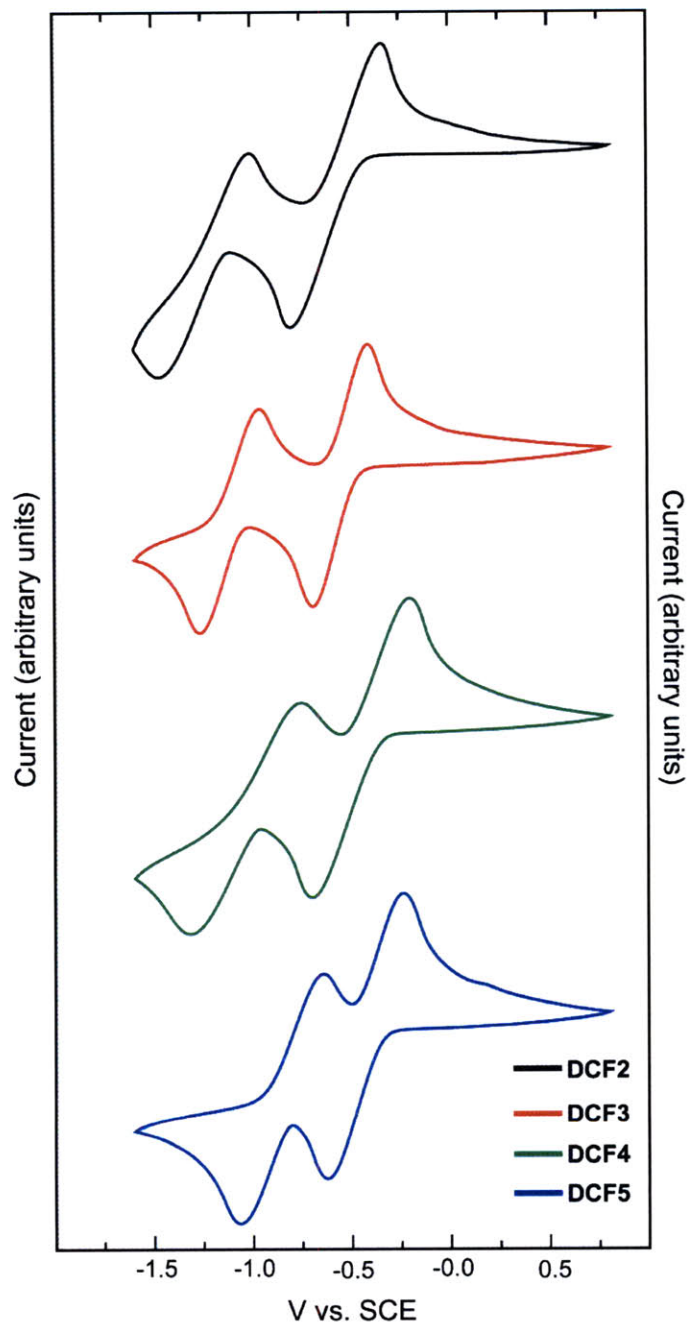


Figure 5.7. Cyclic voltammograms of **DCF2-5** recorded in 0.1M TBAPF₆ in CH₂Cl₂ using a Pt button electrode at a scan rate of 100 mV/s.

Voltage values are reported vs. standard calomel electrode (SCE).

Table 5.1. Optical and electrochemical properties of **DCF2-5**

Compound	λ_{\max}/nm ($\log \epsilon$)	$E_{\text{red}} / \text{V vs. SCE}$	EA^a / eV
DCF2	275 (4.2), 370 (4.1), 555 (2.5)	-0.57, -1.24	3.83
DCF3	332 (4.6), 641 (2.5)	-0.61, -0.84	3.80
DCF4	270 (4.2), 387 (4.1), 543 (2.6)	-0.45, -1.04	3.95
Tetracyclone	265 (4.3), 338 (3.8), 509 (3.1)	-1.06	--
DCF5	333 (4.7), 638 (2.6)	-0.43, -0.85	3.97
8	334 (4.2), 381 (3.9), 580 (3.1)	-0.95	--

^a $EA = E_{\text{red}} (\text{V vs. SCE}) + 4.4 \text{ eV}$

5.4 Conclusions

A series of substituted 6,6-dicyanofulvenes were synthesized starting from masked, dimeric or monomeric cyclopentadienones. DCFs lacking sufficient steric bulk around the fulvene core tend to reversibly undergo a [4+2] dimerization. In addition to being highly crystalline, DCFs are darkly-colored compounds due to the presence of weak electronic transitions in the visible region of the electromagnetic spectrum. DCFs display two distinct, reversible one-electron reductions by cyclic voltammetry. Based on their high crystallinity and suitable electron affinities, and buoyed by their relatively cheap and straight-forward synthesis, DCFs are interesting candidates for organic electron-transport materials.

5.5 Experimental Section

Materials: Synthetic manipulations that required an inert atmosphere (where noted) were carried out under argon using standard Schlenk techniques. All solvents were of ACS reagent grade or better unless otherwise noted. Anhydrous tetrahydrofuran, toluene and dichloromethane were obtained from J. T. Baker and dried on a solvent column purification system. Silica gel (40-63 μm) was obtained from SiliCycle Inc. Benzil, 3-pentanone, malononitrile, 1,3-diphenylacetone, acenaphthenequinone, tetracyclone, and TiCl_4 were purchased from Aldrich and used without further purification.

NMR Spectroscopy: ^1H and ^{13}C NMR spectra for all compounds were acquired in CHCl_3 on a Bruker Avance Spectrometer operating at 400 and 100 MHz, respectively. The chemical shift data are reported in units of δ (ppm) relative to tetramethylsilane (TMS) and referenced with residual CHCl_3 .

Mass Spectrometry: High-resolution mass spectra (HRMS) were obtained at the MIT Department of Chemistry Instrumentation Facility using a peak-matching protocol to determine the mass and error range of the molecular ion, employing either electron impact or electrospray as the ionization technique.

Infrared (IR) spectroscopy: IR spectra were recorded on a Perkin-Elmer Model 2000 FT-IR spectrophotometer at the MIT Department of Chemistry Instrumentation Facility and are reported as strong (s), medium (m) or weak (w).

X-Ray Diffraction: X-ray crystal structures were determined with a Siemens Platform three-circle diffractometer coupled to a Bruker-AXS Smart Apex CCD detector with graphite-monochromated $\text{Mo K}\alpha$ radiation ($\lambda = 0.71073 \text{ \AA}$), performing ϕ - and ω -scans. All structures

were solved by direct methods using SHELXS²² and refined against F²³ on all data by full-matrix least squares with SHELXL-97.² All non-hydrogen atoms were refined anisotropically.

4-hydroxy-3,4-diphenylcyclopent-2-enone (1). 15 mL of 10% methanolic potassium hydroxide was added to a solution of benzil (30g, 143 mmol) and acetone (23 mL, 317 mmol) in 300 mL refluxing methanol. The mixture was heated at 90 °C for 30 minutes, cooled to room temperature and poured into 500 mL ice/water. The resulting solids were filtered, washed with water and dried to yield 30 g of a faint-yellow powder (84%). m.p. 146-148 °C. ¹H NMR (400 MHz, CHCl₃) δ 2.85 (d, *J* = 18.4 Hz, 1H), 2.90 (broad singlet, 1H), 2.93 (d, *J* = 18.4 Hz, 1H), 6.65 (s, 1H), 7.30 (m, 6H), 7.41 (m, 2H), 7.49 (m, 2H). ¹³C NMR (100 MHz, CHCl₃) δ 56.7, 81.8, 124.3, 127.6, 128.9, 129.1, 129.2, 129.3, 131.1, 131.5, 144.2, 174.2, 205.1. HRMS (ESI) calc for C₁₇H₁₄O₂ [M-H]⁻ 249.0921, found 249.0915. IR (KBr plate) 700 (s), 766 (m), 976 (m), 1049 (m), 1210 (9s), 1249 (m), 1324 (w), 1447 (m), 1569 (s), 1685 (s), 3027 (m), 3061 (m), 3388 (s) cm⁻¹.

2-(4-hydroxy-3,4-diphenylcyclopent-2-en-1-ylidene)malononitrile (3). Compound **1** (10g, 40 mmol) and malononitrile (13.1g, 198 mmol) were dissolved in 200 mL *t*-butyl methyl ether and to this solution was added 15 g ammonium acetate and 10 mL acetic acid. The resulting mixture was heated to 80 °C for 30 h with a Dean-Stark trap to remove excess water. Upon cooling, diethyl ether (50 mL) was added to the reaction and a yellow solid started to precipitate. The solids were isolated by filtration, washed with cold diethyl ether and dried. Purification by flash column chromatography with 1% methanol in dichloromethane afforded 8.3 g of a bright yellow solid (70%). m.p. 192-194 °C. ¹H NMR (400 MHz, CHCl₃) δ 2.83 (broad singlet, 1H), 3.43 (s,

2H), 7.25 (s, 1H), 7.35 (m, 8H), 7.62 (m, 2H). ^{13}C NMR (100 MHz, CHCl_3) δ 27.1, 53.1, 75.2, 85.5, 112.6, 112.98, 124.13, 126.42, 128.3, 129.3, 129.3, 129.6, 130.8, 132.1, 143.2, 169.5, 177.4. HRMS (ESI) calc for $\text{C}_{20}\text{H}_{14}\text{N}_2\text{O}$ $[\text{M}-\text{H}]^-$ 297.1033, found 297.1023. IR (KBr plate) 1564 (m), 1586 (m), 2225 (m), 3426 (m) cm^{-1} .

2,3-Diphenyl-6,6-dicyanofulvene dimer (DCF1b). A mixture of compound **3** (0.10g, 0.33 mmol) and PTSA (20 mg, 105 mmol) in toluene (20 mL) was heated to 80 °C for 3 hours. The initially inhomogeneous reaction mixture was observed to turn homogenous after 5 minutes and the reaction mixture turned dark brown with heating. If, at this point, the reaction mixture was taken off the heat and cooled to room temperature, the dark brown solution was observed to turn bright yellow after approximately 6 hours. If, instead, the solvent from the reaction was evaporated under reduced pressure, the dark brown reaction mixture was observed to turn bright yellow almost immediately as the solvent evaporated. The monomeric **DCF1a** could therefore not be isolated as a solid directly from the reaction mixture. After complete solvent evaporation, the remaining yellow residue was purified by flash column chromatography with 70% dichloromethane in hexanes to afford approximately 0.09g of **DCF1b** as a bright yellow solid (97%). Heating a solution of **DCF1b** to approximately 80 °C turned the initially yellow solution dark brown and subsequent cooling reverts the color back to bright yellow. ^1H NMR (400 MHz, CHCl_3) δ 3.95 (d, $J = 4.4$ Hz, 1H), 4.60 (dd, $J = 2$ Hz, 4.4 Hz, 1H), 4.92 (d, $J = 2$ Hz, 1H), 6.82 (m, 2H), 6.90 (m, 2H), 6.99 (m, 1H), 7.13 (m, 2H), 7.26 (m, 7H), 7.34 (m, 6H), 7.46 (m, 3H). ^{13}C NMR (100 MHz, CHCl_3) δ 27.1, 53.5, 56.5, 60.2, 67.1, 72.3, 110.3, 111.6, 112.2, 113.1, 125.6, 128.2, 128.4, 128.5, 128.9, 129.0, 129.2, 129.3, 129.4, 129.7, 130.4, 130.7, 131.6, 132.2, 132.4, 132.8, 139.1, 139.9, 140.2, 168.6, 177.0, 184.6. HRMS (ESI) calc for $\text{C}_{40}\text{H}_{24}\text{N}_4$ $[\text{M}-\text{H}]^-$

559.1928, found 559.1930. IR (KBr plate) 695 (s), 736 (m), 764 (m), 1345 (m), 1445 (s), 1546 (s), 1566 (s), 1648 (m), 2225 (s), 3028 (m), 3058 (m) cm^{-1} .

4-hydroxy-2,5-dimethyl-3,4-diphenylcyclopent-2-enone (4). 15 mL of 10% methanolic potassium hydroxide was added to a solution of benzil (30g, 143 mmol) and 3-pentanone (15 mL, 150 mmol) in 300 mL refluxing methanol. The mixture was heated at 90 °C for 30 minutes, cooled to room temperature and poured into 500 mL ice/water. The resulting solids were filtered, washed with water and dried to yield 33 g of **4** as an approximately 3:1 mixture of diastereomers, by $^1\text{H-NMR}$ (85% total). The diastereomeric mixture was carried on to the next step without further purification. m.p. 172-174 °C. $^1\text{H NMR}$ (Major diastereomer) (400 MHz, CHCl_3) δ 1.19 (d, $J = 7.2$ Hz, 3H), 1.94 (s, 3H), 2.42 (broad singlet, 1H), 2.68 (quartet, $J = 7.2$ Hz, 1H), 7.23 (m, 10H). $^{13}\text{C NMR}$ (mixture of diastereomers) (100 MHz, CHCl_3) δ 10.0, 10.1, 10.3, 10.4, 56.1, 55.9, 82.7, 85.1, 125.1, 125.8, 127.2, 127.8, 128.4, 128.6, 128.8, 129.1, 129.2, 129.2, 129.5, 130.1, 132.9, 133.6, 135.1, 137.6, 137.9, 141.6, 144.3, 166.4, 167.7, 207.1, 209.8. HRMS (ESI) calc for $\text{C}_{19}\text{H}_{18}\text{O}_2$ $[\text{M}+\text{H}]^+$ 279.1380, found 279.1374. IR (KBr plate) 699 (s), 1341 (m), 1448 (m), 1622 (m), 1693 (s), 2934 (m), 2977 (m), 3060 (m), 3437 (s) cm^{-1} .

Compound 5. Compound **4** (20 g, 71.9 mmol) was dissolved in 50 mL acetic acid and to this solution was added 20 ml acetic anhydride and 1 mL concentrated sulfuric acid. The reaction was stirred at room temperature for 3 hours and then poured over ice (200 g). The solids were filtered, washed with saturated sodium bicarbonate and water, and dried to yield 33.5 g of a yellow powder (90%). m.p. (decomp) 190 °C. $^1\text{H NMR}$ (400 MHz, CHCl_3) δ 0.57 (s, 3H), 1.25 (s, 3H), 1.63 (s, 3H), 2.24 (s, 3H), 6.66 (d, $J = 2$ Hz, 2H), 7.3 (m, 18H), 7.52 (m, 2H), 7.65 (m,

1H), 7.98 (m, 1H). ¹³C NMR (100 MHz, CHCl₃) δ 10.0, 12.5, 12.6, 18.2, 58.6, 59.9, 61.2, 66.9, 127.0, 127.1, 127.2, 127.4, 127.5, 128.1, 129.2, 129.5, 130.1, 130.3, 1301.0, 132.0, 133.5, 134.1, 135.1, 140.3, 143.4, 203.3. HRMS (ESI) calc for C₃₈H₃₂O₂ [M+H]⁺ 521.2475, found 521.2472. IR (KBr plate) 700 (m), 732 (m), 911 (w), 1211 (m), 1335 (m), 1447 (m), 1494 (m), 1598 (m), 1685 (s), 1768 (s), 2938 (m), 2980 (m), 3058 (m) cm⁻¹.

1,4-Dimethyl-2,3-diphenyl-6,6-dicyanofulvene (DCF2). Compound **5** (10g, 19.2 mmol) and malononitrile (8g, 121 mmol) were dissolved in 200 mL t-butyl methyl ether and to this solution was added 15 g ammonium acetate and 10 mL acetic acid. The resulting mixture was heated to 80 °C for 20 h with a Dean-Stark trap to remove excess water. Water (100 mL) was added to the cooled reaction, the layers separated and the aqueous phase extracted with ether (3x 30 mL). The organic layers were combined and dried over magnesium sulfate, and the solvent was evaporated under reduced pressure. The residue thus obtained was purified by flash column chromatography with 40% dichloromethane in hexanes as eluent to yield 4.6 g of a dark purple powder (79%). m.p. 148-150 °C. ¹H NMR (400 MHz, CHCl₃) δ 2.21 (s, 3H), 6.85 (m, 2H), 7.22 (m, 3H). ¹³C NMR (100 MHz, CHCl₃) δ 12.9, 82.7, 113.3, 125.8, 128.1, 128.8, 129.6, 133.0, 151.8, 171.2. HRMS (ESI) calc for C₂₂H₁₆N₂ [M+H]⁺ 309.1386, found 309.1371. IR (KBr plate) 700 (s), 764 (s), 1343 (m), 1444 (m), 1560 (m), 2222 (s), 2919 (m), 2951 (m), 3080 (w) cm⁻¹.

Compound 6. 5 mL of 10% methanolic potassium hydroxide was added to a solution of acenaphthenequinone (5g, 27.5 mmol) and 5-nonanone (6.1 mL, 5.07 g, 35.7 mmol) in 100 mL methanol. The mixture was stirred at room temperature for 3 h and poured into 200 mL ice/water. The resulting solids were filtered, washed with water, dried and purified by flash

column chromatography (5% methanol in dichloromethane eluent) to yield 6.8 g of **6** as an approximately 1:1 mixture of diastereomers by ^1H NMR (80% total). The diastereomeric mixture was carried on to the next step without further purification. ^1H NMR (mixture of diastereomers) (400 MHz, CHCl_3) δ 0.94 (t, $J = 7.6$ Hz, 3H), 1.07 (t, $J = 7.2$ Hz, 3H), 1.58 (septet, $J = 7.6$ Hz, 2H), 1.66 (m, 1H), 1.95 (m, 3H), 2.37 (m, 1H), 2.49 (m, 1H), 2.57 (m, 2H), 7.54 (m, 3H), 7.72 (m, 2H), 7.79 (d, $J = 8.4$ Hz, 1H). ^{13}C NMR (mixture of diastereomers) (100 MHz, CHCl_3) δ 14.4, 14.6, 21.9, 22.3, 26.2, 27.2, 56.6, 85.8, 120.9, 122.4, 125.9, 127.9, 128.5, 128.7, 131.8, 132.9, 136.1, 138.7, 142.6, 169.9, 210.1. HRMS (DART) calc for $\text{C}_{21}\text{H}_{22}\text{O}_2$ $[\text{M}-\text{H}]^-$ 305.1547, found 305.1555. IR (KBr plate) 1341 (m), 1448 (m), 1622 (m), 1697 (s), 2934 (m), 2977 (m), 3060 (m), 3427 (s) cm^{-1} .

Compound 7. A 50 mL round bottom flask was charged with **6** (5 g, 16.3 mmol) and acetyl chloride (10 mL) under a positive flow of argon. The resulting mixture was stirred at room temperature under a positive flow of argon for 12 h and then the residual acetyl chloride was evaporated under reduced pressure. The residual solid was dissolved in 50 mL toluene, 15 mL triethylamine was added and the resulting solution heated to 100 $^\circ\text{C}$ for 3 h in the dark. The solvents were evaporated under reduced pressure and the resulting salmon-colored residue was purified by flash column chromatography (in the dark) with 50% dichloromethane in hexanes as eluent. 3.9 g (83%) of a yellow compound was thus obtained. Upon dissolution in either dichloromethane or chloroform this yellow compound was observed to form a pale-pink solution. Heating the solution to ca. 60 $^\circ\text{C}$ resulted in a dark pink solution. Subsequent cooling to room temperature recovered the aforementioned pale-pink solution. Cooling this solution to 0 $^\circ\text{C}$ did not result in disappearance of the pale pink color. ^1H NMR (mixture of monomeric and

dimeric CPD) (400 MHz, CHCl₃) δ 0.55 (m, 1H), 0.66 (t, $J = 7.2$ Hz, 3H), 1.82 (m, 1H), 0.98 (t, $J = 7.2$ Hz, 1H), 1.09 (t, $J = 7.6$ Hz, 3H), 1.76 (m, 1H), 1.81 (m, 3H), 2.45 (m, 1H), 2.58 (m, 2H), 2.73 (m, 1H), 7.35 (m, 6H), 7.75 (m, 1H). ¹³C NMR (mixture of monomeric and dimeric CPD) (100 MHz, CHCl₃) δ 0.2, 14.4, 14.5, 14.9, 18.8, 22.3, 22.4, 26.1, 26.2, 33.6, 60.5, 67.3, 120.4, 120.8, 123.8, 123.9, 126.4, 127.1, 127.6, 127.6, 128.6, 130.4, 133.6, 138.6, 138.8, 141.1, 174.4, 208.8. HRMS (DART) monomer: calc for C₂₁H₁₉O [M-H]⁻ 287.1436, found 287.1437, dimer: calc for C₄₂H₃₉O₂ [M-H]⁻ 575.2950, found 575.2951. IR (KBr plate) 778 (s), 1365 (m), 1457 (w), 1644 (s), 1695 (s), 2871 (m), 2931 (m), 2958 (m), 3047 (m) cm⁻¹.

2-(7,9-dipropyl-8H-cyclopenta[a]acenaphthylen-8-ylidene)malononitrile (DCF3).

Compound 7 (1 g, 1.7 mmol) and malononitrile (3 g, 45 mmol) were dissolved in 100 mL *t*-butyl methyl ether and to this solution was added 10 g ammonium acetate and 5 mL acetic acid. The resulting mixture was heated to 80 °C for 20 h with a Dean-Stark trap to remove excess water. Water (100 mL) was added to the cooled reaction, the layers separated and the aqueous phase extract with ether (3x 30 mL). The organic layers were combined and dried over magnesium sulfate, and the solvent was evaporated under reduced pressure. The residue thus obtained was purified by flash column chromatography with 40% dichloromethane in hexanes as eluent to yield 0.81 g of dark green needles (69%). m.p. 189 °C. ¹H NMR (400 MHz, CHCl₃) δ 1.05 (t, $J = 7.2$ Hz, 3H), 1.67 (sextet, $J = 7.6$ Hz, 2H), 2.80 (t, $J = 8.0$ Hz, 2H), 7.60 (m, 2H), 7.77 (m, 1H). ¹³C NMR (100 MHz, CHCl₃) δ 0.2, 14.1, 23.6, 28.6, 81.2, 113.1, 120.9, 126.5, 127.0, 128.8, 131.3, 132.3, 148.1, 152.6, 175.1. HRMS (ESI) calc for C₂₄H₂₀N₂ [M-H]⁻ 336.1632, found 336.1633. IR (KBr plate) 767 (m), 776 (m), 822 (m), 1288 (m), 1365 (m), 1463 (m), 1547 (s), 1644 (s), 1694 (s), 2218 (s), 2869 (m), 2957 (m) cm⁻¹.

1,2,3,4-Tetraphenyl-6,6-dicyanofulvene (DCF4). To an ice-cooled solution of tetracyclone (3 g, 7.8 mmol) and malononitrile (1g, 15 mmol) in 100 mL dry dichloromethane was added dropwise TiCl_4 (4.4 mL) over 5 minutes under argon. After the addition was complete, 15 mL pyridine was added to the reaction dropwise over 10 minutes. The reaction mixture was allowed to warm to room temperature and stir under argon for an additional 2 hours. The solvents were evaporated under reduced pressure, and the remaining solids were taken up in 50 mL dichloromethane and washed with 0.1M HCl. The organic layer was dried over magnesium sulfate, solvents evaporated under reduced pressure and the residue purified by flash column chromatography with 40% dichloromethane in hexanes as eluent. 1.5 g of a yellow-green powder was thus obtained (45%). m.p. 220-222 °C. ^1H NMR (400 MHz, CHCl_3) δ 6.83 (m, 2H), 7.02 (t, $J = 8$ Hz, 2H), 7.13 (m, 1H), 7.29 (m, 2H), 7.37 (m, 2H). ^{13}C NMR (100 MHz, CHCl_3) δ 86.7, 111.5, 1127.7, 128.8, 128.9, 129.3, 130.0, 131.3, 131.9, 131.9, 132.6, 151.3, 168.7. HRMS (DART) calc for $\text{C}_{32}\text{H}_{20}\text{N}_2$ [M-] 432.1632, found 432.1618. IR (KBr plate) 697 (m), 1027 (m), 1246 (m), 1376 (m), 1457 (m), 2221 (m), 2868 (m), 2923 (s), 2954 (s) cm^{-1} . Tetracyclone: IR (KBr plate) 1712 cm^{-1} .

7,9-diphenyl-8H-cyclopenta[a]acenaphthylen-8-one (8). 5 mL of 10% methanolic potassium hydroxide was added to a solution of acenaphthenequinone (5g, 27 mmol) and 1,3-diphenylacetone (6 g, 28.5 mmol) in 200 mL refluxing methanol. The mixture was heated at 90 °C for 30 minutes and then placed in a -4 °C refrigerator. After 3 hours, the resulting black crystals were filtered, washed with methanol and dried to yield 7.8g of **6** (80%). ^1H NMR (400 MHz, CHCl_3) δ 7.38 (m, 1H), 7.47 (m, 2H), 7.55 (m, 1H), 7.82 (m, 3H), 8.03 (m, 1H). ^{13}C NMR

(100 MHz, CHCl₃) δ 121.1, 121.8, 127.9, 128.5, 128.6, 128.8, 129.2, 131.6, 131.7, 154.4, 202.1. HRMS (ESI) calc for C₂₇H₁₅O [M-H]⁻ 355.1128, found 355.1134. IR (KBr plate) 697 (m), 799 (m), 1121 (m), 1297 (m), 1696 (m), 2923 (m) cm⁻¹.

2-(7,9-diphenyl-8H-cyclopenta[a]acenaphthylen-8-ylidene)malononitrile (DCF5). To an ice-cooled solution of **8** (3g, 16.8 mmol) and malononitrile (1.5g, 22.7 mmol) in 100 mL dry dichloromethane was added dropwise TiCl₄ (5.5 mL) over 5 minutes under argon. After the addition was complete, 18 mL pyridine was added to the reaction dropwise over 10 minutes. The reaction mixture was allowed to warm to room temperature and stir under argon for an additional 2 hours. The solvents were evaporated under reduced pressure, and the remaining solids were taken up in 50 mL dichloromethane and washed with 0.1M HCl. The organic layer was dried over magnesium sulfate, solvents evaporated under reduced pressure and the residue purified by flash column chromatography with 40% dichloromethane in hexanes as eluent. 1.7 g of a forest green powder was thus obtained (50%). m.p. 275 °C. ¹H NMR (400 MHz, CHCl₃) δ 7.34 (d, *J* = 7.2 Hz, 2H), 7.42 (t, *J* = 8 Hz, 2H), 7.54 (m, 10H), 7.75 (d, *J* = 8 Hz, 2H). ¹³C NMR (100 MHz, CHCl₃) δ 85.3, 111.8, 121.2, 126.5, 127.9, 128.7, 129.2, 129.7, 129.9, 130.4, 131.8, 132.1, 148.1, 152.5, 174.0. HRMS (DART) calc for C₃₀H₁₆N₂ [M-] 404.1319, found 404.1303. IR (KBr plate) 701 (m), 761 (m), 1244 (m), 1551 (m), 2221 (s), 2927 (m) cm⁻¹.

5.6 References and Notes

- (1) (a) Payne, M. M.; Parkin, S. R.; Anthony, J. E.; Kuo, C.-C.; Jackson, T. N. *J. Am. Chem. Soc.* **2005**, *127*, 4986. (b) Ebata, H.; Izawa, T.; Miyazaki, E.; Takimiya, K.; Ikeda, M.; Kuwabara, H.; Yui, T. *J. Am. Chem. Soc.* **2007**, *129*, 15732. (c) Subramanian, S.; Park, S.

- K.; Parkin, S. R.; Podzorov, V.; Jackson, T. N.; Anthony, J. E. J. *Am. Chem. Soc.* **2008**, *130*, 2706. (d) Gao, P.; Beckmann, D.; Tsao, H. N.; Feng, X.; Enkelmann, V.; Baumgarten, M.; Pisula, W.; Müllen, K. *Adv. Mater.* **2009**, *21*, 213. (e) Ortiz, R. P.; Facchetti, A.; Marks, T. J. *Chem Rev.* **2010**, *110*, 205.
- (2) (a) Facchetti, A. *Mater. Today* **2007**, *10*, 28. (b) Chua, L.-L.; Zaumseil, J.; Chang, J.-F.; Ou, E. C.-W.; Ho, P. K.-H.; Sirringhaus, H.; Friend, R. H. *Nature* **2005**, *434*, 194.
- (3) (a) Shirota, Y.; Kageyama, H. *Chem. Rev.* **2007**, *107*, 953. (b) Newman, C. R.; Frisbie, C. D.; da Silva Filho, D. A.; Brédas, J.-L.; Ewbank, P. C.; Mann, K. R. *Chem. Mater.* **2004**, *16*, 4436.
- (4) (a) Strukelj, M.; Papadimitrakopoulos, F.; Miller, T. M.; Rothberg, L. J. *Science* **1995**, *267*, 1969. (b) Kulkarni, A. P.; Tonzola, C. J.; Babel, A.; Jenekhe, S. A. *Chem Mater.* **2004**, *16*, 4556.
- (5) (a) Beaujuge, P. M.; Pisula, W.; Tsao Hoi, N.; Ellinger, S.; Müllen, K.; Reynolds, J. R. *J. Am. Chem. Soc.* **2009**, *131*, 7514. (b) Linder, T.; Badiola, E.; Baumgarnter, T.; Sutherland, T. C. *Org. Lett.* **2010**, ASAP doi 10.1021/ol1018213 and references therein.
- (6) (a) Oriz, R. P.; Herrera, H.; Blanco, R.; Huang, H.; Facchetti, A.; Marks, T. J.; Zheng, Y.; Segura, J. L. *J. Am. Chem. Soc.* **2010**, *132*, 8440. (b) Letizia, J. A.; Salata, M. R.; Tribout, C. M.; Facchetti, A.; Ratner, M. A.; Marks, T. J. *J. Am. Chem. Soc.* **2008**, *130*, 9679. (c) Gao, X.; Di, C.; Hu, Y.; Yang, X.; Fan, H.; Zhang, F.; Liu, Y.; Li, H.; Zhu, D. *J. Am. Chem. Soc.* **2010**, *132*, 3697. (d) Katz, H. E.; Lovinger, A. J.; Johnson, J.; Kloc, C.; Seigrist, T.; Li, W.; Lin, Y.-Y.; Dodabalapur, A. *Nature*, **2000**, *404*, 478. (e) Schmidt, R.; Ling, M. M.; Oh, J. H.; Winkler, M.; Könemann, M.; Bao, Z.; Würthner, F. *Adv. Mater.* **2007**, *19*, 3692. (f) Babel, A.; Jenekhe, S. A. *J. Am. Chem. Soc.* **2003**, *125*, 13656.

- (7) Bao, Z.; Lovinger, A. J.; Brown, J. *J. Am. Chem. Soc.* **1998**, *120*, 207.
- (8) (a) Facchetti, A.; Letizia, J.; Yoon, M.-H.; Mushrush, M.; Katz, H.; Marks, T. J. *Chem. Mater.* **2004**, *16*, 4715. (b) Facchetti, A.; Mushrush, M.; Yoon, M.-H.; Hutchison, G. R.; Ratner, M. A.; Marks, T. J. *J. Am. Chem. Soc.* **2004**, *126*, 13859.
- (9) (a) Haddon, R. C.; Perel, A. S.; Morris, R. C.; Palstra, T. T. M.; Hebard, A. F.; Fleming, R. M. *Appl. Phys. Lett.* **1995**, *67*, 121. (b) Kobayashi, S.; Takenobu, T.; Mori, S.; Fujiwara, A.; Iwasa, Y. *Appl. Phys. Lett.* **2003**, *82*, 4581. (c) Meijer, E. J.; De Leeuw, D. M.; Setayesh, S.; van Veenendaal, E.; Huisman, B. H.; Blom, P. W. M.; Hummelen, J. C.; Scherf, U.; Klapwijk, T. M. *Nat. Mater.* **2003**, *2*, 678.
- (10) Izuhara, D.; Swager, T. M. *J. Am. Chem. Soc.* **2009**, *131*, 17724.
- (11) (a) Usta, H.; Facchetti, A.; Marks, T. J. *Org. Lett.* **2008**, *10*, 1385. (b) Usta, H.; Facchetti, A.; Marks, T. J. *J. Am. Chem. Soc.* **2008**, *130*, 8580. (c) Handa, S.; Miyazaki, E.; Takiyama, K.; Kunugi, Y. *J. Am. Chem. Soc.* **2007**, *129*, 11684. (d) Laquindanum, J. G.; Katz, H. E.; Dodabalapur, A.; Lovinger, A. J. *J. Am. Chem. Soc.* **1996**, *118*, 11331. (e) Pappenfus, T. M.; Chesterfield, R. J.; Frisbie, C. D.; Mann, K. R.; Casado, J.; Raff, J. D.; Miller, L. L. *J. Am. Chem. Soc.* **2002**, *124*, 4184. (f) Moslin, R. M.; Andrew, T. L.; Kooi, S. E.; Swager, T. M. *J. Am. Chem. Soc.* **2009**, *131*, 20.
- (12) Pappenfus, T. M.; Hermanson, B. J.; Helland, T. J.; Lee, G. G. W.; Drew, S. M.; Mann, K. R.; McGee, K. A.; Rasmussen, S. C. *Org. Lett.* **2008**, *10*, 1553 and references therein.
- (13) Yamashita, Y.; Suzuki, T.; Saito, G.; Mukai, T. *Chem. Commun.* **1986**, 1489.
- (14) Lim, Y.-F.; Shu, Y.; Parkin, S. R.; Anthony, J. E.; Malliaras, G. G. *J. Mater. Chem.* **2009**, *19*, 3049.

- (15) (a) Yang, C.; Cho, S.; Chiechi, R. C.; Walker, W.; Coates, N. E.; Moses, D.; Heeger, A. J.; Wudl, F. *J. Am. Chem. Soc.* **2008**, *130*, 16524. (b) Walker, W.; Veldman, B.; Chiechi, R.; Partil, S.; Bendikov, M.; Wudl, F. *Macromolecules*, **2008**, *41*, 7278.
- (16) Ogliaruso, M. A.; Romanelli, M. G.; Becker, E. I. *Chem. Rev.* **1965**, *65*, 261.
- (17) Day, J. H. *Chem. Rev.* **1953**, *53*, 167.
- (18) Becker, H.; King, S. B.; Taniguchi, M.; Vanhessche, K. P. M.; Sharpless, K. B. *J. Org. Chem.* **1995**, *60*, 3940.
- (19) Jones, D. W. *J. Chem. Soc. Perkin Trans. 1*, **1977**, 980.
- (20) Jones, D. W.; McDonald, W. S. *Chem. Commun.* **1980**, 417.
- (21) Fox, M. A.; Campbell, K.; Maier, G.; Franz, L. H. *J. Org. Chem.* **1983**, *48*, 1762.
- (22) Sheldrick, G. M. *Acta Cryst. A* **1990**, *46*, 467.
- (23) Sheldrick, G. M. SHELXL 91, Universität Göttingen, Göttingen, Germany, 1997

5.7 Additional Figures

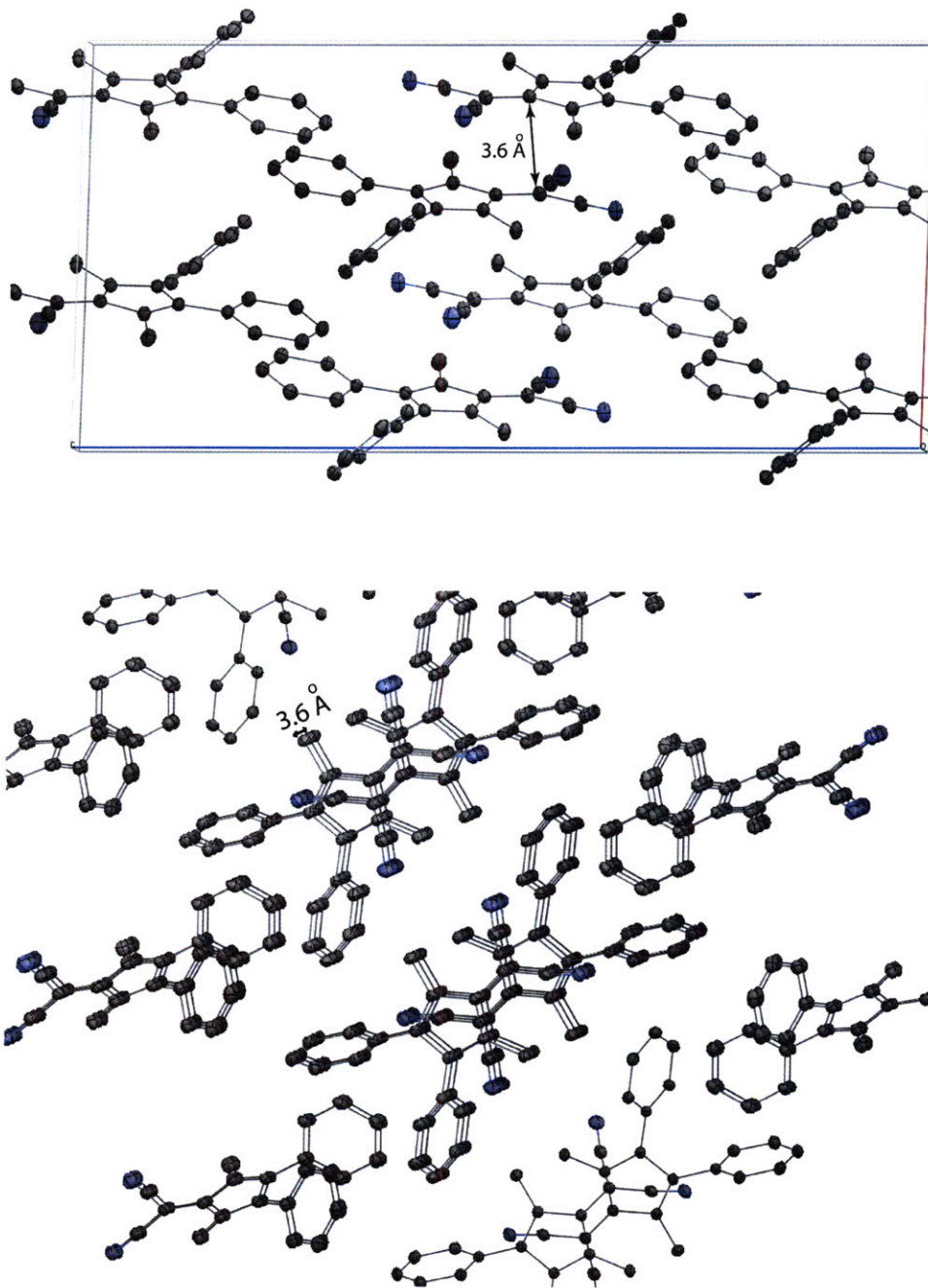


Figure A1. Select views of the packing structure of **DCF2**, showing the absence of herringbone packing between fulvene cores. The intermolecular separation between fulvene cores is ca. 3.6 Å, which is slightly higher than the characteristic π - π stacking distance (3.45 Å). The increased separation between fulvene cores is most likely due to steric crowding arising from the methyl substituents in the 1- and 4-positions.

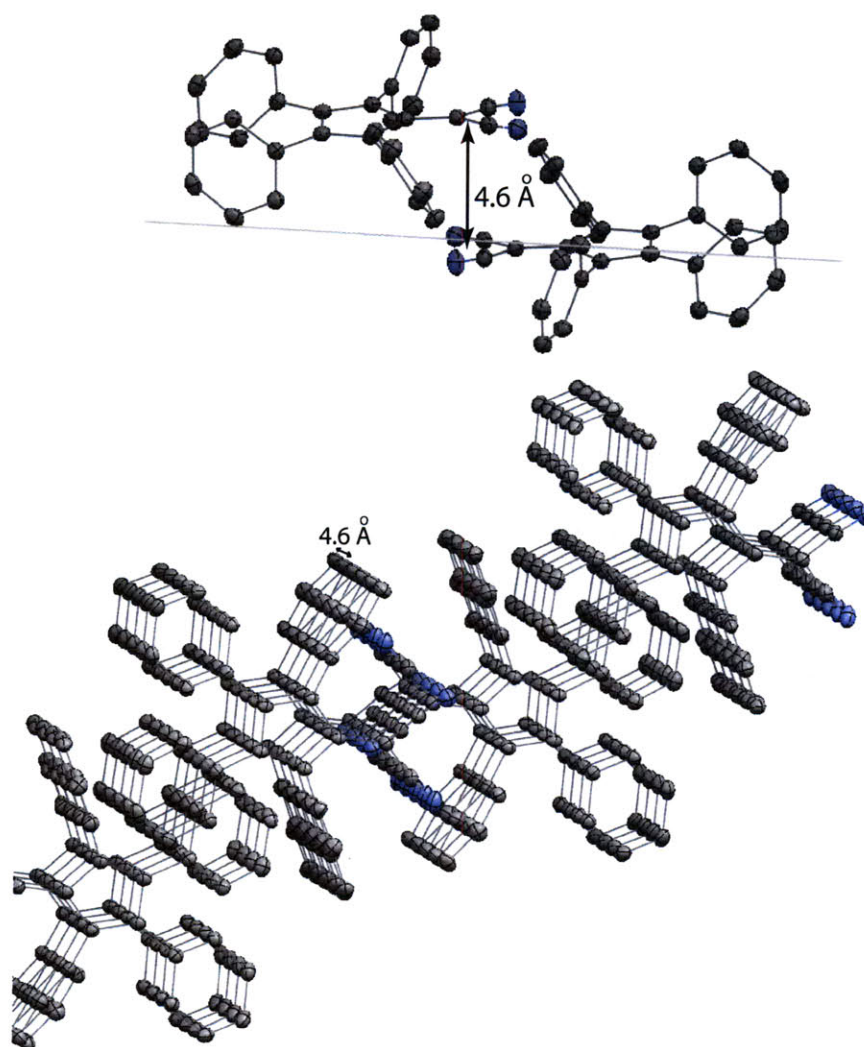


Figure A2. Select views of the packing structure of **DCF3**, showing the absence of herringbone packing between fulvene cores. The intermolecular separation between fulvene cores is ca. 4.6 Å, which is higher than that observed in **DCF2**. The increased separation between fulvene cores is most likely due to relatively greater steric crowding arising from the phenyl substituents in the 1- and 4-positions.

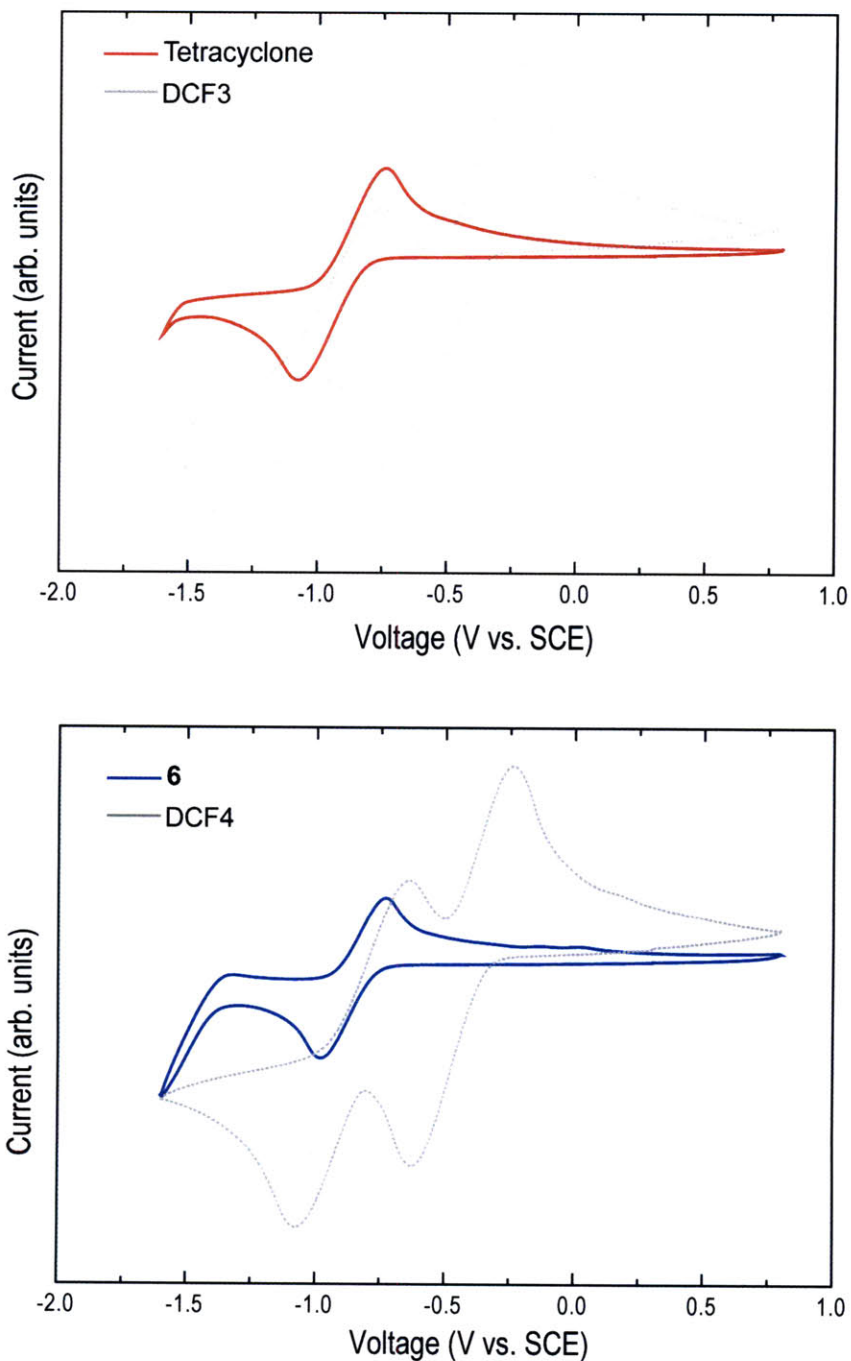


Figure A3. Cyclic voltammograms of monomeric CPDs (tetracyclone in red, **6** in blue) showing only a single reduction peak within the observation window of CH_2Cl_2 . The cyclic voltammograms of the corresponding fulvenes are overlaid (dotted lines) for comparison. Pt button electrode, 0.1M TBAPF_6 in CH_2Cl_2 , 100 mV/s.

CURRICULUM VITAE

TRISHA L. ANDREW

EDUCATION

- 9/2005 – present *Massachusetts Institute of Technology*, Cambridge, MA
Ph.D., Chemistry
Research Advisor: Timothy M. Swager
- 9/2001 – 6/2005 *University of Washington*, Seattle, WA
B.Sc. With Honors, Chemistry
Research Advisor: Natia L. Frank

EXPERIENCE

- 1/2006 – present *Massachusetts Institute of Technology*, Cambridge, MA
Research Assistant, Advisor: Timothy M. Swager
- 3/2007 – present *Student Member, MIT Department of Chemistry Chemical Hygiene and Safety Committee*
- 1/2006 – 12/2009 *Editor, SYNFACTS, Thieme Publishers*
- 9/2006 – 6/2007 *Mentor, MIT Women in Chemistry Program*
- 9/2005 – 12/2005 *Teaching Assistant, Undergraduate introductory chemistry*
- 2/2006 – 5/2006 *Teaching Assistant, Undergraduate chemistry laboratory*
- 6/2002 – 6/2005 *University of Washington*, Seattle, WA
Undergraduate Research Assistant, Advisor: Natia L. Frank
- 6/2004 – 8/2004 *Summer Photonics Intern, NSF Materials and Devices for Information Technology Research Center*
- 3/2002 – 6/2002 *Department of Biochemistry Undergraduate Research Assistant, Advisor: Dr. Hannele Ruohola-Baker*
- 11/2000 – 3/2001 *Intern, University of Washington Human Genome Center, Advisor: Dr. Carl Ton*

PUBLICATIONS

1. **Andrew, T. L.**; Swager, T. M. "Structure Property Relationships for Exciton Transfer in Conjugated Polymers" In *Transport of Charges and Excitons Through Organic Molecular Wires*; Grozema, F. C., Siebbeles, L.D.A., Eds.; Wiley-VCH: Germany, in press.
2. **Andrew, T. L.**; VanVeller, B.; Swager, T. M. "The Synthesis of Azaperylene-9,10-dicarboximides" *Synlett*, **2010**, in press.
3. **Andrew, T. L.**; Cox, J. R.; Swager, T. M. "Synthesis, Reactivity, and Electronic Properties of 6,6-Dicyanofulvenes" *Org. Lett.* **2010**, *12*, 5302-5305.
4. Levine, M.; Song, I.; **Andrew, T. L.**; Kooi, S. E.; Swager, T. M. *J. Polym. Sci. A*, **2010**, *48*, 3382-3391.

5. **Andrew, T. L.**; Tsai, H.-Y.; Menon, R. "Confining Light to Deep Subwavelength Dimensions to Enable Optical Nanopatterning" *Science*, **2009**, 324, 917-921.
6. Moslin, R. M.; **Andrew, T. L.**; Kooi, S. E.; Swager, T. M. "Anionic Oxidative Polymerization: The Synthesis of Poly(phenylenedicyanovinylene) (PPCN2V)" *J. Am. Chem. Soc.* **2009**, 131, 20-21.
7. **Andrew, T. L.** and Swager, T. M. "Reduced Photobleaching of Conjugated Polymer Films Through Small Molecule Additives" *Macromolecules*, **2008**, 41, 8306-8308.
8. **Andrew, T. L.** and Swager, T. M. "A Fluorescence Turn-On Mechanism to Detect the High Explosives RDX and PETN" *J. Am. Chem. Soc.* **2007**, 129, 7254-7255.

ACKNOWLEDGEMENTS

Tim: I couldn't have asked for a better boss/advisor. I know we've had our moments when *I* hoped *you* would be a more involved advisor and *you* hoped *I* would be a more conventional, obedient student, but I think we were, on average, perfect fits for each other. Also, just like real-life parenthood, you are my "father" and are stuck being so, for life, for better or worse.

Koushik Venkatesan, Kazunori Sugiyasu, Ryo Takita, Anne McNeil, Jean Bouffard, Hyuna Kang: Thanks for the **best** years of my life so far. The alchemy of those years can never be recreated.

Hyuna Kang: Our late night chats very seriously saved my soul during an especially dark time. I missed you so when you left and still do.

Jeewoo Lim, Brett VanVeller, Ryan Moslin, and Eric Dane: Even though it lasted only briefly, journal club was my catharsis (do it with protection!).

Jeewoo Lim: You started out being an incidental drinking buddy but grew into one of my closest friends. Your quiet but strong support was much appreciated during my fourth and fifth years. Remember me when you become a ripped K-pop sensation in a few years, babyface.

Jose Miguel Lobez Comeras: You were someone whose presence I ignored in the beginning, but I'm glad I got over that soon because you are one of the funniest, smartest, quickest (multiple senses of the word) people I've met. Thanks for your support toward "the end"; talking with you calmed me down more than you know. It will seriously take me some time to adjust to the fact that I will not see you every morning when I come to work. No matter what you decide to do in your future, I know you will be the best at it; just remember us proletariats when you become a bazillionaire.

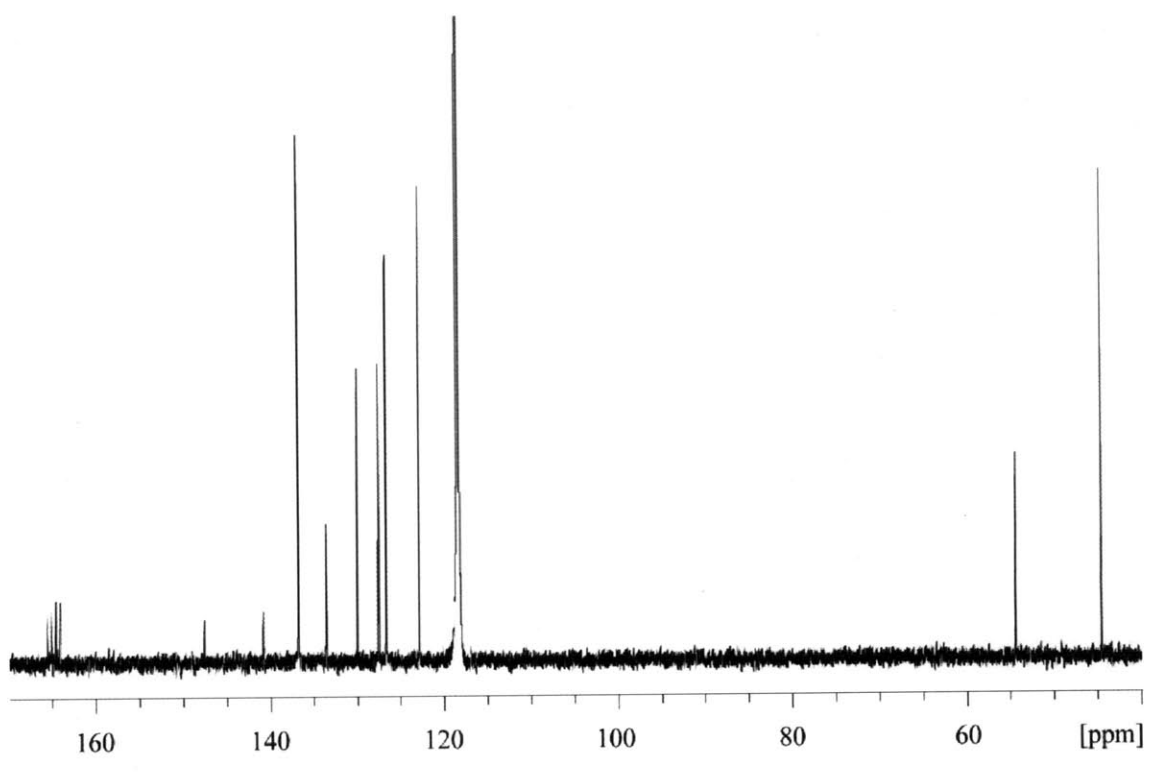
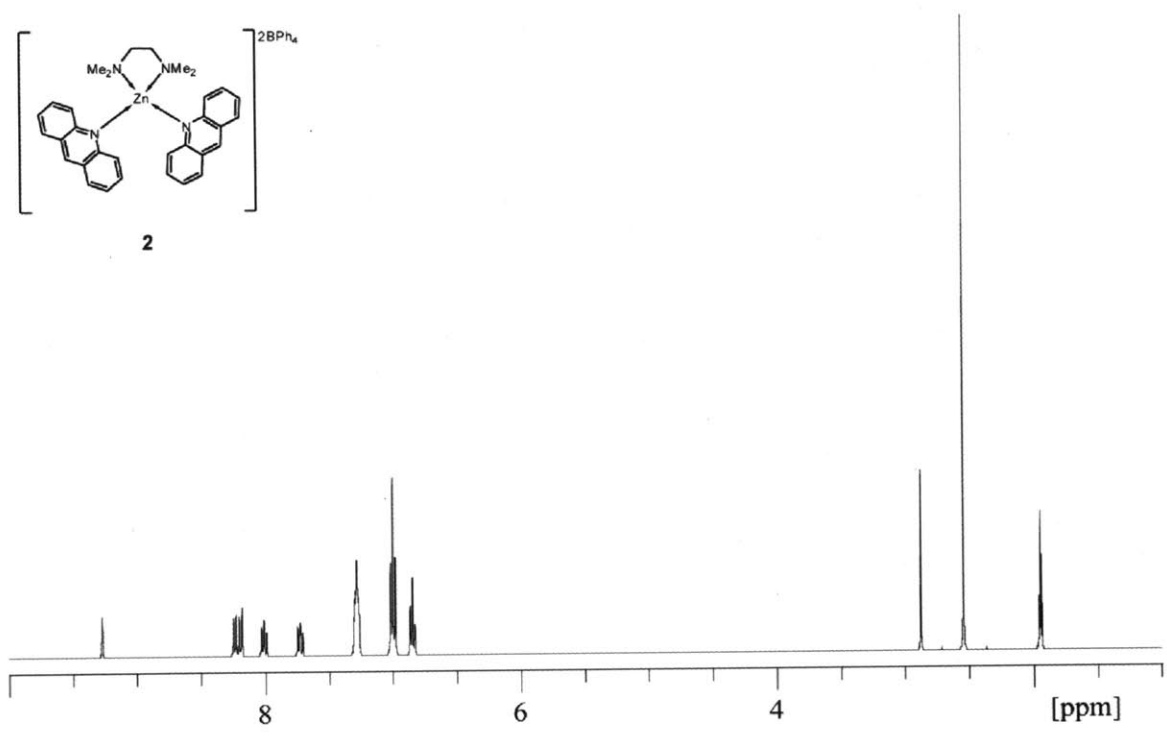
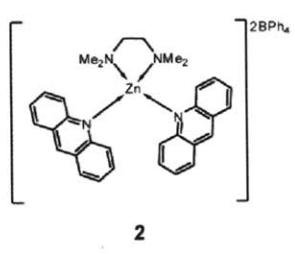
Rebecca Parkhurst: My cohort in all things TV, pop culture, and Sarah Palin-related. You got all my jokes and topical, obscure references when no one else in the room would. I hope your dreams of becoming a naturalized French citizen (or some close approximation) are realized *tout de suite*.

Joel Batson and David Barney Walker: We met only recently, but you are two of the most absurdly entertaining people I've encountered during my tenure in the Swager lab. I can't wait to hear of the crazy/cool things that you two are up to once you move on from MIT.

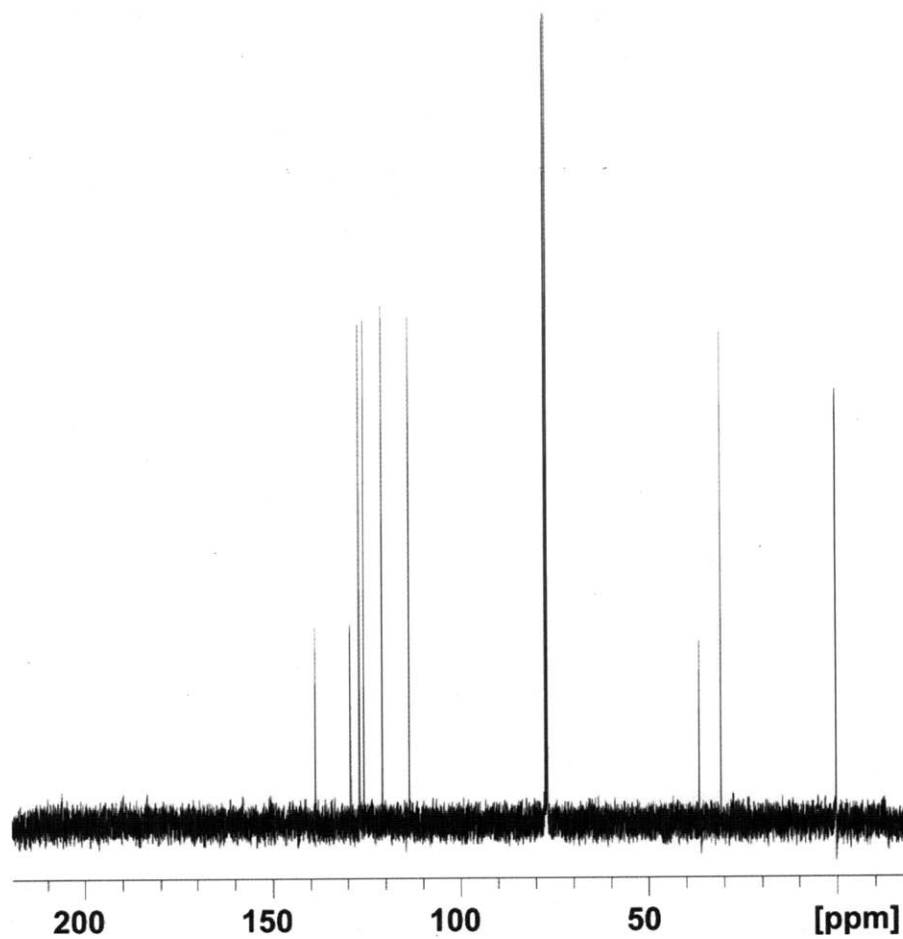
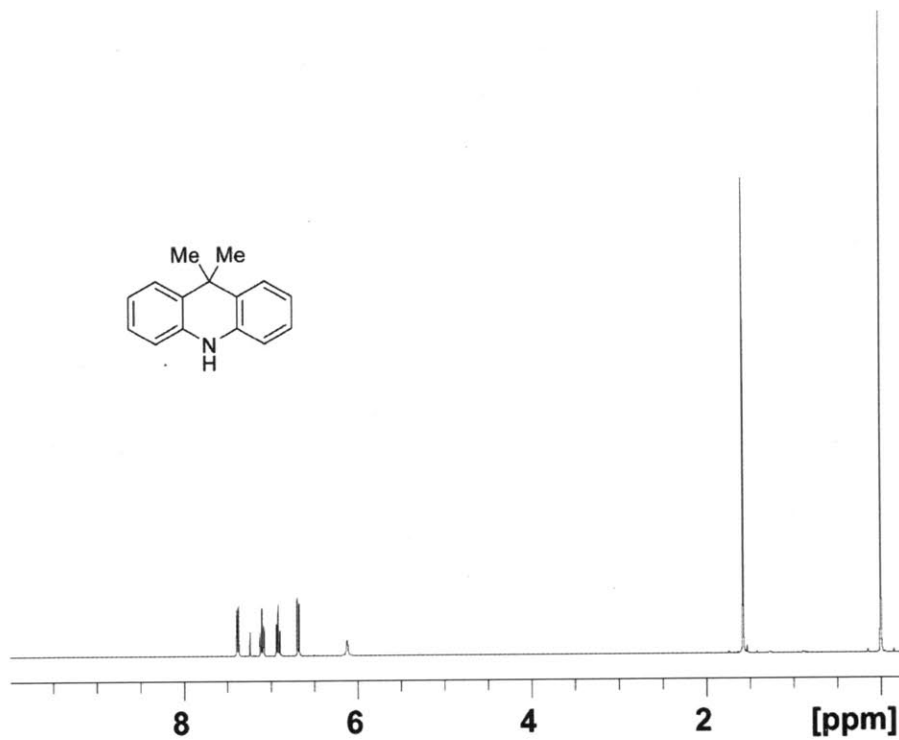
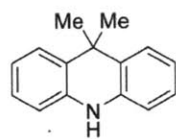
There are most certainly some people I wish I'd never met, but such is life, and the appearance of these people just rendered the presence of good friends all the more precious.

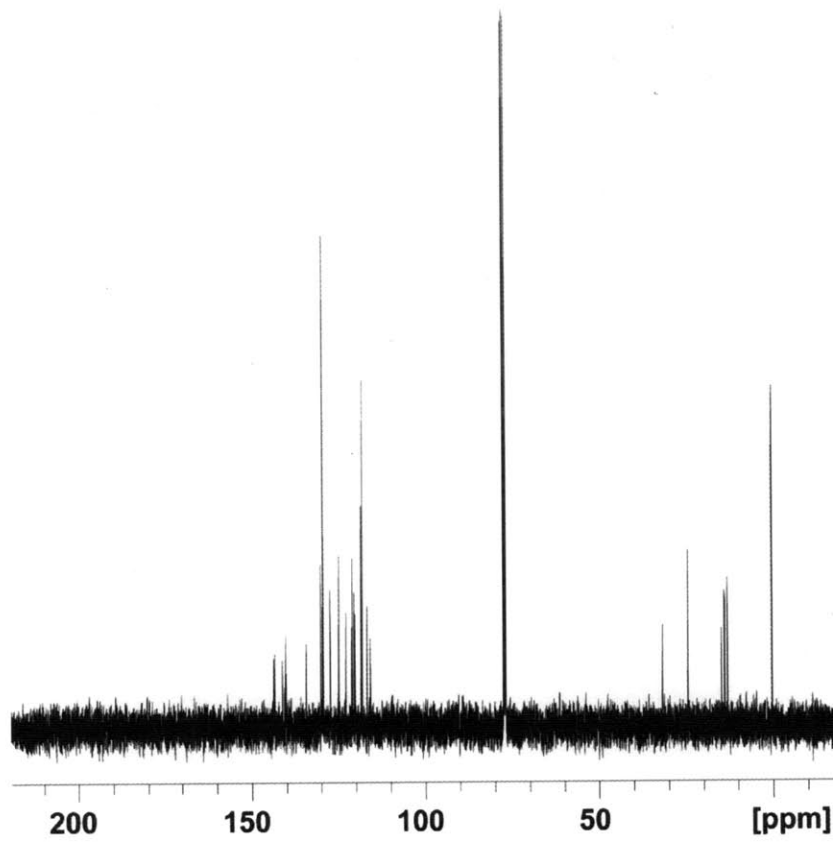
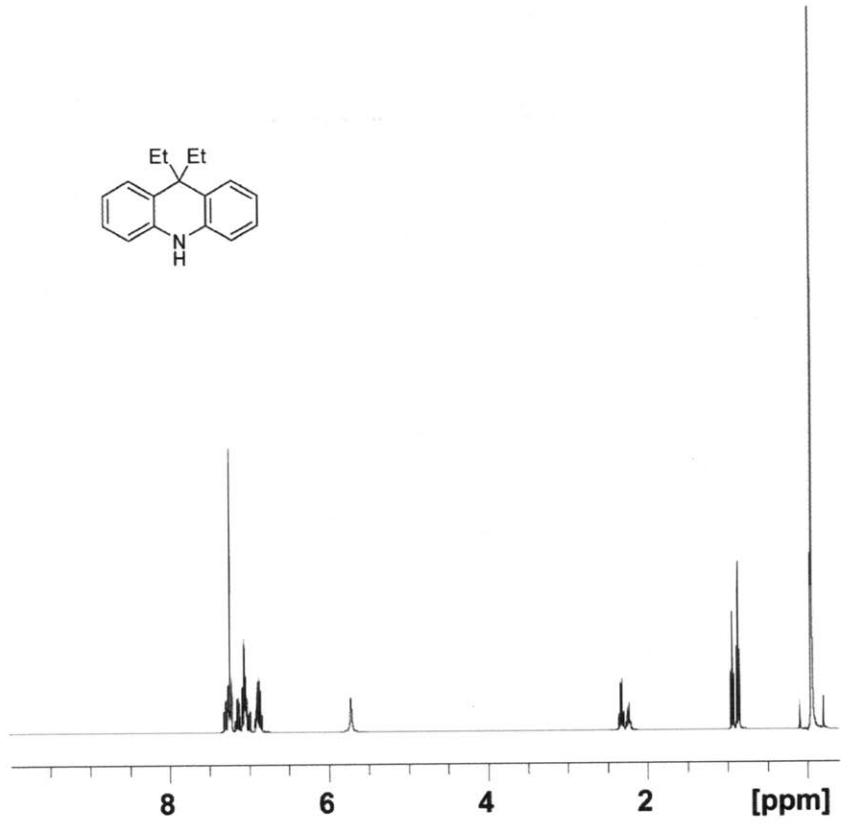
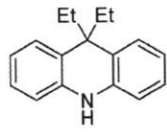
Trisha out.

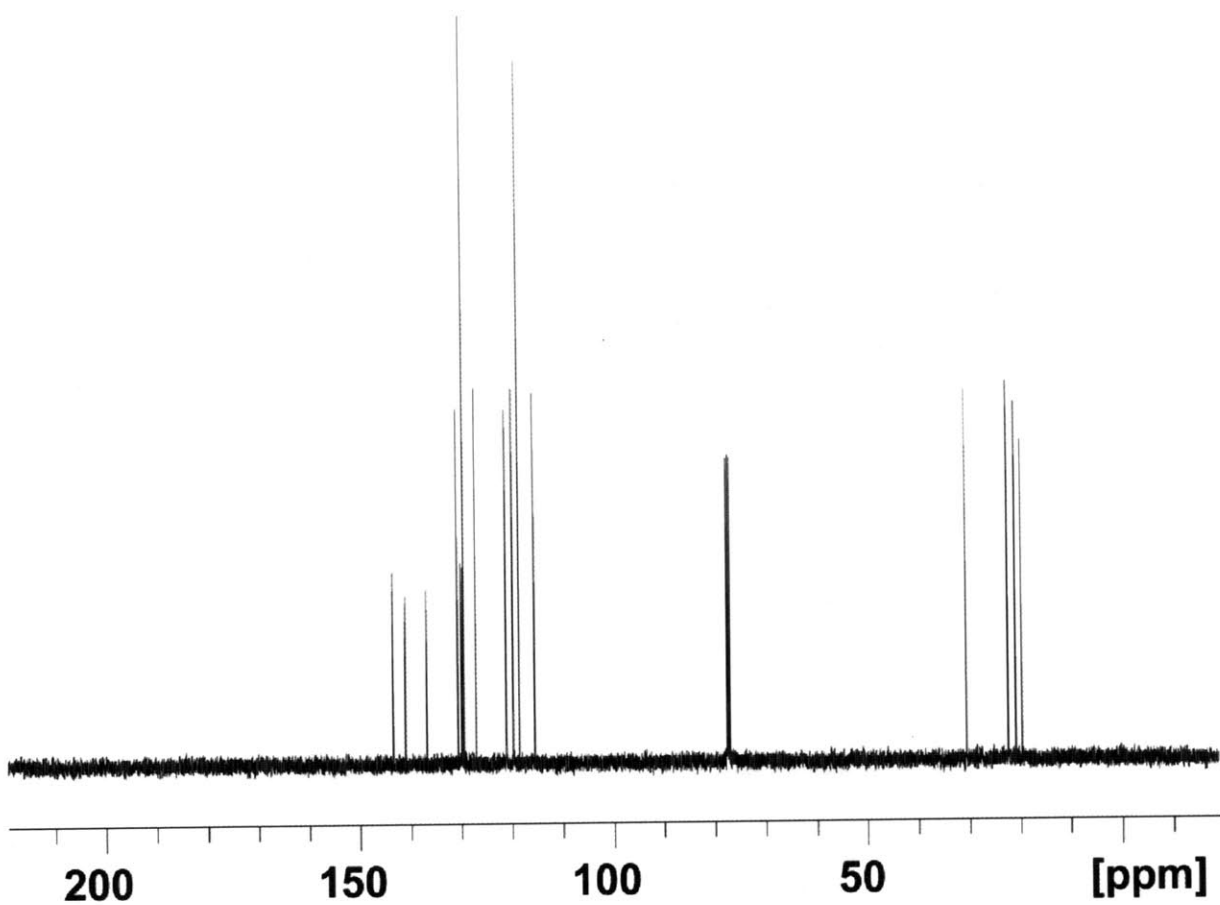
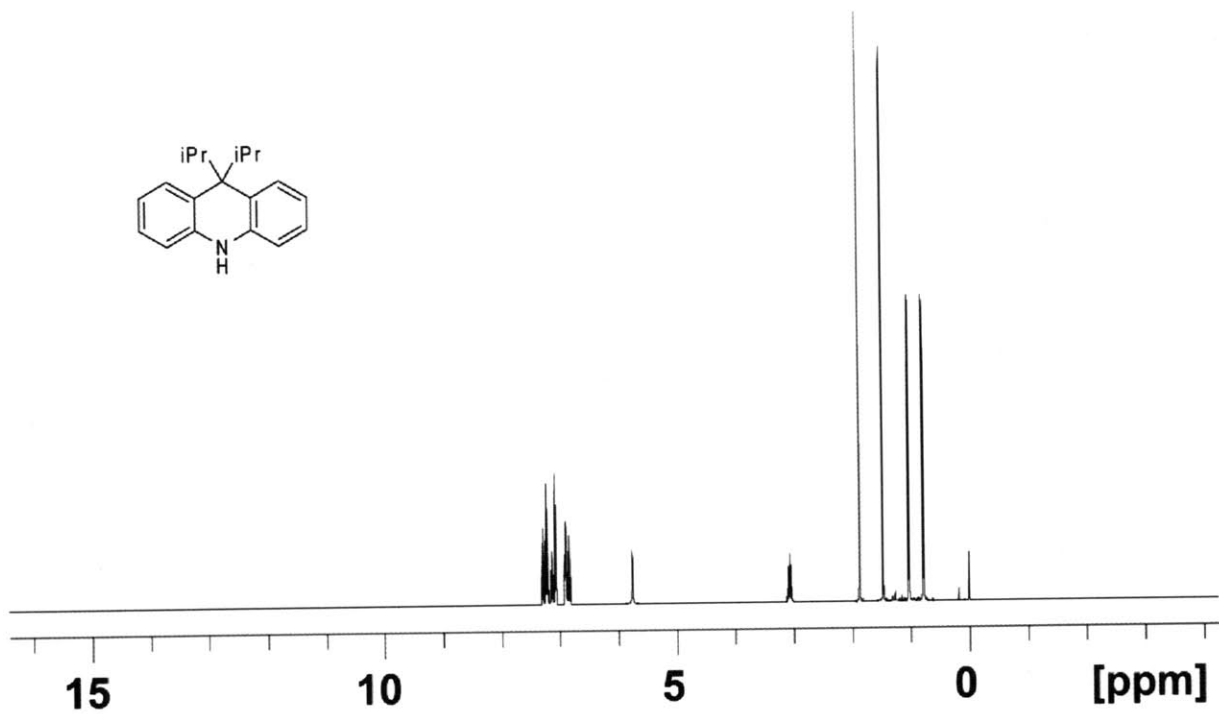
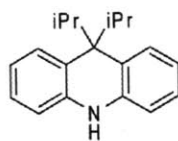
APPENDIX 1
NMR Spectra for Chapter 1

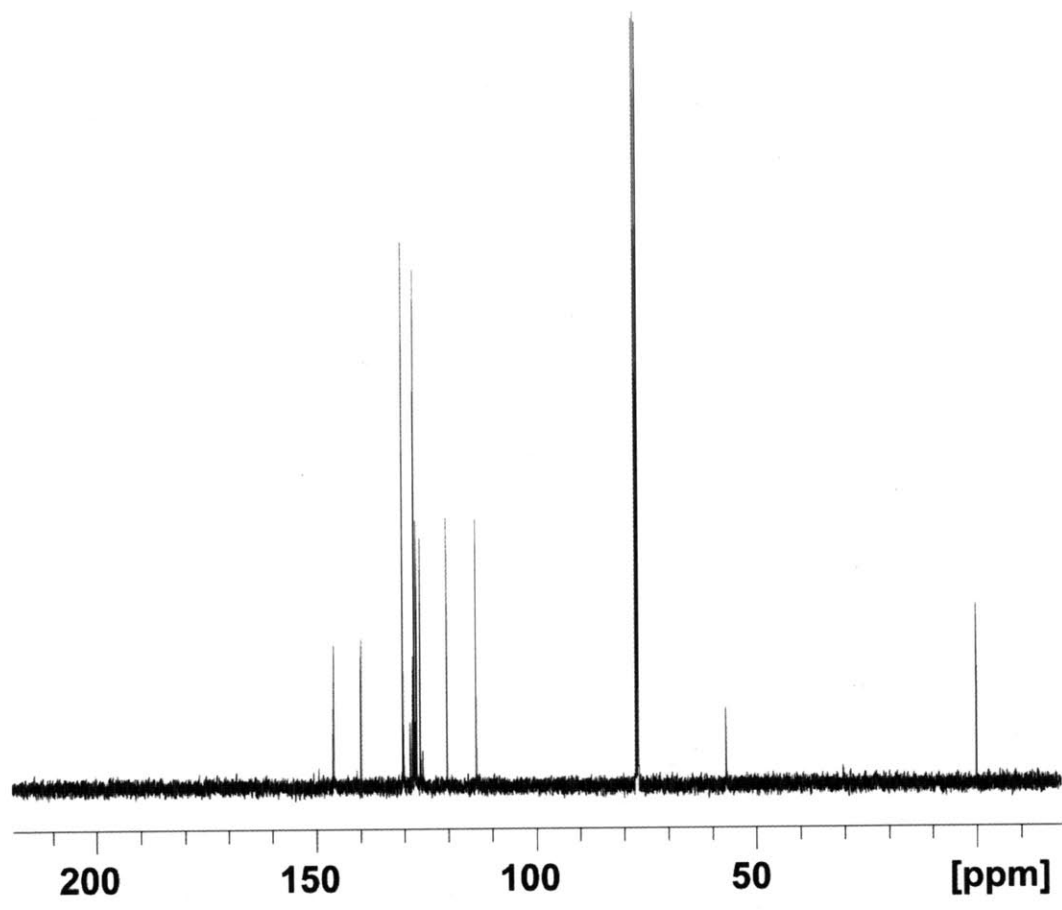
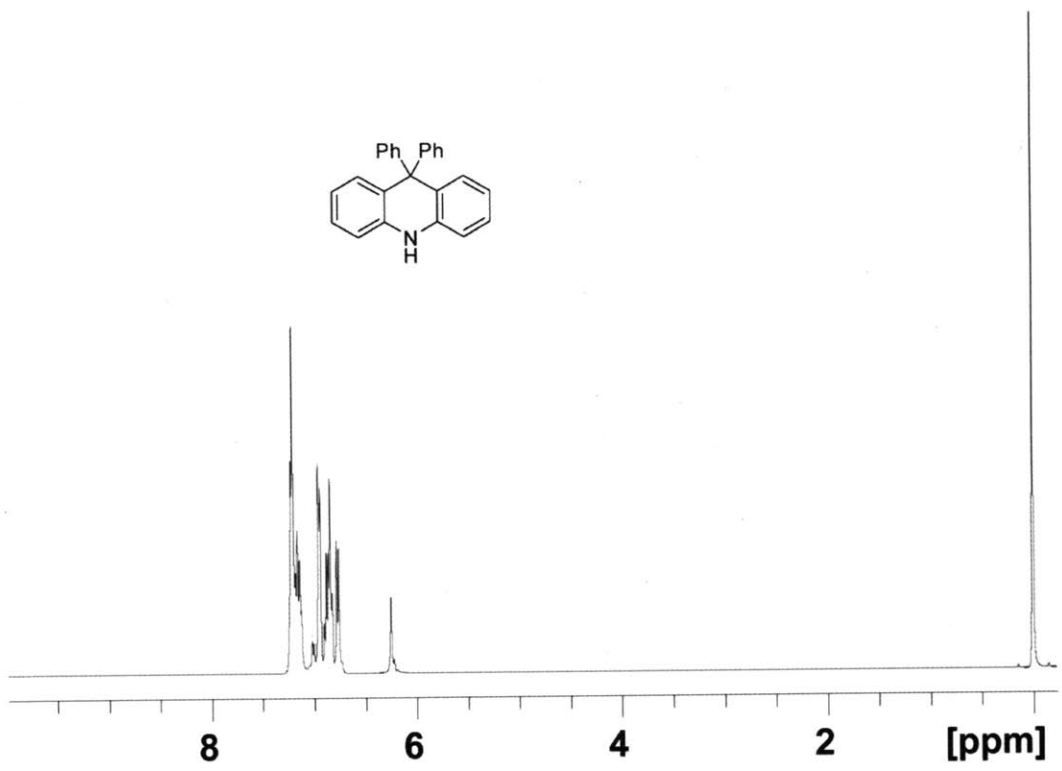
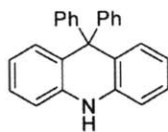


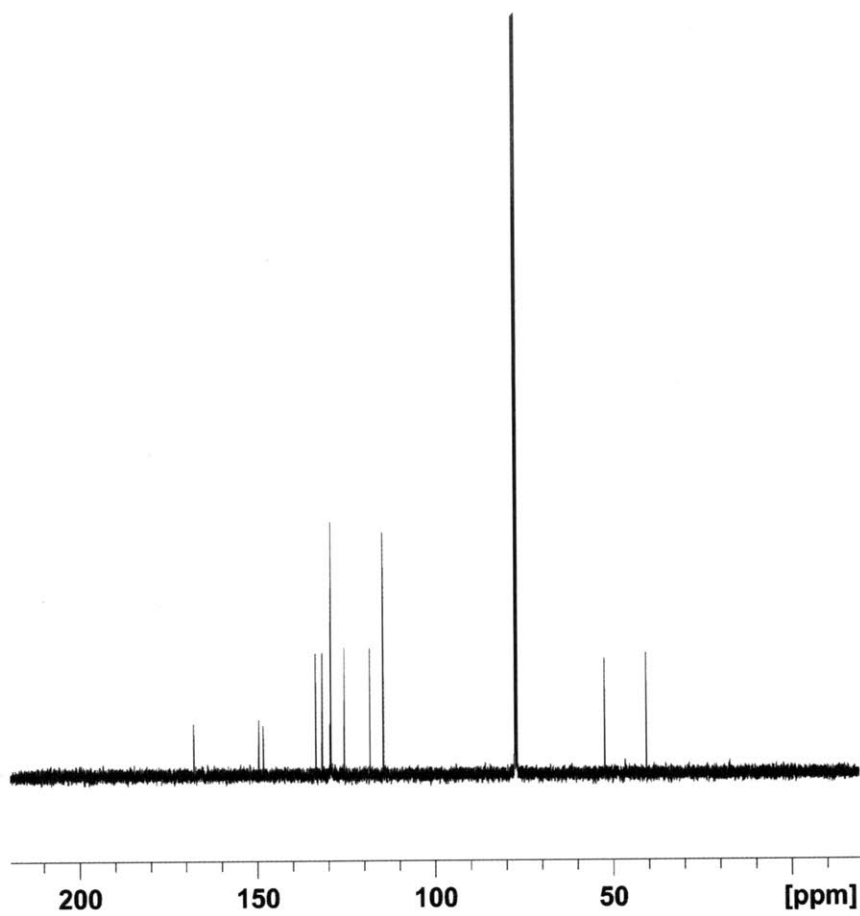
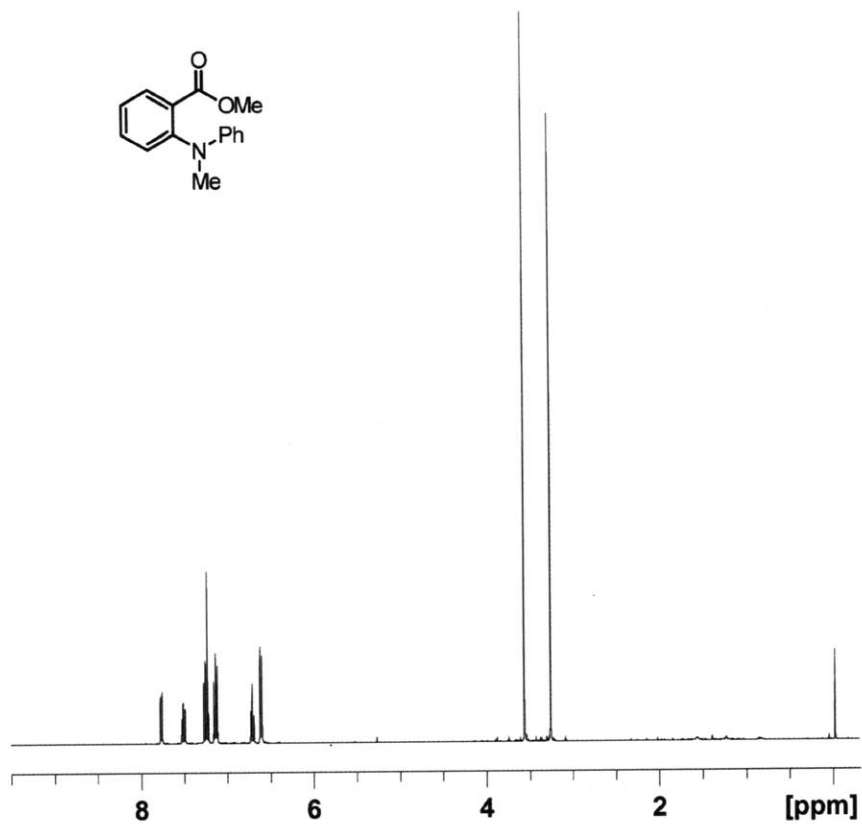
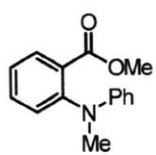
APPENDIX 2
NMR Spectra for Chapter 2

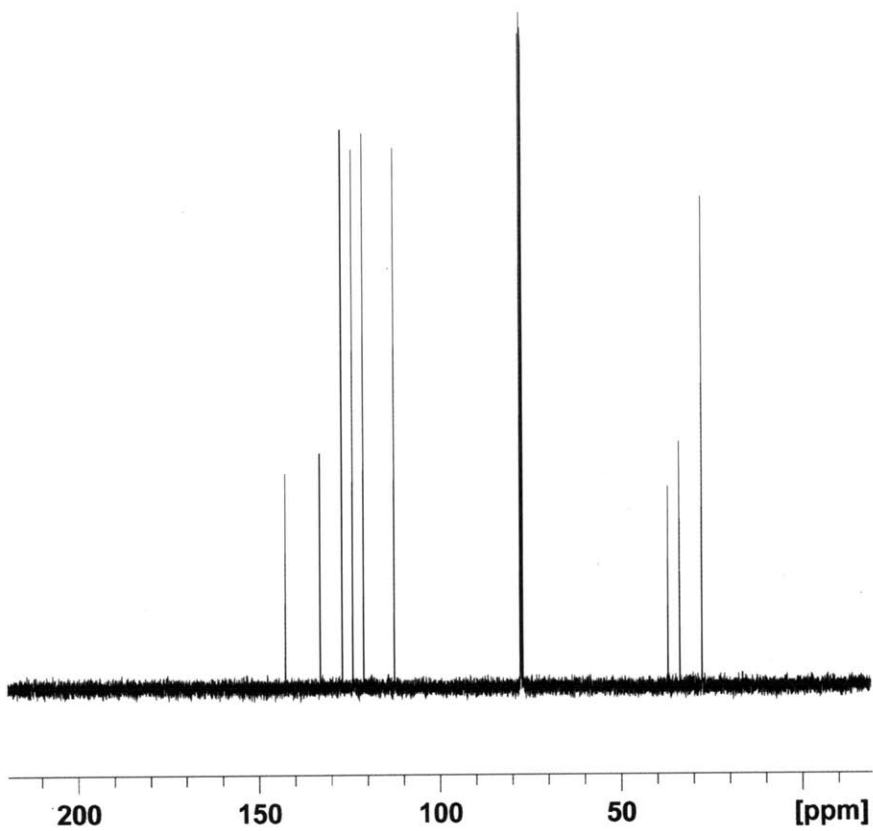
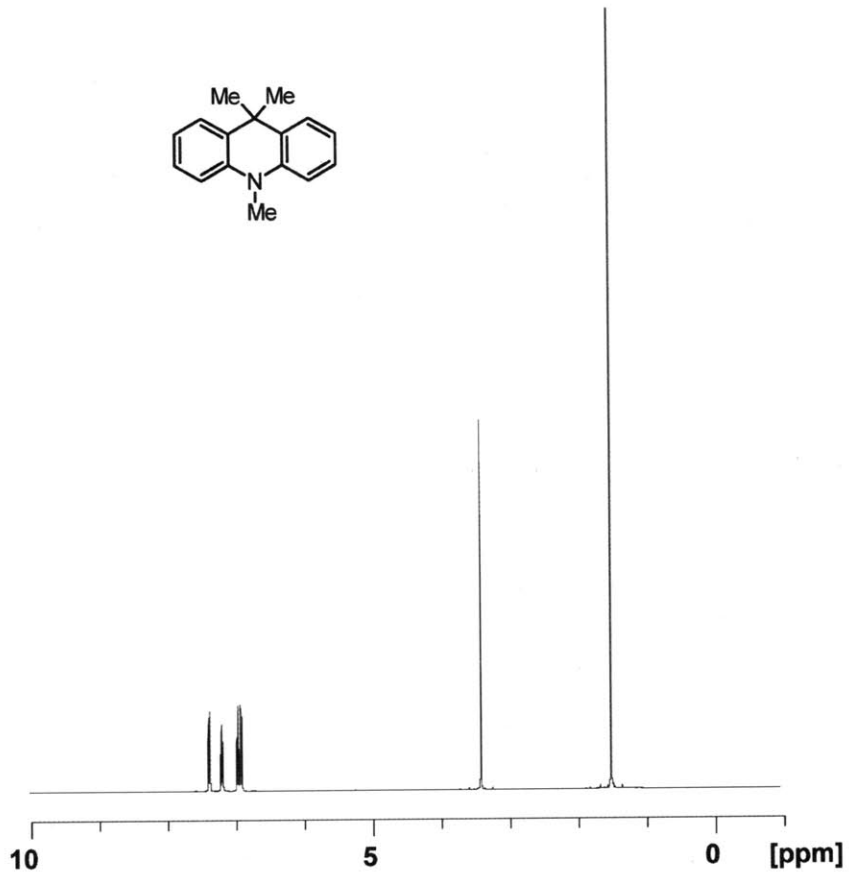
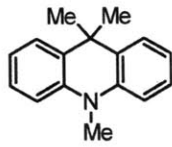


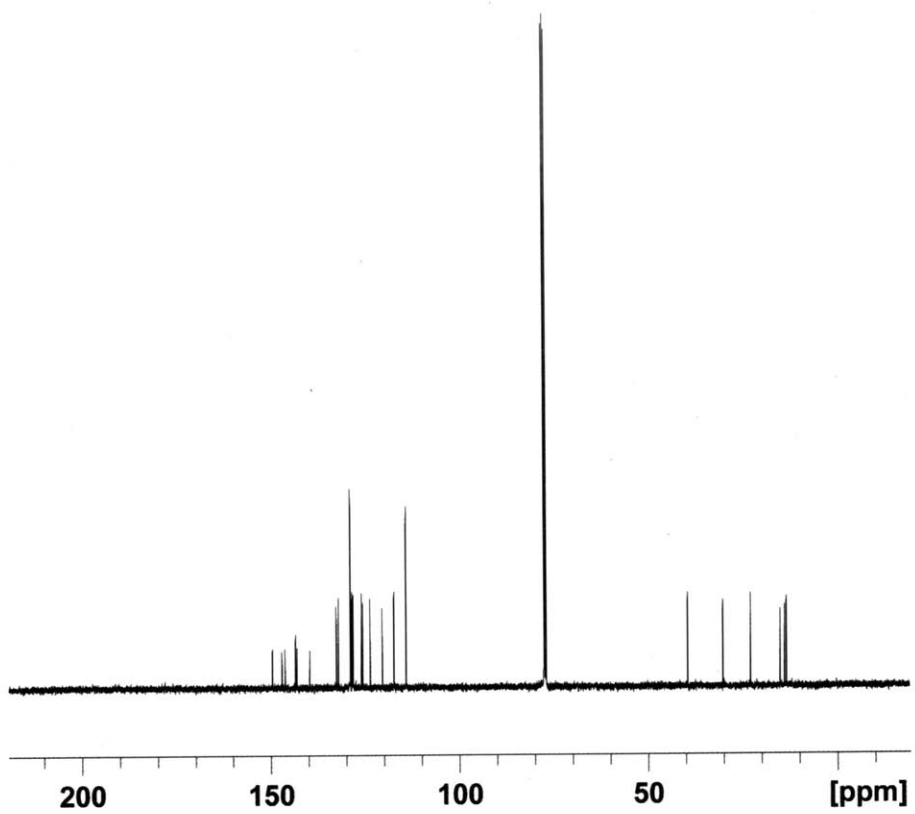
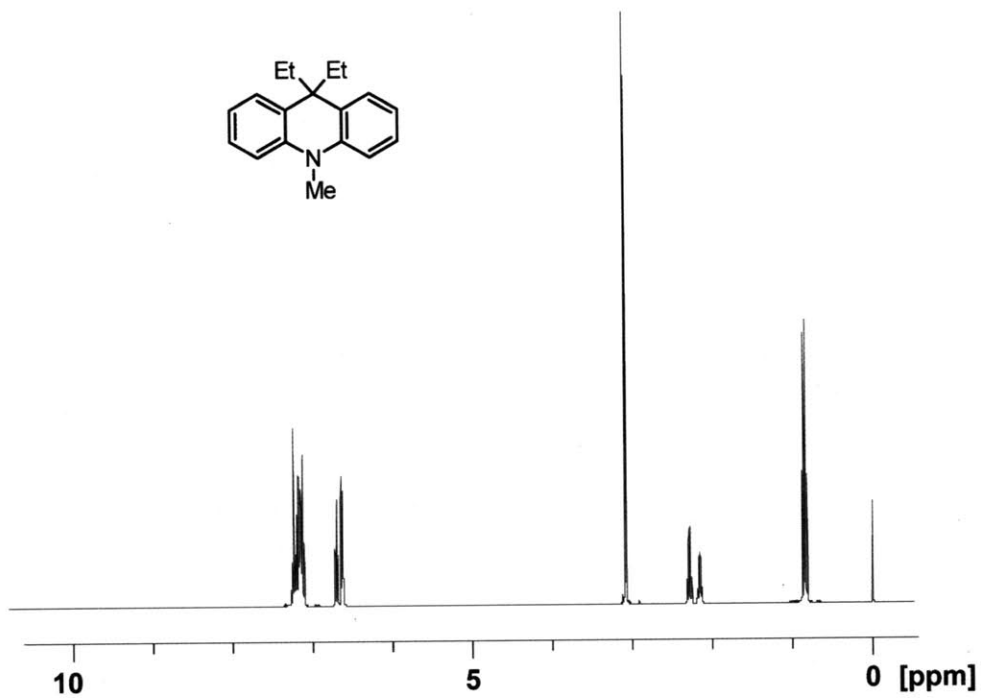
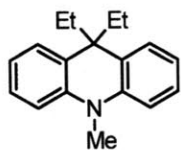


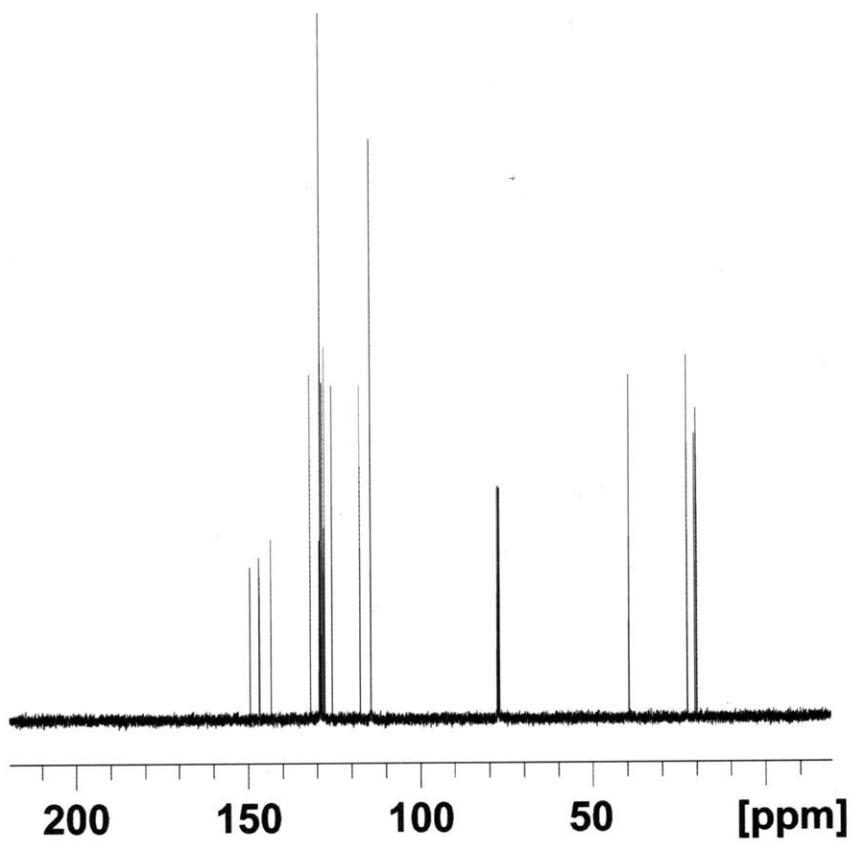
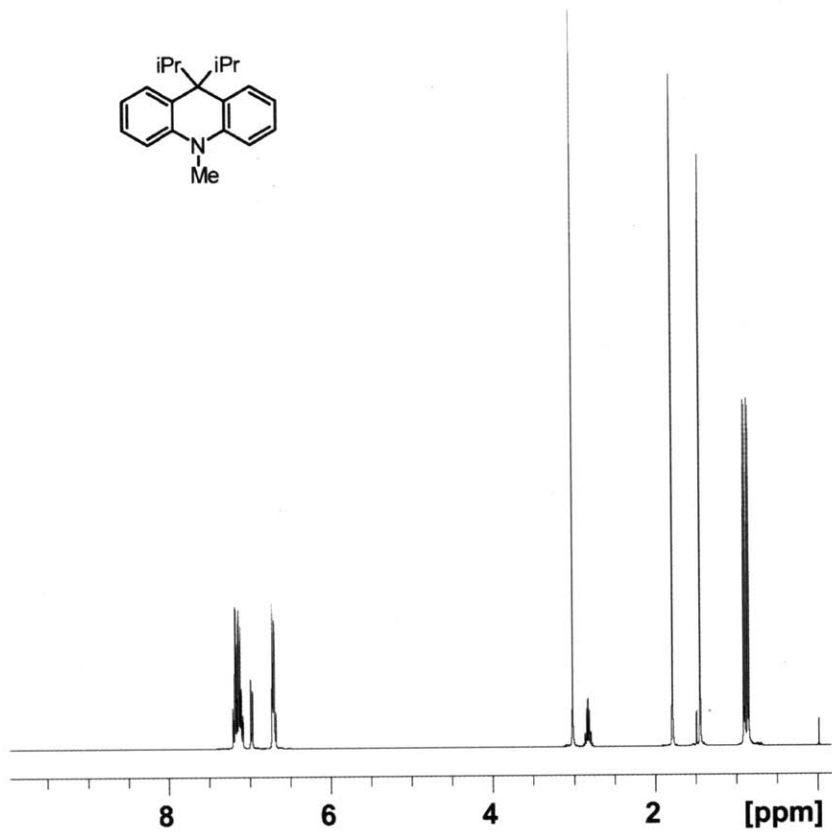
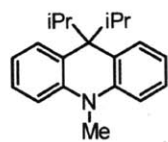


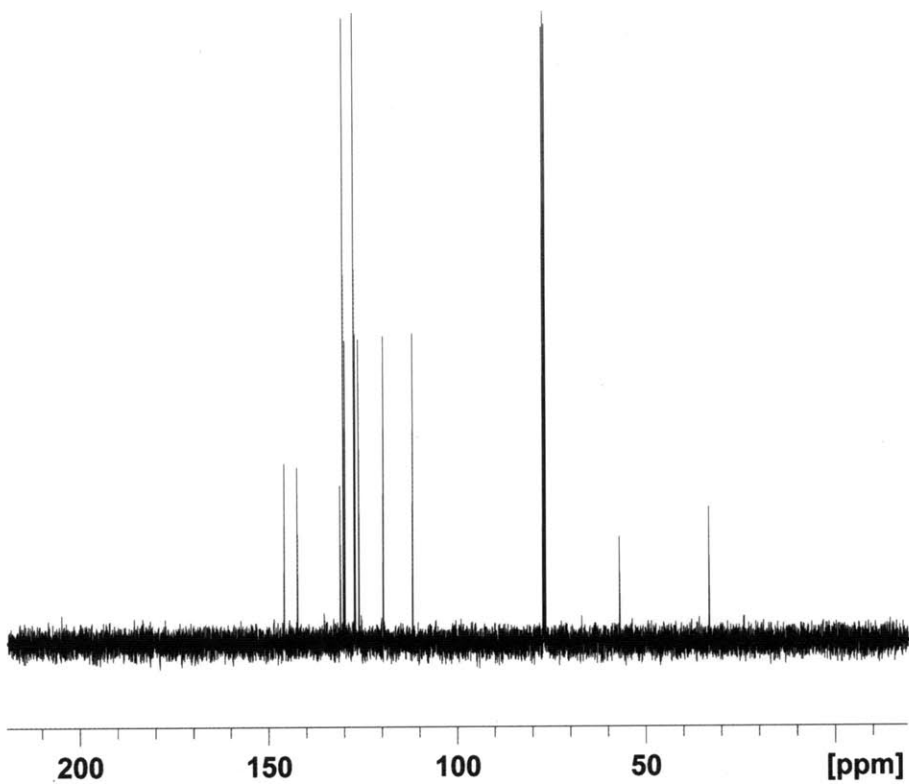
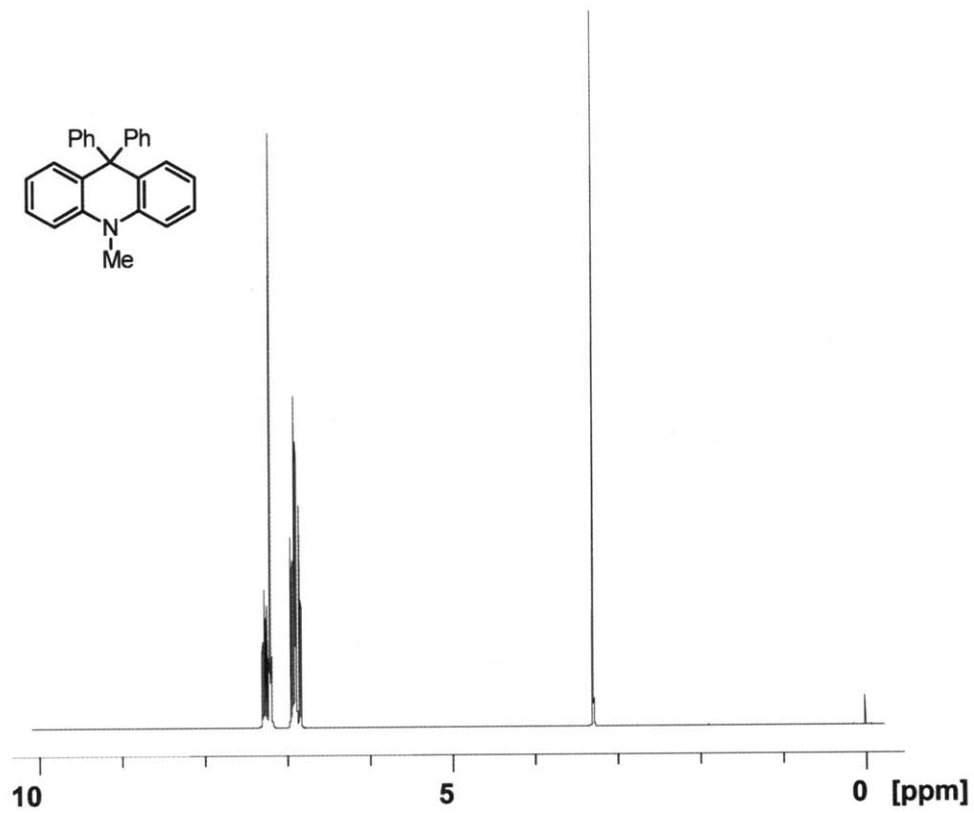


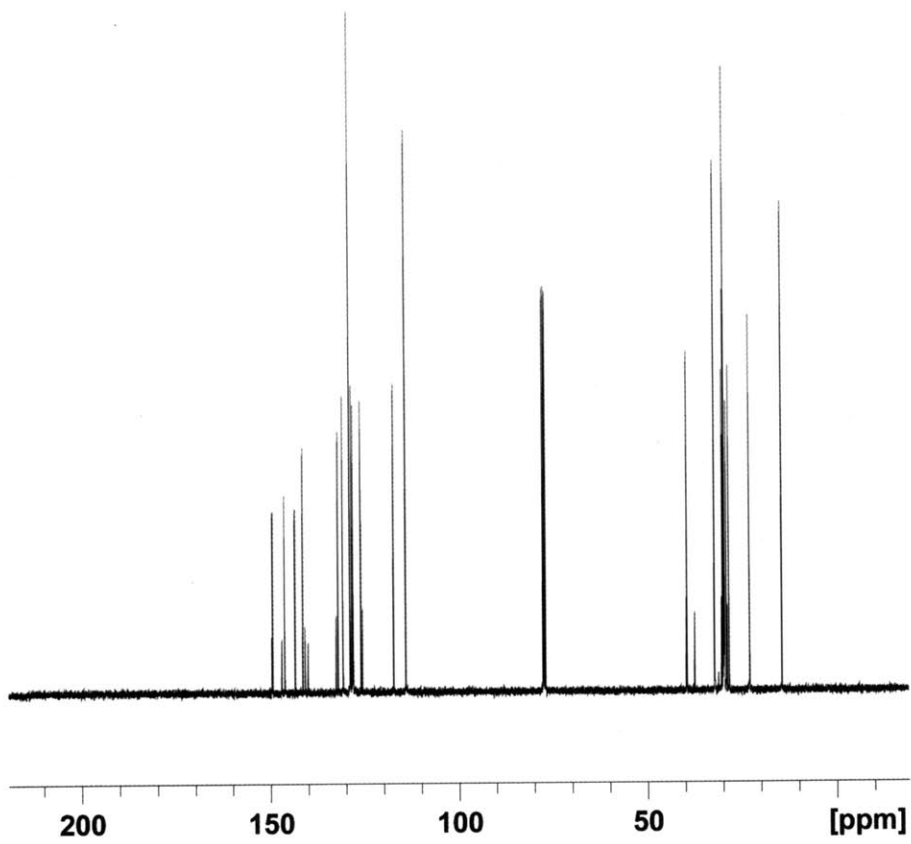
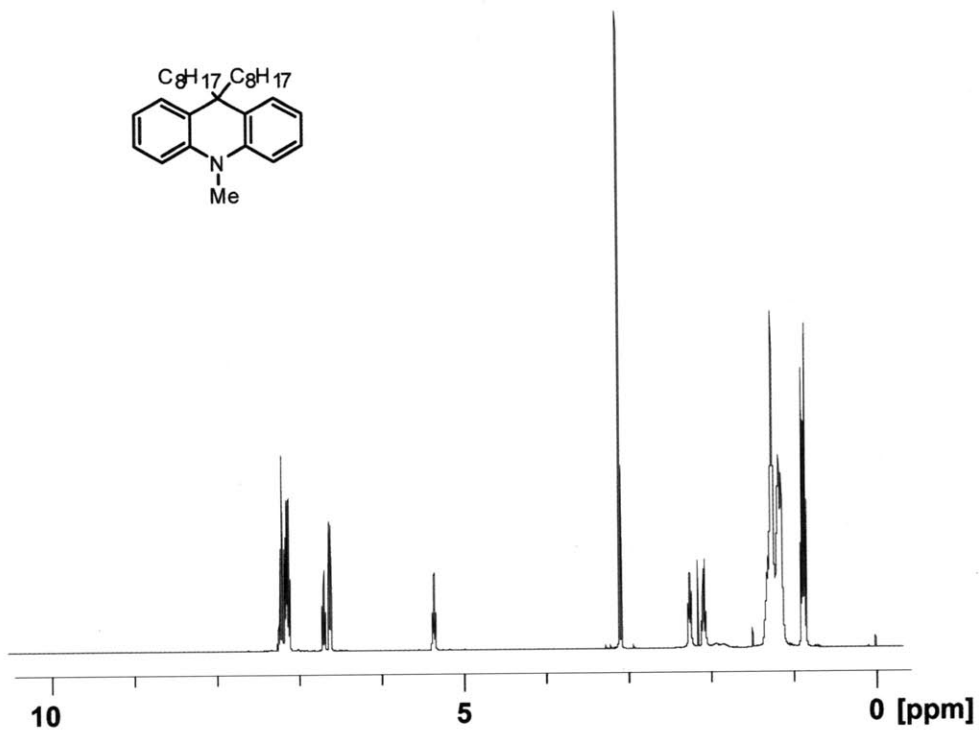
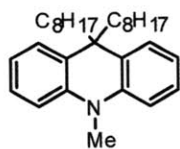


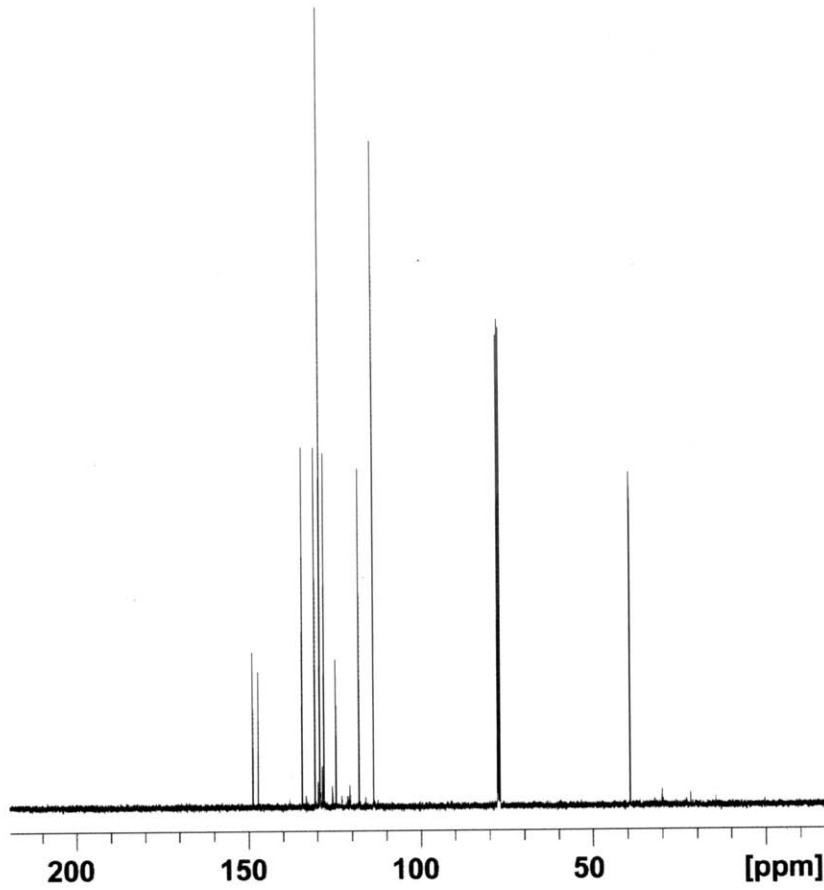
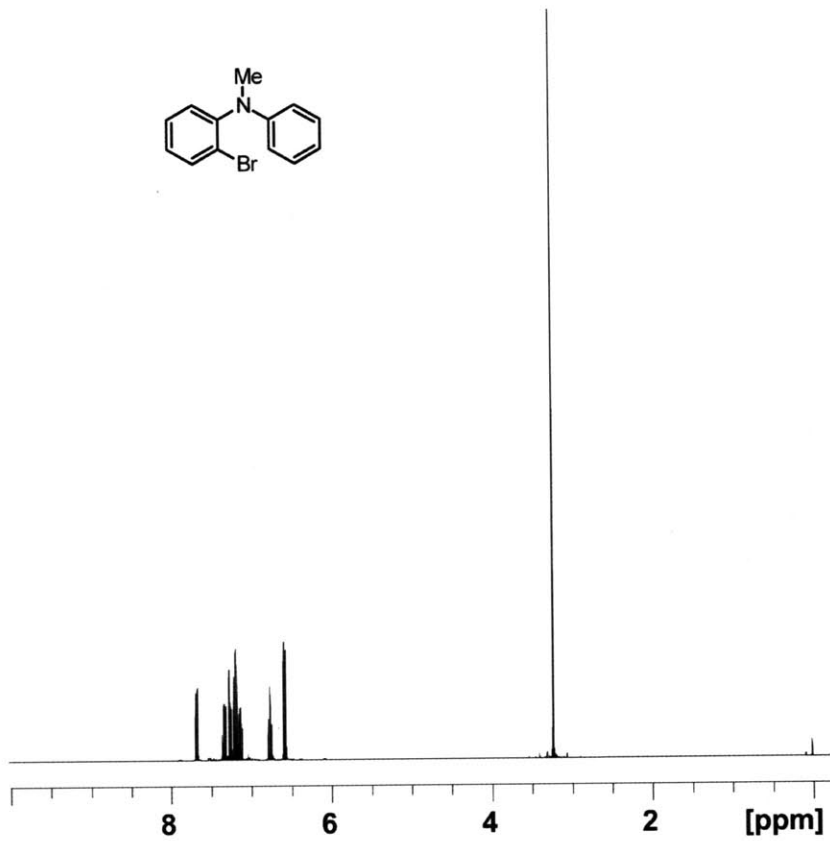
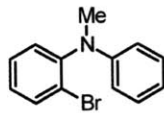


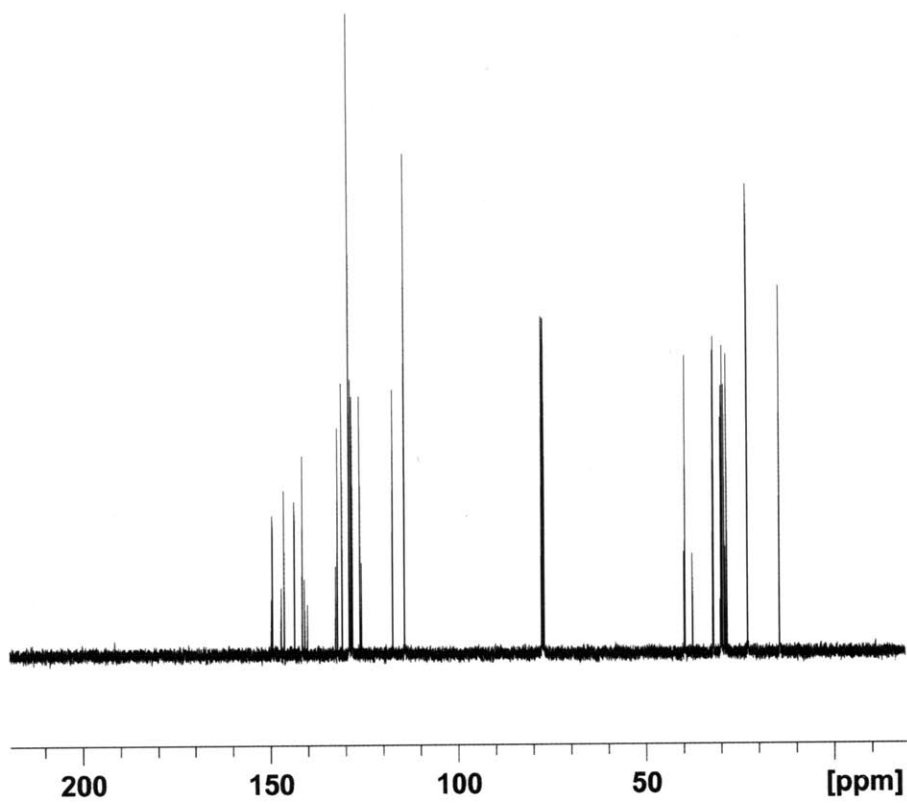
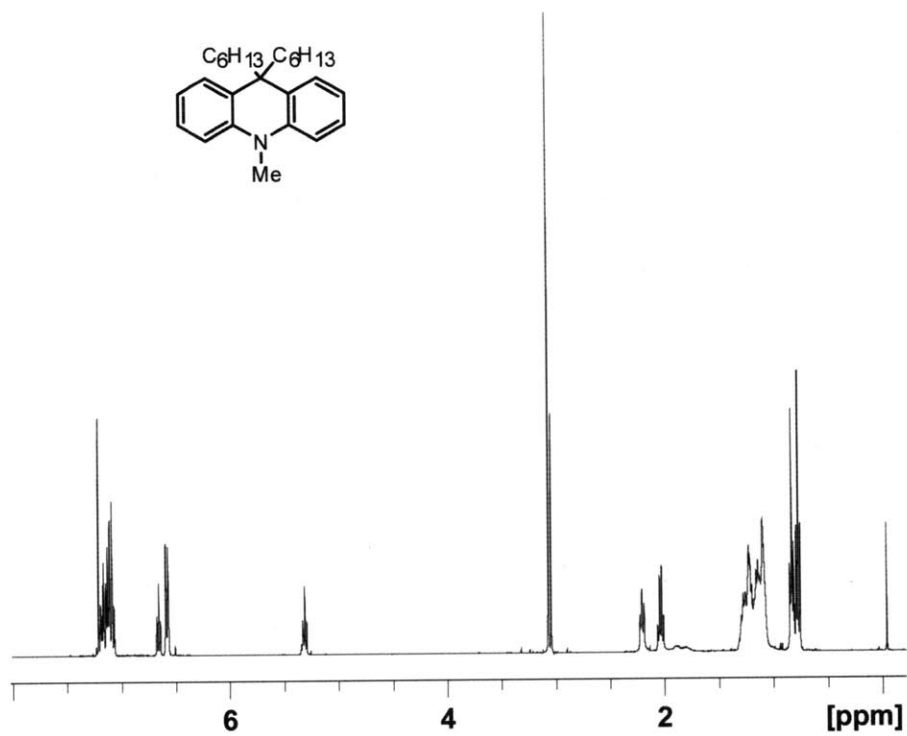
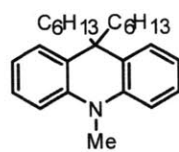


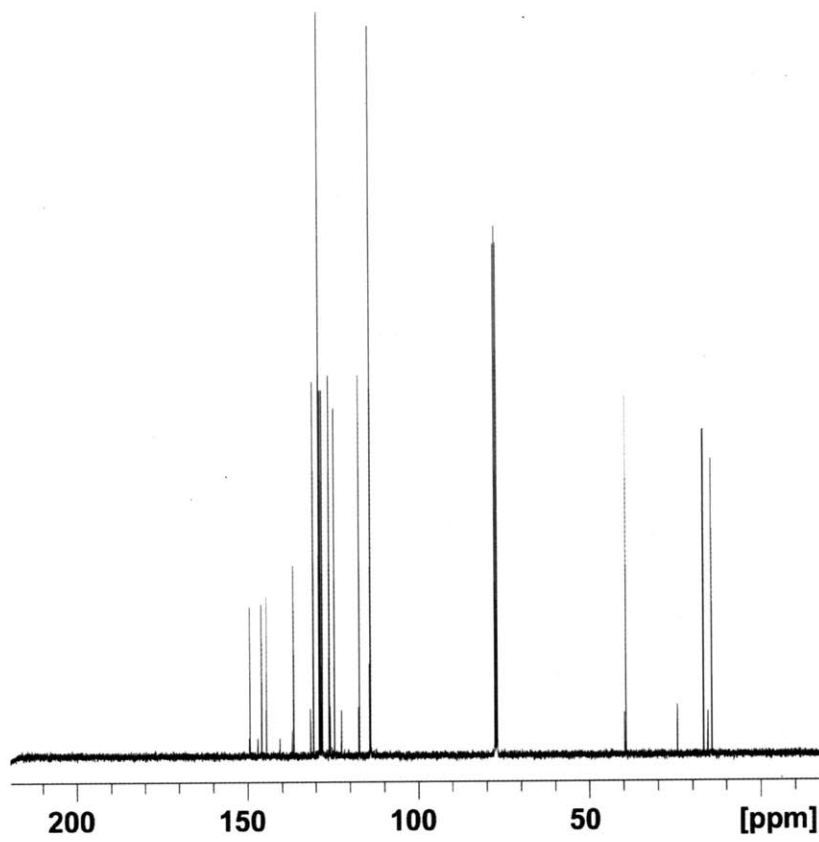
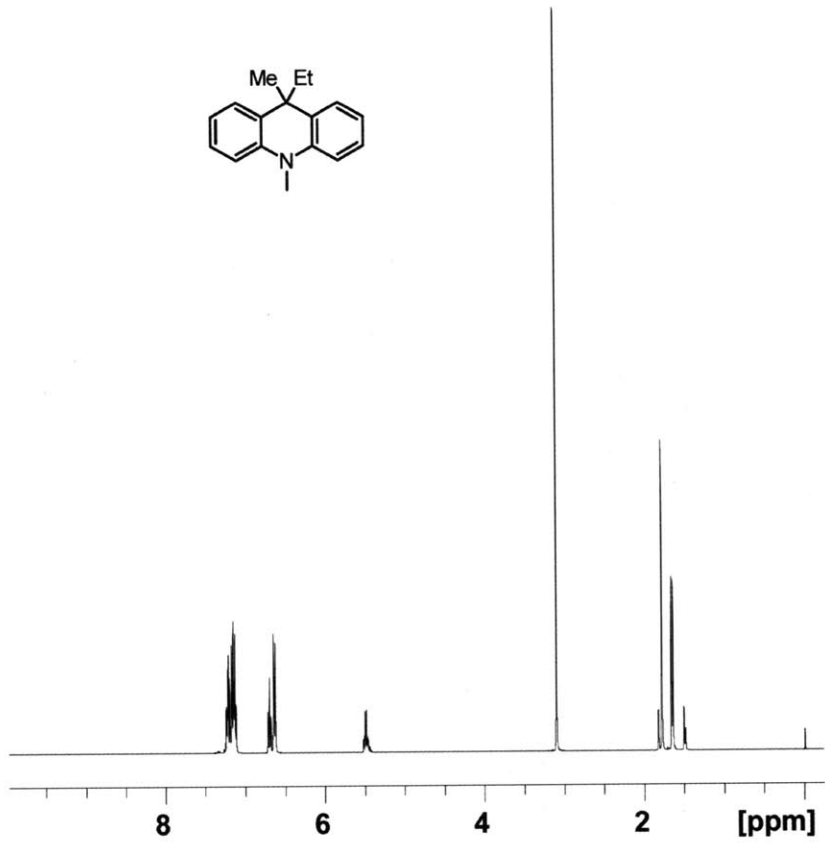
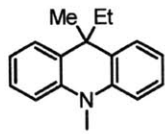


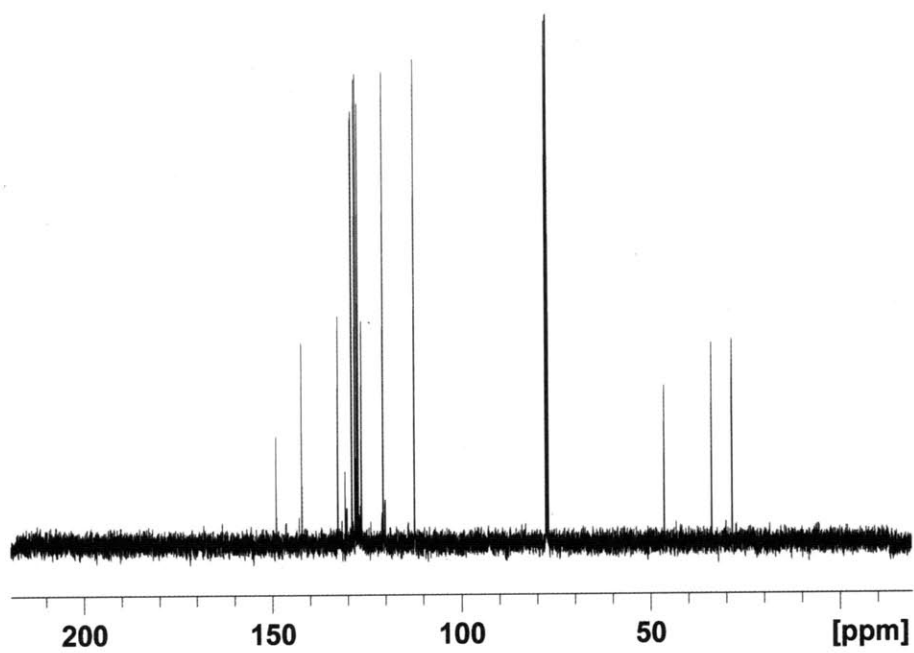
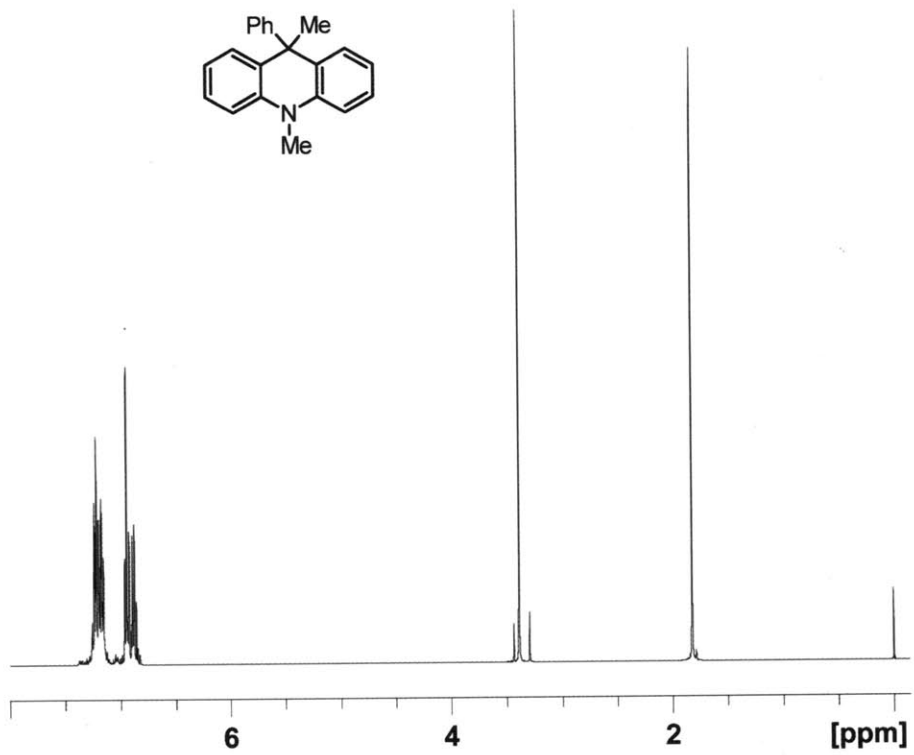
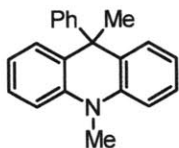


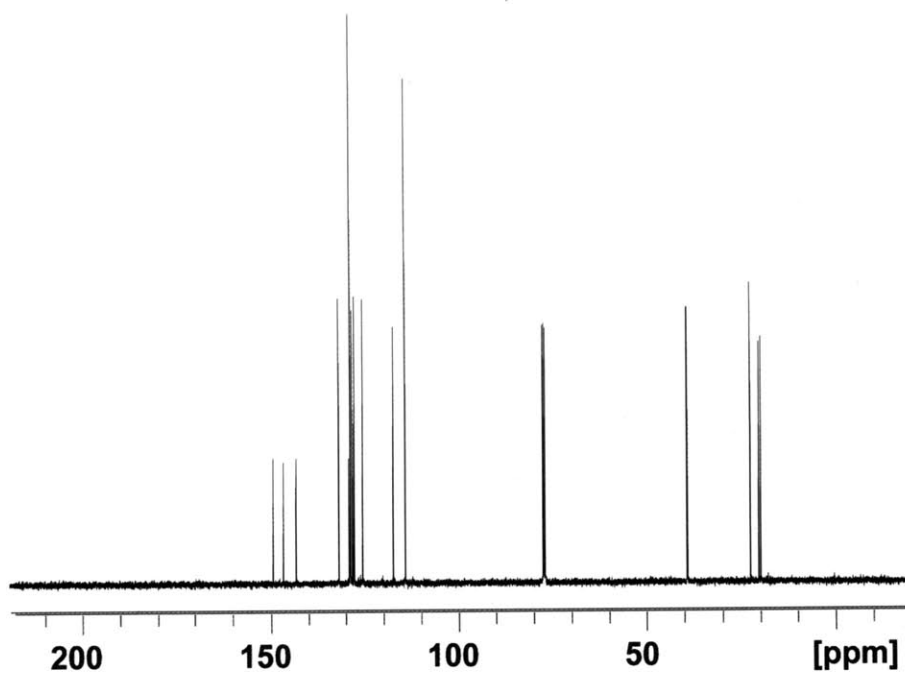
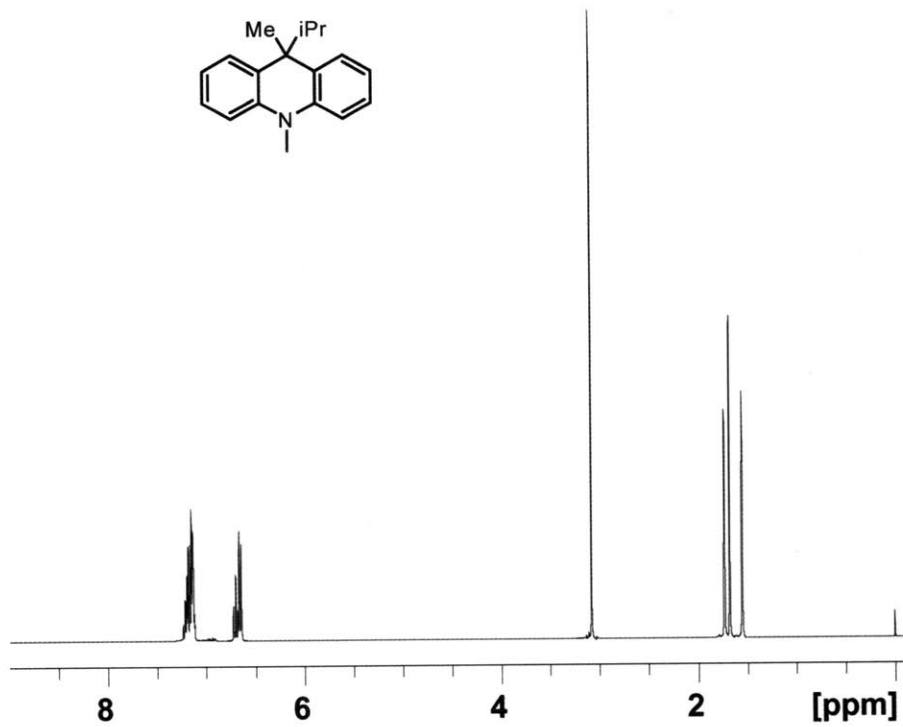
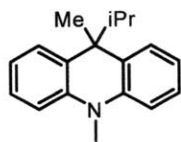


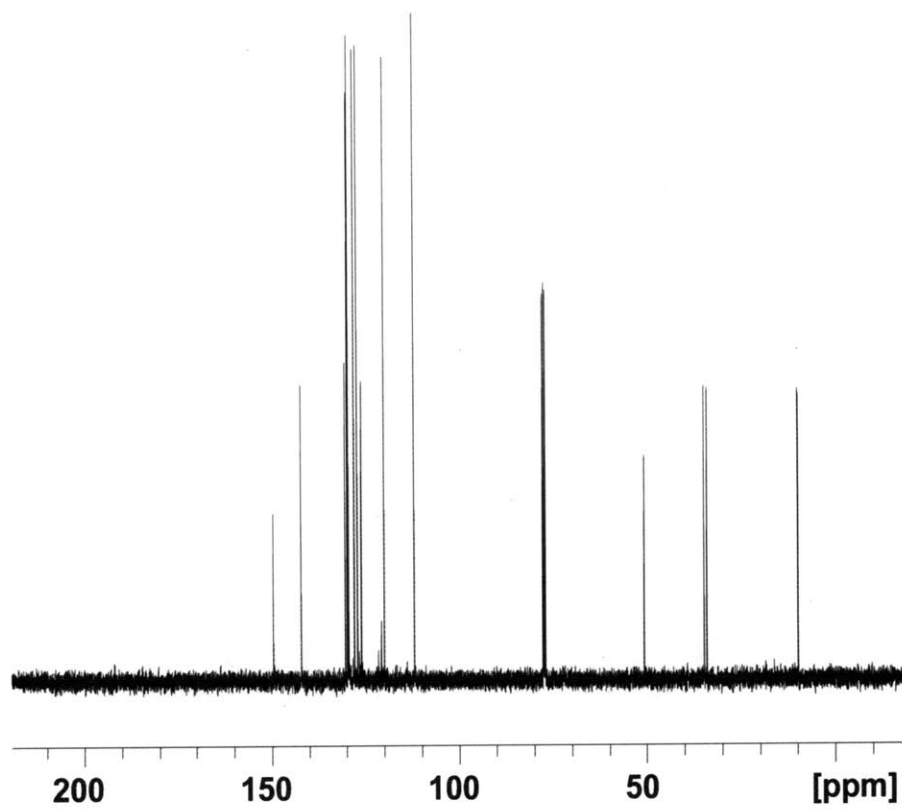
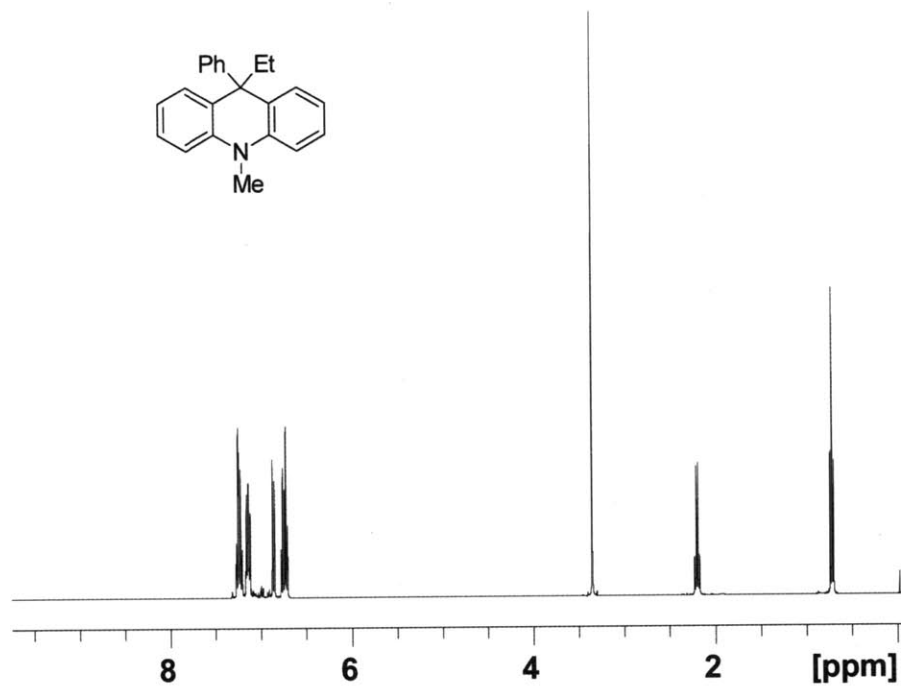
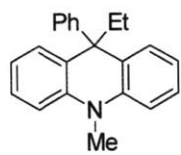


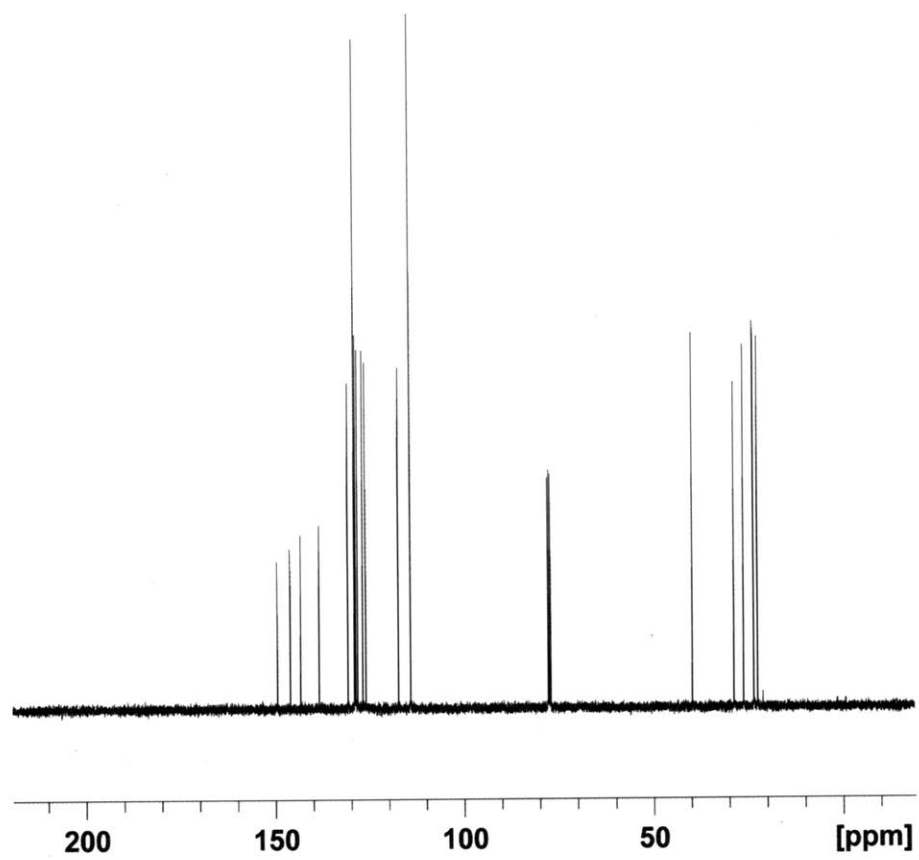
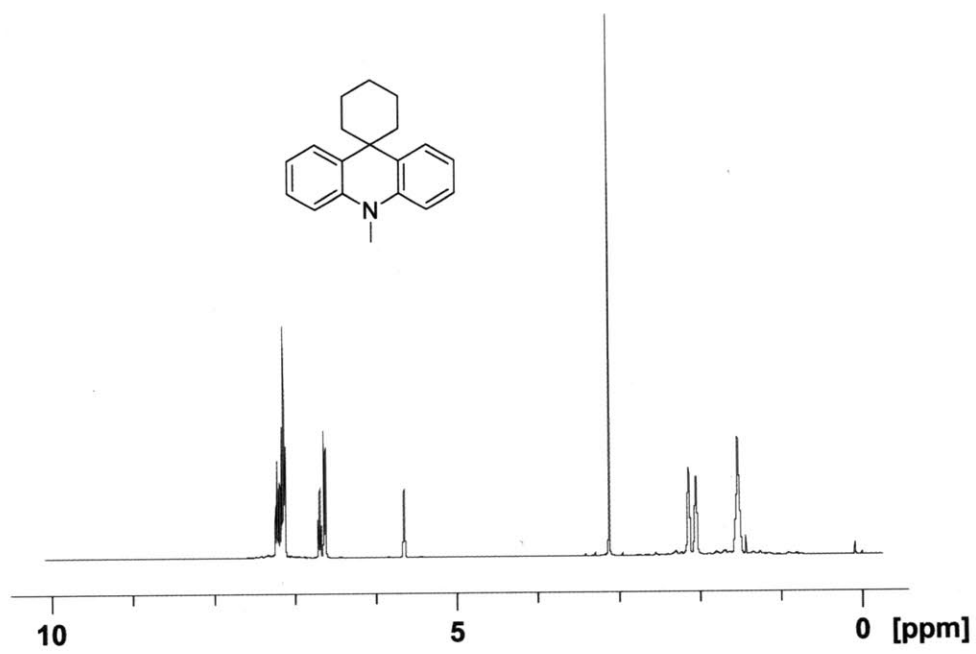


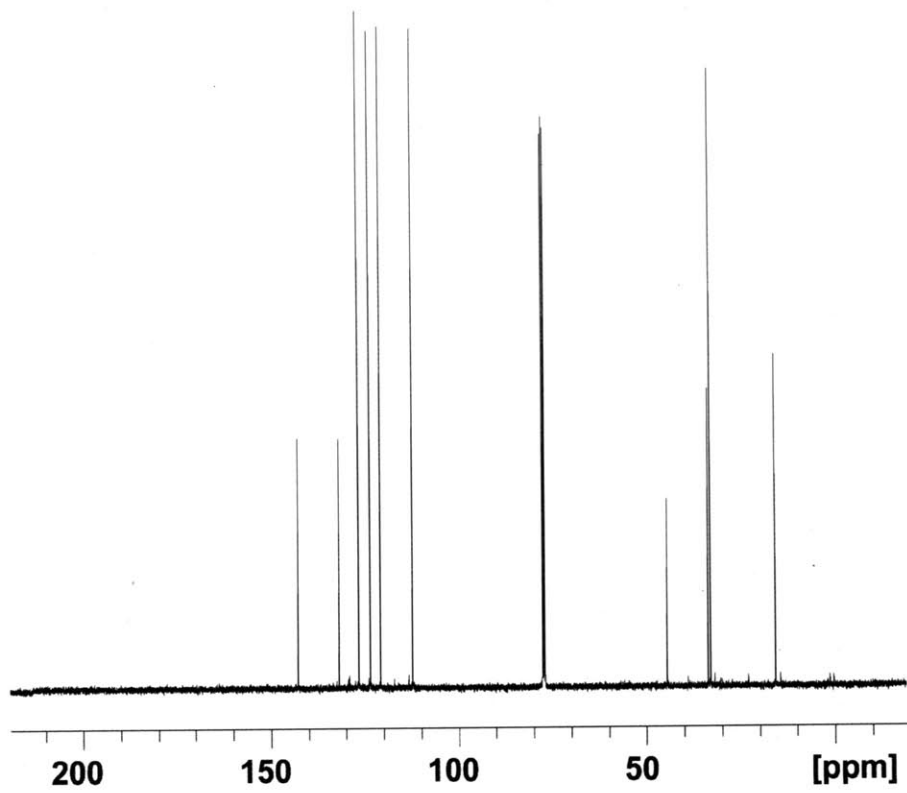
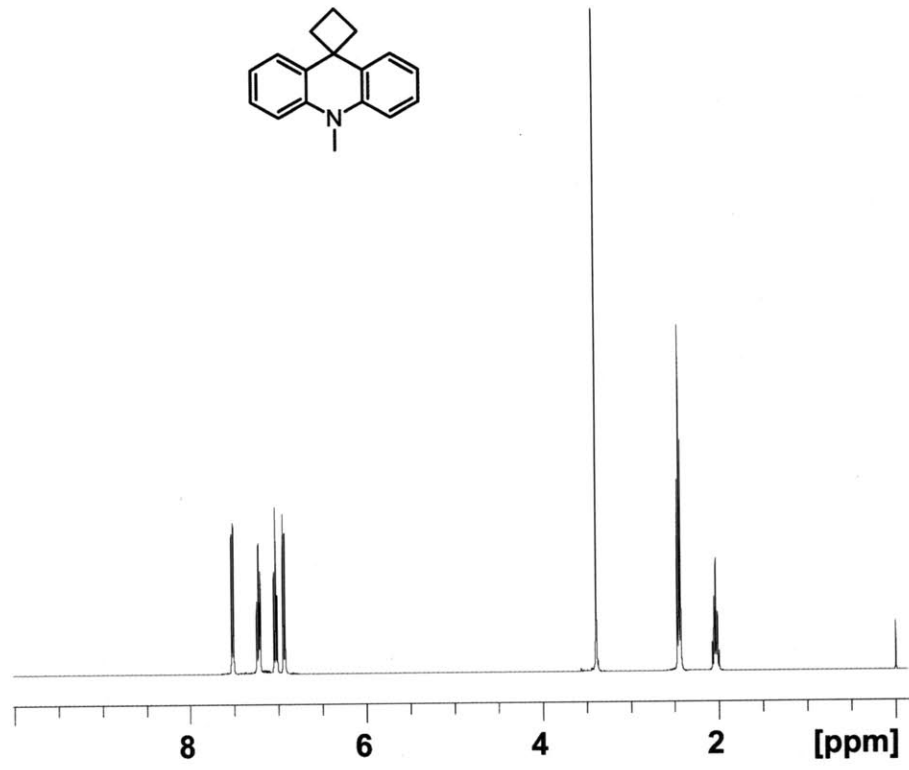
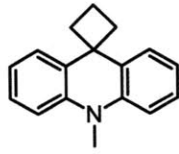


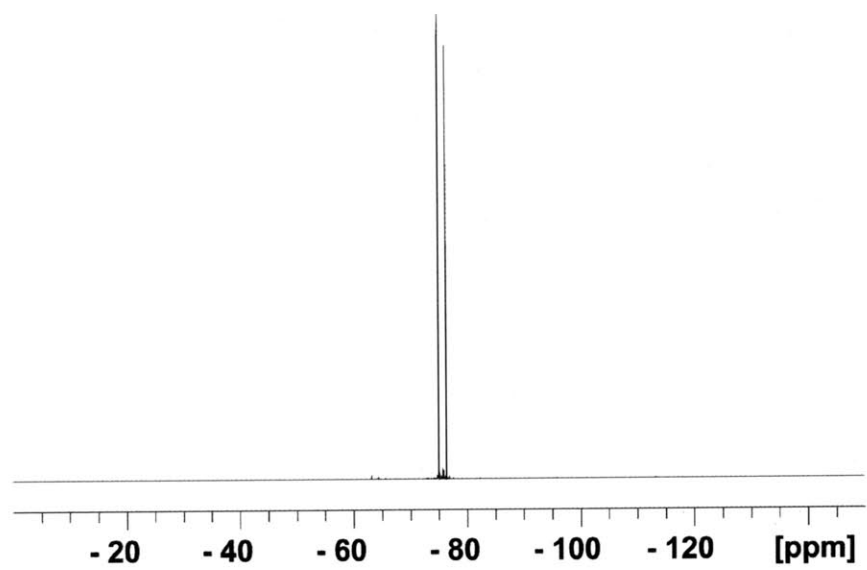
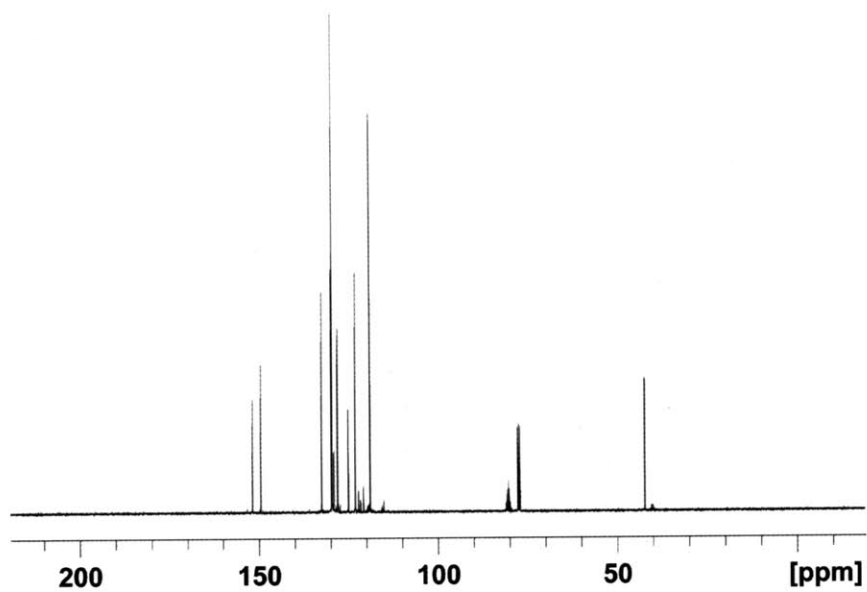
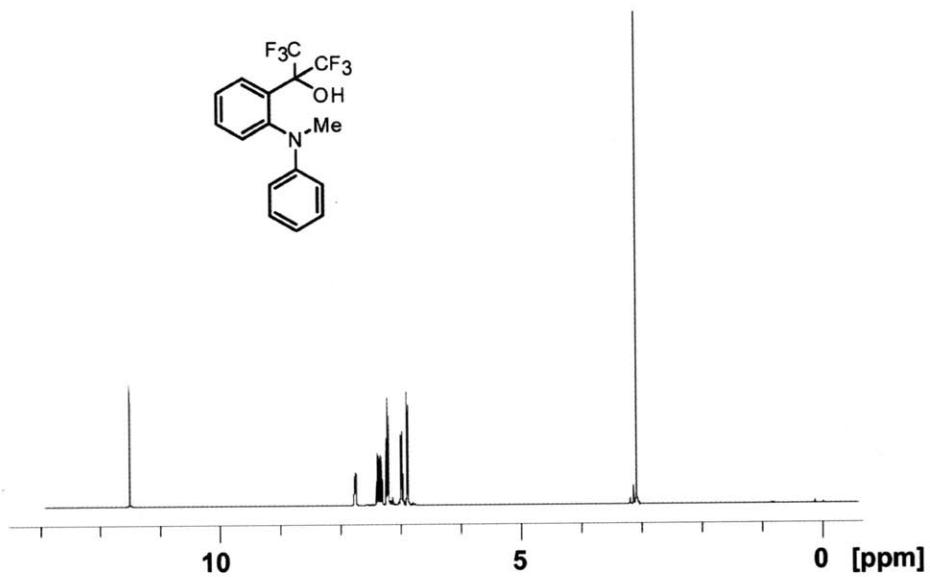
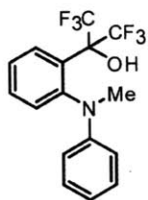


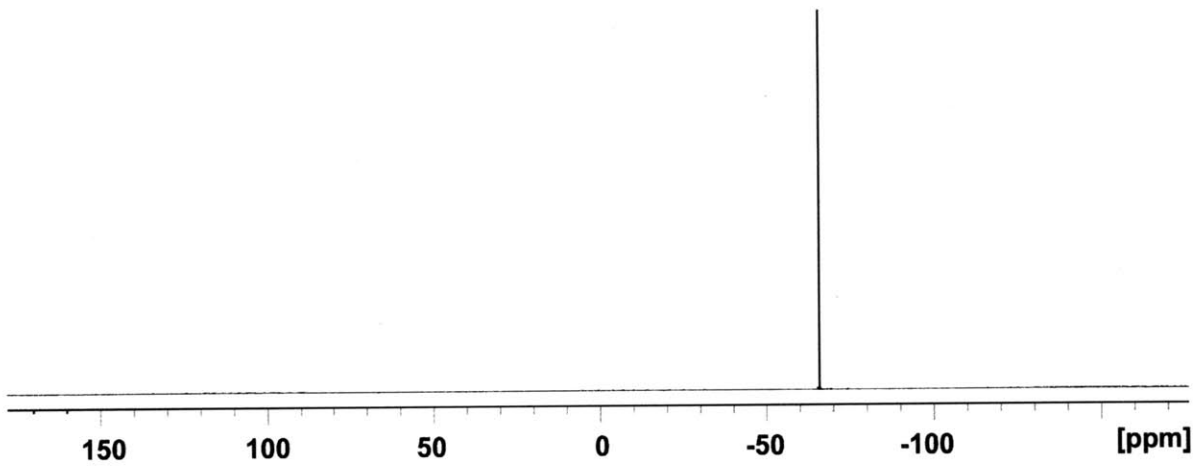
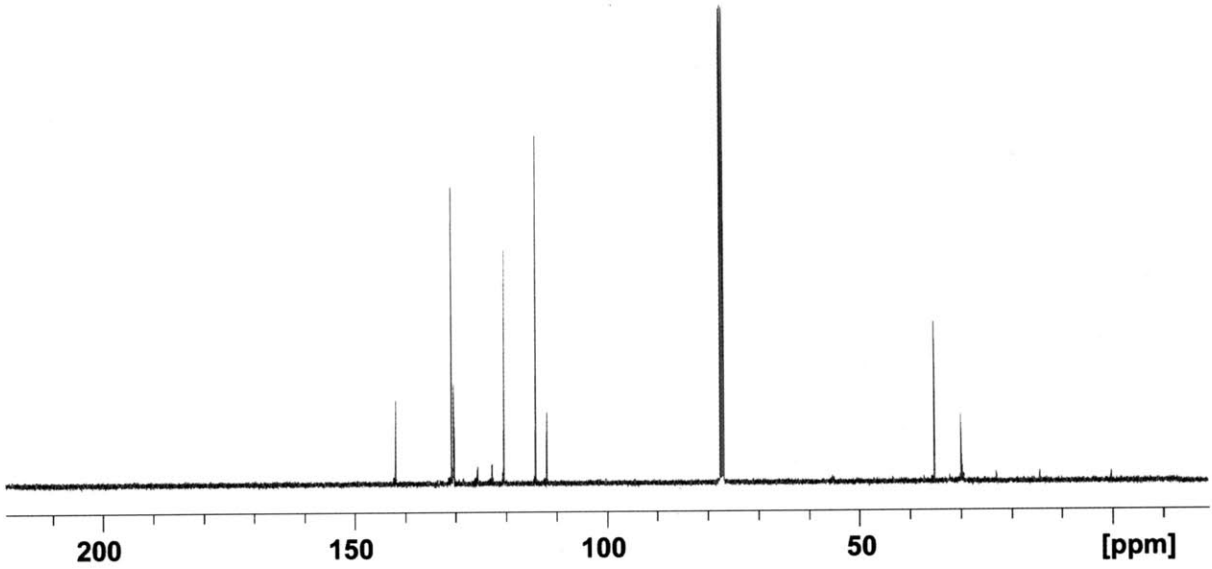
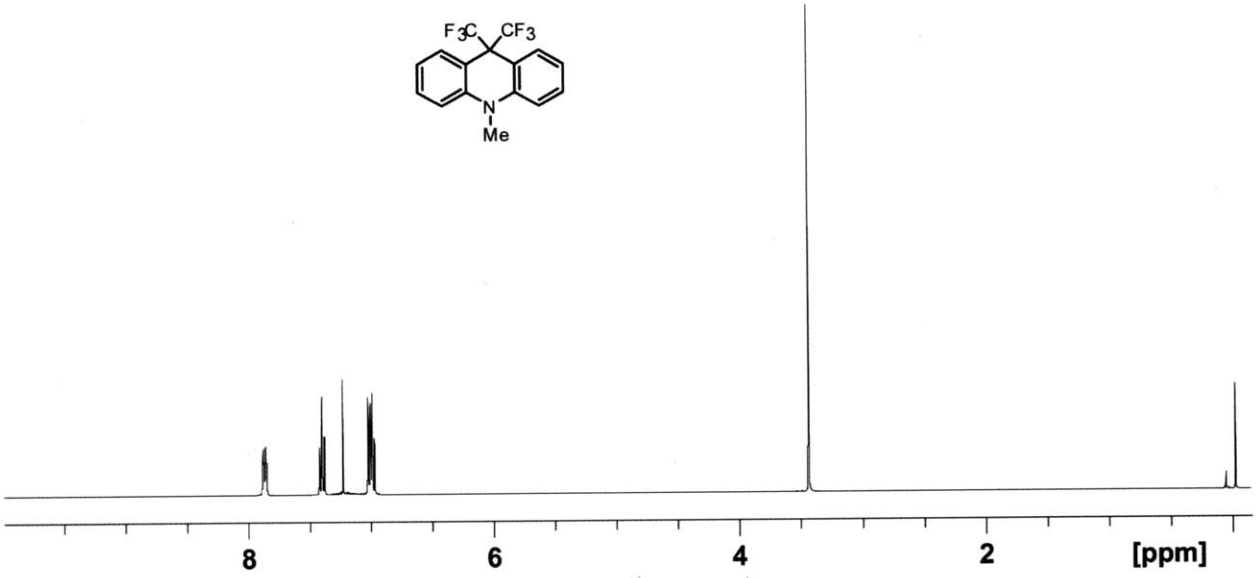
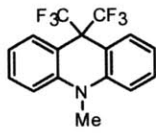


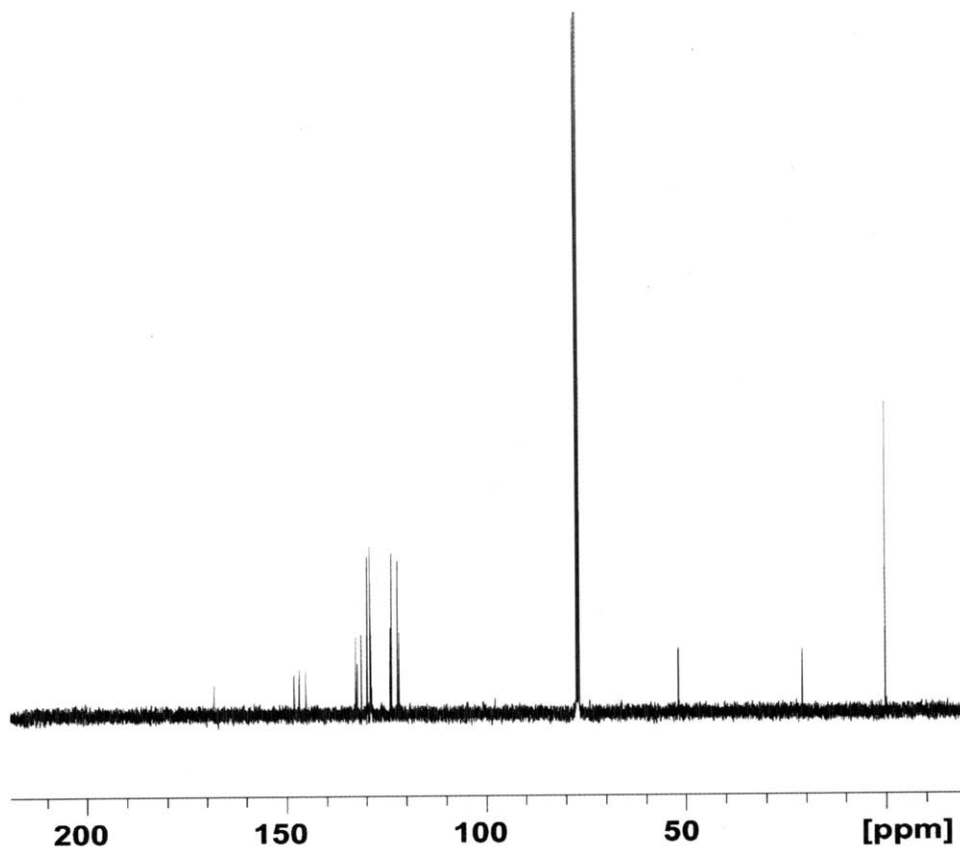
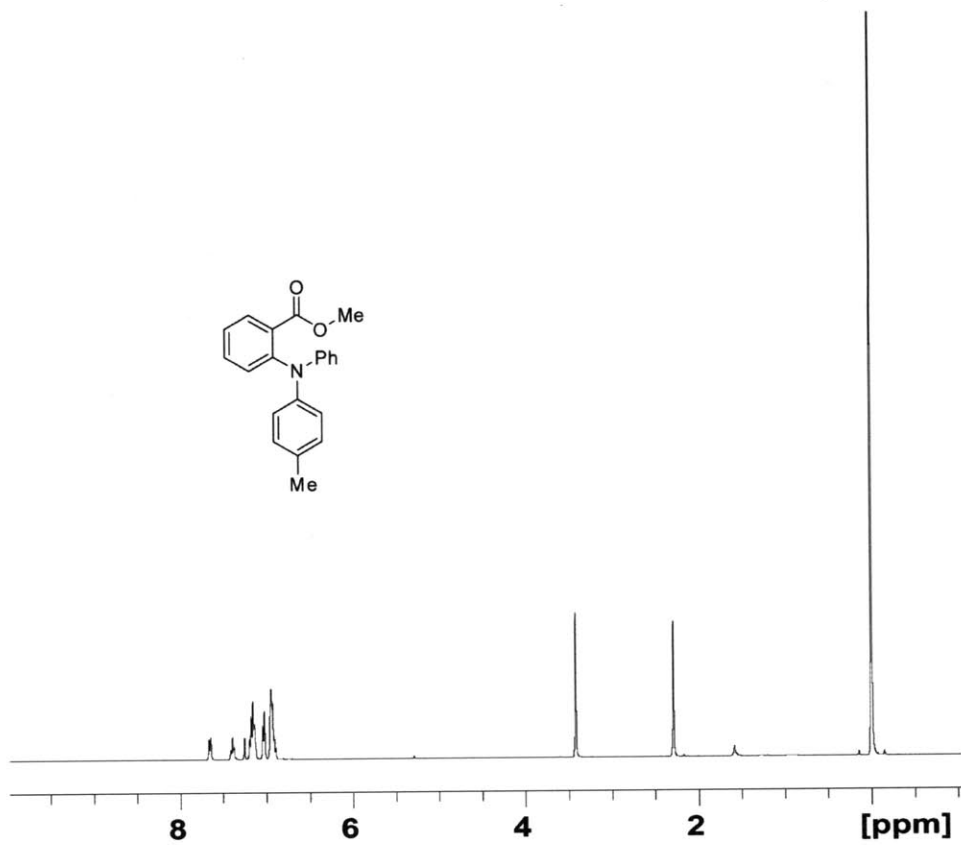
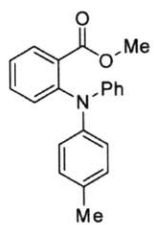


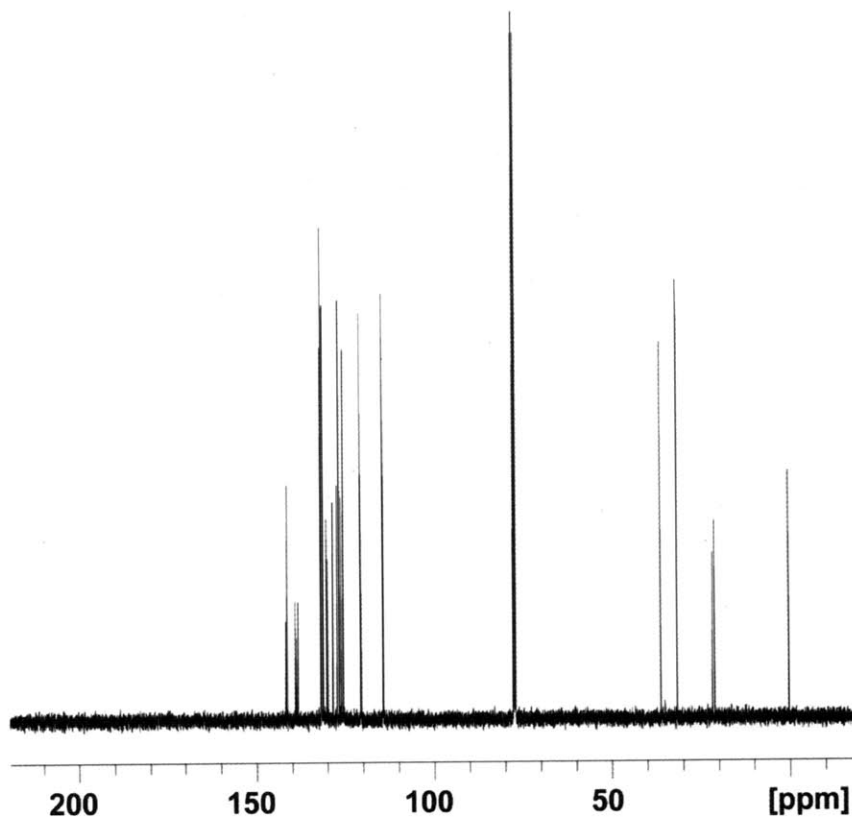
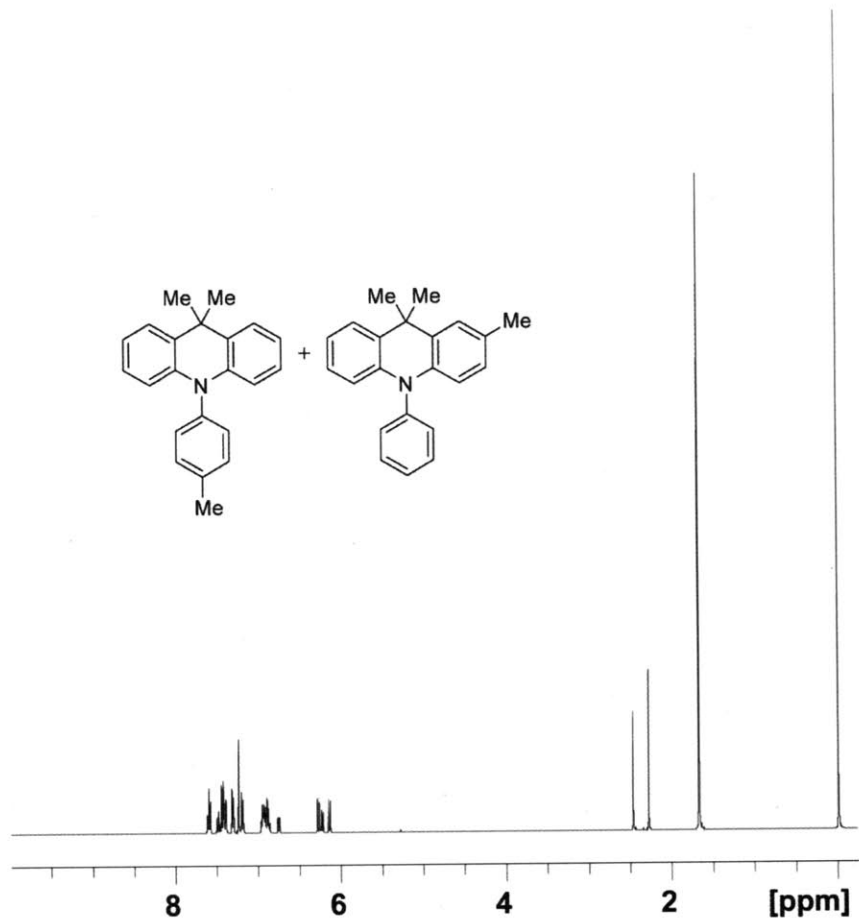


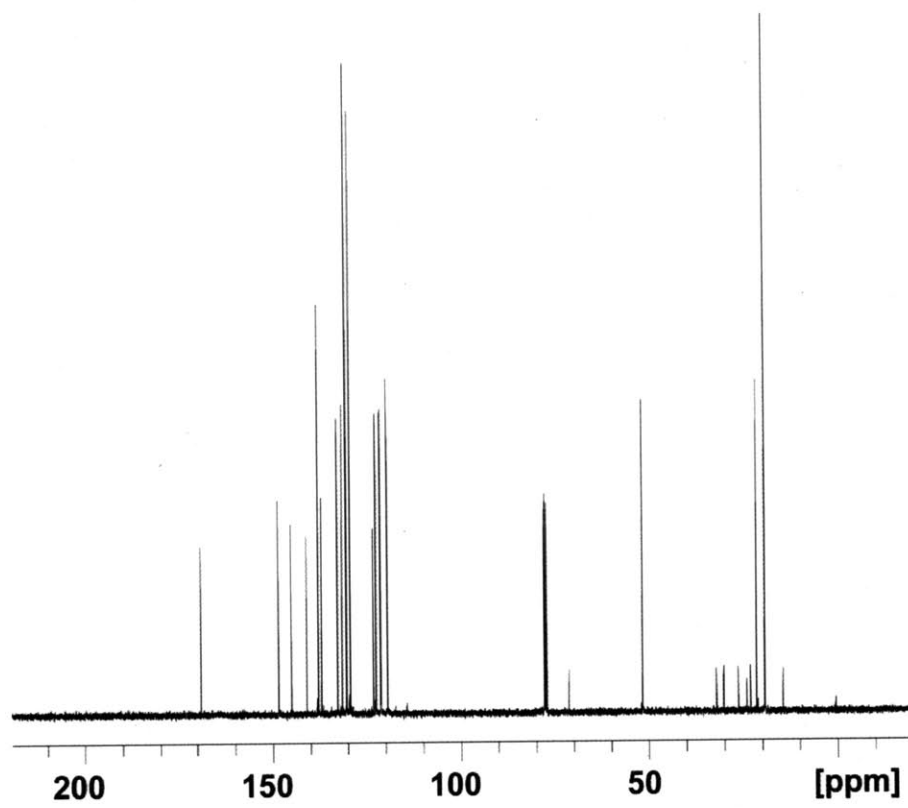
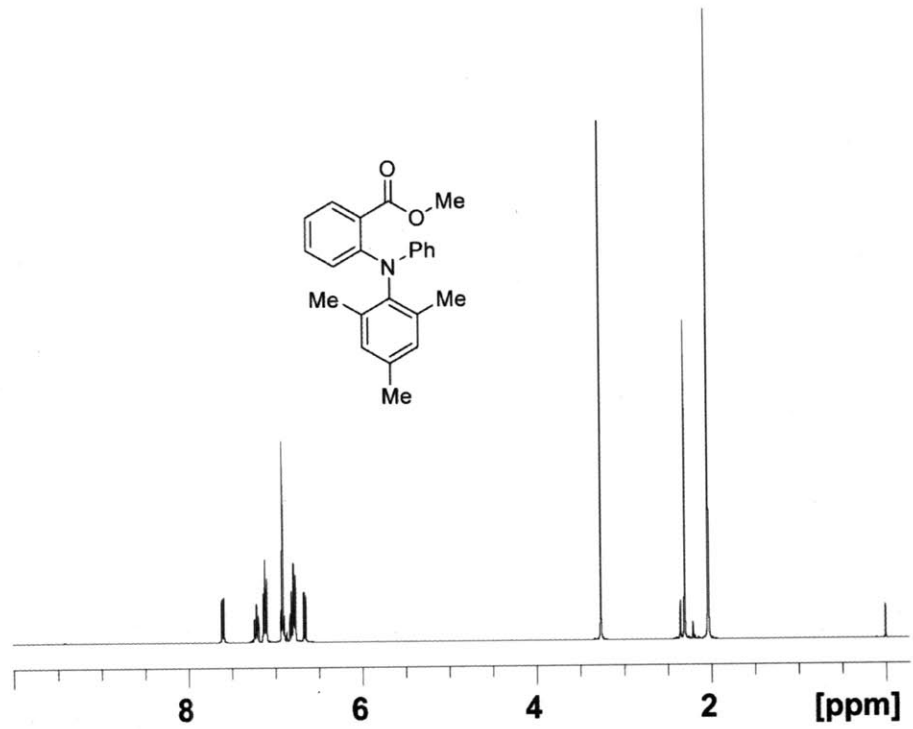


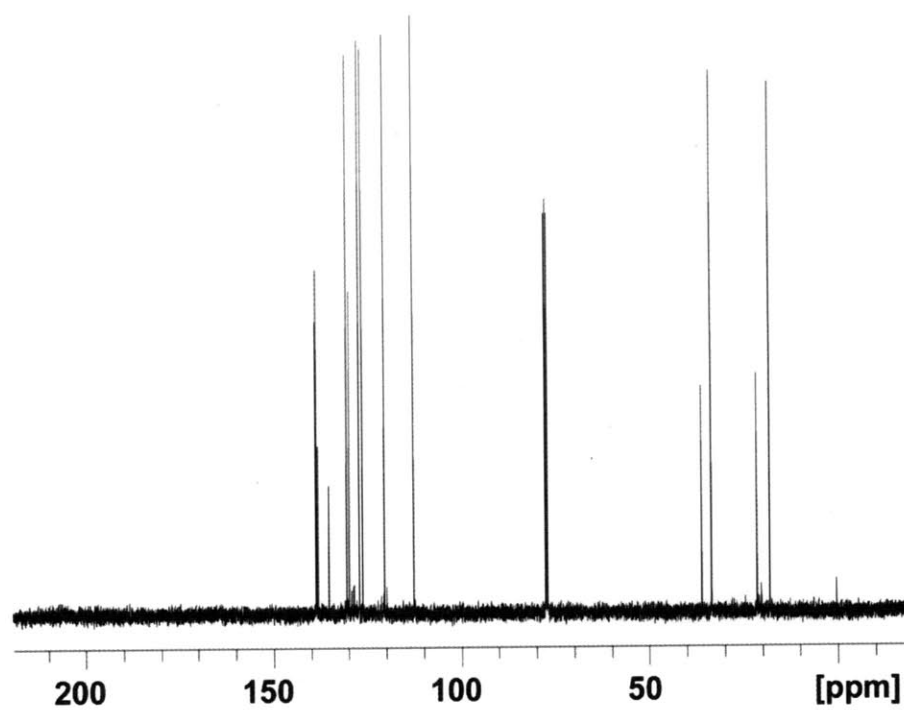
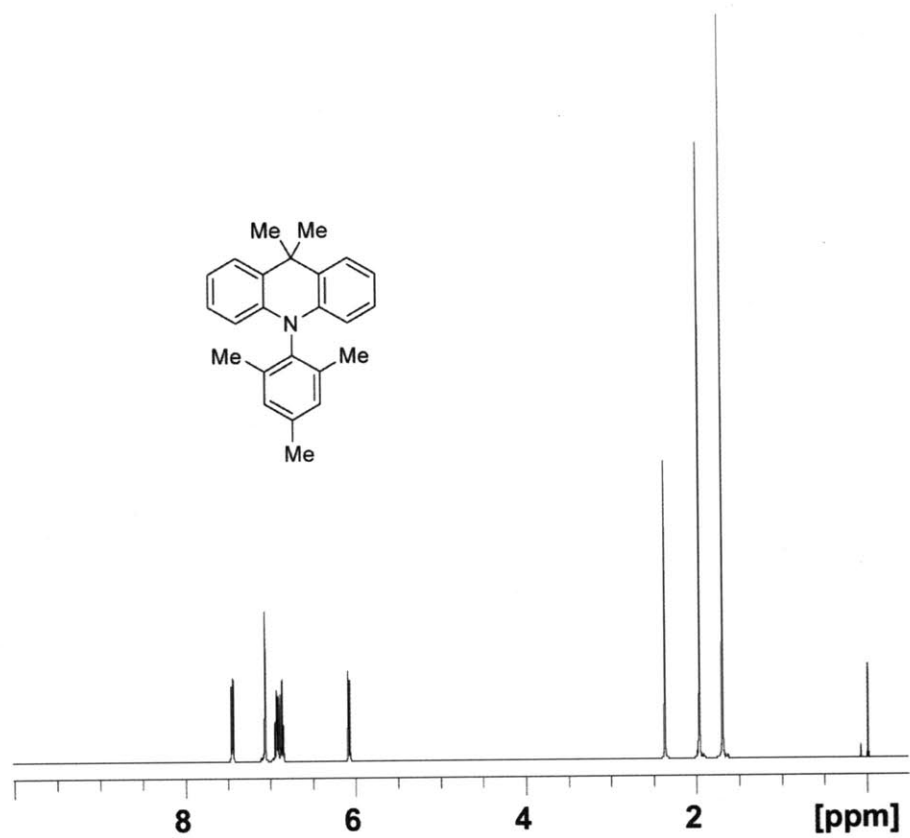


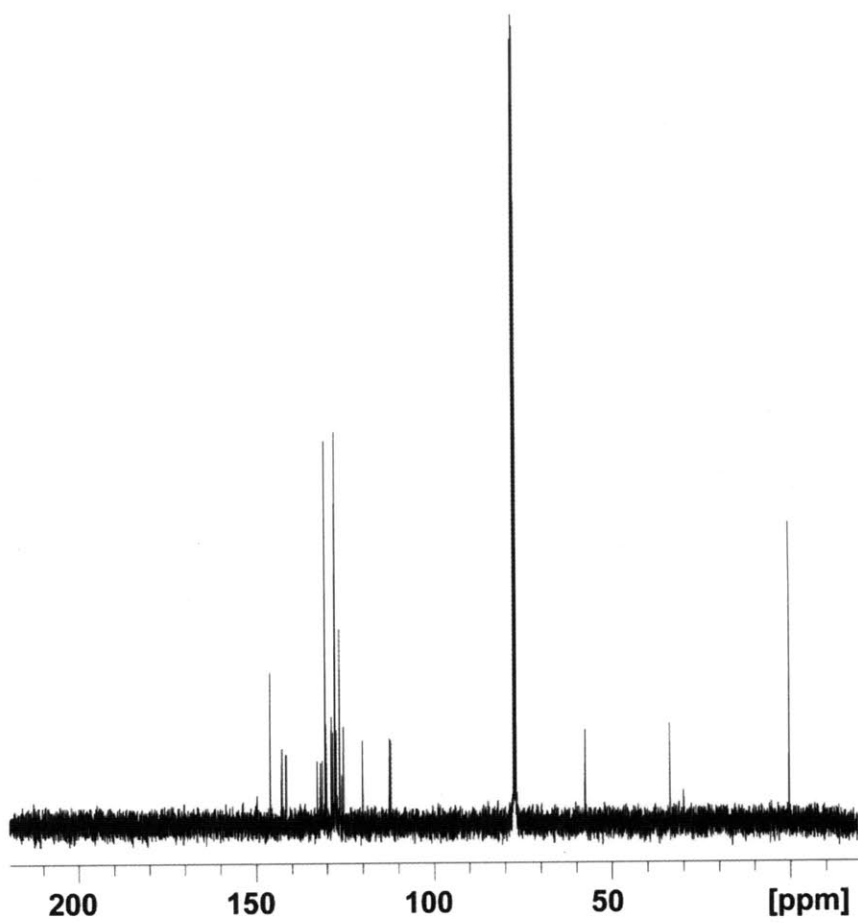
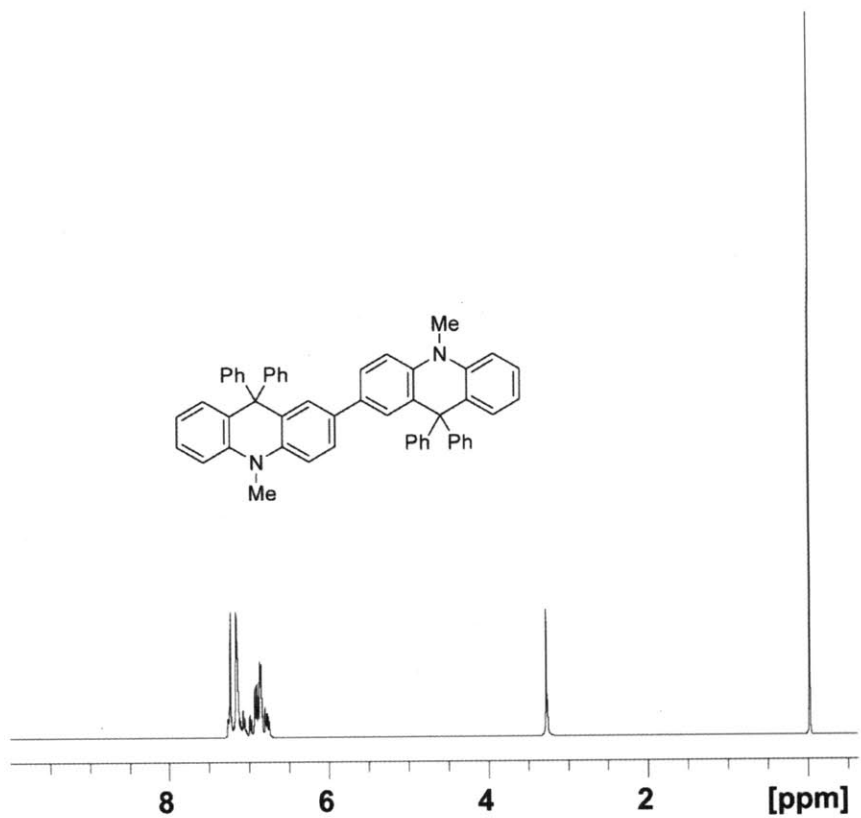


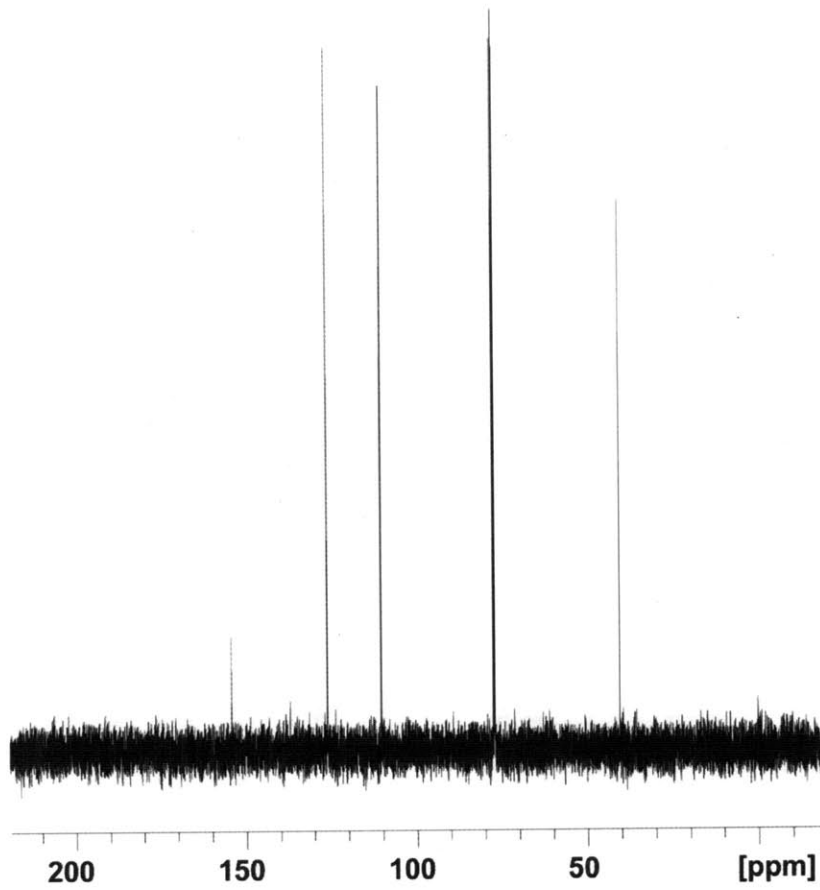
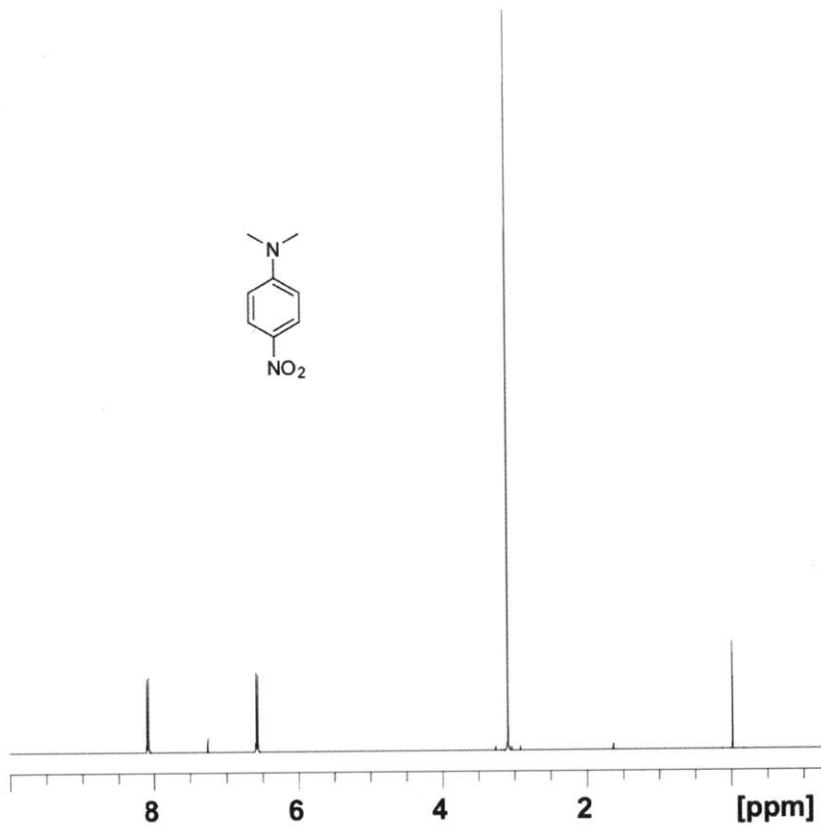
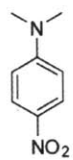


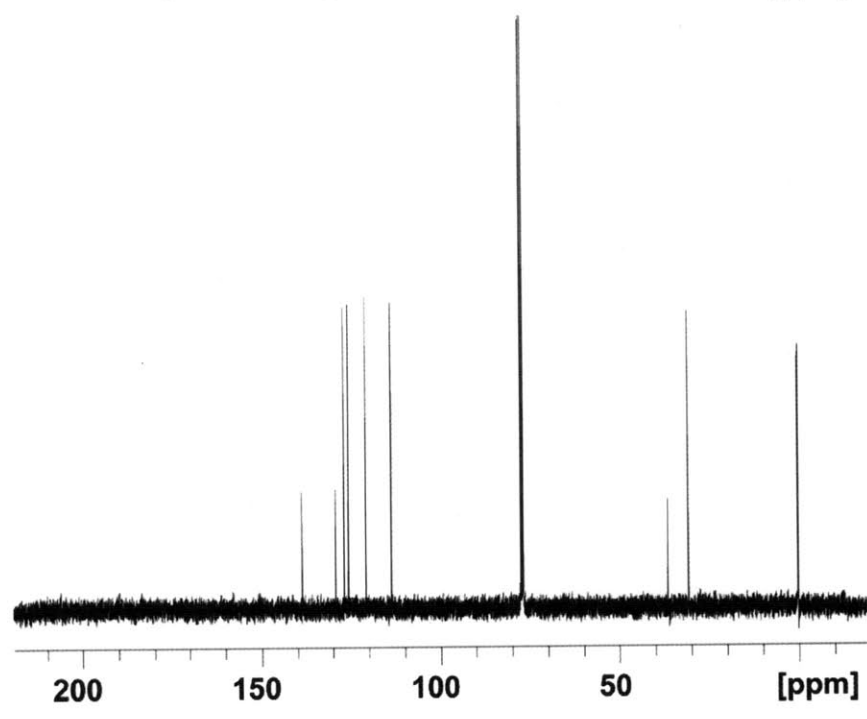
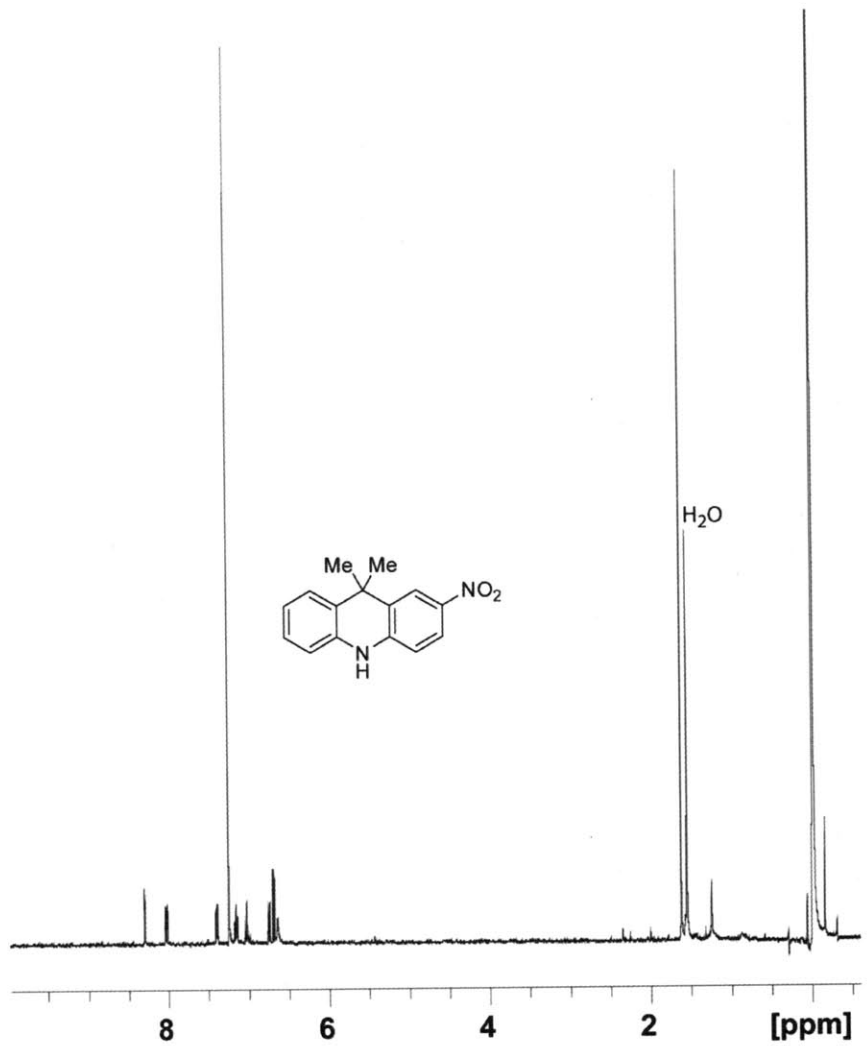


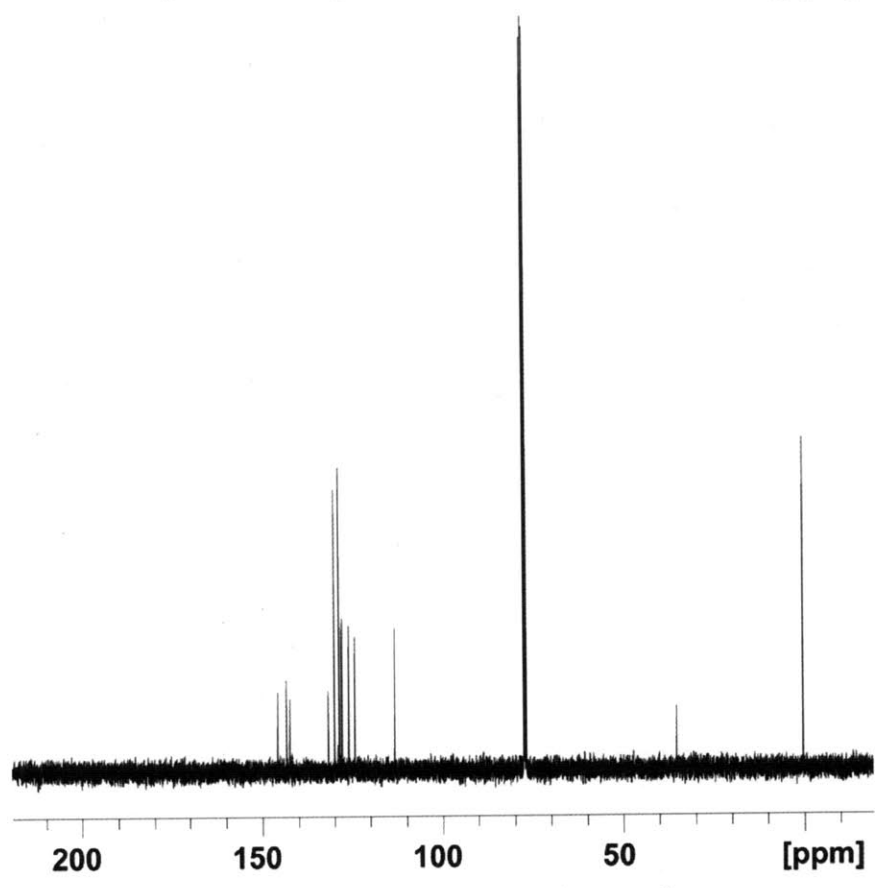
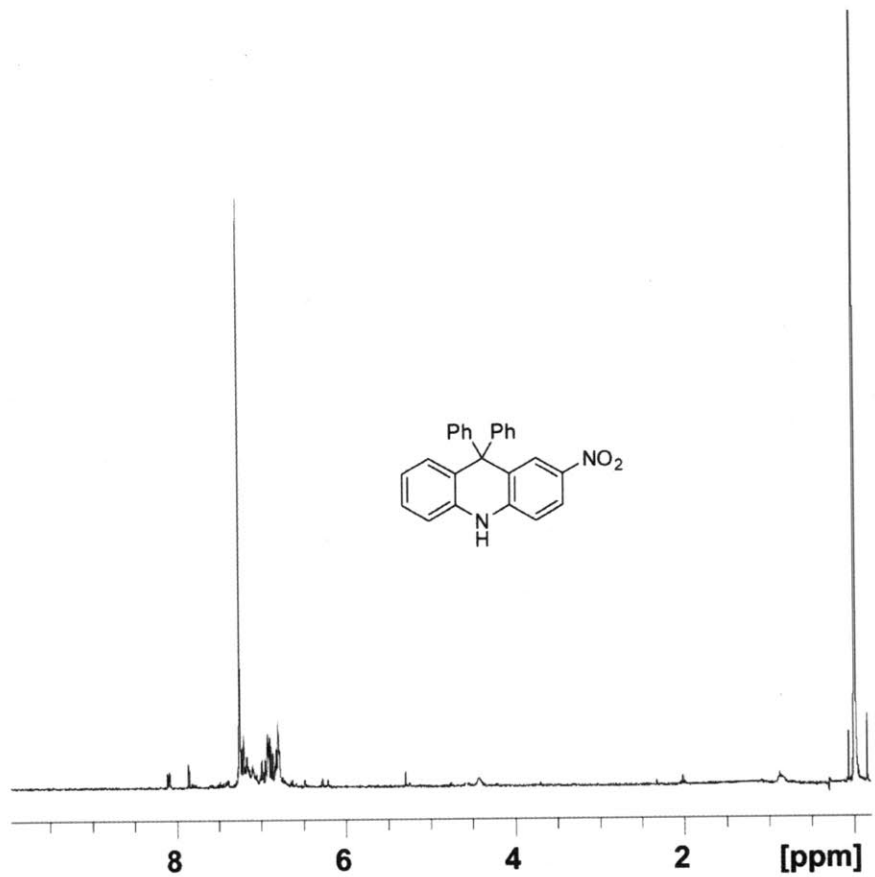


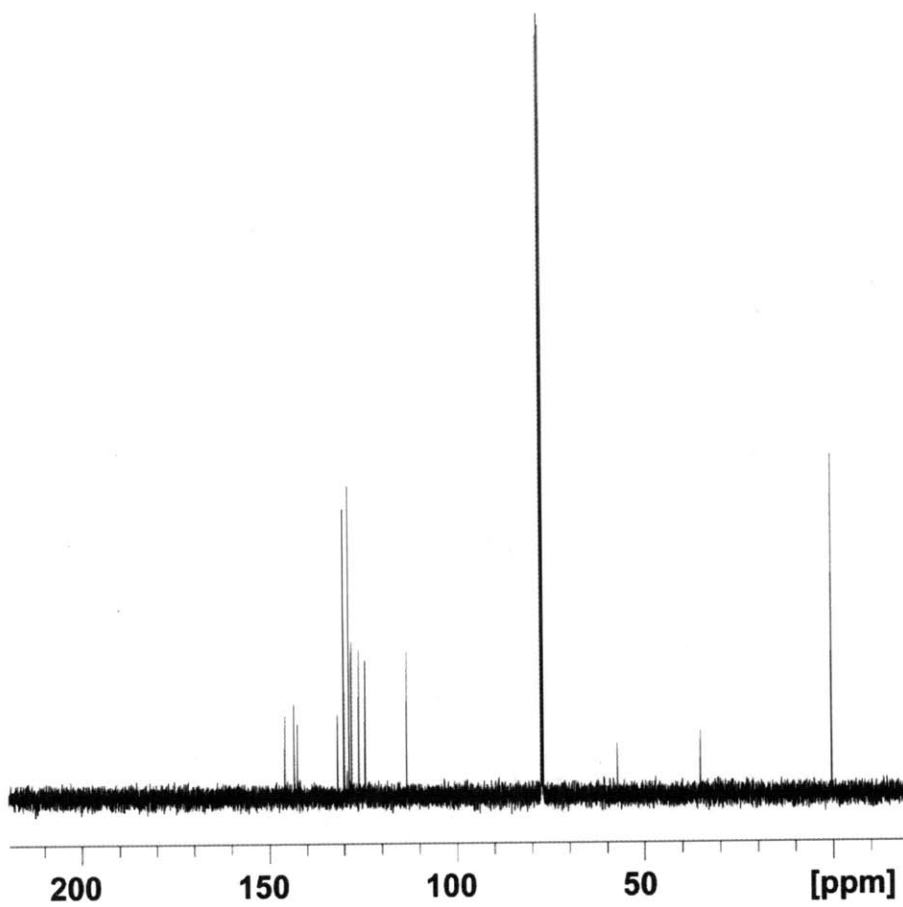
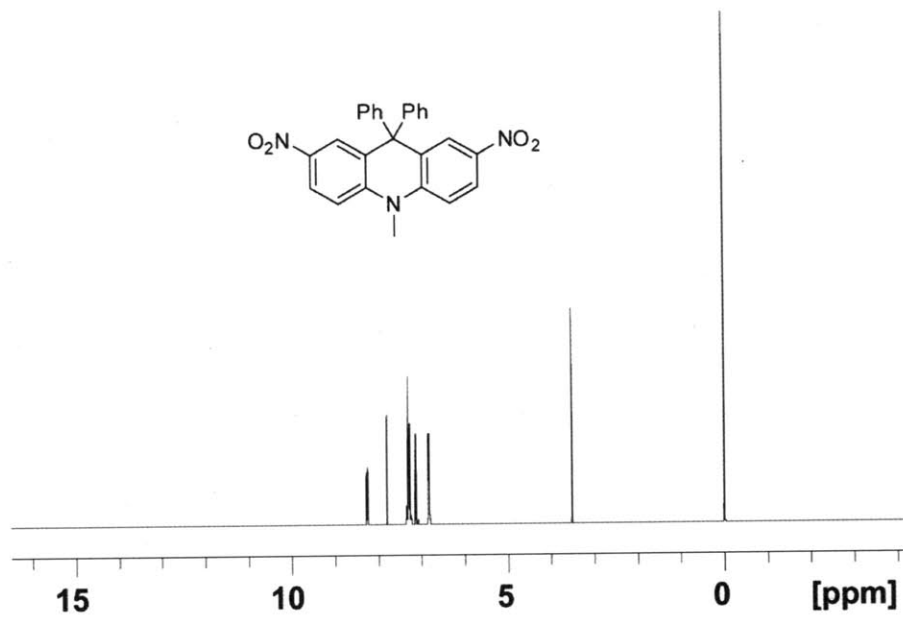


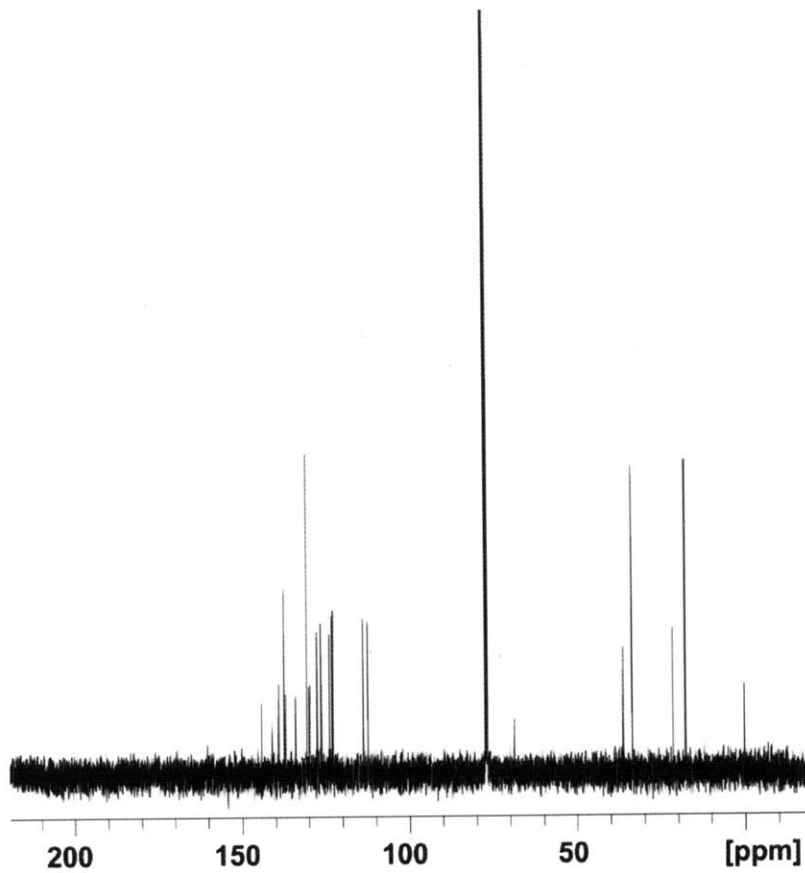
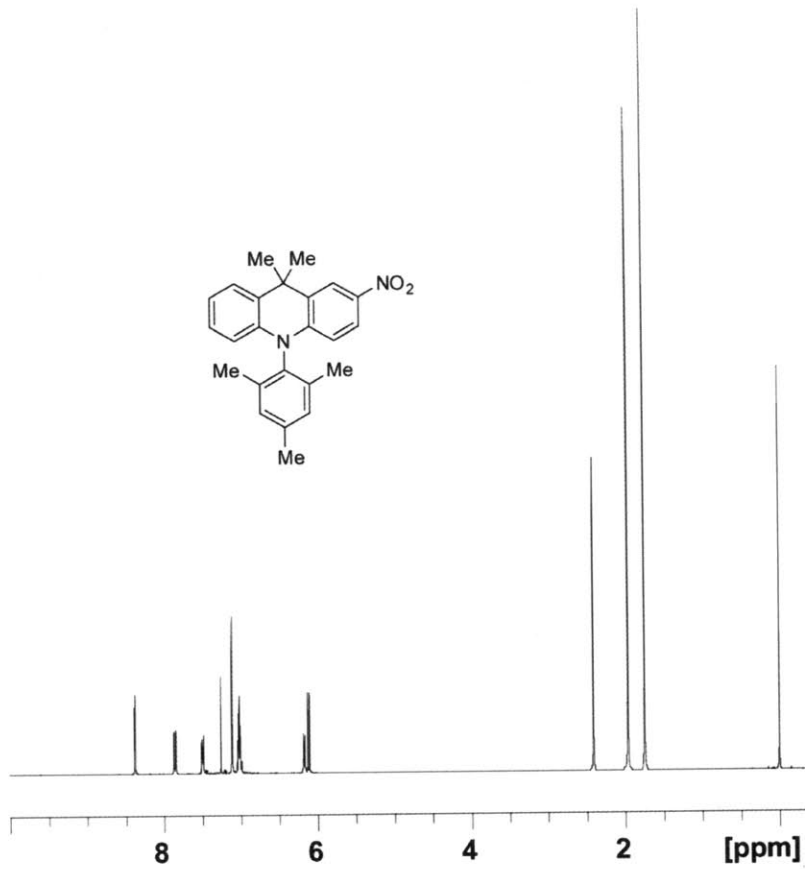
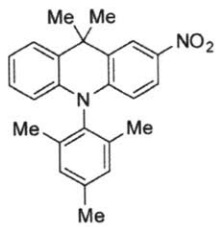


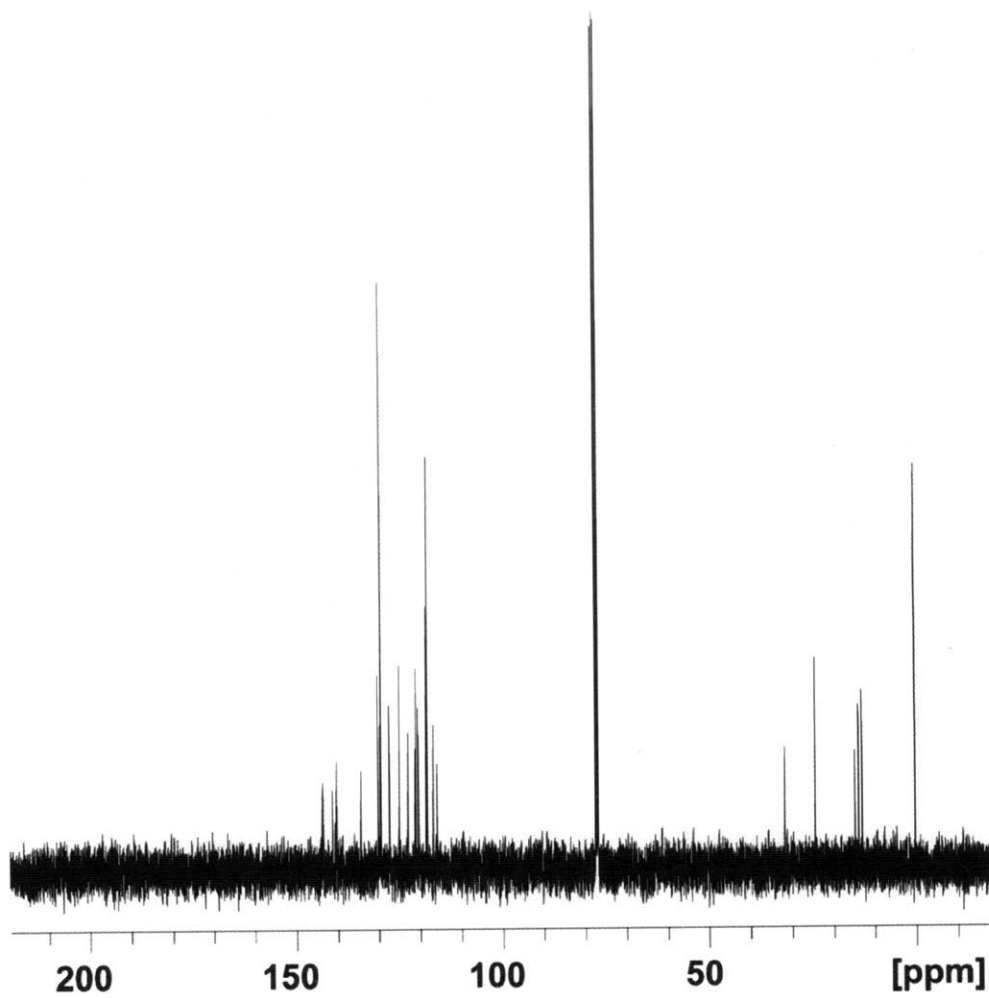
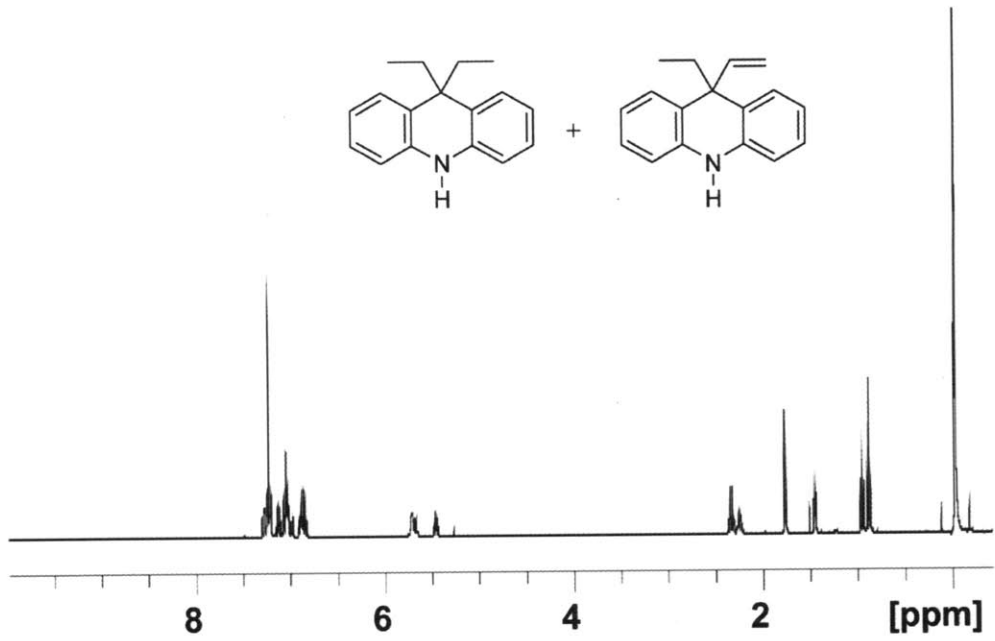


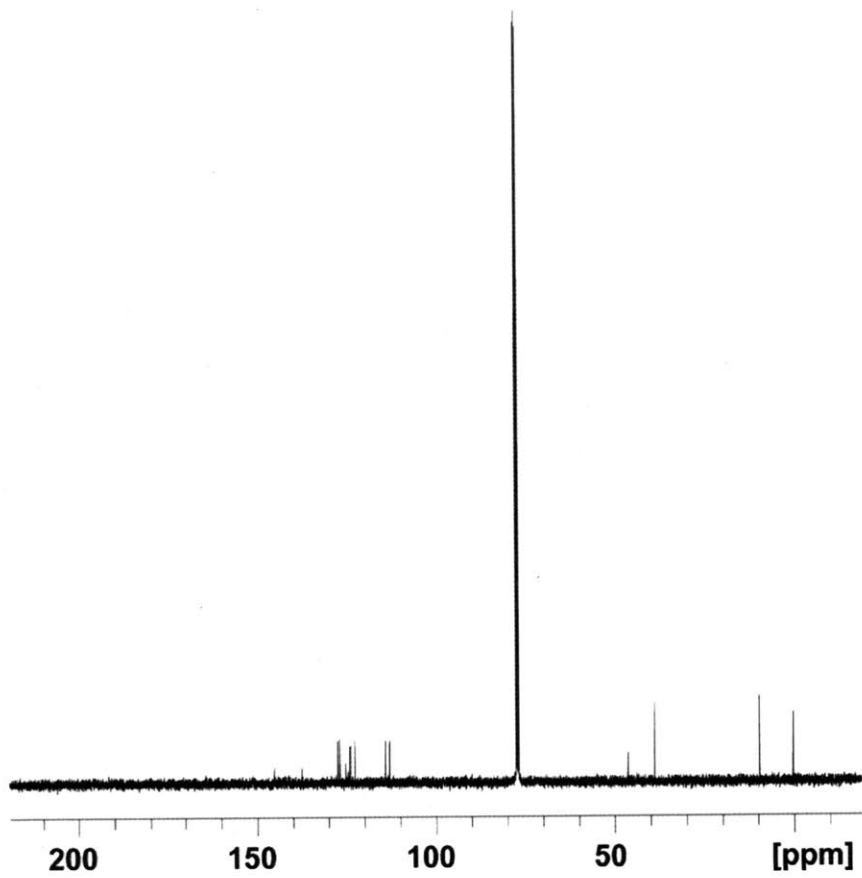
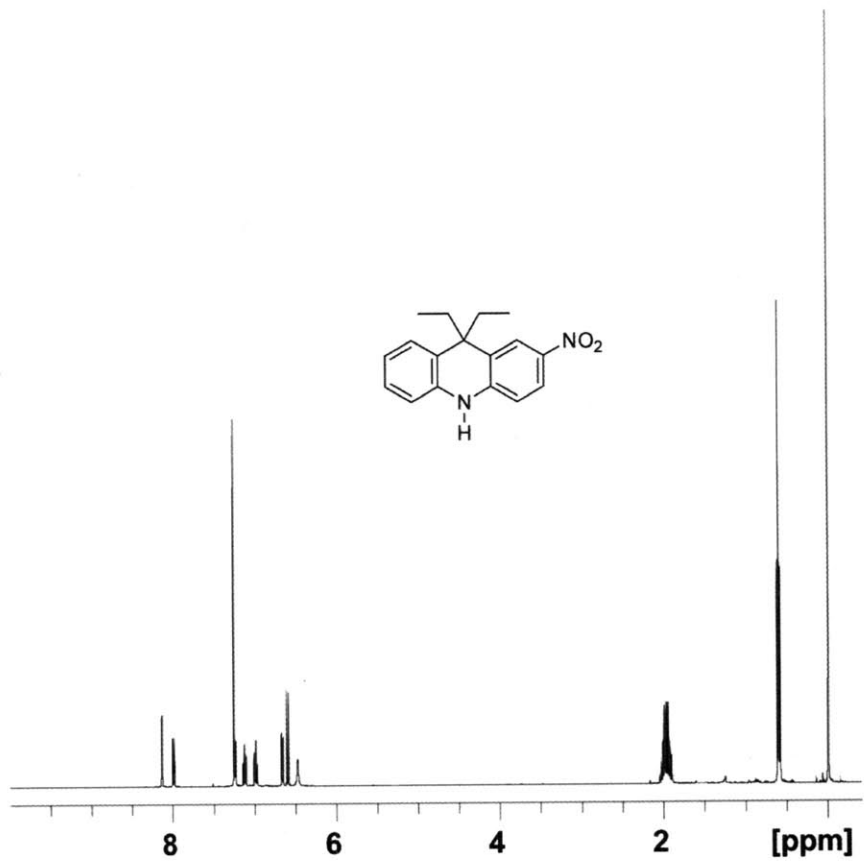
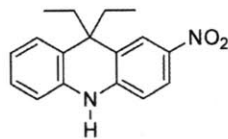




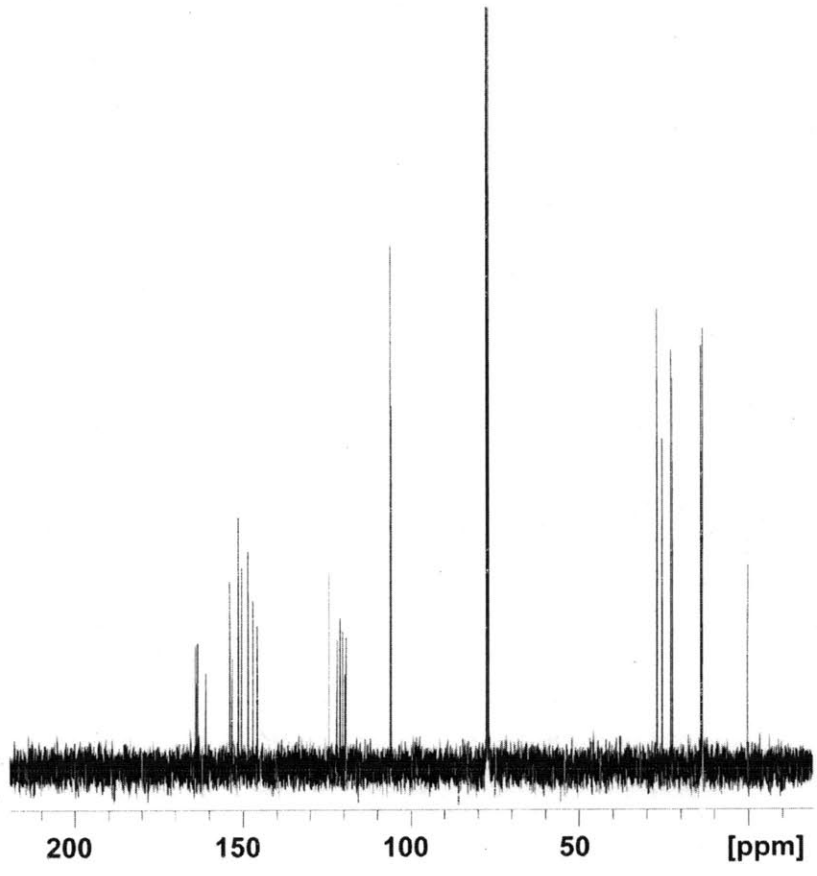
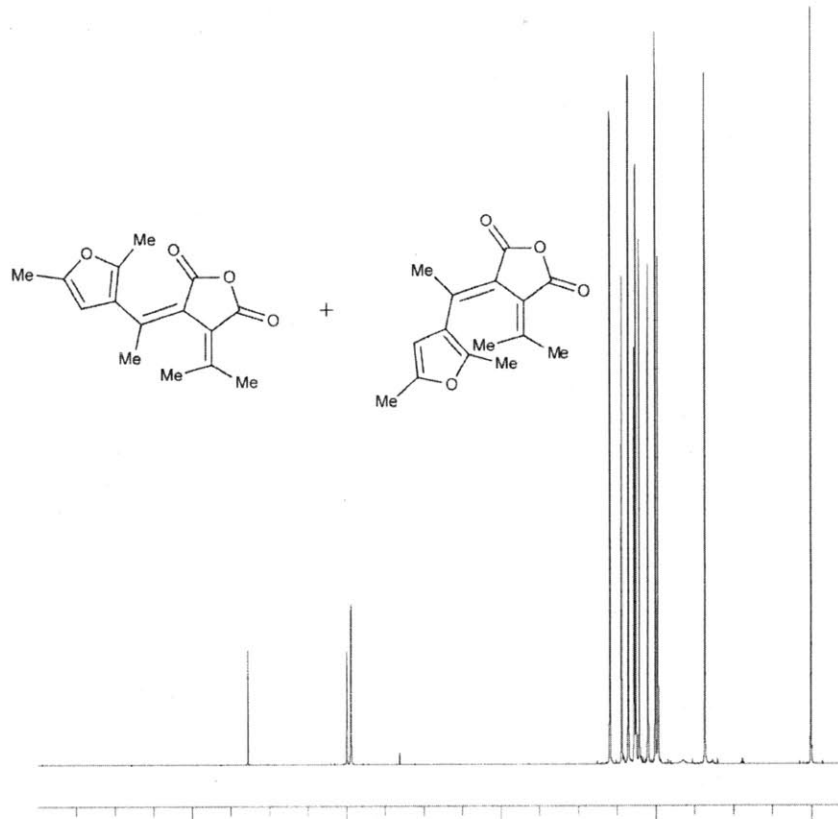


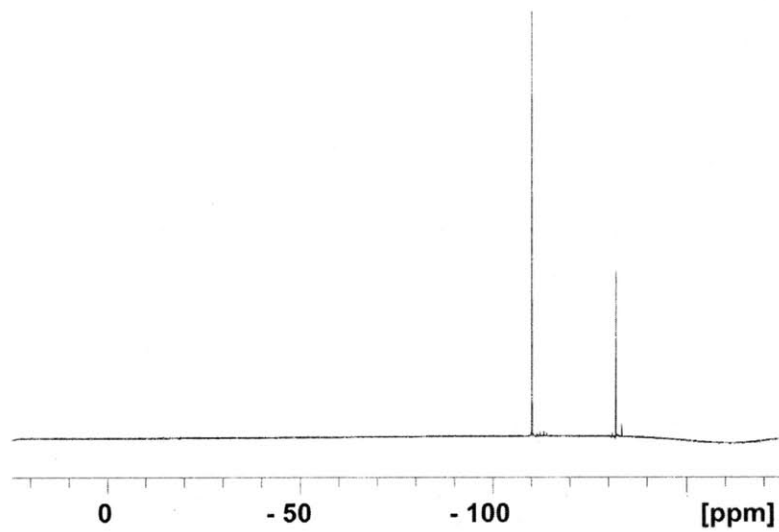
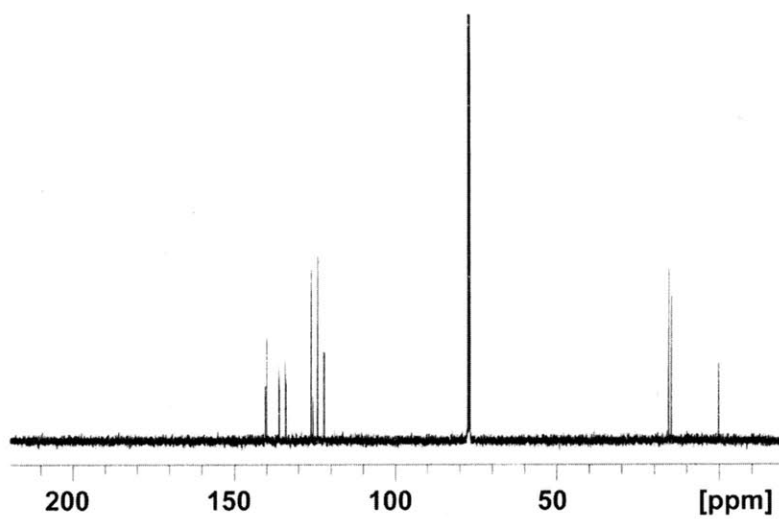
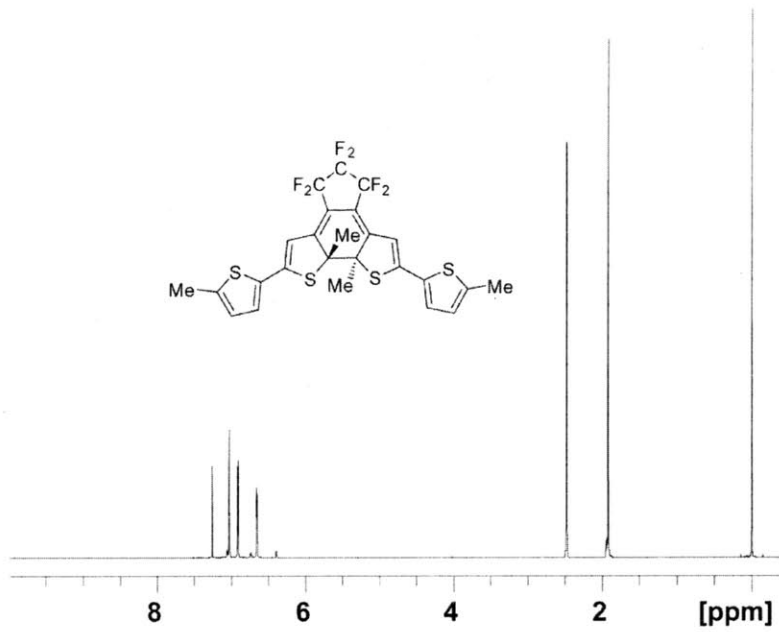




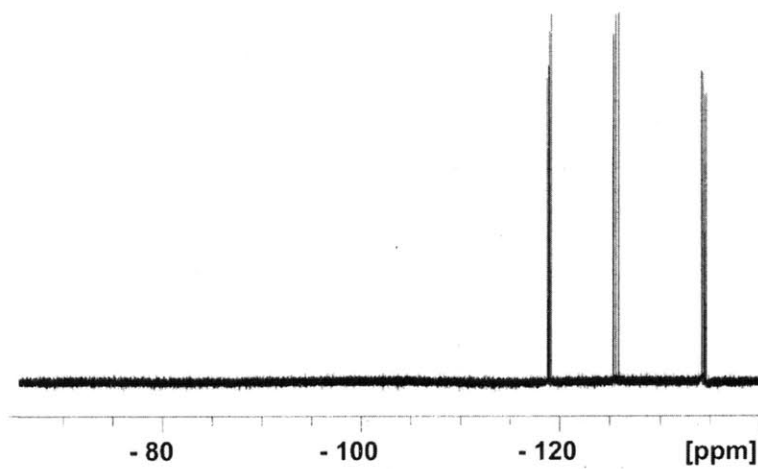
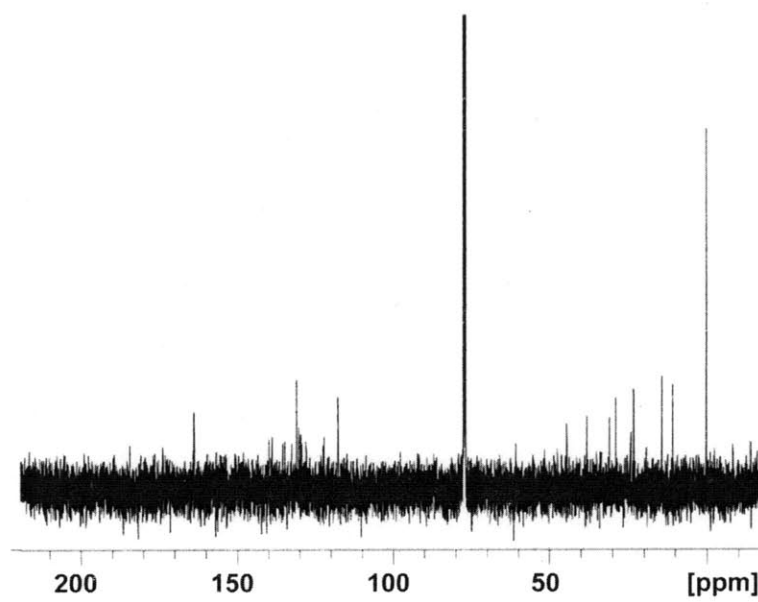
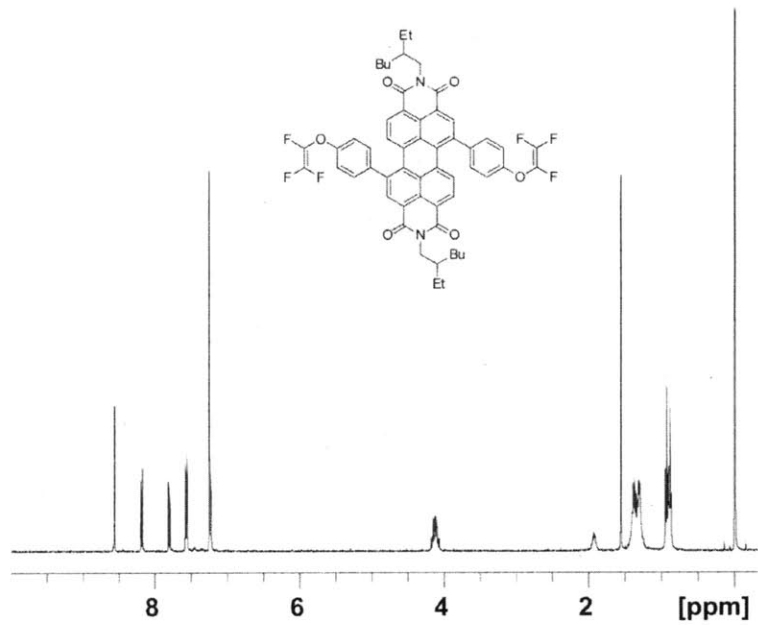


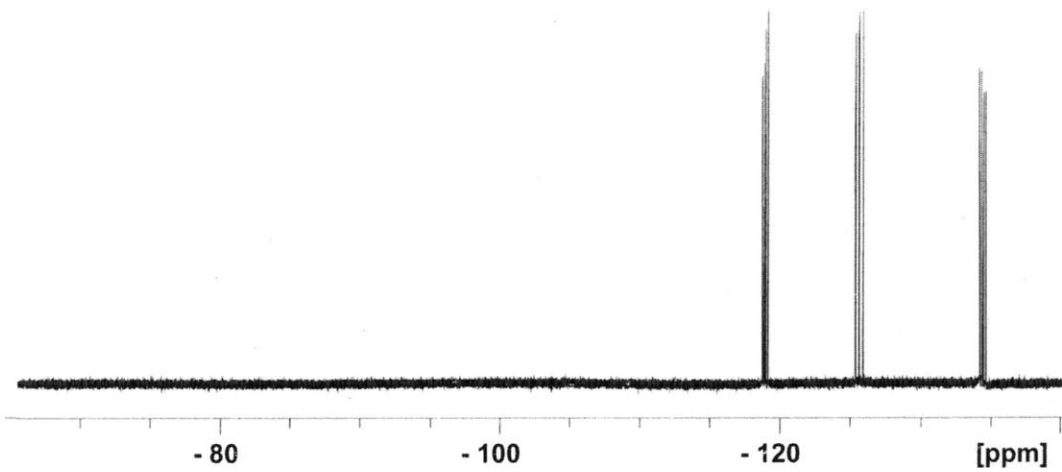
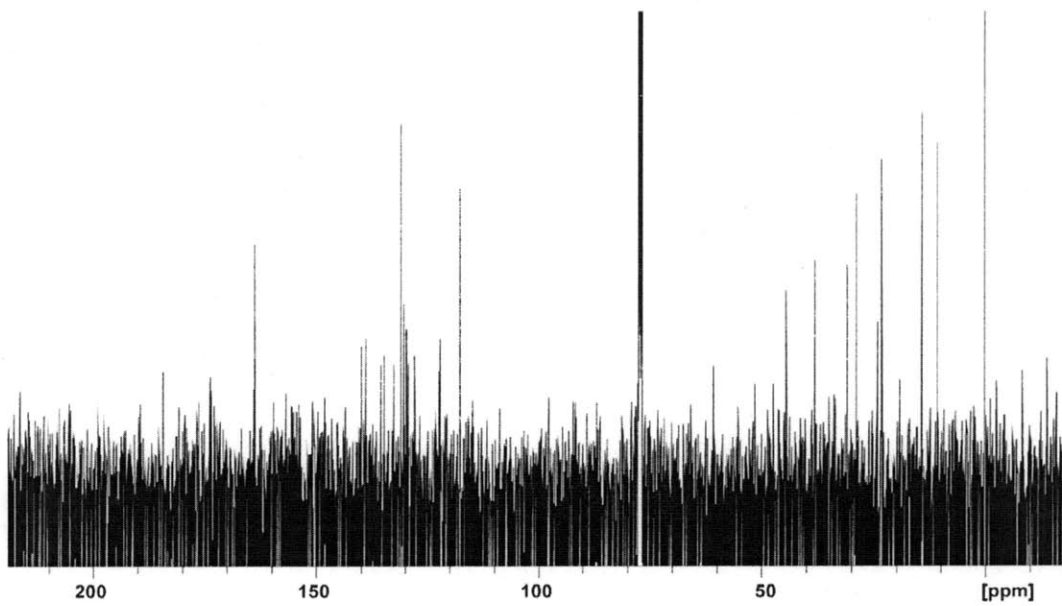
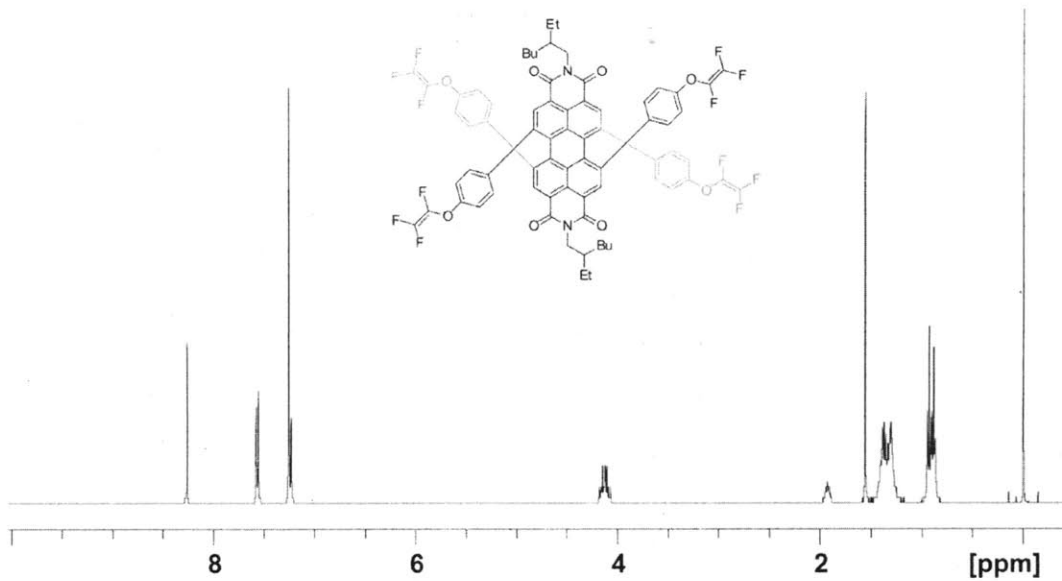
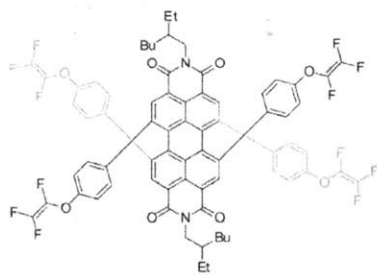
APPENDIX 3
NMR Spectra for Chapter 3

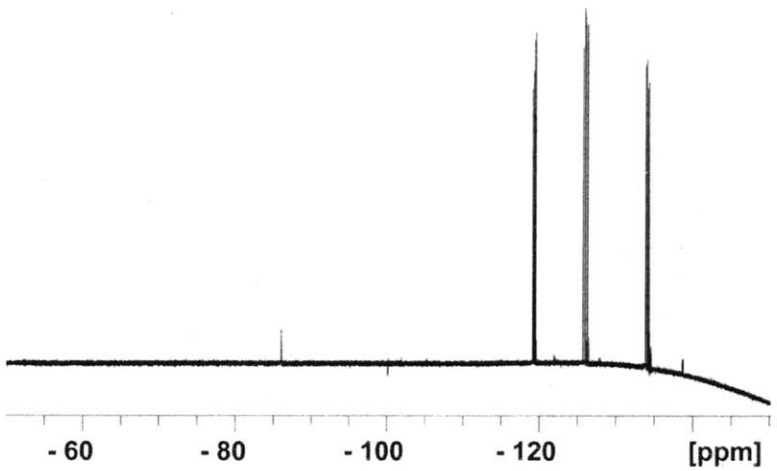
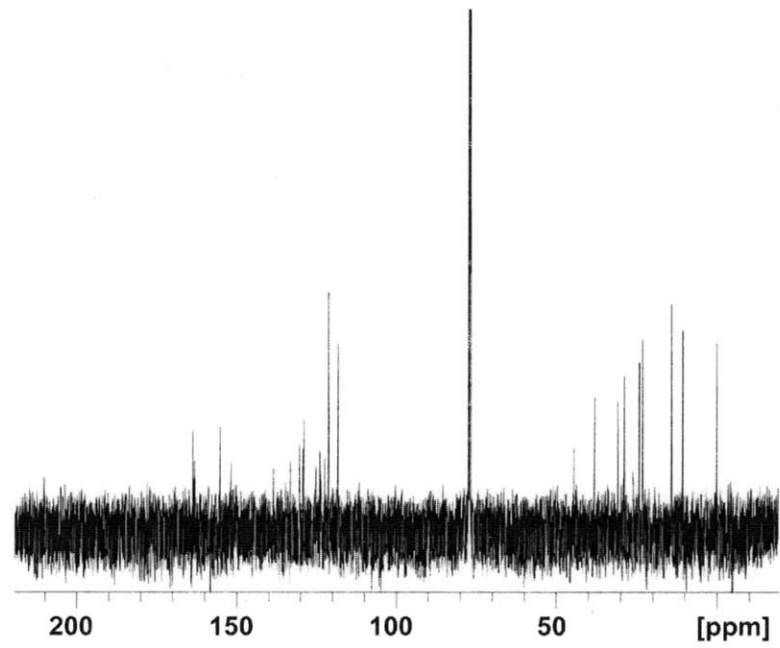
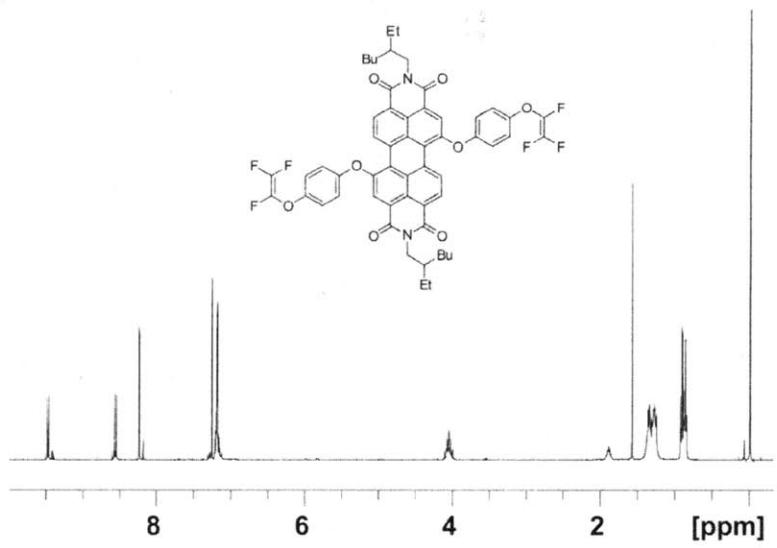


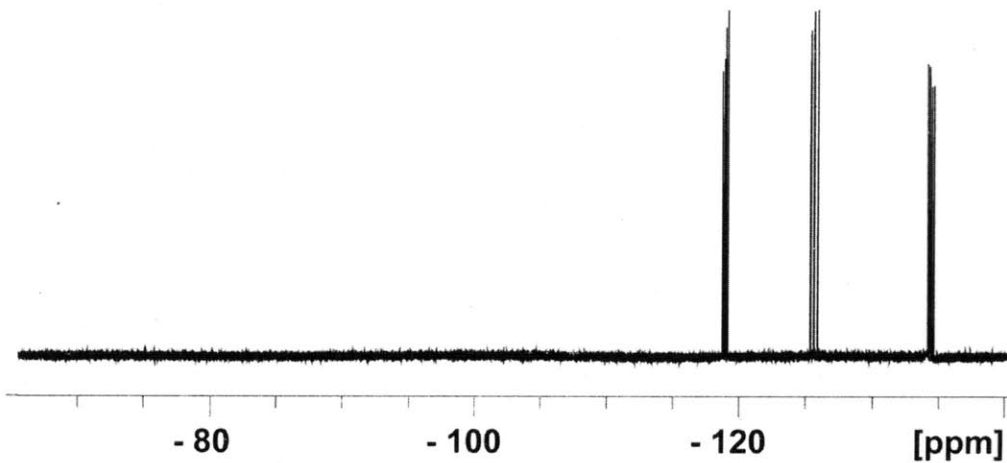
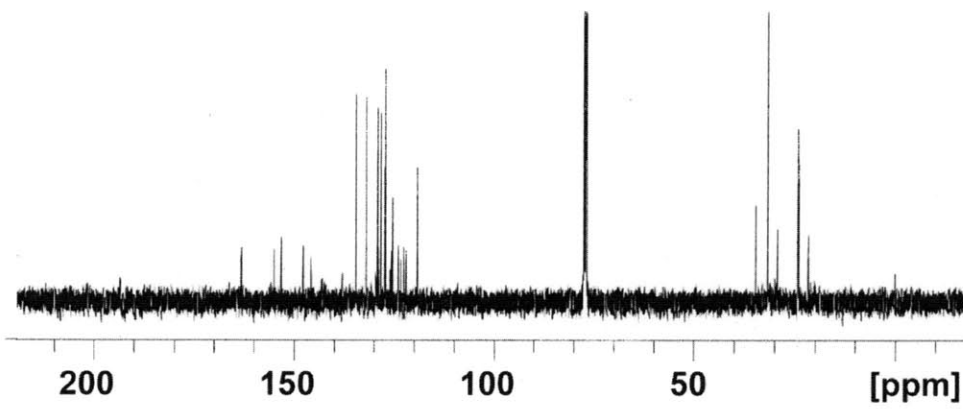
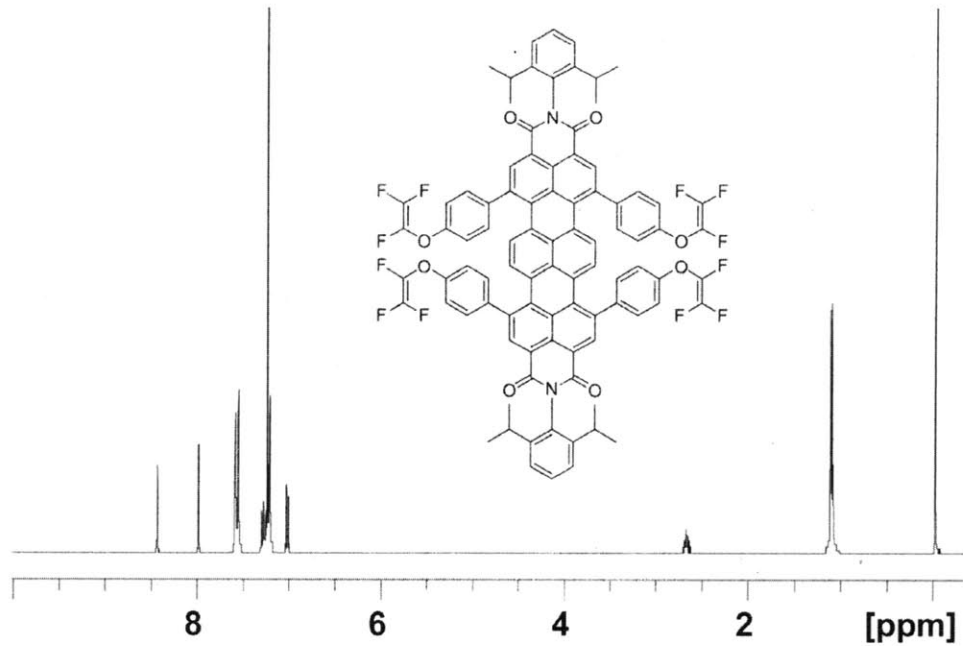


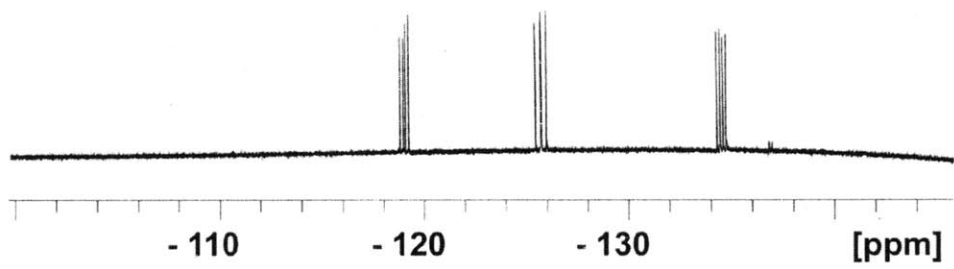
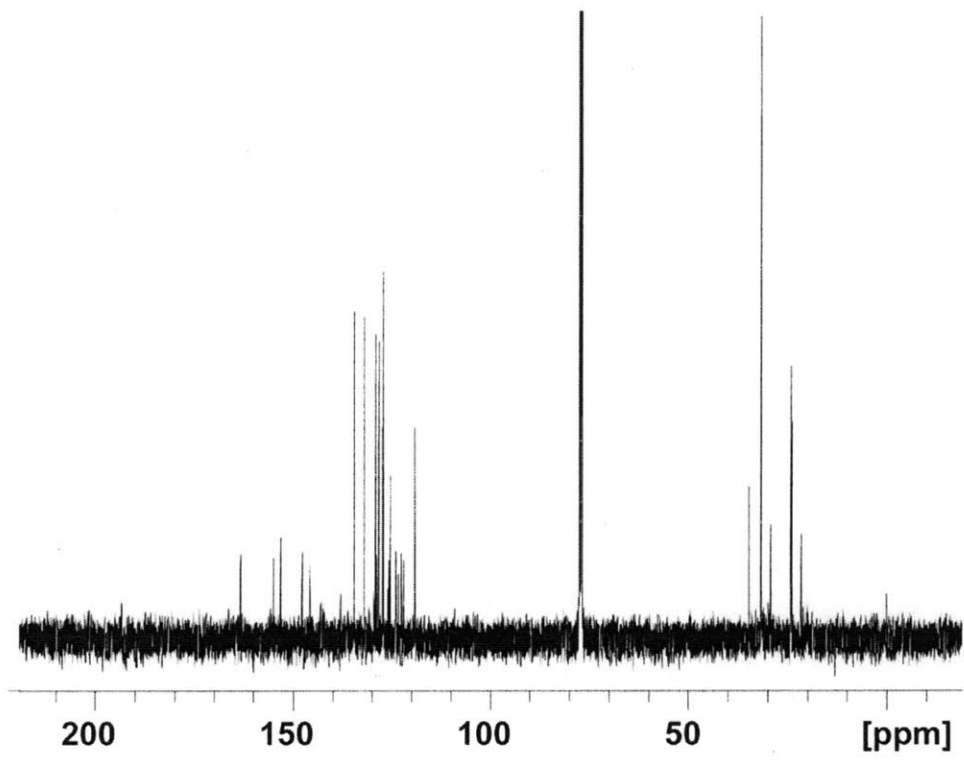
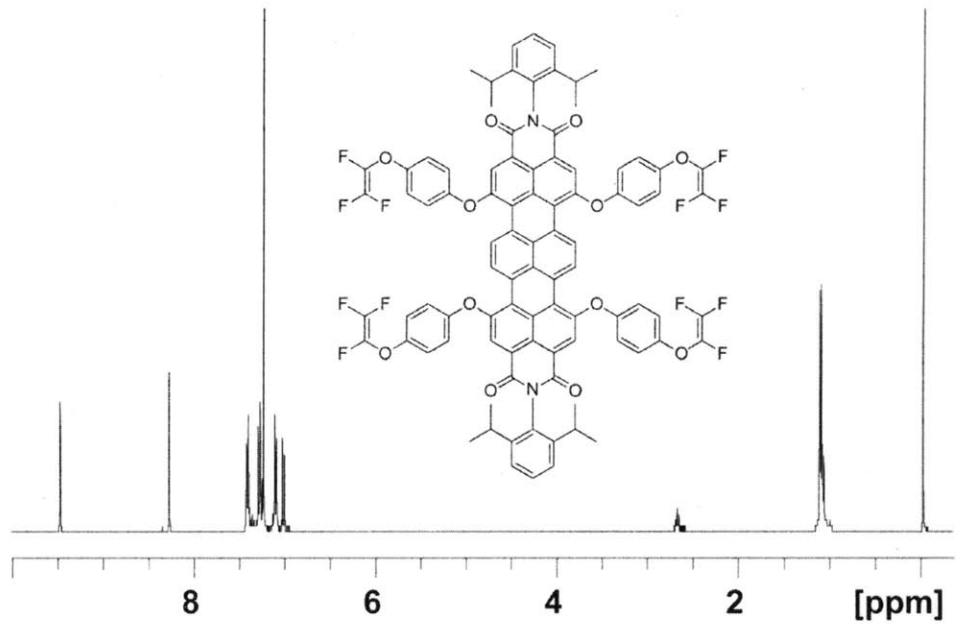
APPENDIX 4
NMR Spectra for Chapter 4



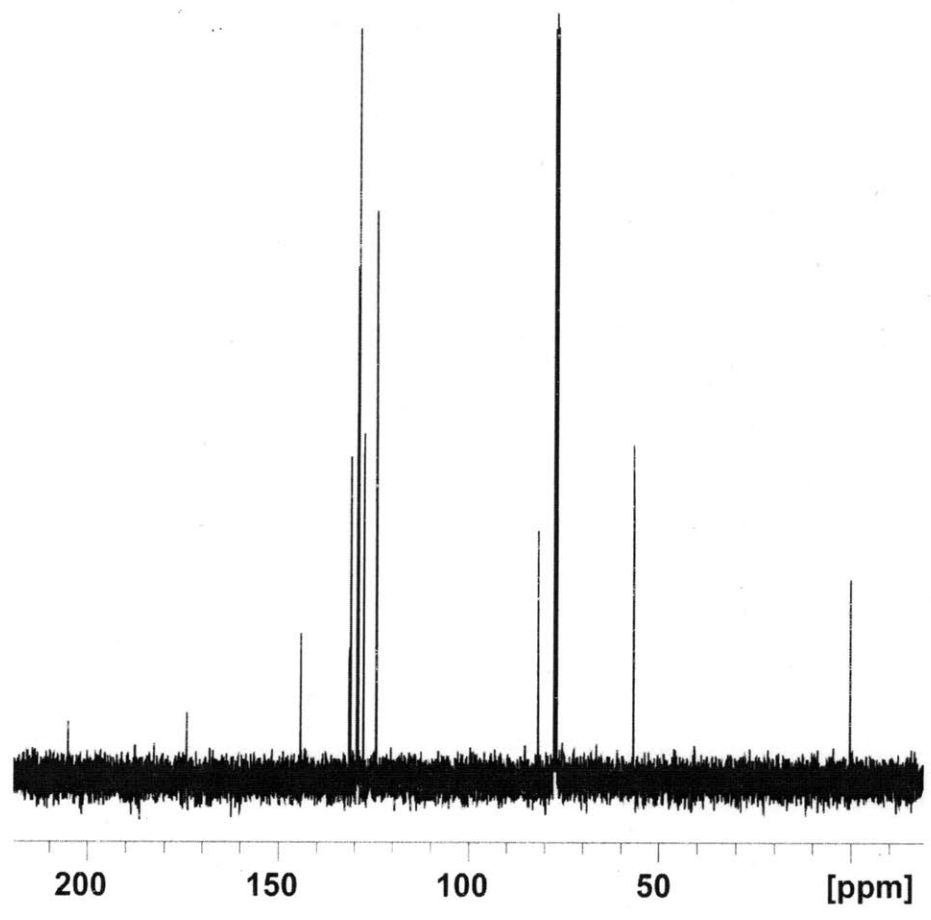
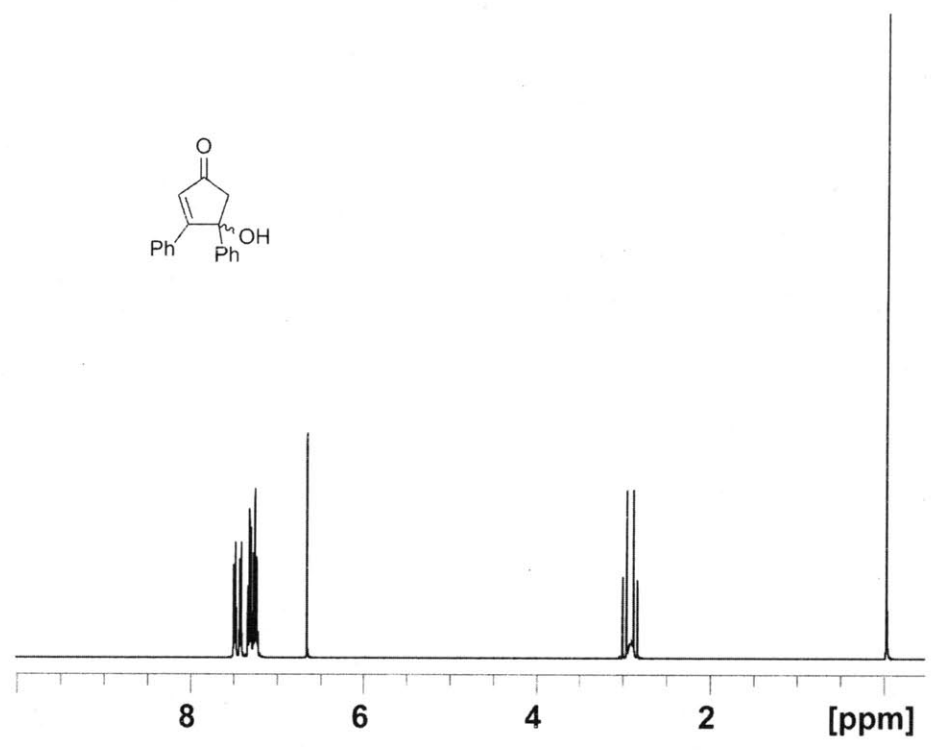
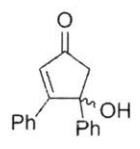


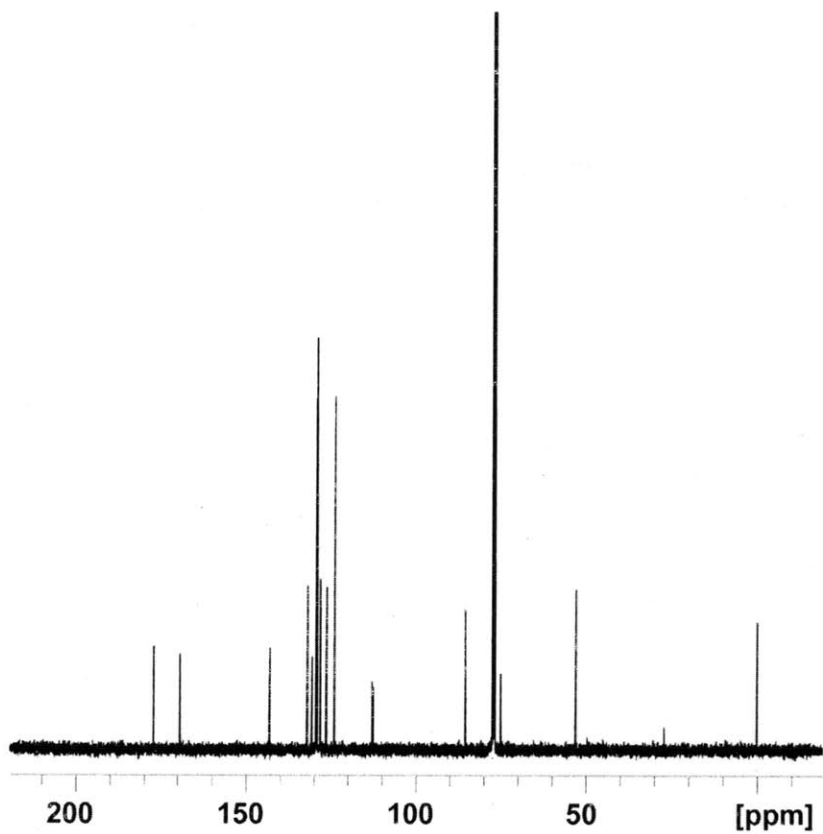
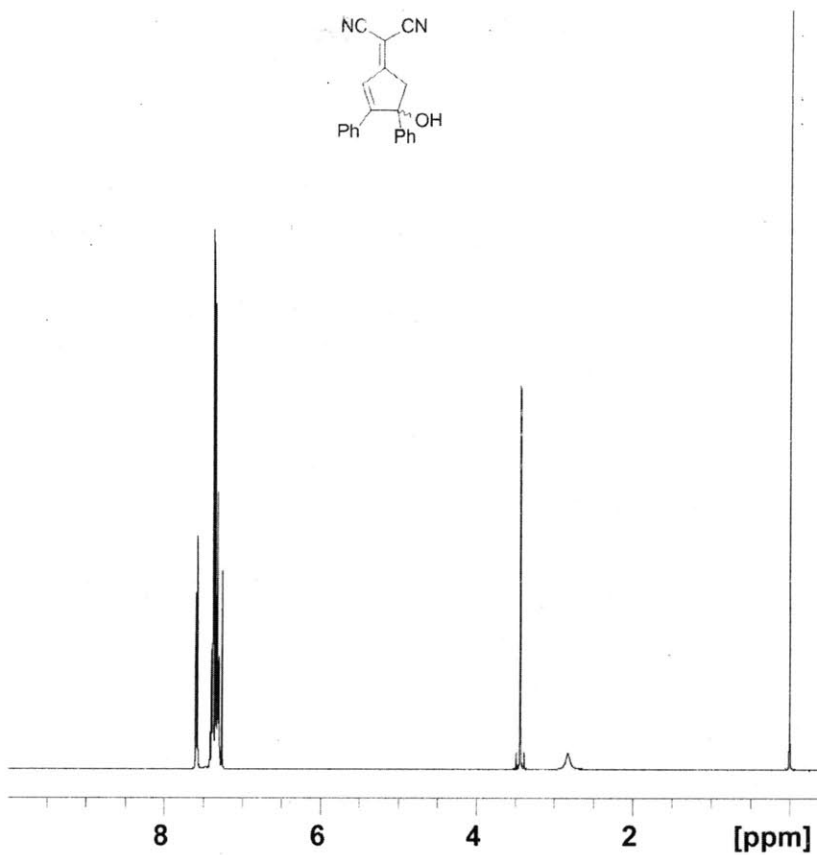
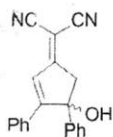


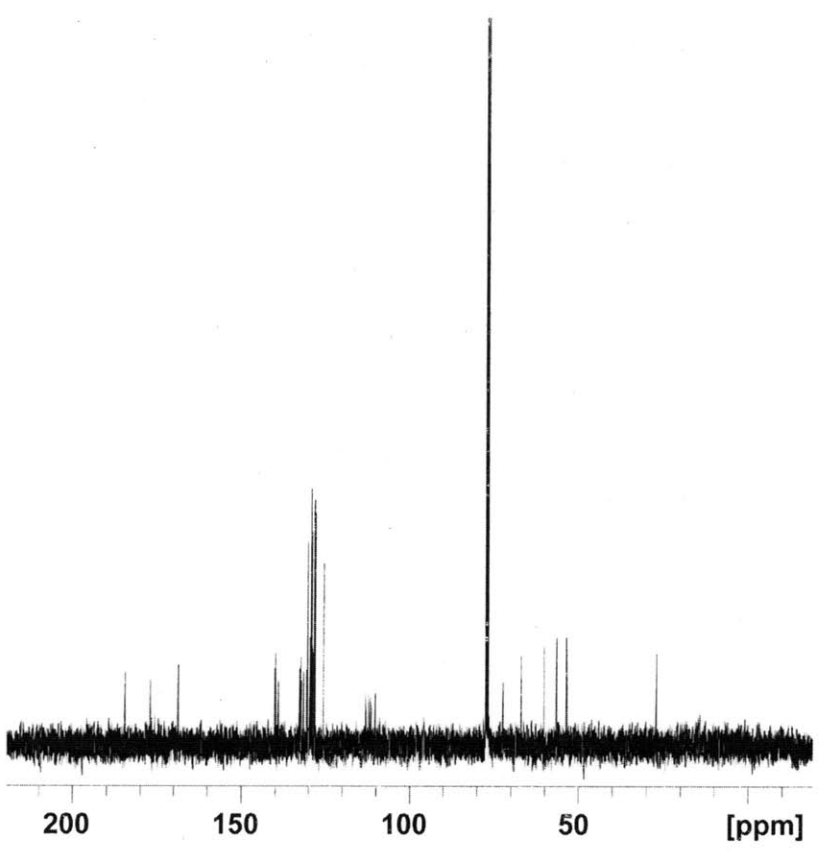
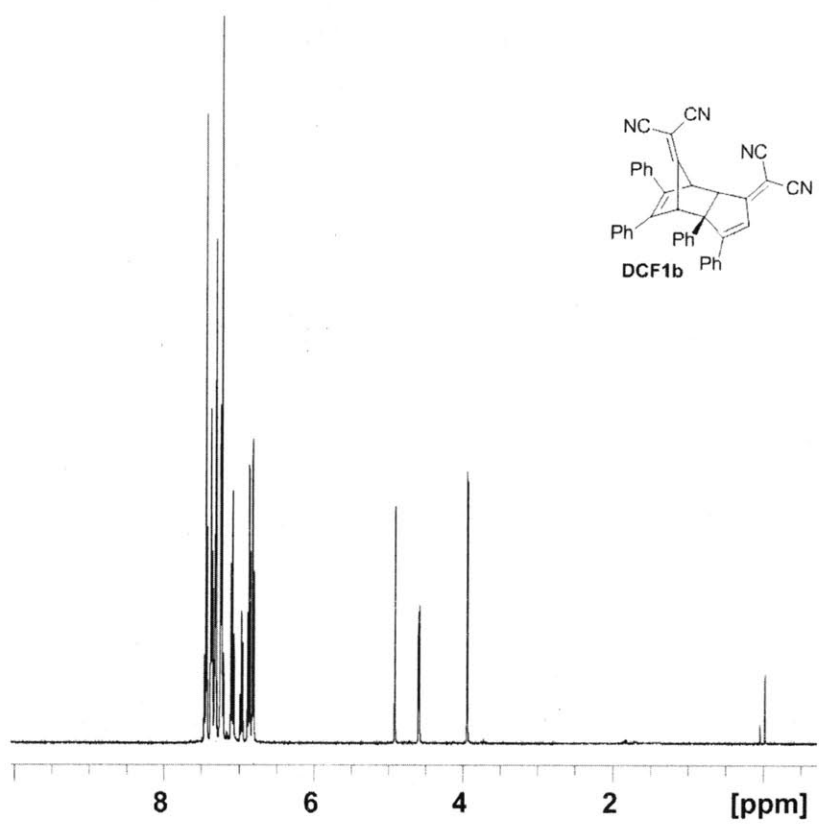


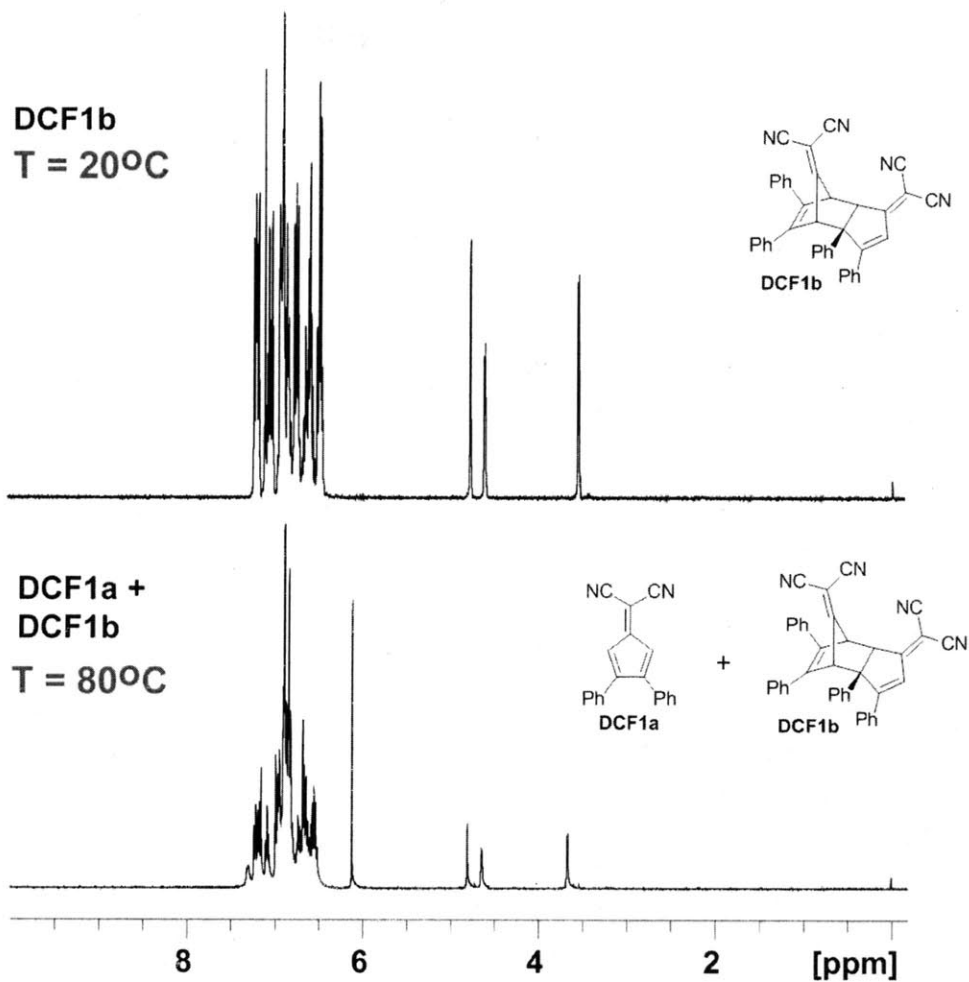


APPENDIX 5
NMR Spectra for Chapter 5









¹H-NMR spectrum of **DCF1b** in toluene-d₈ at room temperature and at 80°C, showing the evolution of **DCF1a** upon heating.

